PASJ: Publ. Astron. Soc. Japan , 1–**??**,

Survey of Period Variations of Superhumps in SU UMa-Type Dwarf Novae. IV: The Fourth Year (2011–2012)

Taichi Kato,[1*] Franz-Josef Hambsch,[2,3,4] Hiroyuki Maehara,[5] Gianluca Masi,[6] Ian Miller,[7] Ryo Noguchi,[8] Chihiro Akasaka,[8] Tomoya Aoki,[8] Hiroshi Kobayashi,[8] Katsura Matsumoto,[8] Shinichi Nakagawa,[8] Takuma Nakazato,[8] Takashi Nomoto,[8] Kazuyuki Ogura,[8] Rikako Ono,[8] Keisuke Taniuchi,[8] William Stein,[9] Arne Henden,[10] Enrique de Miguel,[11,12] Seiichiro Kiyota,[13] Pavol A. Dubovsky,[14] Igor Kudzej,[14] Kazuyoshi Imamura,[15] Hidehiko Akazawa,[15] Ryosuke Takagi,[15] Yuya Wakabayashi,[15] Minako Ogi,[15] Kenji Tanabe,[15] Joseph Ulowetz,[16] Etienne Morelle,[17] Roger D. Pickard,[18,19] Tomohito Ohshima,[1] Kiyoshi Kasai,[20] Elena P. Pavlenko,[21] Oksana I. Antonyuk,[21] Aleksei V. Baklanov,[21] Kirill Antonyuk,[21] Denis Samsonov,[21] Nikolaj Pit,[21] Aleksei Sosnovskij,[21] Colin Littlefield,[22] Richard Sabo,[23] Javier Ruiz,[24,25] Thomas Krajci,[26] Shawn Dvorak,[27] Arto Oksanen,[28] Kenji Hirosawa,[29] William N. Goff,[30] Berto Monard,[31] Jeremy Shears,[32] David Boyd,[33] Irina B. Voloshina,[34] Sergey Yu. Shugarov,[34,35] Drahomir Chochol,[35] Atsushi Miyashita,[36] Jochen Pietz,[37] Natalia Katysheva,[34] Hiroshi Itoh,[38] Greg Bolt,[39] Maksim V. Andreev,[40,41] Nikolai Parakhin,[40] Viktor Malanushenko,[42] Fabio Martinelli,[43] Denis Denisenko,[44] Chris Stockdale,[45] Peter Starr,[46] Mike Simonsen,[10] Paul. J. Tristram,[47] Akihiko Fukui,[48] Tamas Tordai,[49] Robert Fidrich,[49] Kevin B. Paxson,[50] Koh-ichi Itagaki,[51] Youichirou Nakashima,[52] Seiichi Yoshida,[53] Hideo Nishimura,[54] Timur V. Kryachko,[55] Andrey V. Samokhvalov,[55] Stanislav A. Korotkiy,[55] Boris L. Satovski,[55] Rod Stubbings,[56] Gary Poyner,[57] Eddy Muyllaert,[58] Vladimir Gerke,[59] Walter MacDonald II,[60] Michael Linnolt,[10] Yutaka Maeda,[61] Hubert Hautecler,[58]

[1] *Department of Astronomy, Kyoto University, Kyoto 606-8502*
[*] *tkato@kusastro.kyoto-u.ac.jp*
[2] *Groupe Européen d'Observations Stellaires (GEOS), 23 Parc de Levesville, 28300 Bailleau l'Evêque, France*
[3] *Bundesdeutsche Arbeitsgemeinschaft für Veränderliche Sterne (BAV), Munsterdamm 90, 12169 Berlin, Germany*
[4] *Vereniging Voor Sterrenkunde (VVS), Oude Bleken 12, 2400 Mol, Belgium*
[5] *Kwasan and Hida Observatories, Kyoto University, Yamashina, Kyoto 607-8471*
[6] *The Virtual Telescope Project, Via Madonna del Loco 47, 03023 Ceccano (FR), Italy*
[7] *Furzehill House, Ilston, Swansea, SA2 7LE, UK*
[8] *Osaka Kyoiku University, 4-698-1 Asahigaoka, Osaka 582-8582*
[9] *6025 Calle Paraiso, Las Cruces, New Mexico 88012, USA*
[10] *American Association of Variable Star Observers, 49 Bay State Rd., Cambridge, MA 02138, USA*
[11] *Departamento de Física Aplicada, Facultad de Ciencias Experimentales, Universidad de Huelva, 21071 Huelva, Spain*
[12] *Center for Backyard Astrophysics, Observatorio del CIECEM, Parque Dunar, Matalascañas, 21760 Almonte, Huelva, Spain*
[13] *Variable Star Observers League in Japan (VSOLJ), 405-1003 Matsushiro, Tsukuba, Ibaraki 305-0035*
[14] *Vihorlat Observatory, Mierova 4, Humenne, Slovakia*
[15] *Department of Biosphere-Geosphere System Science, Faculty of Informatics, Okayama University of Science, 1-1 Ridai-cho, Okayama, Okayama 700-0005*
[16] *Center for Backyard Astrophysics Illinois, Northbrook Meadow Observatory, 855 Fair Ln, Northbrook, Illinois 60062, USA*
[17] *9 rue Vasco de GAMA, 59553 Lauwin Planque, France*
[18] *The British Astronomical Association, Variable Star Section (BAA VSS), Burlington House, Piccadilly, London, W1J 0DU, UK*
[19] *3 The Birches, Shobdon, Leominster, Herefordshire, HR6 9NG, UK*
[20] *Baselstrasse 133D, CH-4132 Muttenz, Switzerland*
[21] *Crimean Astrophysical Observatory, 98409, Nauchny, Crimea, Ukraine*
[22] *Department of Physics, University of Notre Dame, Notre Dame, Indiana 46556, USA*
[23] *2336 Trailcrest Dr., Bozeman, Montana 59718, USA*
[24] *Observatorio de Cántabria, Ctra. de Rocamundo s/n, Valderredible, Cantabria, Spain*
[25] *Agrupación Astronómica Cántabra, Apartado 573, 39080-Santander, Spain*
[26] *Astrokolkhoz Observatory, Center for Backyard Astrophysics New Mexico, PO Box 1351 Cloudcroft, New Mexico 83117, USA*
[27] *Rolling Hills Observatory, 1643 Nightfall Drive, Clermont, Florida 34711, USA*
[28] *Nyrola observatory, Jyvaskylan Sirius ry, Vertaalantie 419, FI-40270 Palokka, Finland*
[29] *216-4 Maeda, Inazawa-cho, Inazawa-shi, Aichi 492-8217*
[30] *13508 Monitor Ln., Sutter Creek, California 95685, USA*
[31] *Bronberg Observatory, Center for Backyard Astronomy Pretoria, PO Box 11426, Tiegerpoort 0056, South Africa*

[32] "Pemberton", School Lane, Bunbury, Tarporley, Cheshire, CW6 9NR, UK
[33] Silver Lane, West Challow, Wantage, OX12 9TX, UK
[34] Sternberg Astronomical Institute, Lomonosov Moscow University, Universitetsky Ave., 13, Moscow 119992, Russia
[35] Astronomical Institute of the Slovak Academy of Sciences, 05960, Tatranska Lomnica, the Slovak Republic
[36] Seikei Meteorological Observatory, Seikei High School, 3-3-1, Kichijoji-Kitamachi, Musashino-shi, Tokyo 180-8633
[37] Nollenweg 6, 65510 Idstein, Germany
[38] VSOLJ, 1001-105 Nishiterakata, Hachioji, Tokyo 192-0153
[39] Camberwarra Drive, Craigie, Western Australia 6025, Australia
[40] Institute of Astronomy, Russian Academy of Sciences, 361605 Peak Terskol, Kabardino-Balkaria, Russia
[41] International Center for Astronomical, Medical and Ecological Research of NASU, Ukraine 27 Akademika Zabolotnoho Str. 03680 Kyiv, Ukraine
[42] Apache Point Observatory, New Mexico State University, 2001 Apache Point Road, P.O. Box 59, Sunspot, New Mexico 88349-0059, USA
[43] Palareta, 18-56040 Montecatini, Val Di Cecina, Italy
[44] Space Research Institute (IKI), Russian Academy of Sciences, Moscow, Russia
[45] 8 Matta Drive, Churchill, Victoria 3842, Australia
[46] Warrumbungle Observatory, Tenby, 841 Timor Rd, Coonabarabran NSW 2357, Australia
[47] Mt. John Observatory, P.O. Box 56, Lake Tekapo 8770, New Zealand
[48] Okayama Astrophysical Observatory, National Astronomical Observatory of Japan, Asakuchi, Okayama 719-0232
[49] Polaris Observatory, Hungarian Astronomical Association, Laborc utca 2/c, 1037 Budapest, Hungary
[50] 20219 Eden Pines, Spring, Texas 77379, USA
[51] Itagaki Astronomical Observatory, Teppo-cho, Yamagata 990-2492
[52] 968-4 Yamadanoshou, Oku-cho, Setouchi-City, Okayama 701-4246
[53] 2-4-10-708 Tsunashima-nishi, Kohoku-ku, Yokohama-City, Kanagawa 223-0053
[54] Miyawaki 302-6, Kakegawa, Shizuoka 436-0086
[55] Astrotel-Caucasus Observatory, 41 Lenin Street, village Zelenchukskaya Karachay-Cherkessiya, 369140 Russia
[56] Tetoora Observatory, Tetoora Road, Victoria, Australia
[57] BAA Variable Star Section, 67 Ellerton Road, Kingstanding, Birmingham B44 0QE, UK
[58] Vereniging Voor Sterrenkunde (VVS), Moffelstraat 13 3370 Boutersem, Belgium
[59] 39-28 Razvilka, Moscow region, 142717 Russia
[60] Winchester Observatory, P. O. Box 142, Winchester, ON K0C 2K0, Canada
[61] Kaminishiyamamachi 12-14, Nagasaki, Nagasaki 850-0006

(Received 201 0; accepted 201 0)

Abstract

Continuing the project described by Kato et al. (2009), we collected times of superhump maxima for 86 SU UMa-type dwarf novae mainly observed during the 2011–2012 season. We confirmed the general trends recorded in our previous studies, such as the relation between period derivatives and orbital periods. There are some systems showing positive period derivatives despite the long orbital periods. We observed the 2011 outburst of the WZ Sge-type dwarf nova BW Scl, and recorded an $O-C$ diagram similar to those of previously known WZ Sge-type dwarf novae. The WZ Sge-type dwarf nova OT J184228.1+483742 showed an unusual pattern of double outbursts composed of an outburst with early superhumps and one with ordinary superhumps. We propose an interpretation that a very small growth rate of the 3:1 resonance due to an extremely low mass-ratio led to a quenching of the superoutburst before the ordinary superhumps appeared. We systematically studied ER UMa-type dwarf novae and found that V1159 Ori showed positive superhumps similar to ER UMa in the 1990s. The recently recognized ER UMa-type object BK Lyn dominantly showed negative superhumps, and its behavior was very similar to the present-day state of ER UMa. The pattern of period variations in AM CVn-type objects were very similar to short-period hydrogen-rich SU UMa-type dwarf novae, making them helium analogue of hydrogen-rich SU UMa-type dwarf novae. SBS 1108+574, a peculiar hydrogen-rich dwarf nova below the period minimum, showed a very similar pattern of period variations to those of short-period SU UMa-type dwarf novae. The mass-ratio derived from the detected orbital period suggests that this secondary is a somewhat evolved star whose hydrogen envelope was mostly stripped during the mass-exchange. CC Scl, MASTER OT J072948.66+593824.4 and OT J173516.9+154708 showed only low-amplitude superhumps with complex profiles. These superhumps are likely a combination of closely separated two periods.

Key words: accretion, accretion disks — stars: novae, cataclysmic variables — stars: dwarf novae

1. Introduction

In papers Kato et al. (2009), Kato et al. (2010) and Kato et al. (2012a), we systematically surveyed period variations of superhumps in SU UMa-type dwarf novae (for general information of SU UMa-type dwarf novae and superhumps, see e.g. Warner 1995). The period variation of superhumps in many SU UMa-type dwarf novae is generally composed of three distinct stages: early evolutionary stage with a longer superhump period ($P_{\rm SH}$) (stage A), middle stage with systematically varying periods (stage B), final stage with a shorter, stable superhump period (stage C). These stages are most distinct in objects with short orbital periods ($P_{\rm orb}$). Objects with longer orbital periods tend to show more gradual changes around the transition from stage B to C. It was also shown that the period derivatives ($P_{\rm dot} = \dot{P}/P$) during stage B is correlated with $P_{\rm SH}$, or binary mass-ratios ($q = M_2/M_1$). In Kato et al. (2012a), we also studied global trends in the amplitudes of superhumps, and found that the amplitudes of superhumps are strongly correlated with orbital periods, and the dependence on the inclination is weak in non-eclipsing systems.

In the present study, we extended the survey to newly recorded objects and superoutbursts since the publication of Kato et al. (2012a).

2. Observation and Analysis

The data were obtained under campaigns led by the VSNET Collaboration (Kato et al. 2004b). In some objects, we used the public data from the AAVSO International Database[1]. The majority of the data were acquired by time-resolved CCD photometry by using 30 cm-class telescopes, whose observational details on individual objects will be presented in future papers dealing with analysis and discussion on individual objects. The list of outbursts and observers is summarized in table 1. The data analysis was performed just in the same way described in Kato et al. (2009) and Kato et al. (2012a). We particularly refer to Phase Dispersion Minimization (PDM; Stellingwerf 1978). We also used the Least Absolute Shrinkage and Selection Operator (Lasso) method (Kato, Uemura 2012) for separating closely spaced periods. The times of all observations are expressed in Barycentric Julian Dates (BJD). We also use the same abbreviations: $P_{\rm orb}$ for the orbital period and $\epsilon = P_{\rm SH}/P_{\rm orb} - 1$ for the fractional superhump excess.

The derived $P_{\rm SH}$, $P_{\rm dot}$ and other parameters are listed in table 2 in same format as in Kato et al. (2009). The definitions of parameters P_1, P_2, E_1, E_2 and $P_{\rm dot}$ are the same as in Kato et al. (2009). We also present comparisons of $O-C$ diagrams between different superoutbursts since this has been one of the motivations of these surveys (cf. Uemura et al. 2005).

We use the same terminology of superhumps summarized in Kato et al. (2012a). We especially call reader's attention to the term "late superhumps". We only use "traditional" late superhumps when an ∼0.5 phase shift is confirmed. Early superhumps are superhumps seen during the early stages of WZ Sge-type dwarf novae, and have period close to the orbital periods (Kato et al. 1996a; Kato 2002a).

[1] <http://www.aavso.org/data-download>.

Table 3. Superhump maxima of EG Aqr (2011).

E	max*	error	$O-C$†	N‡
0	55740.8707	0.0002	−0.0044	221
5	55741.2672	0.0004	−0.0007	119
12	55741.8181	0.0008	0.0001	88
13	55741.9023	0.0007	0.0058	78
93	55748.1819	0.0010	−0.0008	146

*BJD−2400000.
†Against max $= 2455740.8750 + 0.078577E$.
‡Number of points used to determine the maximum.

3. Individual Objects

3.1. *V725 Aquilae*

Y. Nakashima detected an outburst of this object on 2012 April 16 (vsnet-alert 14450). Subsequent observations confirmed that it is indeed a superoutburst (vsnet-alert 14460). Due to the short visibility in the morning, observations only on two nights were obtained. A PDM analysis yielded a period of 0.09047(5) d. We obtained a single superhump maximum of BJD 2456036.9734(8) ($N = 137$). It is noticeable that a likely superoutburst occurred in 2011 May (vsnet-alert 14460), and the interval between the superoutburst was only ∼340 d, which is much shorter than previously considered (Uemura et al. 2001). The object faded quickly (unfiltered CCD magnitude 17.6 on April 24) and we probably observed the final stage of the superoutburst. There was a visual detection at a magnitude of 14.6 on April 27. The object may have shown a rebrightening as in the 1999 one (Uemura et al. 2001).

3.2. *EG Aquarii*

The 2011 June superoutburst of this object was detected by R. Stubbings at a visual magnitude of 12.5 (vsnet-alert 13460). The object was rather unfavorably located and the observations were limited than in the past studies (Imada et al. 2008b; Kato et al. 2009). The times of superhump maxima are listed in table 3. Although there was likely a stage B–C transition between $E = 13$ and $E = 93$, the epoch of this transition was not covered by observations. The $P_{\rm dot}$ listed in table 2 refers to the global $P_{\rm dot}$. A comparison of $O-C$ diagrams of EG Aqr between different superoutbursts is shown in figure 1.

3.3. *SV Arietis*

SV Ari was discovered by Wolf, Wolf (1905) who recorded the object at magnitude 12 on three Heidelberg plates taken on 1905 November 6. The object was not

Table 1. List of Superoutbursts.

Subsection	Object	Year	Observers or references*	ID†
3.1	V725 Aql	2012	AKz	
3.2	EG Aqr	2011	LCO, Kis, KU	
3.3	SV Ari	2011	KU, HaC, OKU, MEV, Mhh, OUS, Mas, DPV, SRI, AAVSO, Kis, PKV	
3.4	TT Boo	2012	IMi, OUS, Mhh, PXR	
3.5	CR Boo	2012	AAVSO, UJH, Nyr, MEV, DPV, GFB, SRI, HMB	
	CR Boo	2012b	UJH, SWI, AAVSO, MEV, Nyr, HMB, DKS	
3.6	NN Cam	2011	OKU, Mhh, SWI, IMi	
3.7	SY Cap	2011	Mhh, OUS	
3.8	GZ Cet	2011	Mhh, IMi, Hsk	
3.9	AK Cnc	2012	OUS	
3.10	CC Cnc	2011	SWI, OKU, KU, Mhh	
3.11	GO Com	2012	DPV, OKU, Mhh, PXR, IMi, Pol	
3.12	TU Crt	2011	Kis	
3.13	V503 Cyg	2011	Ter, LCO, KU, CRI, OKU, DPV, IMi, HMB	
	V503 Cyg	2011b	CRI	
3.14	V1454 Cyg	2012	IMi	
3.15	AQ Eri	2011	HMB, SWI	
3.16	UV Gem	2011	MEV, AAVSO	
3.17	NY Her	2011	AKz	
3.18	PR Her	2011	Kai, OUS, OKU, JSh, DPV, deM, SXN, IMi, Ioh, SAc, PXR	
3.19	V611 Her	2012	Mas	
3.20	V844 Her	2012	OUS, Vol, DPV, PXR, HMB, Hsk	
3.21	MM Hya	2012	HMB, Mhh, IMi, AAVSO	
3.22	VW Hyi	2011	HaC, AAVSO	
3.23	RZ LMi	2012	MEV, HMB	
	RZ LMi	2012b	HMB, DKS, AAVSO	
	RZ LMi	2012c	HMB, AAVSO	
3.24	BK Lyn	2012	HMB, AAVSO, MEV, DKS, Boy, UJH, Mhh, GFB, Kai, SRI	
	BK Lyn	2012b	UJH, Nyr, AAVSO, DKS, Boy, SRI	
3.25	V585 Lyr	2012	Mhh	
3.26	FQ Mon	2011	Kis	
3.27	V1032 Oph	2012	Kai, Mhh	
3.28	V2051 Oph	2012	Mhh	
3.29	V1159 Ori	2012	UJH, SWI	
3.30	AR Pic	2011	HaC	
3.31	GV Psc	2011	SWI, IMi, Mas, OKU	
3.32	BW Scl	2011	HaC, MLF, Mhh, SPE, Kis, Sto, DKS, KU, MOA, Hsk, Nyr, AAVSO	
3.33	CC Scl	2011	HaC	
3.34	V1208 Tau	2011	SWI, IMi, OKU	
3.35	V1212 Tau	2011b	MEV, IMi	
3.36	DI UMa	2007	Rutkowski et al. (2009)	
	DI UMa	2007b	Rutkowski et al. (2009)	
3.37	IY UMa	2011	OUS	
3.38	KS UMa	2012	OUS	
3.39	MR UMa	2012	DPV	
3.40	PU UMa	2012	IMi, Kai, LCO, CRI, Mhh, PXR, OKU, JSh	
3.41	SS UMi	2012	HMB, AKz, AAVSO, Kai, UJH	

*Key to observers: AKz (Astrokolkhoz Obs.), APO (Apache Point Obs.), Boy‡(D. Boyd), CRI (Crimean Astrophys. Obs.), deM (E. de Miguel), DKS‡(S. Dvorak), DPV (P. Dubovsky), GBo (G. Bolt), GFB‡(W. Goff), HaC (F.-J. Hambsch, remote obs. in Chile), HMB (F.-J. Hambsch), Hsk (K. Hirosawa), IMi‡(I. Miller), Ioh (H. Itoh), JSh‡(J. Shears), Kai (K. Kasai), Kis (S. Kiyota), Kra (T. Krajci), KU (Kyoto U., campus obs.), LCO‡(C. Littlefield), Mas (G. Masi), MEV‡(E. Morelle), Mhh (H. Maehara), MLF‡(B. Monard), MOA (MOA team), Mtc (Montecatini Obs.), NKa (N. Katysheva), Nyr (Nyrola and Hankasalmi Obs.), OKU (Osaya Kyoiku U.), OUS (Okayama U. of Science), PIE (J. Pietz), PKV‡(K. Paxson), Pol (Polaris Obs.), PXR‡(R. Pickard), Rui (J. Ruiz), SAc (Seikei High School), Shu (S. Shugarov), SPE‡(P. Starr), SRI‡(R. Sabo), Sto (C. Stockdale), SWI‡(W. Stein), SXN‡(M. Simonsen), Ter (Terskol Obs.), UJH‡(J. Ulowetz), Vol (I. Voloshina)

†Original identifications or discoverers.

‡Inclusive of observations from the AAVSO database.

Table 1. List of Superoutbursts (continued).

Subsection	Object	Year	Observers or references*	ID†
3.42	1RXS J231935	2011	MEV, Rui, PIE, OKU, PXR, deM, Mhh, AAVSO, Mtc	
3.43	ASAS J224349	2011	IMi	
3.44	DDE 19	2011	SWI	
3.45	MASTER J072948	2012	deM, SWI, Shu, IMi, Mhh	Balanutsa et al. (2012c)
3.46	MASTER J174305	2012	Kra	Balanutsa et al. (2012a)
3.47	MASTER J182201	2012	Mas	Balanutsa et al. (2012b)
3.48	MisV 1446	2012	GBo, MLF, Kis, Kai, KU, deM, HaC	
3.49	SBS 1108	2012	Kai, deM, Vol, LCO, APO, GFB, Mhh, NKa, CRI, OKU, Kis, Shu	
3.50	SDSS J073208	2012	SRI, PXR	Wils et al. (2010)
3.51	SDSS J080303	2011	deM, OKU, Rui, IMi	
3.52	SDSS J165359	2012	IMi, Mhh, PXR, OKU, deM	
3.53	SDSS J170213	2011	MEV, OKU, IMi, DPV, Mas, LCO, Boy, HMB	
3.54	SDSS J172102	2012	GFB, Mas	Rau et al. (2010)
3.55	SDSS J210449	2011	IMi	
3.56	SDSS J220553	2011	SWI, Mhh, NKa	
3.57	OT J001952	2012	deM	CSS120131:001952+433901
3.58	OT J011516	2012	Mas	CSS101008:011517+245530
3.59	OT J050716	2012	Mas	CSS081221:050716+125314
3.60	OT J055721	2011	HaC, Mhh	SSS111229:055722−363055
3.61	OT J064608	2011	SWI, Mas, Rui	CSS080512:064608+403305
3.62	OT J081117	2011	Rui, Mhh	CSS111030:081117+152003
3.63	OT J084127	2012	Mas, OKU, PXR	CSS090525:084127+210054
3.64	OT J094854	2012	HMB, SWI, Mas	CSS120315:094854+014911
3.65	OT J102842	2012	OKU, Kis, UJH, SWI, deM, HMB	CSS090331:102843−081927
3.66	OT J105122	2012	SWI, CRI	CSS120101:105123+672528
3.67	OT J125905	2012	Mas	CSS120424:125906+242634
3.68	OT J131625	2012	Mas	CSS080427:131626−151313
3.69	OT J142548	2011	Mas	CSS110628:142548+151502
3.70	OT J144252	2012	MLF, HaC, LCO	CSS120417:144252−225040
3.71	OT J144453	2012	Mhh, HaC	CSS120424:144453−131118
3.72	OT J145921	2011	Kra, Mas, PIE	CSS110613:145922+354806
3.73	OT J155631	2012	GBo, HMB	CSS090321:155631−080440
3.74	OT J160410	2012	Mas	CSS120326:160411+145618
3.75	OT J162806	2011	Mas, Mhh	CSS110611:162806+065316
3.76	OT J163942	2012	IMi	CSS080131:163943+122414
3.77	OT J170609	2011	Mas	CSS090205:170610+143452
3.78	OT J173516	2011	OKU, Mas, Mhh, DPV, KU, HMB, Kis	CSS110623:173517+154708
3.79	OT J184228	2011	Mas, Mhh, OKU, DPV, OUS, Ioh, deM, SRI, UJH, KU, AAVSO, HMB, LCO, CRI, Hsk, IMi	Nishimura (Nakano et al. 2011)
3.80	OT J210950	2011	DKS, Rui, DPV, OUS, Kis, SRI, IMi, LCO, Mhh, AAVSO	Itagaki (Yamaoka et al. 2011)
3.81	OT J214738	2011	Mas, SWI, deM, HMB, OKU, Nyr, UJH, CRI	CSS111004:214738+244554
3.82	OT J215818	2011	SWI, Rui, JSh, deM, OKU, SRI, IMi, UJH, Mas, MEV	PNV J21581852+2419246
3.83	OT J221232	2011	SWI, Kai, Mas, CRI, SAc	CSS 090911:221232+160140
3.84	OT J224736	2012	Mas	CSS120616:224736+250436
3.85	TCP J084616	2012	deM, Mas	TCP J08461690+3115554
3.86	TCP J231308	2011	Rui, Mas, Mhh, Kra, Kis	TCP J23130812+2337018

Table 2. Superhump Periods and Period Derivatives

Object	Year	P_1 (d)	err	E_1*		$P_{\rm dot}$†	err†	P_2 (d)	err	E_2*		$P_{\rm orb}$ (d)	Q‡
EG Aqr	2011	0.078577	0.000055	0	93	−17.6	7.2	–	–	–	–	–	CGM
SV Ari	2011	0.055524	0.000014	19	311	4.0	0.2	0.055350	0.000052	307	366	–	A
TT Boo	2012	0.078083	0.000015	0	113	1.6	0.8	–	–	–	–	–	C
CR Boo	2012	0.017265	0.000002	0	247	2.0	0.2	0.017193	0.000006	237	395	0.017029	B
CR Boo	2012b	0.017257	0.000002	0	245	1.9	0.2	–	–	–	–	0.017029	B
NN Cam	2011	0.074197	0.000023	0	57	7.1	3.8	0.073843	0.000013	54	109	0.0717	B
SY Cap	2011	0.063750	0.000026	0	31	–	–	–	–	–	–	–	CG
AK Cnc	2012	0.067239	0.000123	0	46	–	–	–	–	–	–	0.0651	C
CC Cnc	2011	0.075887	0.000001	0	27	–	–	0.075456	0.000028	42	103	0.07352	C
GO Com	2012	0.063016	0.000019	0	128	4.8	1.5	0.062492	0.000150	127	144	–	B
TU Crt	2011	–	–	–	–	–	–	0.084962	0.000043	0	82	0.08209	C
V503 Cyg	2011	0.081309	0.000062	0	25	–	–	0.081046	0.000048	35	78	0.07777	B
V503 Cyg	2011b	0.081241	0.000057	0	87	−11.6	3.4	–	–	–	–	0.07777	CGM
V1454 Cyg	2012	0.057494	0.000015	0	18	–	–	–	–	–	–	–	C
AQ Eri	2011	–	–	–	–	–	–	0.061648	0.000247	143	161	0.06094	CG
UV Gem	2011	0.092822	0.000094	0	13	–	–	–	–	–	–	–	C
NY Her	2011	0.075802	0.000121	0	37	–	–	–	–	–	–	–	CG
PR Her	2011	0.055022	0.000026	0	92	8.8	3.7	–	–	–	–	0.05422	CE
V844 Her	2012	0.055901	0.000021	22	124	12.4	1.5	0.055873	0.000031	124	183	0.054643	B
MM Hya	2012	0.058872	0.000026	0	122	–	–	0.058625	0.000049	119	201	0.057590	C
VW Hyi	2011	0.076914	0.000026	25	68	8.2	5.8	0.076540	0.000019	77	146	0.074271	A
RZ LMi	2012	0.059441	0.000021	0	126	2.4	1.5	–	–	–	–	–	C
RZ LMi	2012b	0.059472	0.000026	0	84	4.5	3.6	–	–	–	–	–	C
RZ LMi	2012c	0.059408	0.000011	0	133	2.9	0.4	–	–	–	–	–	B
BK Lyn	2012b	0.078510	0.000028	25	127	3.2	2.7	–	–	–	–	0.07498	B
V585 Lyr	2012	0.060350	0.000038	0	19	–	–	–	–	–	–	–	C
FQ Mon	2011	–	–	–	–	–	–	0.072718	0.000180	0	14	–	C
V1032 Oph	2012	0.085965	0.000288	0	47	–	–	–	–	–	–	0.081055	C
AR Pic	2011	–	–	–	–	–	–	0.083154	0.000149	0	50	0.0801	CP
GV Psc	2011	0.094313	0.000018	0	62	−3.1	2.3	–	–	–	–	–	C2
BW Scl	2011	0.055000	0.000008	25	210	4.4	0.3	–	–	–	–	0.054323	A
CC Scl	2011	–	–	–	–	–	–	0.060012	0.000028	0	152	0.05858	C
V1208 Tau	2011	–	–	–	–	–	–	0.070481	0.000066	0	49	–	B
V1212 Tau	2011b	0.069692	0.000055	0	18	–	–	–	–	–	–	–	C2
DI UMa	2007	0.055306	0.000015	18	182	4.1	0.8	–	–	–	–	0.054566	B
DI UMa	2007b	0.055340	0.000040	0	126	9.3	4.3	–	–	–	–	0.054566	B
MR UMa	2012	–	–	–	–	–	–	0.064746	0.000021	0	48	–	C
PU UMa	2012	0.081090	0.000048	11	84	−14.3	2.6	0.080724	0.000100	84	121	0.077881	B
SS UMi	2012	0.070358	0.000128	0	33	–	–	–	–	–	–	0.06778	C
1RXS J231935	2011	0.065989	0.000019	0	79	11.6	1.7	0.065528	0.000014	75	159	–	B
DDE 19	2011	–	–	–	–	–	–	0.091210	0.000043	0	35	–	C
MisV 1446	2012	0.078072	0.000088	0	35	–	–	0.077304	0.000098	35	69	–	C
SBS 1108	2012	0.039118	0.000003	0	403	1.2	0.1	0.038869	0.000004	399	876	0.038449	CP
SDSS J073208	2012	0.079571	0.000021	0	72	–	–	–	–	–	–	–	CG
SDSS J080303	2011	0.091949	0.000119	17	31	–	–	0.090393	0.000022	27	88	–	C
SDSS J165359	2012	–	–	–	–	–	–	0.065105	0.000150	91	121	–	C
SDSS J170213	2011	0.105005	0.000056	32	117	17.0	2.8	–	–	–	–	0.100082	B
SDSS J172102	2012	–	–	–	–	–	–	0.026673	0.000008	0	463	–	C
SDSS J210449	2011	0.075315	0.000045	0	27	–	–	–	–	–	–	–	C
SDSS J220553	2011	0.058151	0.000021	0	99	7.7	0.9	–	–	–	–	0.05752	B

*Interval used for calculating the period (corresponding to E in section 3).

†Unit 10^{-5}.

‡Data quality and comments. A: excellent, B: partial coverage or slightly low quality, C: insufficient coverage or observations with large scatter, G: $P_{\rm dot}$ denotes global $P_{\rm dot}$, M: observational gap in middle stage, 2: late-stage coverage, the listed period may refer to P_2, E: $P_{\rm orb}$ refers to the period of early superhumps. P: $P_{\rm orb}$ refers to a shorter stable periodicity recorded in outburst.

Table 2. Superhump Periods and Period Derivatives (continued)

Object	Year	P_1	err	E_1		$P_{\rm dot}$	err	P_2	err	E_2		$P_{\rm orb}$	Q
OT J001952	2012	0.056770	0.000039	0	18	–	–	–	–	–	–	–	C
OT J050716	2012	0.065916	0.000080	0	15	–	–	–	–	–	–	–	C
OT J055721	2011	0.059756	0.000017	0	153	4.6	0.9	–	–	–	–	–	B
OT J064608	2011	0.061105	0.000023	0	82	11.1	2.6	–	–	–	–	–	B
OT J081117	2011	0.058035	0.000027	0	63	–	–	–	–	–	–	–	C
OT J084127	2012	0.087686	0.000252	0	4	–	–	–	–	–	–	–	C
OT J094854	2012	0.057499	0.000021	0	77	8.3	2.8	–	–	–	–	–	C
OT J102842	2012	0.038168	0.000008	70	151	–	–	–	–	–	–	–	C
OT J105122	2012	0.061054	0.000109	0	30	–	–	–	–	–	–	0.0596	C2
OT J144252	2012	0.065126	0.000028	0	59	13.6	4.3	0.064639	0.000054	59	107	–	B
OT J144453	2012	–	–	–	–	–	–	0.082289	0.000060	0	58	–	C
OT J145921	2011	0.085114	0.000059	0	74	10.9	7.2	–	–	–	–	–	C
OT J155631	2012	0.089309	0.000053	0	41	−21.3	5.8	–	–	–	–	–	CG
OT J162806	2011	0.068847	0.000008	0	140	–	–	–	–	–	–	–	CGM
OT J163942	2012	0.088585	0.000052	0	23	–	–	–	–	–	–	–	C
OT J170609	2011	0.059460	0.000076	0	16	–	–	–	–	–	–	–	C
OT J184228	2011	0.072342	0.000018	64	206	−0.9	1.5	–	–	–	–	0.07168	BE
OT J210950	2011	0.060045	0.000026	34	188	8.5	0.6	0.059742	0.000022	187	289	0.05865	BP
OT J214738	2011	0.097147	0.000021	21	107	8.8	1.0	–	–	–	–	0.09273	BP
OT J215818	2011	0.067397	0.000027	0	56	6.9	4.5	0.066852	0.000020	50	127	–	B
OT J221232	2011	0.090322	0.000097	0	29	–	–	0.090051	0.000028	29	106	–	B
OT J224736	2012	0.056673	0.000020	0	37	–	–	–	–	–	–	–	C
TCP J084616	2012	0.096333	0.000106	0	12	–	–	–	–	–	–	0.09139	C
TCP J231308	2011	0.071364	0.000044	0	24	–	–	0.071016	0.000033	28	85	–	C

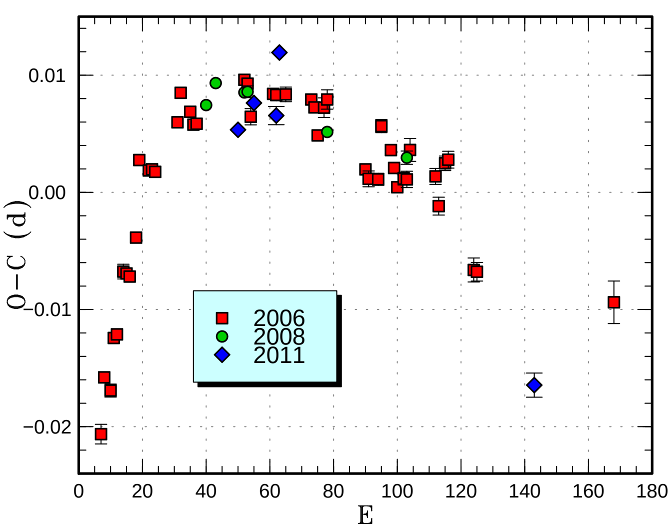

Fig. 1. Comparison of $O-C$ diagrams of EG Aqr between different superoutbursts. A period of 0.07885 d was used to draw this figure. Approximate cycle counts (E) after the start of the superoutburst were used. Since the starts of the 2008 and 2011 superoutbursts were not well constrained, we shifted the $O-C$ diagrams to best fit the best-recorded 2006 one.

detected on November 1, and it quickly faded to magnitude 13.5 on November 21. According to Duerbeck (1987), there was a possible detection of a brightening to magnitude 15.7 on 1943 September 2 by Himpel and Jansch. Although Duerbeck (1987) even suggested an intergalactic nova, many observers, mostly amateur observers, intensively monitored the object suspecting that it is a dwarf nova. Robertson et al. (1998) identified a $B = 22.1$ mag quiescent counterpart [see also Robertson et al. (2000); Duerbeck (1987) had also proposed the same 22-nd mag counterpart]. After a long period of unsuccessful detection of an outburst, R. Stubbings finally detected an outburst at a visual magnitude of 15.0 on 2011 August 2 (vsnet-outburst 13091). The outburst was immediately confirmed by T. Tordai and G. Masi who detected superhumps (vsnet-alert 13541, 13552; figure 2).

The times of superhump maxima are listed in table 4 The early to middle portion of the $O-C$ diagram shows clear stages of A and B. During the period of BJD 2455789–2477912, there were sometimes two hump maxima, and humps with phases different from main humps ($E = 240, 253, 272$) were also included in the table. There was some indication of a stage C around the terminal stage ($E \geq 364$). The values given in table 2 were determined after rejecting humps at $E = 240, 253, 272$. The resultant $P_{\rm dot}$ for stage B superhumps was $+4.0(0.2) \times 10^{-5}$, comparable to those of extreme WZ Sge-type dwarf novae.

The 2011 outburst was much fainter than the 1905 outburst. This difference can be understood as a combina-

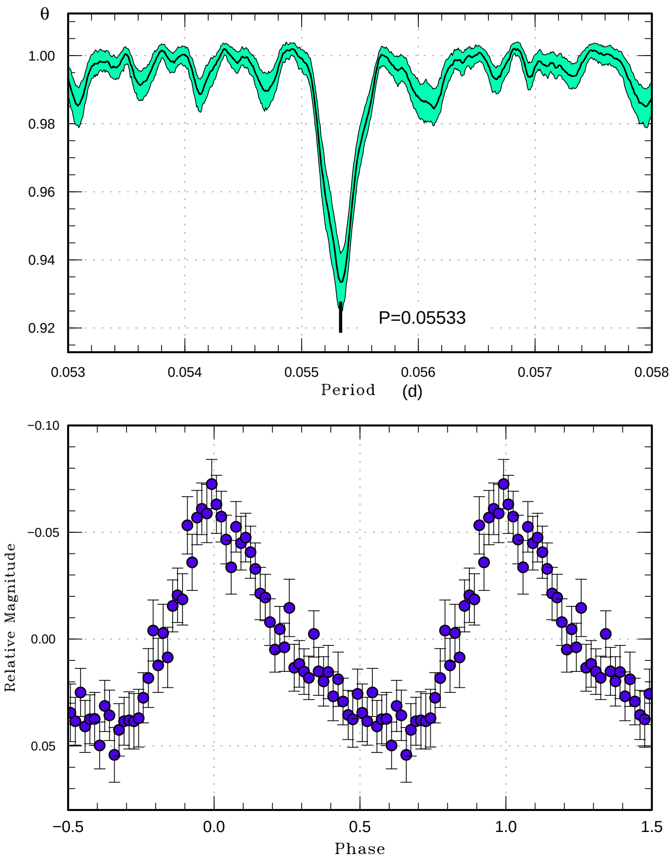

Fig. 2. Superhumps in SV Ari (2011). (Upper): PDM analysis. (Lower): Phase-averaged profile.

tion of two effects: (1) the magnitude scale in Wolf, Wolf (1905) was about 2 mag brighter than the present scale, which is confirmed from a comparison of the magnitudes of the comparison stars, and (2) the brightness maximum of the 2011 outburst was missed because there were no observations in that season before the Stubbings' detection. The lack of a stage of early superhumps, which is expected for such a WZ Sge-type dwarf nova, can also be understood for the same reason. No post-superoutburst rebrightening was recorded.

3.4. TT Bootis

We observed the early part of the 2012 superoutburst. The times of superhump maxima are listed in table 5. There were no detectable superhumps 0.8 d prior to the initial epoch of superhump maximum. The resultant $P_{\rm dot}$ for stage B was smaller than in 2004 and 2010, and it is probably a result of the limited observation of stage B and possibly from contamination of stage A or C superhumps (figure 3).

3.5. CR Bootis

CR Boo is one of the prototypical "helium dwarf novae" [Patterson et al. (1997); Provencal et al. (1997); Kato et al. (2000b); for representative theoretical analyses, see

Table 4. Superhump maxima of SV Ari (2011).

E	max*	error	$O-C$†	N‡
0	55776.5824	0.0026	0.0059	66
5	55776.8591	0.0010	0.0052	47
7	55776.9722	0.0011	0.0072	99
11	55777.1956	0.0009	0.0086	250
12	55777.2464	0.0007	0.0039	358
13	55777.3083	0.0014	0.0103	154
16	55777.4748	0.0013	0.0104	41
17	55777.5259	0.0015	0.0059	30
18	55777.5860	0.0006	0.0106	49
19	55777.6419	0.0003	0.0109	37
23	55777.8629	0.0003	0.0099	53
24	55777.9167	0.0004	0.0082	38
30	55778.2477	0.0010	0.0062	84
34	55778.4729	0.0014	0.0095	32
35	55778.5252	0.0009	0.0063	31
36	55778.5792	0.0003	0.0048	91
37	55778.6356	0.0004	0.0056	50
41	55778.8563	0.0006	0.0043	34
43	55778.9637	0.0010	0.0008	28
54	55779.5730	0.0003	−0.0004	38
59	55779.8498	0.0005	−0.0012	36
60	55779.9032	0.0005	−0.0033	28
66	55780.2370	0.0028	−0.0024	186
67	55780.2891	0.0016	−0.0059	167
77	55780.8425	0.0010	−0.0074	29
78	55780.9012	0.0010	−0.0043	75
79	55780.9551	0.0008	−0.0059	70
83	55781.1839	0.0031	0.0009	100
84	55781.2324	0.0012	−0.0060	224
85	55781.2897	0.0008	−0.0043	252
95	55781.8415	0.0005	−0.0074	36
96	55781.8981	0.0005	−0.0064	32
102	55782.2312	0.0010	−0.0063	238
103	55782.2838	0.0006	−0.0092	288
109	55782.6183	0.0006	−0.0077	44
113	55782.8402	0.0005	−0.0078	35
114	55782.8950	0.0006	−0.0085	35
127	55783.6165	0.0005	−0.0085	51
131	55783.8384	0.0008	−0.0086	35
132	55783.8941	0.0007	−0.0083	35
145	55784.6161	0.0007	−0.0079	51
150	55784.8916	0.0013	−0.0099	65
162	55785.5544	0.0037	−0.0131	26
163	55785.6194	0.0010	−0.0036	49
167	55785.8358	0.0019	−0.0092	30
168	55785.8944	0.0010	−0.0061	30
185	55786.8424	0.0035	−0.0016	28
186	55786.8891	0.0035	−0.0104	19
192	55787.2249	0.0039	−0.0076	105
203	55787.8394	0.0019	−0.0036	28
204	55787.8962	0.0024	−0.0023	28

*BJD−2400000.

†Against max $= 2455776.5764 + 0.055500E$.

‡Number of points used to determine the maximum.

Table 4. Superhump maxima of SV Ari (2011) (continued).

E	max*	error	$O-C$†	N‡
222	55788.8967	0.0043	−0.0008	29
240	55789.8813	0.0061	−0.0152	20
252	55790.5667	0.0027	0.0042	51
253	55790.5904	0.0023	−0.0276	51
253	55790.6199	0.0007	0.0020	37
257	55790.8503	0.0093	0.0103	19
270	55791.5773	0.0049	0.0158	51
272	55791.6554	0.0045	−0.0171	29
307	55793.6346	0.0020	0.0196	22
310	55793.7952	0.0024	0.0137	30
311	55793.8603	0.0009	0.0233	40
364	55796.7895	0.0039	0.0110	20
365	55796.8452	0.0034	0.0112	20
366	55796.8987	0.0016	0.0092	16

*BJD−2400000.
†Against max $= 2455776.5764 + 0.055500E$.
‡Number of points used to determine the maximum.

Table 5. Superhump maxima of TT Boo (2012).

E	max*	error	$O-C$†	N‡
0	56016.4443	0.0002	−0.0010	81
1	56016.5239	0.0002	0.0005	83
2	56016.6011	0.0002	−0.0003	83
35	56019.1732	0.0039	−0.0034	30
36	56019.2549	0.0011	0.0002	56
37	56019.3315	0.0014	−0.0012	42
38	56019.4122	0.0005	0.0015	73
39	56019.4881	0.0005	−0.0007	78
40	56019.5673	0.0005	0.0005	82
60	56021.1277	0.0032	0.0001	44
61	56021.2069	0.0023	0.0013	58
62	56021.2861	0.0013	0.0024	54
113	56025.2689	0.0007	0.0054	56
139	56027.2870	0.0016	−0.0054	55

*BJD−2400000.
†Against max $= 2456016.4454 + 0.078036E$.
‡Number of points used to determine the maximum.

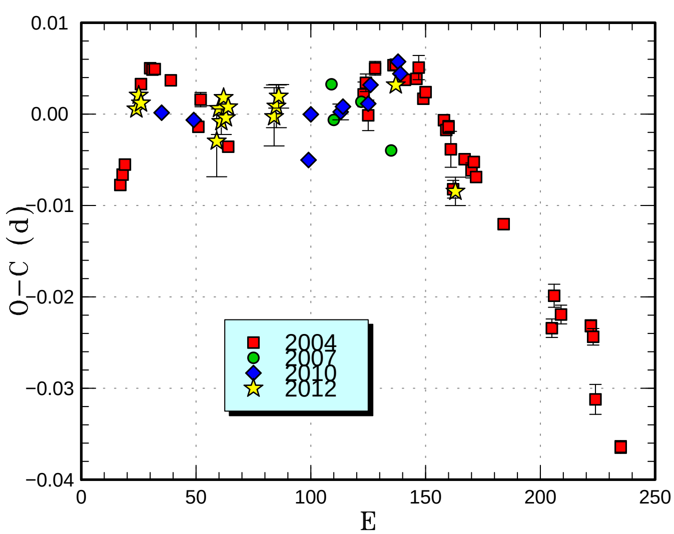

Fig. 3. Comparison of $O-C$ diagrams of TT Boo between different superoutbursts. A period of 0.07807 d was used to draw this figure. Approximate cycle counts (E) after the start of the superoutburst were used.

Tsugawa, Osaki (1997), Kotko et al. (2012); for recent observational reviews of AM CVn stars, see Solheim (2010), Ramsay et al. (2011), Ramsay et al. (2012)]. Although superhumps in this object was well established in the past, the published observations were either obtained in an anomalous state (Patterson et al. 1997) or not very ideally sampled (Kato et al. 2000b). The object was in a state of regular pattern of outbursts (cf. Kato et al. 2000b) with a supercycle of ∼50 d in 2011–2012 and is ideal to study the behavior of superhumps in helium dwarf novae.

We present here an analysis of a superoutburst in 2012 March mainly using the AAVSO observations. The superoutburst was first detected by G. Gualdoni on March 3 at $V = 13.61$ (AAVSO data). The existence of superhumps was soon recognized (vsnet-alert 14305). Although the object stayed in its plateau phase for six days, it started oscillations with a quasi-period of 1.0 d similar to Patterson et al. (1997), and this state lasted for six days. The object apparently entered a more stable state, and finally started fading rapidly on March 25. Although the overall behavior of the superoutburst was similar to those of hydrogen-rich SU UMa-type dwarf novae, the presence of oscillatory state is different. The relatively large scatter in the supercycle-phase-folded light curve (figure 4 of Kato et al. 2000b) may have been a result of these oscillations.

The times of superhump maxima until the early stage of the oscillatory state are shown in table 6. The $O-C$ diagram shows a pattern very similar to stages B and C in hydrogen-rich SU UMa-type dwarf novae. The $P_{\rm dot}$ for stage B was $+2.0(0.2) \times 10^{-5}$ and the ϵ for stage B and C superhumps (figures 4 and 5, respectively) were 1.39(1)%, and 0.97(4)%, similar to those of WZ Sge-type dwarf novae, but are larger than what is expected only from the mass-ratio. The stage B–C transition occurred when the oscillation started (figure 6). This may be analogous to WZ Sge-type dwarf novae, which usually do not show stage C superhumps by the end of plateau phase (Kato et al. 2009; Kato et al. 2010; Kato et al. 2012a). The oscillatory phase in CR Boo may correspond to post-superoutburst stage in WZ Sge-type dwarf novae, when these objects tend to show various kinds of rebrightenings (cf. Kato et al. 2009). We might recall the past examples of V803 Cen (Kato et al. 2004a) and V406 Hya (Nogami et al. 2004), both of which showed rebrightenings similar to WZ Sge-type dwarf novae. Ramsay et al. (2011) also noted the presence of a "dip" during superoutbursts of short-$P_{\rm orb}$ AM CVn-type objects (see also Levitan et al. 2011; Kotko et al. 2012). Such phenomena may be more prevalent than had been thought.

Although the superhumps in the later stages were not readily recognizable, we could detect the period with the PDM method: 0.017183(5) d for BJD 2455997.8–2456002.0 (oscillatory phase) and 0.017265(3) d for BJD 2456002.0–2456009.0 (second stable plateau). These periods indicate the persistence of superhumps until the end of the superoutburst.

After one supercycle, the object underwent another superoutburst in 2012 April. The times of superhump maxima are listed in table 7. Although the object started oscillatory behavior as in the March superoutburst, the later part of the superoutburst was not as well observed as in the March one. The resultant period and period derivatives were quite similar to those of the March superoutburst. The $O-C$ diagram of the stage B very well reproduced that of the March superoutburst (figure 6, lower panel).

3.6. NN Camelopardalis

We observed a superoutburst in 2011 December. The times of superhump maxima are listed in table 8. Although stage A and early part of stage B were missed, a clear pattern of stage B–C superhumps was detected.

A comparison of $O-C$ diagrams between different superoutbursts is shown in figure 7. The 2007 superoutburst, whose start of the main superoutburst was not observed, was shifted by 63 cycles to best match the others. This cycle count placed the initial epoch of superhump evolution around BJD 2454358.9, shortly after the precursor outburst. It was likely that superhumps started to grow just following the precursor outburst, and it is likely the true start of the main superoutburst was missed.

3.7. SY Capricorni

We observed a superoutburst in 2011 August–September. The times of superhump are listed in table 9. Since only a limited fragment of observation was obtained, we adopted a period with the PDM analysis in table 2.

3.8. GZ Ceti

This object (=SDSS J013701.06−091234.9) is an unusual short-$P_{\rm orb}$ dwarf nova with a massive secondary (Imada et al. 2006; Ishioka et al. 2007). We observed the 2011 superoutburst. We only observed the initial and final parts of the outburst. The times of superhump maxima

Table 6. Superhump maxima of CR Boo (2012 March).

E	max*	error	$O-C$†	N‡
0	55990.7536	0.0001	−0.0006	5
1	55990.7724	0.0004	0.0010	6
2	55990.7893	0.0005	0.0006	6
3	55990.8066	0.0009	0.0006	5
4	55990.8237	0.0007	0.0006	6
5	55990.8416	0.0009	0.0011	6
6	55990.8583	0.0005	0.0006	8
39	55991.4270	0.0005	0.0001	14
40	55991.4433	0.0003	−0.0008	17
41	55991.4613	0.0006	−0.0001	16
42	55991.4779	0.0005	−0.0008	16
43	55991.4946	0.0003	−0.0013	16
44	55991.5125	0.0006	−0.0006	12
45	55991.5295	0.0003	−0.0009	14
46	55991.5479	0.0006	0.0003	13
47	55991.5641	0.0004	−0.0007	8
48	55991.5819	0.0005	−0.0003	12
49	55991.5985	0.0003	−0.0009	15
50	55991.6161	0.0004	−0.0006	16
51	55991.6341	0.0005	0.0002	15
52	55991.6503	0.0007	−0.0008	17
53	55991.6677	0.0009	−0.0007	14
59	55991.7716	0.0006	−0.0003	7
60	55991.7888	0.0003	−0.0003	6
61	55991.8053	0.0005	−0.0011	6
62	55991.8235	0.0002	−0.0002	5
63	55991.8403	0.0002	−0.0006	6
64	55991.8569	0.0004	−0.0012	7
65	55991.8746	0.0002	−0.0007	7
66	55991.8921	0.0003	−0.0005	6
96	55992.4093	0.0008	−0.0007	28
97	55992.4267	0.0006	−0.0006	33
98	55992.4445	0.0004	−0.0001	30
99	55992.4615	0.0004	−0.0004	30
100	55992.4778	0.0004	−0.0013	22
101	55992.4952	0.0011	−0.0012	21
102	55992.5129	0.0008	−0.0007	20
103	55992.5302	0.0006	−0.0006	24
104	55992.5472	0.0011	−0.0009	19
105	55992.5626	0.0007	−0.0027	17
106	55992.5814	0.0006	−0.0012	18
118	55992.7889	0.0012	−0.0006	15
119	55992.8061	0.0004	−0.0007	13
120	55992.8238	0.0008	−0.0002	15
121	55992.8413	0.0004	0.0000	16
122	55992.8585	0.0012	−0.0001	15
124	55992.8925	0.0005	−0.0005	15
125	55992.9103	0.0009	0.0000	15
126	55992.9277	0.0006	0.0002	12
237	55994.8466	0.0010	0.0045	16
239	55994.8783	0.0011	0.0017	15
240	55994.8970	0.0006	0.0031	16

*BJD−2400000.

†Against max $= 2455990.7542 + 0.017249E$.

‡Number of points used to determine the maximum.

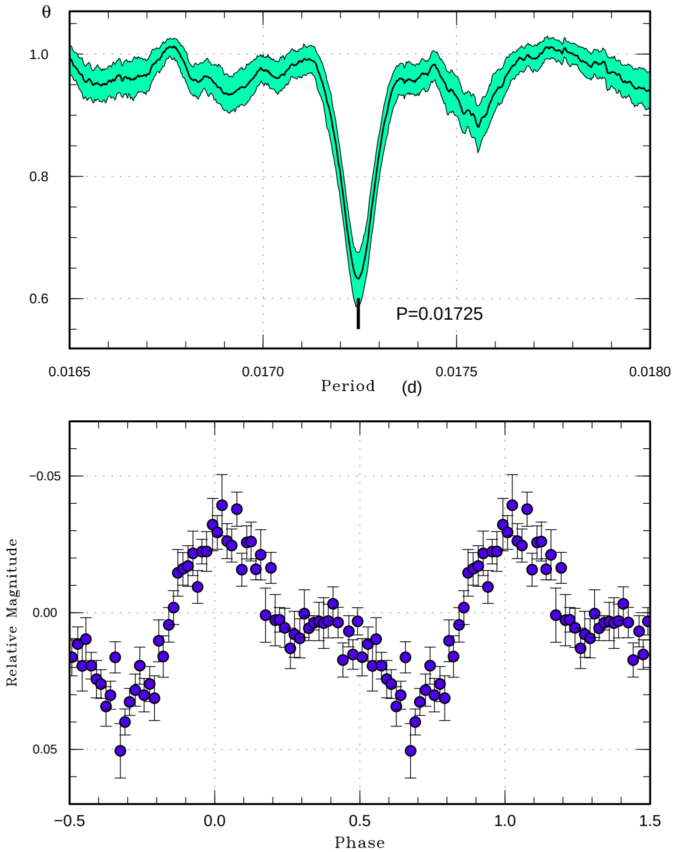

Fig. 4. Superhumps in CR Boo (2012 March) before the oscillatory phase. (Upper): PDM analysis. (Lower): Phase-averaged profile.

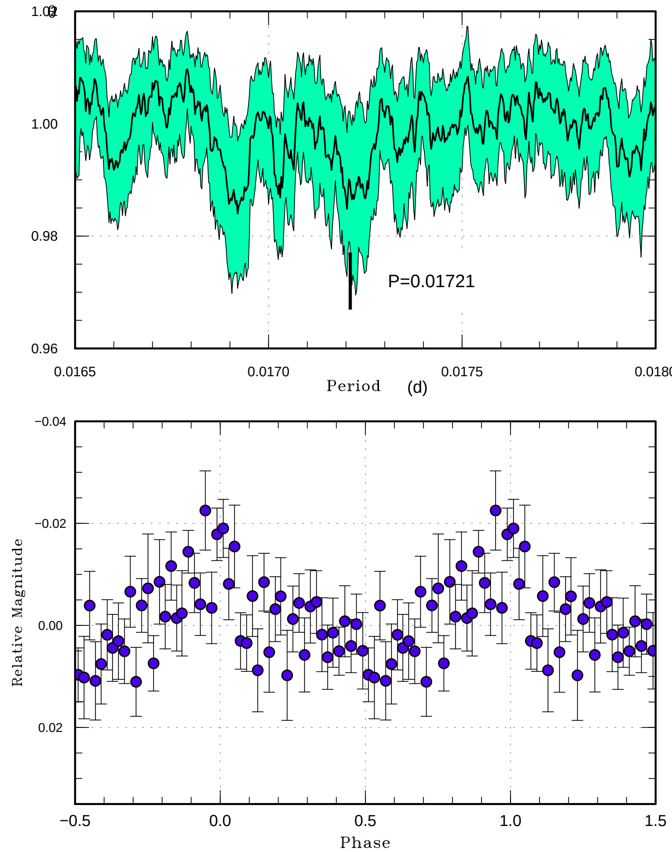

Fig. 5. Superhumps in CR Boo (2012 March) during the oscillatory phase. (Upper): PDM analysis. (Lower): Phase-averaged profile.

are listed in table 10. On BJD 2455923, the amplitudes of superhumps were still less than 0.1 mag, and we must have caught the initial stage of the outburst. A comparison of $O-C$ diagrams between different outbursts is shown in figure 8. Despite its unusual properties, the $O-C$ curve is composed of stages B and C similar to those of ordinary SU UMa-type dwarf novae. The $P_{\rm dot}$ during stage B appears to be smaller than those of ordinary SU UMa-type dwarf novae with similar $P_{\rm SH}$, consistent with the result in Kato et al. (2009).

3.9. AK Cancri

We observed a superoutburst in 2012 January. Due to the short duration of the observation, the recorded superhumps were limited (table 11). The resultant period suggests that we observed stage B superhumps.

3.10. CC Cancri

We observed a superoutburst in 2011 December. The times of superhump maxima are listed in table 12. Although the data were rather sparse, stages B and C were recorded. The obtained periods were similar to those in 2001 (Kato et al. 2009).

A comparison of $O-C$ diagrams between different superoutburst is shown in figure 9. Early stage observations are still lacking for this object.

3.11. GO Comae Berenices

We observed the 2012 superoutburst of this object. The times of superhump maxima are listed in table 13. Both typical stages B and C can be clearly identified. The $O-C$ variation during this outburst was similar to those in previous outbursts (figure 10).

3.12. TU Crateris

We observed the late stage of the 2011 superoutburst of TU Crt. The times of superhump maxima are listed in table 14. We most likely observed only stage C superhumps. The measured period is in good agreement with that of stage C superhumps recorded in 1998 (Mennickent et al. 1999) and analyzed in Kato et al. (2009). A comparison of $O-C$ diagrams between different superoutburst is shown in figure 11.

3.13. V503 Cygni

Harvey et al. (1995) established the SU UMa-type nature of this object and reported a mean $P_{\rm SH}$ of 0.08101(4) d. They also detected negative superhumps in quiescence. Although there may have been some evidence of a hump corresponding to negative superhumps during

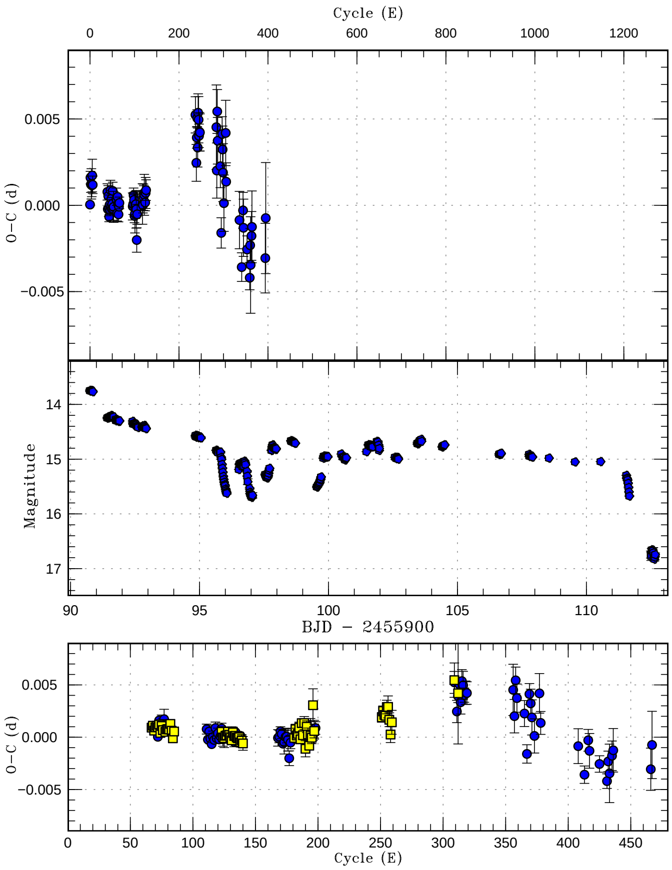

Fig. 6. $O-C$ diagram of superhumps in CR Boo. (Upper:) $O-C$ for the 2012 March superoutburst. We used a period of 0.017249 d for calculating the $O-C$ residuals. (Middle:) Light curve for the 2012 March superoutburst. (Lower:) Comparison of $O-C$ diagrams between two superoutbursts in 2012 March (filled circles) and April (filled squares). Approximate cycle counts (E) after the start of the superoutburst were used.

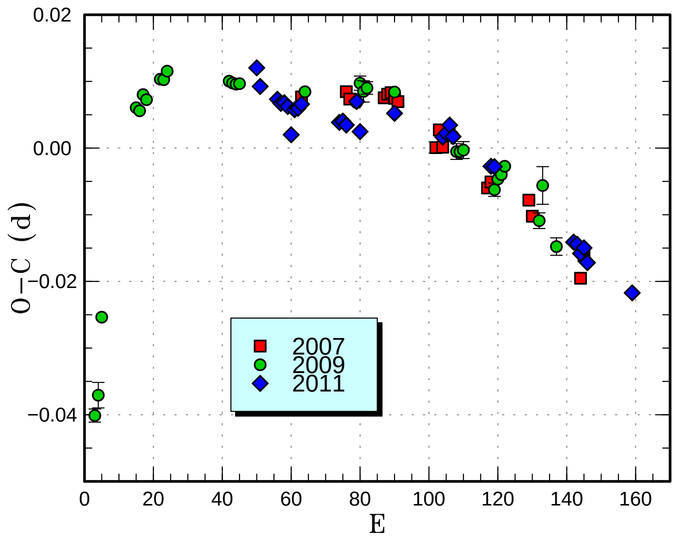

Fig. 7. Comparison of $O-C$ diagrams of NN Cam between different superoutbursts. A period of 0.0743 d was used to draw this figure. Approximate cycle counts (E) after the start of the superoutburst were used. The 2007 superoutburst was shifted by 63 cycles to best match the others.

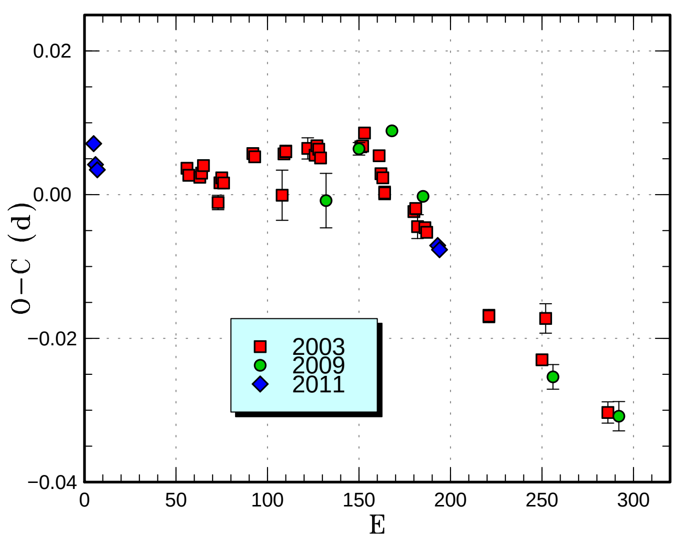

Fig. 8. Comparison of $O-C$ diagrams of GZ Cet between different superoutbursts. A period of 0.05672 d was used to draw this figure. Approximate cycle counts (E) after the start of the superoutburst were used. We assumed that the 2011 superoutburst was caught around its peak based on the brightness and evolution of superhumps, and assumed it to be the start of the superoutburst.

superoutburst, its presence was not well established.

We observed the 2011 July superoutburst, subsequent phase with normal outbursts and 2011 October superoutburst. The times of superhump maxima during the July superoutburst are listed in table 15. There was some hint of a break in the $O-C$ diagram for the superhumps during the superoutburst between $E = 25$ and $E = 35$, and we attributed this to be a stage B–C transition. A global $P_{\rm dot}$ corresponded to $-3.8(2.6) \times 10^{-5}$.

The signals of the ordinary superhumps already became difficult to trace even before the rapid fading (BJD 2455751). A PDM analysis, however, to the data for the interval BJD 2455751–2455754 yielded a period of 0.0814(1) d, suggesting that the ordinary superhumps were still the dominant signal, rather than negative superhumps.

After BJD 2455754, large-amplitude modulations appeared again. The times of maxima were not on a smooth extension of the times of superhump maxima during the superoutburst plateau. These new signals appear to cor-

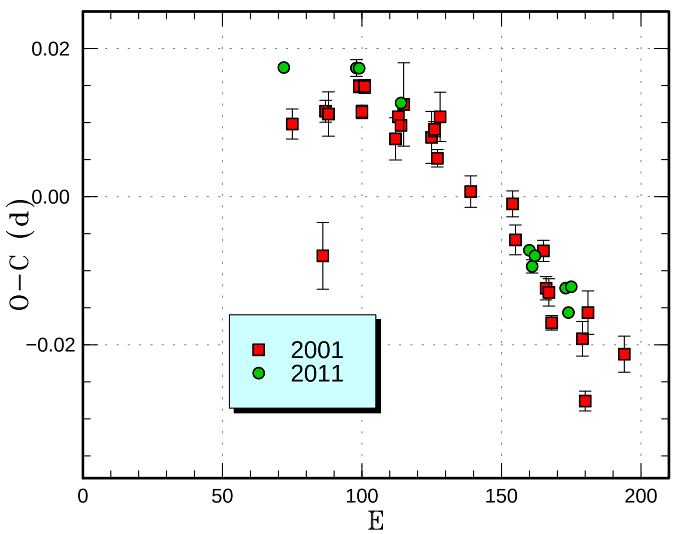

Fig. 9. Comparison of $O-C$ diagrams of CC Cnc between different superoutbursts. A period of 0.07589 d was used to draw this figure. Approximate cycle counts (E) after the start of the superoutburst were used. Since the start of the 2001 superoutburst was not well constrained, we shifted the $O-C$ diagrams to best fit the best-recorded 2011 one.

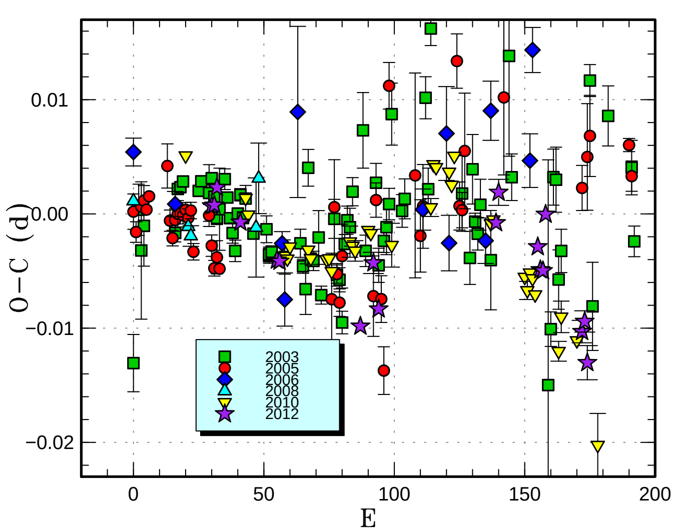

Fig. 10. Comparison of $O-C$ diagrams of GO Com between different superoutbursts. A period of 0.06303 d was used to draw this figure. Approximate cycle counts (E) after the start of the superoutburst were used.

Table 6. Superhump maxima of CR Boo (2012 March) (continued).

E	max*	error	$O-C$†	N‡
241	55994.9154	0.0005	0.0043	16
242	55994.9310	0.0011	0.0026	14
243	55994.9502	0.0011	0.0046	25
244	55994.9671	0.0013	0.0042	24
245	55994.9834	0.0007	0.0032	25
246	55995.0009	0.0011	0.0035	25
247	55995.0181	0.0011	0.0034	13
284	55995.6566	0.0024	0.0037	21
285	55995.6713	0.0016	0.0012	21
286	55995.6920	0.0013	0.0046	21
287	55995.7075	0.0014	0.0029	22
293	55995.8095	0.0012	0.0015	6
295	55995.8402	0.0009	−0.0024	11
297	55995.8804	0.0010	0.0033	14
298	55995.8967	0.0014	0.0024	15
299	55995.9126	0.0017	0.0011	14
301	55995.9454	0.0016	−0.0007	24
305	55996.0184	0.0019	0.0034	9
306	55996.0329	0.0011	0.0005	9
336	55996.5481	0.0017	−0.0017	22
341	55996.6316	0.0008	−0.0044	17
344	55996.6866	0.0010	−0.0011	37
345	55996.7029	0.0017	−0.0022	36
353	55996.8396	0.0008	−0.0034	10
359	55996.9414	0.0007	−0.0051	12
360	55996.9606	0.0010	−0.0032	7
361	55996.9767	0.0028	−0.0043	15
363	55997.0128	0.0014	−0.0026	9
364	55997.0306	0.0021	−0.0021	8
394	55997.5462	0.0020	−0.0039	16
395	55997.5658	0.0032	−0.0016	18

*BJD−2400000.
†Against max $= 2455990.7542 + 0.017249E$.
‡Number of points used to determine the maximum.

respond to the traditional late superhumps (e.g. Vogt 1983), rather than "stage C superhumps" in our designation (table 17).

The times of superhump maxima during the October superoutburst are listed in table 16. Although the epoch $E = 114$ is possibly a late superhump as in the 2011 July superoutburst, the lack of subsequent observations made the identification unclear. We listed a global $P_{\rm orb}$ and $P_{\rm dot}$ in table 2. A period derived from $E \le 27$ (stage B) was 0.08151(8) d.

We were not able to detect a signal of negative superhumps during the fading stage and subsequent quiescence, and the signal was dominated by positive superhumps. The situation was thus different from ER UMa (Ohshima et al. 2012). The mean period of (traditional late) superhumps during the post-superoutburst stage was 0.08032(3) d (PDM method), 3.4% longer than $P_{\rm orb}$, and was significantly shorter than that of ordinary superhumps. Although the superhump signal persisted

Table 7. Superhump maxima of CR Boo (2012 April).

E	max*	error	$O-C$†	N‡
0	56039.6483	0.0002	0.0009	21
1	56039.6657	0.0002	0.0011	33
2	56039.6825	0.0001	0.0006	33
3	56039.7001	0.0003	0.0009	33
4	56039.7175	0.0001	0.0010	34
5	56039.7346	0.0002	0.0009	34
6	56039.7521	0.0002	0.0011	34
7	56039.7685	0.0002	0.0003	34
8	56039.7865	0.0001	0.0010	33
9	56039.8033	0.0002	0.0006	34
11	56039.8376	0.0002	0.0004	24
12	56039.8551	0.0002	0.0006	32
13	56039.8724	0.0002	0.0006	33
14	56039.8896	0.0003	0.0006	33
15	56039.9074	0.0002	0.0011	33
16	56039.9240	0.0002	0.0005	33
17	56039.9405	0.0003	−0.0003	33
18	56039.9584	0.0002	0.0004	33
56	56040.6138	0.0005	0.0000	15
57	56040.6305	0.0004	−0.0005	16
58	56040.6477	0.0003	−0.0006	16
59	56040.6652	0.0004	−0.0004	15
60	56040.6825	0.0003	−0.0004	14
61	56040.7001	0.0004	−0.0000	16
62	56040.7170	0.0003	−0.0003	16
63	56040.7340	0.0005	−0.0006	14
64	56040.7510	0.0003	−0.0009	16
65	56040.7690	0.0005	−0.0001	13
66	56040.7859	0.0004	−0.0005	14
67	56040.8031	0.0003	−0.0005	15
68	56040.8202	0.0003	−0.0006	15
69	56040.8374	0.0003	−0.0007	14
70	56040.8548	0.0005	−0.0006	15
71	56040.8715	0.0003	−0.0011	13
72	56040.8890	0.0006	−0.0009	13
73	56040.9059	0.0007	−0.0012	15
114	56041.6136	0.0004	−0.0011	16
115	56041.6317	0.0005	−0.0003	16
116	56041.6483	0.0007	−0.0009	16
117	56041.6657	0.0009	−0.0007	13
118	56041.6836	0.0005	−0.0001	15
119	56041.6997	0.0004	−0.0013	15
120	56041.7185	0.0004	0.0003	15
121	56041.7346	0.0003	−0.0009	11
122	56041.7530	0.0006	0.0003	15
123	56041.7678	0.0008	−0.0022	14
124	56041.7872	0.0006	−0.0001	16
125	56041.8037	0.0006	−0.0008	15
126	56041.8198	0.0004	−0.0019	12
127	56041.8381	0.0005	−0.0009	16
128	56041.8551	0.0006	−0.0012	15
129	56041.8754	0.0016	0.0019	14

*BJD−2400000.
†Against max $= 2456039.6474 + 0.017257E$.
‡Number of points used to determine the maximum.

Table 7. Superhump maxima of CR Boo (2012 April) (continued).

E	max*	error	$O-C$†	N‡
130	56041.8902	0.0007	−0.0006	15
184	56042.8229	0.0005	0.0003	15
185	56042.8408	0.0005	0.0009	17
186	56042.8577	0.0004	0.0005	18
187	56042.8748	0.0003	0.0004	17
188	56042.8929	0.0006	0.0012	18
189	56042.9102	0.0010	0.0012	17
190	56042.9262	0.0007	0.0000	18
191	56042.9420	0.0008	−0.0014	18
192	56042.9604	0.0011	−0.0003	18
242	56043.8269	0.0016	0.0033	16
245	56043.8774	0.0048	0.0021	15

*BJD−2400000.
†Against max $= 2456039.6474 + 0.017257E$.
‡Number of points used to determine the maximum.

Table 8. Superhump maxima of NN Cam (2011).

E	max*	error	$O-C$†	N‡
0	55904.9897	0.0002	0.0015	254
1	55905.0612	0.0001	−0.0010	241
6	55905.4308	0.0005	−0.0017	75
7	55905.5044	0.0005	−0.0021	63
8	55905.5788	0.0004	−0.0017	68
9	55905.6526	0.0005	−0.0020	56
10	55905.7226	0.0010	−0.0060	42
11	55905.8007	0.0004	−0.0020	78
12	55905.8752	0.0004	−0.0016	78
13	55905.9501	0.0004	−0.0007	76
24	55906.7647	0.0005	−0.0007	77
25	55906.8392	0.0004	−0.0003	77
26	55906.9129	0.0005	−0.0006	78
29	55907.1393	0.0002	0.0037	294
30	55907.2091	0.0003	−0.0006	294
40	55907.9548	0.0003	0.0046	261
54	55908.9915	0.0002	0.0045	279
55	55909.0664	0.0003	0.0053	433
56	55909.1419	0.0005	0.0068	216
57	55909.2145	0.0004	0.0053	156
68	55910.0273	0.0004	0.0036	156
69	55910.1016	0.0005	0.0038	101
92	55911.7991	0.0005	−0.0019	79
93	55911.8731	0.0007	−0.0020	78
94	55911.9460	0.0003	−0.0031	307
95	55912.0212	0.0004	−0.0020	236
96	55912.0932	0.0006	−0.0040	159
109	55913.0546	0.0007	−0.0053	135

*BJD−2400000.
†Against max $= 2455904.9881 + 0.074053E$.
‡Number of points used to determine the maximum.

Table 9. Superhump maxima of SY Cap (2011).

E	max*	error	$O-C$†	N‡
0	55803.0789	0.0005	0.0012	172
1	55803.1409	0.0006	−0.0005	154
16	55804.0964	0.0017	−0.0014	43
31	55805.0550	0.0007	0.0007	50

*BJD−2400000.
†Against max $= 2455803.0777 + 0.063761E$.
‡Number of points used to determine the maximum.

Table 10. Superhump maxima of GZ Cet (2011).

E	max*	error	$O-C$†	N‡
0	55924.2865	0.0011	0.0021	31
1	55924.3403	0.0003	−0.0007	54
2	55924.3963	0.0003	−0.0014	46
188	55934.9357	0.0003	0.0003	164
189	55934.9918	0.0002	−0.0003	165

*BJD−2400000.
†Against max $= 2455924.2844 + 0.056654E$.
‡Number of points used to determine the maximum.

Table 11. Superhump maxima of AK Cnc (2012).

E	max*	error	$O-C$†	N‡
0	55952.0678	0.0047	−0.0045	42
1	55952.1424	0.0007	0.0028	74
2	55952.2086	0.0007	0.0018	54
45	55955.1043	0.0016	0.0062	74
46	55955.1591	0.0011	−0.0062	69

*BJD−2400000.
†Against max $= 2455952.0723 + 0.067239E$.
‡Number of points used to determine the maximum.

Table 12. Superhump maxima of CC Cnc (2011).

E	max*	error	$O-C$†	N‡
0	55910.1871	0.0006	−0.0065	155
26	55912.1601	0.0011	0.0028	91
27	55912.2360	0.0006	0.0031	154
42	55913.3697	0.0002	0.0038	200
88	55916.8407	0.0004	0.0003	77
89	55916.9144	0.0009	−0.0015	37
90	55916.9918	0.0007	0.0003	73
101	55917.8222	0.0006	−0.0001	79
102	55917.8948	0.0008	−0.0031	77
103	55917.9741	0.0005	0.0008	79

*BJD−2400000.
†Against max $= 2455910.1935 + 0.075532E$.
‡Number of points used to determine the maximum.

Table 13. Superhump maxima of GO Com (2012).

E	max*	error	$O-C$†	N‡
0	55983.5944	0.0002	0.0015	63
1	55983.6575	0.0003	0.0017	61
2	55983.7221	0.0003	0.0032	65
11	55984.2863	0.0003	0.0006	107
25	55985.1654	0.0002	−0.0022	130
26	55985.2284	0.0003	−0.0023	128
57	55987.1766	0.0003	−0.0067	145
62	55987.4973	0.0009	−0.0009	54
64	55987.6193	0.0008	−0.0049	53
109	55990.4632	0.0005	0.0045	129
110	55990.5289	0.0011	0.0072	92
125	55991.4696	0.0004	0.0030	128
126	55991.5306	0.0005	0.0011	131
127	55991.5936	0.0005	0.0010	122
128	55991.6615	0.0008	0.0060	71
142	55992.5337	0.0010	−0.0037	55
143	55992.5976	0.0009	−0.0028	48
144	55992.6570	0.0015	−0.0063	45

*BJD−2400000.
†Against max $= 2455983.5929 + 0.062990E$.
‡Number of points used to determine the maximum.

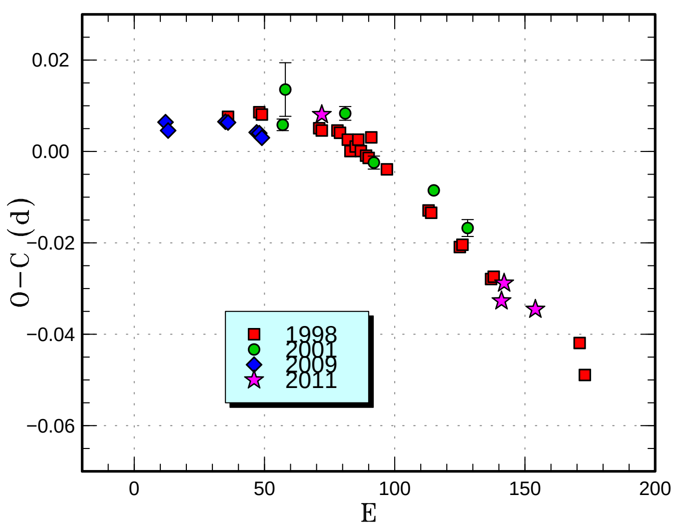

Fig. 11. Comparison of $O-C$ diagrams of TU Crt between different superoutbursts. A period of 0.08550 d was used to draw this figure. Approximate cycle counts (E) after the start of the superoutburst were used.

Table 14. Superhump maxima of TU Crt (2011).

E	max*	error	$O-C$†	N‡
0	55925.2955	0.0003	0.0004	151
69	55931.1543	0.0017	−0.0033	99
70	55931.2437	0.0005	0.0011	151
82	55932.2639	0.0007	0.0018	151

*BJD−2400000.
†Against max $= 2455925.2952 + 0.084962E$.
‡Number of points used to determine the maximum.

during the quiescent state following the superoutburst, the signal became dominated by P_{orb} after the next normal outburst. The P_{orb} determined from all the observations between BJD 2455744–2455802 was 0.077773(2) d. This period is in agreement with an analysis of the data set restricted to the phase when the object did not show superhumps within respective errors. The period is also in good agreement with the period obtained from the 2010 observations (Pavlenko et al. 2012b). We used this refined P_{orb} in table 2.

The lack of negative superhumps during these observations made a clear contrast to the observation by Harvey et al. (1995). V503 Cyg is known to display highly variable number of normal outbursts between superoutbursts (Kato et al. 2002), and normal outbursts were very infrequent (every ∼30 d) during the observation by Harvey et al. (1995), while the current observations showed much more frequent ones (every ∼10 d). Kato et al. (2002) suggested that mechanisms for suppressing normal outbursts may have worked when normal outbursts were very infrequent. As discussed by various authors (Cannizzo et al. 2010; Kato et al. 2012a; Ohshima et al. 2012), the state with negative superhumps prevents the disk-instability to occur. The condition to produce negative superhumps (likely a disk tilt) seems to naturally explain the association of the presence of negative superhumps with the reduced number of normal outbursts in V503 Cyg.

3.14. V1454 Cygni

This SU UMa-type dwarf nova undergoes outbursts relatively rarely and the last outburst was in 2009 (Kato et al. 2010). The new observation during the 2012 superoutburst confirmed the period selection as stated in Kato et al. (2010). The times of superhump maxima are listed in table 18. A. Henden reported that there is a $V \sim 20.5$-mag blue quiescent counterpart (cf. vsnet-alert 14568), whose position is in good agreement with the astrometry ($19^{\mathrm{h}}53^{\mathrm{m}}38^{\mathrm{s}}.47$, $+35^{\circ}21'45''.8$) measured during the outburst (vsnet-alert 14566).

3.15. AQ Eridani

The 2011 superoutburst of AQ Eri was observed only for its early and late stages. Although well-developed superhumps were observed on the first night, we could not measure the superhump period precisely. The late stage of the superoutburst and post-superoutburst stage were

Table 15. Superhump maxima of V503 Cyg (2011 July).

E	max*	error	$O-C$†	N‡
0	55744.5173	0.0005	−0.0041	89
1	55744.6008	0.0008	−0.0017	47
10	55745.3315	0.0016	−0.0007	21
12	55745.4959	0.0009	0.0016	31
24	55746.4683	0.0008	0.0010	92
25	55746.5524	0.0009	0.0039	82
35	55747.3620	0.0023	0.0027	16
36	55747.4410	0.0006	0.0006	75
37	55747.5227	0.0008	0.0012	75
39	55747.6836	0.0004	−0.0000	129
40	55747.7639	0.0005	−0.0008	150
41	55747.8465	0.0005	0.0007	133
47	55748.3339	0.0014	0.0016	30
61	55749.4612	0.0024	−0.0063	30
73	55750.4418	0.0186	0.0013	101
74	55750.5206	0.0021	−0.0010	126
77	55750.7689	0.0011	0.0041	136
78	55750.8419	0.0026	−0.0040	116

*BJD−2400000.
†Against max $= 2455744.5214 + 0.081084E$.
‡Number of points used to determine the maximum.

Table 16. Superhump maxima of V503 Cyg (2011 October).

E	max*	error	$O-C$†	N‡
0	55831.1911	0.0014	−0.0055	33
1	55831.2718	0.0004	−0.0059	58
2	55831.3537	0.0004	−0.0049	59
3	55831.4366	0.0005	−0.0030	58
4	55831.5186	0.0007	−0.0020	36
25	55833.2234	0.0012	0.0018	24
26	55833.3128	0.0020	0.0101	28
27	55833.3946	0.0019	0.0110	29
87	55838.2578	0.0016	0.0142	45
114	55840.4147	0.0042	−0.0159	45

*BJD−2400000.
†Against max $= 2455831.1966 + 0.081000E$.
‡Number of points used to determine the maximum.

Table 17. Superhump maxima of V503 Cyg (2011 July) (late superhumps).

E	max*	error	$O-C$†	N‡
0	55753.4128	0.0018	−0.0076	30
1	55753.4995	0.0019	−0.0015	30
10	55754.2291	0.0006	0.0041	82
16	55754.7127	0.0018	0.0050	60
17	55754.7878	0.0008	−0.0003	145
24	55755.3518	0.0012	0.0006	30
25	55755.4300	0.0021	−0.0017	30
26	55755.5117	0.0010	−0.0004	29
38	55756.4835	0.0016	0.0060	30
42	55756.8034	0.0007	0.0040	144
43	55756.8821	0.0008	0.0023	75
47	55757.2020	0.0006	0.0004	146
48	55757.2768	0.0008	−0.0052	148
60	55758.2381	0.0010	−0.0094	74
66	55758.7351	0.0010	0.0050	136
67	55758.8125	0.0008	0.0019	141
70	55759.0506	0.0008	−0.0013	65
71	55759.1311	0.0007	−0.0013	160
72	55759.2122	0.0010	−0.0007	179

*BJD−2400000.
†Against max $= 2455753.4205 + 0.080450E$.
‡Number of points used to determine the maximum.

Table 18. Superhump maxima of V1454 Cyg (2012).

E	max*	error	$O-C$†	N‡
0	56059.5294	0.0005	−0.0001	60
1	56059.5872	0.0006	0.0002	58
17	56060.5067	0.0006	−0.0002	60
18	56060.5647	0.0004	0.0002	61

*BJD−2400000.
†Against max $= 2456059.5296 + 0.057494E$.
‡Number of points used to determine the maximum.

well observed. The superhumps apparently persisted after the rapid decline. The times of superhump maxima are listed in table 19. By using the PDM analysis, the signal of the superhumps was detected until BJD 2455586. The signal, however, was not significantly detected after this epoch. The present case appears to be different from long-persisting stage C superhumps in many short-$P_{\rm orb}$ dwarf novae, such as QZ Vir (Ohshima et al. 2011).

3.16. UV Geminorum

We observed the middle part of the 2011 superoutburst. The times of superhump maxima are listed as table 20. A comparison of $O-C$ diagram between different superoutbursts is shown in figure 12. Despite the large variation of the superhump period, the periods during the middle stage of superoutbursts were almost the same in different superoutbursts.

Table 19. Superhump maxima of AQ Eri (2011).

E	max*	error	$O-C$†	N‡
0	55875.8290	0.0005	−0.0016	121
1	55875.8930	0.0003	0.0001	103
143	55884.7372	0.0006	0.0079	77
144	55884.7964	0.0007	0.0049	98
145	55884.8561	0.0009	0.0024	80
159	55885.7152	0.0013	−0.0098	24
160	55885.7813	0.0029	−0.0059	22
161	55885.8513	0.0008	0.0019	15

*BJD−2400000.
†Against max $= 2455875.8306 + 0.062228E$.
‡Number of points used to determine the maximum.

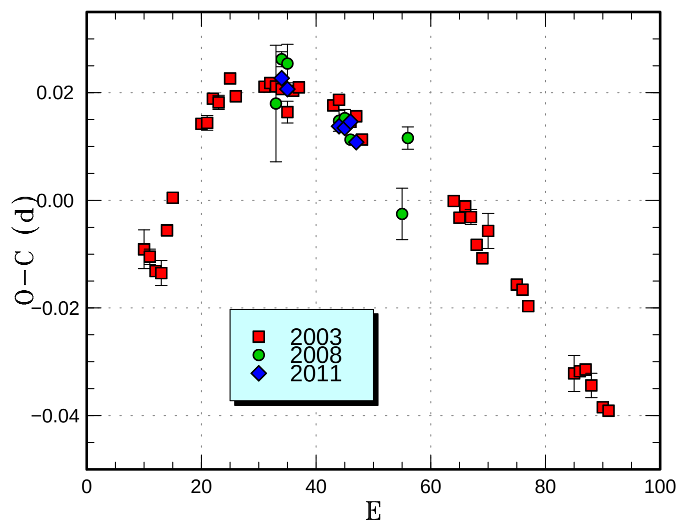

Fig. 12. Comparison of $O-C$ diagrams of UV Gem between different superoutbursts. A period of 0.0936 d was used to draw this figure. Approximate cycle counts (E) after the start of the superoutburst were used.

Table 20. Superhump maxima of AW Gem (2011).

E	max*	error	$O-C$†	N‡
0	55892.6080	0.0004	0.0006	62
1	55892.6996	0.0005	−0.0007	80
10	55893.5351	0.0005	−0.0005	84
11	55893.6284	0.0004	−0.0001	83
12	55893.7231	0.0007	0.0019	51
13	55893.8129	0.0004	−0.0012	60

*BJD−2400000.
†Against max $= 2455892.6074 + 0.092822E$.
‡Number of points used to determine the maximum.

Table 21. Superhump maxima of NY Her (2011).

E	max*	error	$O-C$†	N‡
0	55724.6932	0.0013	−0.0023	77
1	55724.7690	0.0009	−0.0022	79
2	55724.8466	0.0009	−0.0005	78
3	55724.9220	0.0006	−0.0009	78
13	55725.6829	0.0014	0.0020	78
14	55725.7585	0.0072	0.0018	40
26	55726.6702	0.0027	0.0039	65
27	55726.7455	0.0031	0.0034	34
29	55726.8994	0.0040	0.0057	77
37	55727.4892	0.0044	−0.0109	28

*BJD−2400000.
†Against max $= 2455724.6955 + 0.075802E$.
‡Number of points used to determine the maximum.

3.17. NY Herculis

NY Her was discovered by Hoffmeister (1949) as a Mira-type variable with a photographic range of 15.0 to fainter than 16.5. Gessner (1966) classified this object as a Cepheid (likely a W Vir-type variable) with a period of 6.3146 d. Pastukhova (1988), however, did not confirm this classification. Pastukhova (1988) identified the object as an 18-mag blue object on POSS plates and obtained a mean period of 67.7067 d. In addition to this mean period, short outbursts were irregularly observed. The object varied at a rate up to 2 mag d^{-1}, and Pastukhova (1988) classified the object to be a blue irregular variable.

On 2011 June 10, CRTS detected an outburst of this object. T. Kato suggested that the known behavior of this object resembles that of ER UMa (cf. vsnet-alert 13410). Follow-up observation indicated the presence of superhumps (vsnet-alert 13418). The best superhump period with the PDM method was 0.07602(14) d (figure 13).

The times of superhump maxima are listed in table 21. CRTS data suggest a supercycle of 80–90 d. As judged from the relatively long superhump period, the object may be more similar to V503 Cyg (Harvey et al. 1995) rather than ER UMa. Further intensive observations are particularly needed to determine the true cycle length for such a rare variety of SU UMa-type dwarf novae.

3.18. PR Herculis

PR Her was discovered as a dwarf nova (S 4247) by Hoffmeister (1951) with a photographic range of 14.0 to fainter than 17.5. Although this star was monitored by amateur observes since the early 1990s, no outburst had been recorded. In the meantime, A. Henden identified the object as a $V = 21$-mag blue star in 1999 (vsnet-chat 1800).[2] The large outburst amplitude made the object a good candidate for a WZ Sge-type dwarf nova.

On 2011 November 21, Walter MacDonald II reported a very bright outburst at a magnitude of $V = 12.84$ (cf. cvnet-outburst 4406). Subsequent observations confirmed the presence of typical double-wave early superhumps (figure 14). Due to the unfavorable location, the object soon became hard to access in the low evening sky. Ordinary superhumps were detected despite this unfavorable condition (vsnet-alert 13932; figure 15). The times of superhump maxima are listed in table 22. The large outburst amplitude, the low frequency of outbursts, and the existence of prominent early superhumps qualify PR Her as a WZ Sge-type dwarf nova.

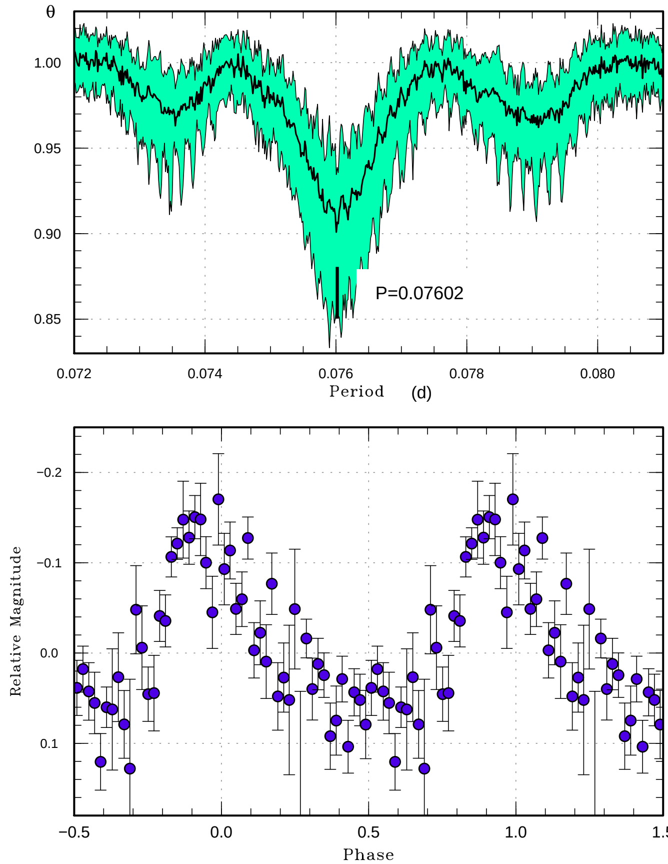

Fig. 13. Superhumps in NY Her (2011). (Upper): PDM analysis. (Lower): Phase-averaged profile.

Table 22. Superhump maxima of PR Her (2011).

E	max*	error	$O-C$†	N‡
0	55900.2456	0.0006	0.0008	74
1	55900.3034	0.0006	0.0035	54
11	55900.8507	0.0015	0.0006	31
12	55900.9020	0.0021	−0.0031	51
19	55901.2905	0.0005	0.0002	43
37	55902.2771	0.0008	−0.0036	51
91	55905.2512	0.0004	−0.0008	114
92	55905.3094	0.0011	0.0025	58

*BJD−2400000.
†Against max $= 2455900.2449 + 0.055022E$.
‡Number of points used to determine the maximum.

[2] See also <ftp://ftp.aavso.org/upload/chartteam/MISC/seq/Her%20PR.txt>.

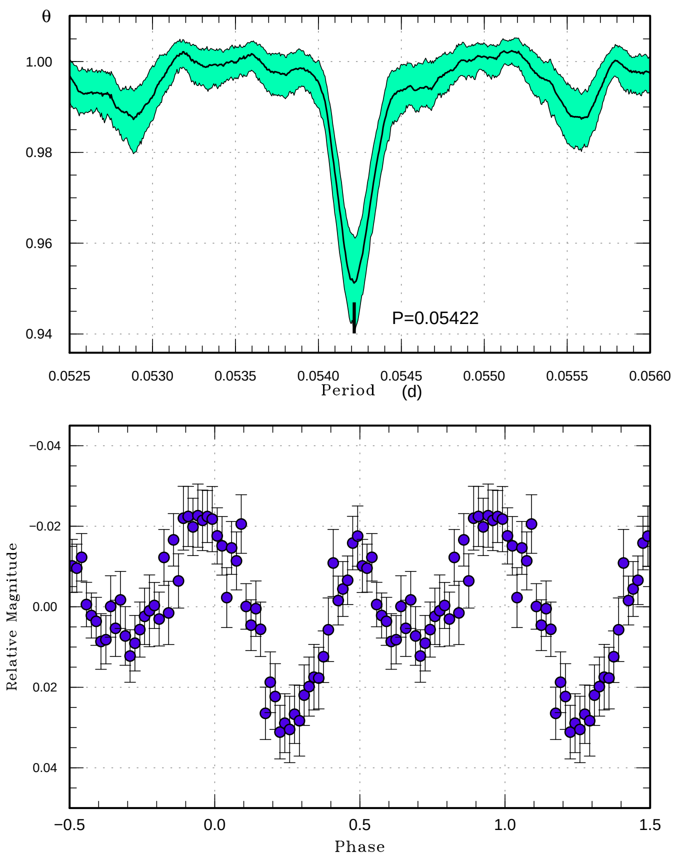

Fig. 14. Early superhumps in PR Her (2011). (Upper): PDM analysis. (Lower): Phase-averaged profile.

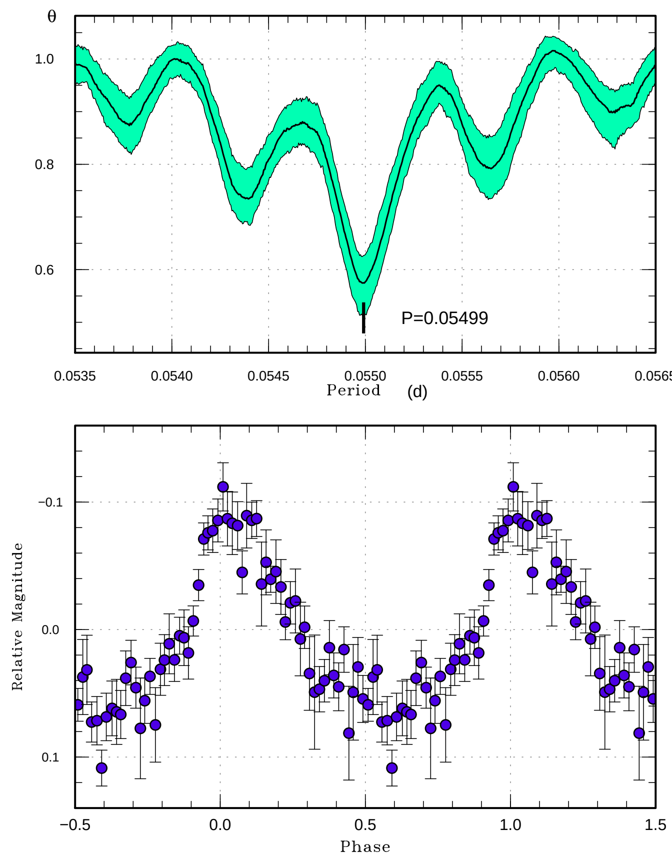

Fig. 15. Ordinary superhumps in PR Her (2011). (Upper): PDM analysis. (Lower): Phase-averaged profile.

3.19. V611 Herculis

Little had been known about this dwarf nova since its discovery (Hoffmeister 1968). CRTS detected four past outbursts. An analysis of the SDSS colors of the quiescent counterpart suggested an object below the period gap (Kato et al. 2012b). A new outburst was detected by CRTS on 2012 June 8 (cf. vsnet-alert 14647). Subsequent observations detected superhumps (vsnet-alert 14648; figure 16). We detected two superhump maxima at BJD 2456087.4232(5) ($N = 62$) and 2456087.4877(6) ($N = 27$). The best period determined by the PDM method was 0.0636(4) d.

3.20. V844 Herculis

The well-known SU UMa-type dwarf nova V844 Her underwent a superoutburst in 2012 May (vsnet-alert 14525). After a period of frequent outburst in 2009–2011, the object again entered a relatively inactive phase in 2011–2012 and the superoutburst occurred ∼370 d after the 2011 superoutburst. The times of superhump maxima are listed in table 23. Although a clear pattern of stages A–C was observed, the period of stage A was not determined due to the limited observations in this stage. The $P_{\rm dot}$ for stage B was clearly positive as in other superoutbursts in this object.

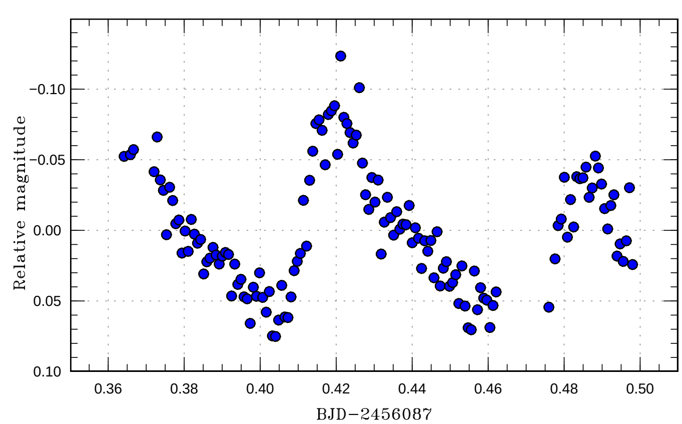

Fig. 16. Superhumps in V611 Her.

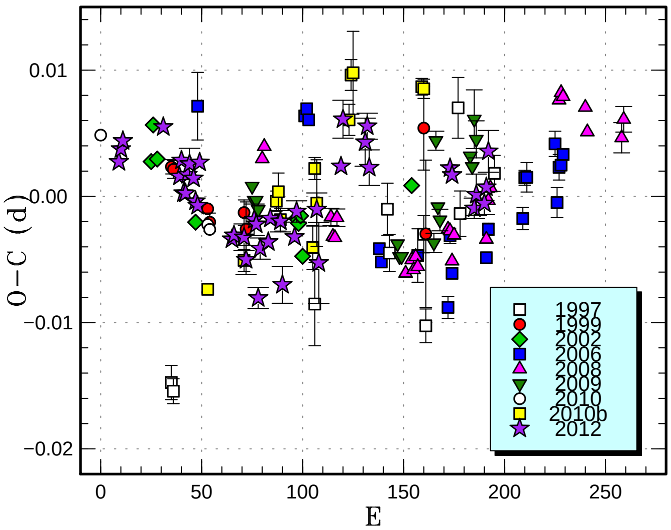

Fig. 17. Comparison of $O-C$ diagrams of V844 Her between different superoutbursts. A period of 0.05590 d was used to draw this figure. Approximate cycle counts (E) after the start of the superoutburst were used. For descriptions of the 2009, 2010 and 2010b superoutburst see Kato et al. (2012a).

Figure 17 illustrates a comparison of $O-C$ diagrams between different superoutbursts. As noted in Kato et al. (2012a), the epoch of stage B–C transition is different between different superoutbursts. The B–C transition in the 2012 superoutburst appears to have occurred earlier than in other superoutbursts.

3.21. MM Hydrae

We observed the early and late stages of the 2012 superoutburst of this object. The times of superhump maxima are listed in table 24. The $O-C$ diagram indicates that we missed the middle-to-end part of stage B, and it was impossible to determine $P_{\rm dot}$. Although a comparison of $O-C$ diagrams can be drawn (figure 18), middle to late part of stage B has not yet been well recorded in this object.

3.22. VW Hydri

Although this object is one of the best and oldest known prototypical SU UMa-type dwarf novae, no high-quality photometric data for superhumps had been publicly available. The present observation (Hambsch 2012) recorded the 2011 November–December superoutburst and two normal outbursts in 2011 December and 2012 January. Although the data were not as uninterrupted as Kepler observations, the data provide an opportunity to analyze observations of this well-known object in a modern way and with modern knowledge.

The times of superhump maxima during the superoutburst are listed in table 25.

The outburst started with a precursor (figure 19, lower pnel), after a stage of short fading branch and entered the plateau phase. During the plateau phase, stage A and two segments of almost constant periods, which we attribute

Table 23. Superhump maxima of V844 Her (2012).

E	max*	error	$O-C$†	N‡
0	56050.3428	0.0002	0.0028	108
1	56050.3997	0.0001	0.0038	117
2	56050.4563	0.0001	0.0044	71
22	56051.5754	0.0004	0.0055	51
30	56052.0187	0.0004	0.0016	91
31	56052.0758	0.0003	0.0029	92
32	56052.1291	0.0003	0.0003	93
33	56052.1850	0.0003	0.0002	81
34	56052.2424	0.0008	0.0017	23
35	56052.2992	0.0012	0.0026	22
37	56052.4098	0.0002	0.0014	68
38	56052.4639	0.0002	−0.0004	75
39	56052.5194	0.0003	−0.0007	61
40	56052.5788	0.0004	0.0027	41
56	56053.4671	0.0003	−0.0034	76
57	56053.5233	0.0002	−0.0031	76
62	56053.8026	0.0011	−0.0032	11
63	56053.8568	0.0011	−0.0050	12
67	56054.0835	0.0012	−0.0018	67
68	56054.1391	0.0005	−0.0022	92
69	56054.1891	0.0008	−0.0080	108
70	56054.2490	0.0008	−0.0041	57
74	56054.4731	0.0003	−0.0036	74
75	56054.5308	0.0003	−0.0018	76
80	56054.8101	0.0008	−0.0020	12
81	56054.8610	0.0015	−0.0070	12
87	56055.2002	0.0007	−0.0032	61
88	56055.2581	0.0008	−0.0012	62
98	56055.8172	0.0013	−0.0010	12
99	56055.8689	0.0032	−0.0053	12
110	56056.4915	0.0006	0.0024	75
111	56056.5511	0.0015	0.0061	69
122	56057.1642	0.0019	0.0043	35
123	56057.2213	0.0010	0.0055	40
124	56057.2740	0.0014	0.0023	38
164	56059.5099	0.0007	0.0022	46
165	56059.5653	0.0004	0.0017	42
176	56060.1775	0.0008	−0.0010	42
177	56060.2345	0.0016	0.0001	40
181	56060.4574	0.0009	−0.0006	59
182	56060.5146	0.0008	0.0007	62
183	56060.5734	0.0017	0.0035	62

*BJD−2400000.

†Against max $= 2456050.3401 + 0.055900E$.

‡Number of points used to determine the maximum.

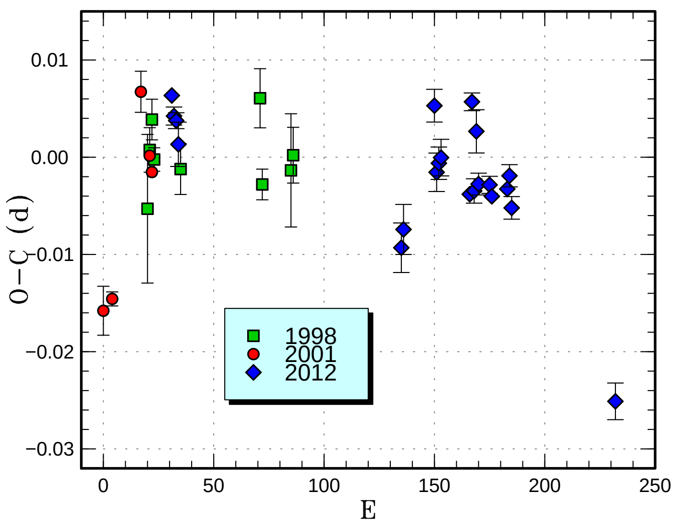

Fig. 18. Comparison of $O-C$ diagrams of MM Hya between different superoutbursts. A period of 0.05892 d was used to draw this figure. Approximate cycle counts (E) after the start of the superoutburst were used.

Table 24. Superhump maxima of MM Hya (2012).

E	max*	error	$O-C$†	N‡
0	55993.5863	0.0008	0.0008	12
1	55993.6431	0.0009	−0.0012	17
2	55993.7015	0.0008	−0.0016	18
3	55993.7580	0.0023	−0.0040	20
104	55999.6983	0.0025	−0.0078	9
105	55999.7591	0.0026	−0.0058	14
119	56000.5967	0.0017	0.0078	16
120	56000.6488	0.0020	0.0011	19
121	56000.7086	0.0017	0.0021	14
122	56000.7681	0.0019	0.0027	10
135	56001.5303	0.0005	−0.0002	44
136	56001.5987	0.0009	0.0094	23
137	56001.6485	0.0013	0.0003	18
138	56001.7135	0.0022	0.0065	6
139	56001.7670	0.0011	0.0011	15
144	56002.0616	0.0009	0.0014	122
145	56002.1193	0.0008	0.0003	99
152	56002.5325	0.0007	0.0015	40
153	56002.5928	0.0011	0.0029	23
154	56002.6484	0.0012	−0.0003	18
201	56005.3977	0.0019	−0.0170	61

*BJD−2400000.

†Against max $= 2455993.5854 + 0.058852E$.

‡Number of points used to determine the maximum.

to stage B and C. The stage B–C transition occurred between $E = 68$ and $E = 77$ and was apparently relatively smooth compared to short-$P_{\rm orb}$ systems (cf. Kato et al. 2009 figure 4).

During the rapid fading stage of the superoutburst a phase reversal occurred as described as for "traditional" late superhumps (Schoembs, Vogt 1980; Vogt 1983), and this signal persisted during the quiescent period after this superoutburst (figure 19). The times of maxima of these superhumps are listed in table 26. In contrast to V344 Lyr (Kato et al. 2012a; Wood et al. 2011), there was no prominent signal of "secondary maxima" during the late plateau stage of the superoutburst, and it looks like that the phase suddenly jumped by an $\sim$0.5 $P_{\rm SH}$. Although "traditional" late superhumps were usually considered to arise from an ordinary stream-impact hot spot,[3] the apparent absence of the corresponding signal before the rapid fading, as recorded in V344 Lyr, would make this traditional explanation worth reconsideration. The unavoidable gap between BJD 2455904.9 and 2455905.4 made it difficult to examine how this phase jump occurred.

The times of the late superhumps, measured after subtracting the mean orbital variation, are listed in table 26. These late superhumps persisted until the second next normal outburst, as observed in V344 Lyr (Kato et al. 2012a; Wood et al. 2011). After this second normal outburst, superhumps still persisted with a shorter period [0.075333(4) d] and there was a well-recognizable signal in PDM analysis (figure 20).

3.23. RZ Leonis Minoris

We analyzed three superoutbursts in 2012 from the AAVSO data (tables 27, 28, 29). The first two superoutbursts were observed for their later parts and the last superoutburst was mainly observed for the earlier part. In measuring $P_{\rm dot}$, we did not use $E \geq 176$ for the first outburst, which were obtained during the fading stage and the identification of the phases was ambiguous. A comparison of $O-C$ diagrams is shown in figure 21. Although a combined $O-C$ analysis of Olech et al. (2008) in Kato et al. (2009) was suggestive of a positive $P_{\rm dot}$, the current analysis of the new data more strongly supports the positive $P_{\rm dot}$ in this very unusual object. Although there was a hint of emergence of double-wave modulations during the fading stage, we could not detect secure stage C superhumps. It would be worth noting that the epochs of superhump maxima for these three superoutbursts can be reasonably well (within 0.005 d) expressed by a single period of 0.059432(2) d, which might strengthen the finding by Olech et al. (2008) that there was no phase shift of superhumps between different superhumps. A direct analysis of the photometric data (PDM method, figure 22), however, strongly preferred a period of 0.059585(1) d with larger (0.010 d) and systematically variable $O-C$ values. Since the $O-C$ analysis of individual superoutbursts gives only small residuals for the period of 0.05940 d, this preference

[3] See also a discussion in Hessman et al. (1992), who reported that the traditional model of late superhumps by Vogt (1983) did not trivially explain the observed eclipse depths in OY Car.

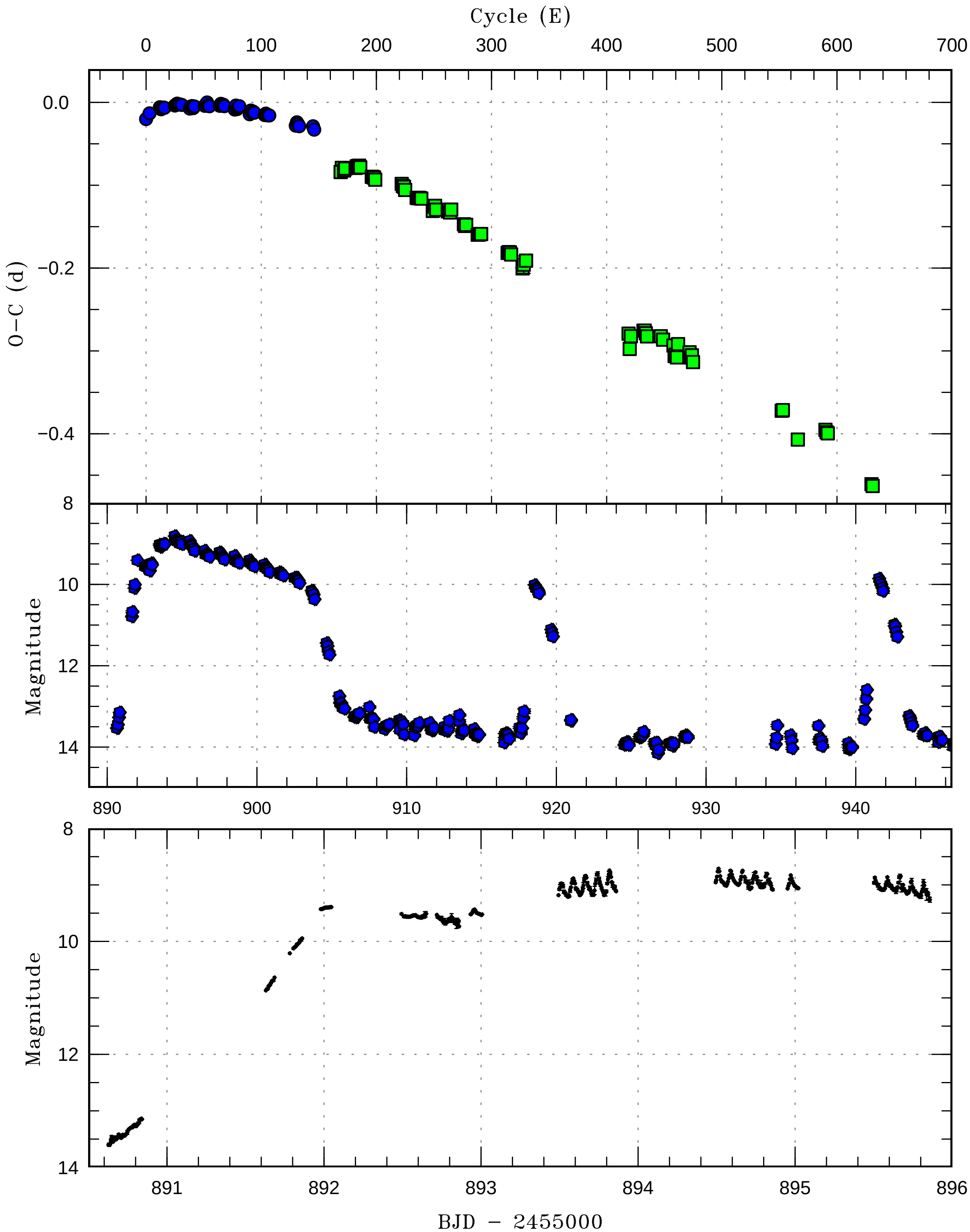

Fig. 19. $O-C$ diagram of superhumps in VW Hyi (2011). (Upper): $O-C$. Filled circles and filled squares represent superhumps and late superhumps after the rapid fading. We used a period of 0.076914 d for calculating the $O-C$ residuals. (Middle): Light curve. (Lower): Enlarged light curve of showing the precursor and evolution of superhumps.

Table 25. Superhump maxima of VW Hyi (2011).

E	max*	error	$O-C$†	N‡
0	55892.5748	0.0007	−0.0202	840
3	55892.8124	0.0024	−0.0128	26
12	55893.5120	0.0006	−0.0041	33
13	55893.5865	0.0004	−0.0064	42
14	55893.6647	0.0005	−0.0050	24
15	55893.7424	0.0004	−0.0040	22
16	55893.8190	0.0005	−0.0042	25
25	55894.5140	0.0001	−0.0001	721
26	55894.5919	0.0001	0.0011	834
27	55894.6701	0.0003	0.0025	371
28	55894.7459	0.0007	0.0016	19
29	55894.8231	0.0013	0.0020	21
31	55894.9762	0.0002	0.0016	180
38	55895.5102	0.0015	−0.0018	28
39	55895.5896	0.0008	0.0009	42
40	55895.6670	0.0012	0.0015	29
41	55895.7415	0.0012	−0.0008	21
42	55895.8203	0.0014	0.0013	22
51	55896.5134	0.0004	0.0034	647
52	55896.5924	0.0002	0.0057	839
53	55896.6712	0.0004	0.0078	353
54	55896.7447	0.0011	0.0045	20
55	55896.8205	0.0024	0.0035	22
64	55897.5133	0.0010	0.0054	32
65	55897.5926	0.0013	0.0079	42
66	55897.6672	0.0014	0.0058	21
67	55897.7454	0.0017	0.0072	22
68	55897.8205	0.0010	0.0056	22
77	55898.5086	0.0013	0.0028	26
78	55898.5903	0.0009	0.0077	42
79	55898.6630	0.0008	0.0036	30
80	55898.7420	0.0011	0.0058	31
81	55898.8203	0.0017	0.0074	34
90	55899.5028	0.0038	−0.0010	25
91	55899.5842	0.0007	0.0036	42
92	55899.6586	0.0006	0.0013	30
93	55899.7368	0.0014	0.0027	31
94	55899.8123	0.0010	0.0015	33
103	55900.5017	0.0022	−0.0000	25
104	55900.5804	0.0013	0.0019	21
105	55900.6553	0.0015	0.0000	30
106	55900.7322	0.0011	0.0002	30
107	55900.8089	0.0012	0.0001	34
130	55902.5656	0.0020	−0.0088	25
131	55902.6465	0.0038	−0.0046	30
132	55902.7214	0.0016	−0.0066	30
133	55902.7957	0.0015	−0.0090	34
145	55903.7186	0.0016	−0.0073	30
146	55903.7915	0.0015	−0.0112	34

*BJD−2400000.
†Against max $= 2455892.5949 + 0.076765E$.
‡Number of points used to determine the maximum.

Table 26. Late superhumps in VW Hyi (2011).

E	max*	error	$O-C$†	N‡
0	55905.5093	0.0016	−0.0199	32
1	55905.5913	0.0018	−0.0140	21
0	55905.5093	0.0015	−0.0199	30
3	55905.7420	0.0014	−0.0155	32
4	55905.8211	0.0019	−0.0124	33
13	55906.5142	0.0015	−0.0042	33
14	55906.5930	0.0015	−0.0015	19
15	55906.6703	0.0014	−0.0004	28
16	55906.7476	0.0012	0.0009	34
17	55906.8225	0.0021	−0.0003	33
27	55907.5803	0.0011	−0.0035	21
28	55907.6569	0.0013	−0.0030	30
29	55907.7331	0.0009	−0.0029	33
30	55907.8075	0.0025	−0.0046	34
53	55909.5714	0.0009	0.0090	22
54	55909.6458	0.0010	0.0073	28
55	55909.7218	0.0015	0.0072	31
56	55909.7949	0.0014	0.0042	32
66	55910.5545	0.0008	0.0029	20
67	55910.6310	0.0010	0.0032	21
68	55910.7084	0.0008	0.0045	22
69	55910.7847	0.0010	0.0048	27
70	55910.8612	0.0023	0.0051	14
80	55911.6155	0.0027	−0.0016	15
81	55911.6975	0.0007	0.0044	24
82	55911.7755	0.0007	0.0062	27
83	55911.8477	0.0016	0.0024	20
93	55912.6148	0.0021	0.0085	16
94	55912.6937	0.0012	0.0113	20
95	55912.7673	0.0019	0.0088	26
96	55912.8477	0.0009	0.0130	18
107	55913.6761	0.0015	0.0043	20
108	55913.7510	0.0010	0.0031	25
109	55913.8291	0.0016	0.0052	26
119	55914.5864	0.0022	0.0015	15
120	55914.6634	0.0008	0.0024	20
121	55914.7410	0.0019	0.0039	27
122	55914.8180	0.0014	0.0048	26
145	55916.5642	0.0016	0.0007	15
146	55916.6421	0.0019	0.0025	21
147	55916.7187	0.0015	0.0030	26
148	55916.7930	0.0020	0.0012	26
158	55917.5454	0.0023	−0.0074	28
159	55917.6268	0.0105	−0.0021	13
161	55917.7855	0.0047	0.0044	19
250	55924.5427	0.0012	−0.0112	46
251	55924.6012	0.0035	−0.0288	22
252	55924.6934	0.0016	−0.0126	25
263	55925.5463	0.0011	0.0031	41
264	55925.6232	0.0026	0.0039	23

*BJD−2400000.
†Against max $= 2455905.5291 + 0.076099E$.
‡Number of points used to determine the maximum.

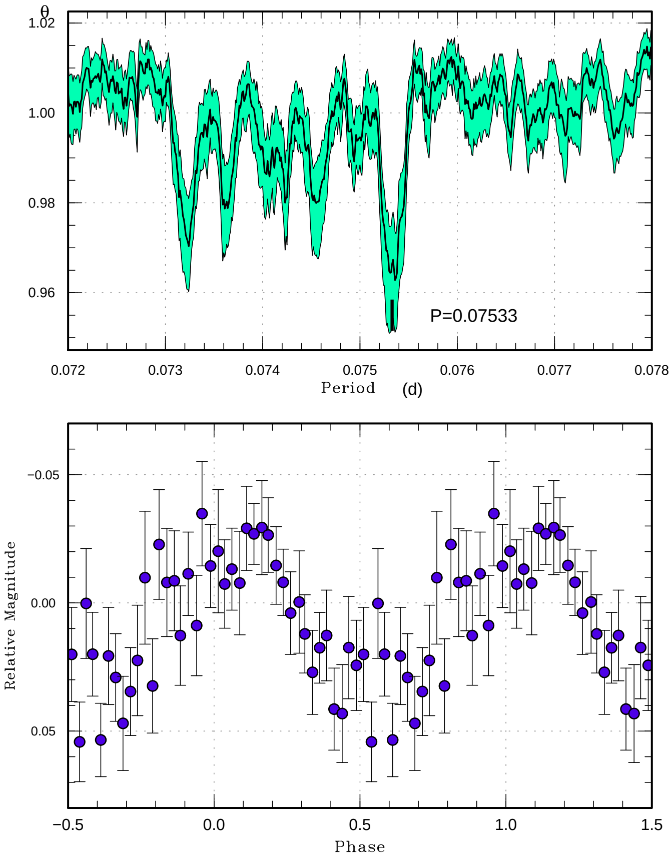

Fig. 20. Late superhumps in VW Hyi after a normal outburst. (Upper): PDM analysis after removing the mean orbital variation. The rejection rate for bootstrapping was reduced to 0.2 for better visualization. (Lower): Phase-averaged profile.

Table 26. Late superhumps in VW Hyi (2011) (continued).

E	max*	error	$O-C$†	N‡
265	55925.6969	0.0017	0.0016	26
266	55925.7700	0.0022	−0.0015	32
278	55926.6932	0.0046	0.0085	13
280	55926.8429	0.0028	0.0060	9
289	55927.5281	0.0021	0.0063	23
290	55927.5923	0.0015	−0.0056	18
291	55927.6709	0.0013	−0.0031	19
292	55927.7444	0.0025	−0.0056	21
293	55927.8374	0.0021	0.0112	14
303	55928.5967	0.0027	0.0095	17
304	55928.6673	0.0010	0.0040	18
305	55928.7469	0.0010	0.0075	22
306	55928.8156	0.0025	0.0002	13
383	55934.6792	0.0017	0.0042	17
384	55934.7569	0.0012	0.0057	14
397	55935.7212	0.0034	−0.0192	18
421	55937.5789	0.0010	0.0121	16
422	55937.6529	0.0007	0.0099	18
423	55937.7285	0.0014	0.0095	18
461	55940.5898	0.0008	−0.0210	19
462	55940.6646	0.0015	−0.0223	22

*BJD−2400000.
†Against max $= 2455905.5291 + 0.076099E$.
‡Number of points used to determine the maximum.

of a different period over the 0.05940 d is an unnatural behavior. This suggests that the apparent coherence of superhumps in the combined $O-C$ analysis with a period of 0.059432(2) d may simply be superficial, and that the true underlying period may be different. This possibility should be clarified by a larger set of data.

While most of the weak signal in figure 22 corresponds to aliases of the main superhump signal as is evident from the window function, the period at 0.059053(2) d does not arise from an alias. Since ϵ for objects around these P_{SH} is usually 1.0% or slightly less (cf. Kato et al. 2012a), we regard this period to be a candidate orbital period. The waveform of this periodicity is shown in figure 23. If this is the true orbital period, the ϵ for stage B superhumps is 0.6%. Further testing for the stability of this signal needs to be confirmed.

3.24. BK Lyncis

BK Lyn has been a well-known permanent superhumper below the period gap (Skillman, Patterson 1993). The object, however, has recently been demonstrated to show dwarf nova-type outbursts, and the pattern of outbursts is quite similar to those of ER UMa stars (E. de Miguel,

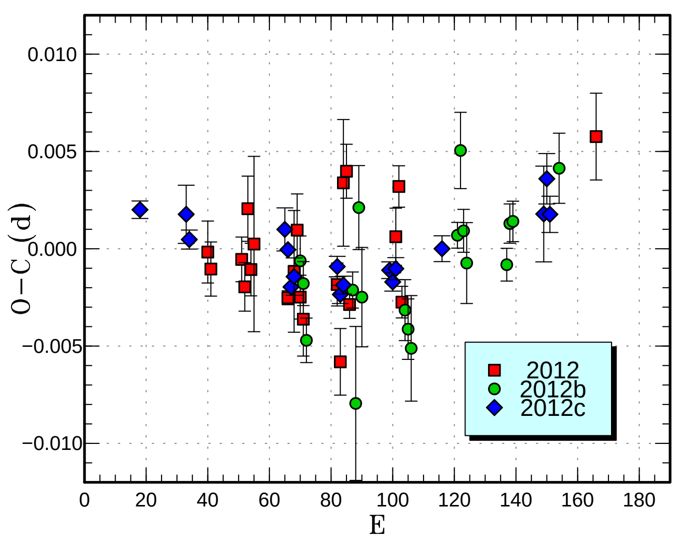

Fig. 21. Comparison of $O-C$ diagrams of RZ LMi between different superoutbursts. A period of 0.05940 d was used to draw this figure. Approximate cycle counts (E) after the start of the superoutburst were used.

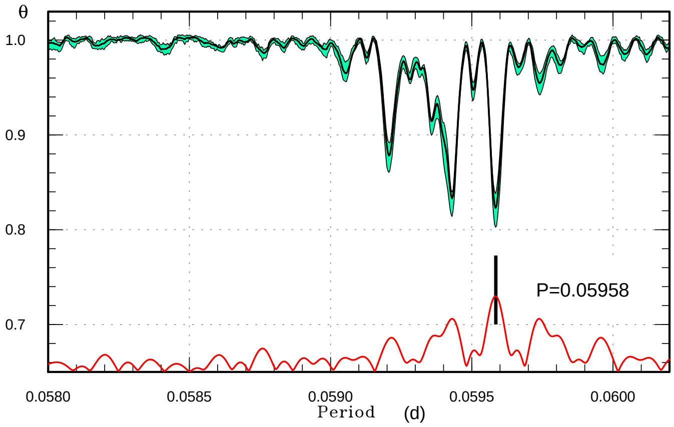

Fig. 22. Period analysis of plateau phases of three subsequent superoutbursts of RZ LMi. The curve at the bottom of the figure represents the window function.

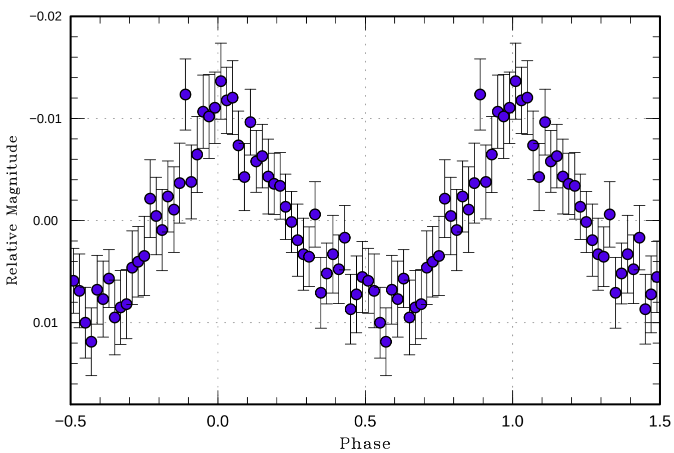

Fig. 23. Waveform of the candidate orbital period (0.059053 d) of RZ LMi.

see also Kemp et al. 2012). According to the Northern Sky Variability Survey (NSVS), the object was still in novalike (NL)-type state in 2002.[4] The CRTS data indicate that the object already entered a DN state in 2005. The outburst-like variations were also recorded in AAVSO observations in 2005–2006. We here analyze observations in 2012, mostly from the AAVSO database.

As in recent ER UMa (Ohshima et al. 2012), the object showed negative superhumps during most of its outburst cycle, and showed positive superhumps during the ∼10 d initial part of superoutbursts. We first identified the period of positive superhumps using the best observed superoutburst in 2012 April. The period was identified to be 0.07859(1) d (figure 24). With the help of this period, we could identify the times of superhump maxima during the less-observed 2012 February–March superoutburst (table 30). Although the maxima for $E \leq 3$ were those of negative

[4] <http://skydot.lanl.gov/nsvs/star.php?num=7454712&mask=32004>

Table 27. Superhump maxima of RZ LMi (2012 February–March).

E	max*	error	$O-C$†	N‡
0	55985.8946	0.0016	0.0046	10
1	55985.9531	0.0014	0.0036	7
11	55986.5476	0.0011	0.0027	18
12	55986.6056	0.0012	0.0011	14
13	55986.6690	0.0017	0.0050	14
14	55986.7253	0.0014	0.0017	15
15	55986.7866	0.0057	0.0035	13
26	55987.4366	0.0004	−0.0014	40
28	55987.5568	0.0031	−0.0003	12
29	55987.6183	0.0019	0.0016	14
30	55987.6743	0.0011	−0.0019	14
31	55987.7325	0.0019	−0.0032	13
42	55988.3877	0.0011	−0.0030	38
43	55988.4431	0.0017	−0.0071	34
44	55988.5117	0.0033	0.0020	44
45	55988.5717	0.0014	0.0024	57
46	55988.6243	0.0007	−0.0045	55
61	55989.5188	0.0015	−0.0032	42
62	55989.5808	0.0011	−0.0007	42
63	55989.6342	0.0008	−0.0068	41
126	55993.3849	0.0022	−0.0071	38
176	55996.3719	0.0012	0.0030	35
177	55996.4281	0.0040	−0.0004	35
178	55996.4921	0.0011	0.0040	43
179	55996.5485	0.0008	0.0009	43
180	55996.6107	0.0011	0.0036	43

*BJD−2400000.
†Against max $= 2455985.8900 + 0.059540E$.
‡Number of points used to determine the maximum.

superhumps [P =0.071(2) d], we included these epochs to illustrate the smooth transition from negative superhumps to positive superhumps in phase as recorded in ER UMa (Ohshima et al. 2012). The times of superhump maxima during the 2012 April superoutburst are shown in table 32. Since the epochs $E = 1, 2$ were obtained before the maximum of the superoutburst, we did not use them in calculating the period and $P_{\rm dot}$. During the later stage ($E \geq 114$), the structure of superhumps became complex and both negative and positive superhumps appeared to coexist. Although the superhump period during the superoutburst was not very different from those recorded during its NL-type state (Skillman, Patterson 1993), the amplitudes of superhumps were much larger than those in its former NL-type state, implying that 3:1 resonance is more strongly excited during a superoutburst.

A comparison of the $O-C$ diagrams of positive superhumps between different superhumps is shown in figure 25. The disagreement between the $O-C$ diagrams was slightly larger than in other SU UMa-type dwarf novae, which may be a result of remnant, overlapping negative superhumps. Particularly, the relatively large scatter in the $O-C$ diagram in the later part of this figure was caused by profile variations caused by evolving negative

Table 28. Superhump maxima of RZ LMi (2012 March–April).

E	max*	error	$O-C$†	N‡
0	56013.6575	0.0013	0.0032	48
1	56013.7157	0.0011	0.0019	48
2	56013.7722	0.0011	−0.0011	47
17	56014.6658	0.0009	0.0004	47
18	56014.7193	0.0040	−0.0055	61
19	56014.7888	0.0022	0.0045	72
20	56014.8436	0.0026	−0.0002	25
34	56015.6745	0.0016	−0.0018	47
35	56015.7329	0.0016	−0.0029	49
36	56015.7914	0.0027	−0.0040	47
50	56016.6273	0.0017	−0.0006	64
51	56016.6882	0.0006	0.0008	63
52	56016.7519	0.0020	0.0051	91
53	56016.8072	0.0011	0.0009	76
54	56016.8649	0.0021	−0.0009	20
67	56017.6371	0.0009	−0.0018	62
68	56017.6986	0.0010	0.0002	62
69	56017.7581	0.0010	0.0002	63
84	56018.6517	0.0017	0.0017	60

*BJD−2400000.
†Against max $= 2456013.6543 + 0.059472E$.
‡Number of points used to determine the maximum.

Table 29. Superhump maxima of RZ LMi (2012 April).

E	max*	error	$O-C$†	N‡
0	56030.8288	0.0004	0.0026	18
15	56031.7195	0.0015	0.0022	37
16	56031.7776	0.0005	0.0009	32
47	56033.6196	0.0011	0.0012	34
48	56033.6779	0.0004	0.0001	81
49	56033.7354	0.0003	−0.0018	88
50	56033.7953	0.0010	−0.0013	21
64	56034.6275	0.0005	−0.0009	63
65	56034.6854	0.0005	−0.0023	99
66	56034.7453	0.0005	−0.0018	96
81	56035.6371	0.0004	−0.0012	67
82	56035.6959	0.0005	−0.0018	94
83	56035.7560	0.0006	−0.0011	74
98	56036.6480	0.0007	−0.0002	62
131	56038.6100	0.0025	0.0013	44
132	56038.6712	0.0013	0.0031	63
133	56038.7287	0.0009	0.0012	61

*BJD−2400000.
†Against max $= 2456030.8262 + 0.059408E$.
‡Number of points used to determine the maximum.

Table 30. Superhump maxma of BK Lyn (2012 February–March).

E	max*	error	$O-C$†	N‡
0	55971.6983	0.0012	0.0155	69
1	55971.7771	0.0012	0.0159	75
2	55971.8456	0.0011	0.0061	76
3	55971.9115	0.0015	−0.0062	71
9	55972.3785	0.0006	−0.0088	39
10	55972.4569	0.0005	−0.0087	41
21	55973.3168	0.0021	−0.0099	21
22	55973.3992	0.0008	−0.0059	40
23	55973.4779	0.0012	−0.0054	40
24	55973.5590	0.0008	−0.0026	39
25	55973.6400	0.0009	0.0001	39
26	55973.7193	0.0010	0.0012	20
73	55977.3967	0.0015	−0.0006	72
74	55977.4807	0.0049	0.0051	43
76	55977.6363	0.0027	0.0041	71

*BJD−2400000.
†Against max $= 2455971.6828 + 0.078280E$.
‡Number of points used to determine the maximum.

superhumps.

The behavior of negative superhumps was very similar to that of ER UMa (figure 26; cf. figure 2 of Ohshima et al. 2012). The mean period of negative superhumps during the superoutburst was 0.072793(7) d ($0 \le E \le 280$). The period slightly lengthened later, and stabilized to a slightly longer period during the phase showing normal outbursts [mean period 0.072922(6) d for $280 \le E \le 544$] (table 31). It is noteworthy that there was no jump in phase when superhumps switched from negative ones to positive ones. The same phenomenon was observed in ER UMa (Ohshima et al. 2012). The amplitudes of negative superhumps were well correlated with the system magnitude, and the amplitudes became larger when the system gets fainter. This relation was also observed in V344 Lyr (cf. figure 79 of Kato et al. 2012a), V503 Cyg (Harvey et al. 1995), MN Dra (Pavlenko et al. 2010a) and ER UMa, although Ohshima et al. (2012) did not present the corresponding figure.

Kemp et al. (2012) proposed that a transition from a permanent superhumper to a dwarf nova may a result of cooling of the white dwarf following a nova eruption. The time-scale (several years) of this transition, however, appears to be too short compared to the proposed duration ($\sim$ 1900 yr) of the post-nova state. The change of state may also be a result of variable mass-transfer rate as recorded in other ER UMa-type dwarf novae such as V1159 Ori (Kato 2001) rather than secular evolution.

3.25. V585 Lyrae

Although the object was extensively observed during the 2003 superoutburst (cf. Kato et al. 2009), no secure record of an outburst had been recorded until 2012. The 2012 superoutburst was detected by P. A. Dubovsky (vsnet-alert 14494). We obtained two nights of observa-

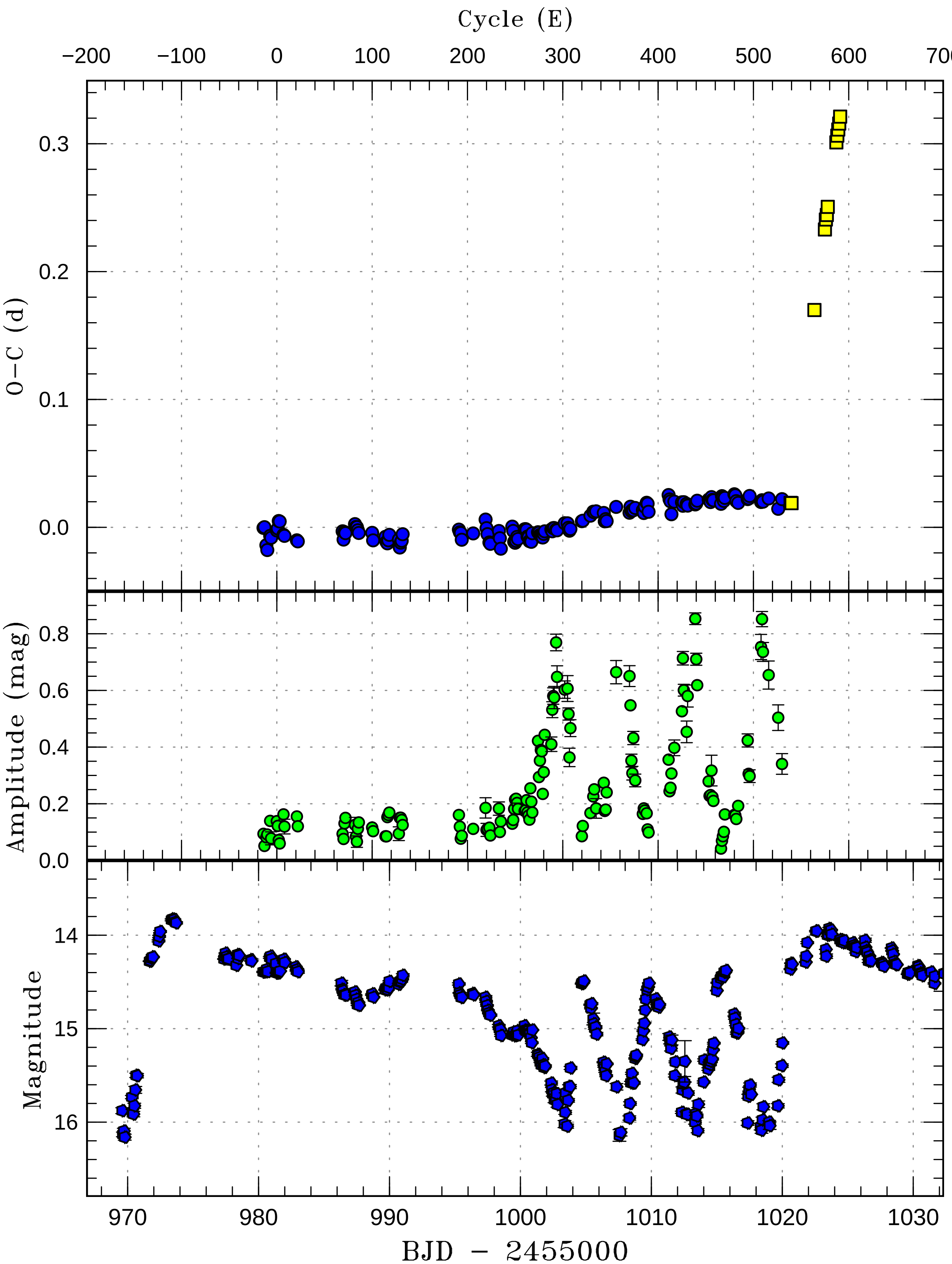

Fig. 26. $O-C$ diagram of negative superhumps in BK Lyn (2012). (Upper:) $O-C$. Filled circles and filled squares represent negative superhumps and positive superhumps, respectively. The positive superhumps appeared as the next superoutburst started, and the phase of the hump maximum was continuous with that of the preceding negative superhumps. The maxima of positive superhumps during the first superoutburst are not shown. We used a period of 0.07280 d for calculating the $O-C$ residuals. (Middle:) Amplitudes of negative superhumps. The amplitudes become larger when the system fades. (Lower:) Light curve. The supercycle is ∼50 d and there were three normal outbursts between the superoutbursts.

Table 31. Times of negative superhumps in BK Lyn.

E	max*	error	$O-C$†	N‡
0	55980.3754	0.0007	0.0147	38
1	55980.4487	0.0017	0.0153	38
3	55980.5802	0.0018	0.0010	37
4	55980.6492	0.0011	−0.0028	38
7	55980.8787	0.0011	0.0080	33
8	55980.9500	0.0028	0.0065	35
14	55981.3926	0.0006	0.0118	39
15	55981.4669	0.0007	0.0133	37
16	55981.5455	0.0014	0.0191	37
17	55981.6180	0.0020	0.0186	38
21	55981.8987	0.0005	0.0079	33
22	55981.9707	0.0020	0.0071	35
35	55982.9136	0.0006	0.0027	37
36	55982.9856	0.0014	0.0018	35
83	55986.4151	0.0016	0.0066	38
84	55986.4814	0.0014	0.0001	33
85	55986.5601	0.0013	0.0059	34
86	55986.6320	0.0009	0.0050	37
96	55987.3671	0.0016	0.0114	34
97	55987.4377	0.0017	0.0091	37
98	55987.5104	0.0029	0.0089	20
99	55987.5807	0.0010	0.0064	37
100	55987.6514	0.0012	0.0042	74
114	55988.6707	0.0007	0.0034	70
115	55988.7376	0.0010	−0.0026	70
128	55989.6868	0.0011	−0.0006	107
129	55989.7556	0.0009	−0.0047	109
130	55989.8273	0.0006	−0.0059	76
131	55989.9025	0.0008	−0.0036	38
132	55989.9795	0.0006	0.0006	27
142	55990.7038	0.0018	−0.0037	29
143	55990.7704	0.0006	−0.0100	28
144	55990.8470	0.0009	−0.0063	37
145	55990.9213	0.0009	−0.0049	36
146	55990.9992	0.0013	0.0002	32
205	55995.2980	0.0015	−0.0001	37
206	55995.3687	0.0010	−0.0022	105
207	55995.4409	0.0019	−0.0029	61
208	55995.5085	0.0016	−0.0082	30
220	55996.3870	0.0015	−0.0040	37
233	55997.3443	0.0015	0.0060	28
234	55997.4104	0.0020	−0.0008	37
235	55997.4785	0.0015	−0.0056	36
237	55997.6176	0.0013	−0.0122	37
238	55997.6893	0.0015	−0.0134	26
247	55998.3545	0.0010	−0.0039	33
248	55998.4217	0.0017	−0.0096	36
249	55998.4863	0.0012	−0.0179	37
261	55999.3772	0.0008	−0.0014	149
262	55999.4466	0.0006	−0.0049	155
263	55999.5109	0.0006	−0.0134	85
264	55999.5829	0.0004	−0.0142	83

*BJD−2400000.
†Against max $= 2455980.3606 + 0.072866E$.
‡Number of points used to determine the maximum.

Table 31. Times of negative superhumps in BK Lyn.

E	max*	error	$O-C$†	N‡
265	55999.6572	0.0009	−0.0128	80
266	55999.7331	0.0010	−0.0098	76
267	55999.8042	0.0010	−0.0115	69
274	56000.3215	0.0007	−0.0043	59
275	56000.3944	0.0005	−0.0043	94
276	56000.4666	0.0004	−0.0049	96
277	56000.5342	0.0008	−0.0102	74
278	56000.6064	0.0006	−0.0109	118
279	56000.6762	0.0006	−0.0139	144
280	56000.7488	0.0003	−0.0142	169
281	56000.8213	0.0004	−0.0146	159
282	56000.9008	0.0010	−0.0079	65
288	56001.3384	0.0004	−0.0076	90
289	56001.4108	0.0003	−0.0080	165
290	56001.4818	0.0003	−0.0099	164
291	56001.5541	0.0004	−0.0104	138
292	56001.6257	0.0004	−0.0117	160
293	56001.6982	0.0005	−0.0120	154
294	56001.7739	0.0004	−0.0092	118
295	56001.8487	0.0003	−0.0073	127
302	56002.3597	0.0005	−0.0064	52
303	56002.4311	0.0005	−0.0078	60
304	56002.5064	0.0005	−0.0054	61
305	56002.5792	0.0006	−0.0054	60
307	56002.7236	0.0004	−0.0068	70
308	56002.7958	0.0006	−0.0074	70
316	56003.3838	0.0005	−0.0024	67
319	56003.6021	0.0007	−0.0026	77
320	56003.6714	0.0004	−0.0062	96
321	56003.7420	0.0008	−0.0085	70
322	56003.8161	0.0006	−0.0073	61
334	56004.6958	0.0008	−0.0020	71
335	56004.7690	0.0007	−0.0016	70
343	56005.3553	0.0007	0.0018	52
346	56005.5768	0.0005	0.0047	31
347	56005.6492	0.0006	0.0041	58
349	56005.7955	0.0019	0.0048	40
357	56006.3766	0.0006	0.0030	150
358	56006.4429	0.0005	−0.0036	161
359	56006.5174	0.0005	−0.0020	150
360	56006.5887	0.0007	−0.0036	119
370	56007.3278	0.0005	0.0069	38
384	56008.3424	0.0005	0.0014	99
385	56008.4199	0.0003	0.0060	99
386	56008.4893	0.0006	0.0025	90
387	56008.5628	0.0007	0.0032	132
388	56008.6355	0.0005	0.0030	82
390	56008.7829	0.0007	0.0047	64
398	56009.3636	0.0008	0.0025	67
399	56009.4342	0.0006	0.0002	67
400	56009.5119	0.0008	0.0051	66
402	56009.6606	0.0008	0.0080	65
403	56009.7327	0.0013	0.0072	70
404	56009.7992	0.0014	0.0008	66

*BJD−2400000.
†Against max $= 2455980.3606 + 0.072866E$.
‡Number of points used to determine the maximum.

Table 31. Times of negative superhumps in BK Lyn.

E	max*	error	$O-C$†	N‡
425	56011.3411	0.0003	0.0125	162
426	56011.4104	0.0004	0.0090	233
427	56011.4817	0.0003	0.0074	238
428	56011.5444	0.0005	−0.0027	136
431	56011.7727	0.0005	0.0069	48
439	56012.3546	0.0003	0.0059	220
440	56012.4247	0.0003	0.0031	212
441	56012.5003	0.0003	0.0059	124
444	56012.7173	0.0008	0.0043	70
445	56012.7888	0.0006	0.0029	61
453	56013.3721	0.0002	0.0033	213
454	56013.4456	0.0003	0.0040	215
455	56013.5206	0.0003	0.0061	111
467	56014.3951	0.0004	0.0062	196
468	56014.4673	0.0004	0.0056	163
469	56014.5387	0.0004	0.0041	131
470	56014.6154	0.0011	0.0080	23
471	56014.6861	0.0008	0.0057	56
472	56014.7585	0.0008	0.0053	56
480	56015.3382	0.0010	0.0020	299
481	56015.4170	0.0006	0.0080	281
482	56015.4887	0.0007	0.0068	201
483	56015.5588	0.0006	0.0041	162
484	56015.6340	0.0005	0.0064	50
494	56016.3649	0.0006	0.0086	211
495	56016.4368	0.0006	0.0077	182
496	56016.5051	0.0005	0.0031	125
498	56016.6493	0.0007	0.0016	46
508	56017.3803	0.0005	0.0039	71
509	56017.4536	0.0007	0.0044	108
510	56017.5283	0.0008	0.0062	74
522	56018.3972	0.0005	0.0007	60
523	56018.4714	0.0003	0.0020	62
524	56018.5430	0.0004	0.0008	61
530	56018.9824	0.0006	0.0030	129
540	56019.7023	0.0011	−0.0058	71
544	56020.0010	0.0010	0.0015	150

*BJD−2400000.
†Against max $= 2455980.3606 + 0.072866E$.
‡Number of points used to determine the maximum.

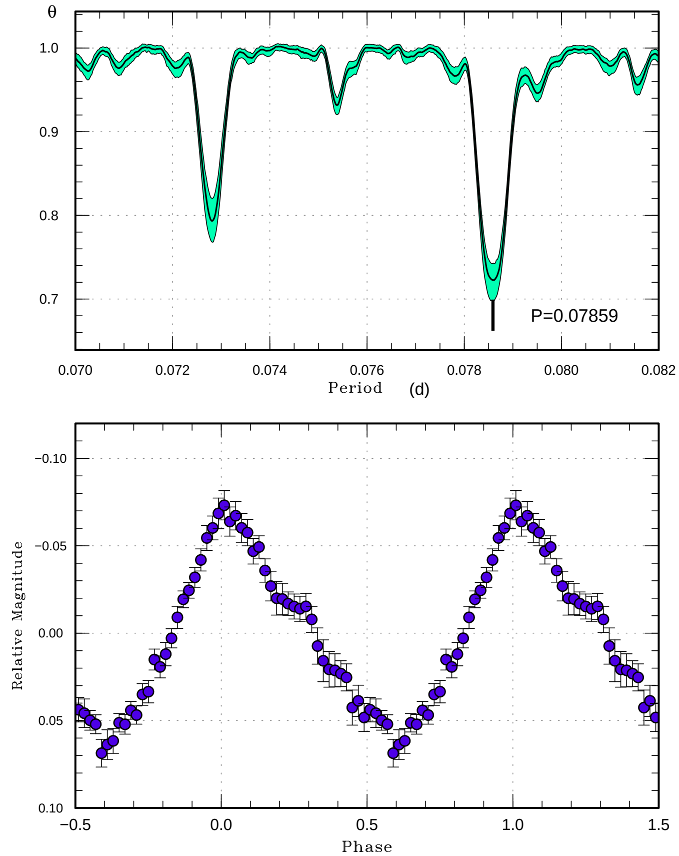

Fig. 24. Positive superhumps in BK Lyn (2012 April). (Upper): PDM analysis. A period at 0.0728 d is a one–day alias of the superhump period. This period coincided the period of negative superhumps by chance. (Lower): Phase-averaged profile.

tions and listed the times of maxima (table 33). The period in table 2 was obtained by the PDM method.

3.26. *FQ Monocerotis*

Only a fragment of the 2011 superoutburst was observed. The times of superhump maxima are listed in table 34. Since the object quickly faded three days after the observation, it is likely we only observed stage C superhumps.

3.27. *V1032 Ophiuchi*

This object is an eclipsing SU UMa-type dwarf nova (Kato et al. 2010). By applying Markov-Chain Monte Carlo (MCMC) method to the phased data using the period and epoch as trial variables (see appendix 1), we obtained an updated orbital ephemeris of

$$\mathrm{Min(BJD)} = 2455286.68256(7) + 0.081055386(10)E \quad (1)$$

based on 2010 and 2012 observations. The times of superhump maxima are listed in table 35. A PDM analysis yielded a consistent result of 0.08599(5) d.

Table 32. Superhump maxima of BK Lyn (2012 April).

E	max*	error	$O-C$†	N‡
0	56020.6533	0.0009	−0.0043	67
1	56020.7259	0.0011	−0.0102	66
25	56022.6242	0.0004	0.0029	142
36	56023.4880	0.0018	0.0027	62
37	56023.5685	0.0011	0.0047	95
38	56023.6449	0.0005	0.0025	71
39	56023.7240	0.0006	0.0031	70
48	56024.4297	0.0005	0.0018	66
49	56024.5077	0.0006	0.0013	73
50	56024.5853	0.0006	0.0003	94
51	56024.6628	0.0004	−0.0007	146
52	56024.7410	0.0005	−0.0011	139
60	56025.3774	0.0005	0.0069	82
61	56025.4519	0.0005	0.0029	82
62	56025.5290	0.0005	0.0014	90
73	56026.3951	0.0008	0.0035	75
74	56026.4729	0.0011	0.0027	75
77	56026.7014	0.0009	−0.0043	76
78	56026.7839	0.0018	−0.0004	43
88	56027.5681	0.0009	−0.0017	43
89	56027.6441	0.0005	−0.0043	70
90	56027.7221	0.0005	−0.0048	66
99	56028.4338	0.0018	−0.0000	88
100	56028.5159	0.0008	0.0035	50
101	56028.5918	0.0007	0.0009	74
102	56028.6665	0.0006	−0.0030	69
103	56028.7423	0.0008	−0.0057	63
114	56029.6190	0.0053	0.0069	51
115	56029.6781	0.0011	−0.0124	66
116	56029.7610	0.0019	−0.0081	40
124	56030.4074	0.0011	0.0098	153
125	56030.4849	0.0024	0.0089	104
126	56030.5569	0.0013	0.0023	69
127	56030.6252	0.0022	−0.0080	91

*BJD−2400000.
†Against max $= 2456020.6576 + 0.078548E$.
‡Number of points used to determine the maximum.

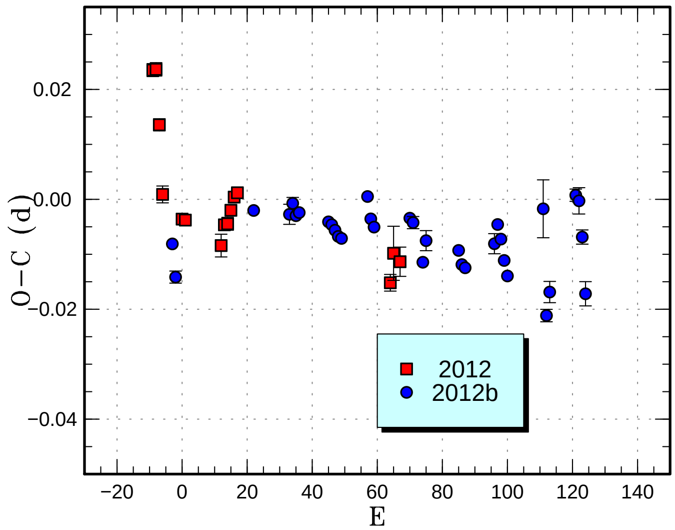

Fig. 25. Comparison of $O-C$ diagrams of positive superhumps of BK Lyn between different superoutbursts. The abbreviation 2012 refers to the 2012 February–March superoutburst and 2012b the 2012 April one, respectively. A period of 0.07859 d was used to draw this figure. Approximate cycle counts (E) after the appearance of the positive superhumps were used. The maxima for $E<0$ are negative superhumps. As known in ER UMa (Ohshima et al. 2012), there were relatively large intranight $O-C$ variations against the mean period of positive superhumps. This can be interpreted as a result of the coexistence of negative superhumps.

Table 33. Superhump maxima of V585 Lyr (2012).

E	max*	error	$O-C$†	N‡
0	56045.1580	0.0005	−0.0005	123
1	56045.2195	0.0006	0.0006	71
18	56046.2441	0.0008	−0.0025	124
19	56046.3094	0.0023	0.0023	68

*BJD−2400000.
†Against max $= 2456045.1584 + 0.060454E$.
‡Number of points used to determine the maximum.

Table 34. Superhump maxima of FQ Mon (2011).

E	max*	error	$O-C$†	N‡
0	55922.0918	0.0011	−0.0015	130
1	55922.1676	0.0033	0.0015	67
13	55923.0405	0.0020	0.0018	91
14	55923.1096	0.0015	−0.0018	130

*BJD−2400000.
†Against max $= 2455922.0934 + 0.072718E$.
‡Number of points used to determine the maximum.

Table 35. Superhump maxima of V1032 Oph (2012).

E	max*	error	$O-C$†	phase‡	N§
0	56076.3539	0.0046	−0.0101	0.52	80
9	56077.1475	0.0015	0.0098	0.23	127
12	56077.3984	0.0009	0.0029	0.15	148
47	56080.4017	0.0012	−0.0026	0.29	150

*BJD−2400000.
†Against max $= 2456076.3640 + 0.085965E$.
‡Orbital phase.
§Number of points used to determine the maximum.

Table 36. Superhump maxima of V1159 Ori (2012).

E	max*	error	$O-C$†	N‡
0	55991.6169	0.0004	0.0065	123
1	55991.6826	0.0004	0.0074	124
16	55992.6410	0.0010	−0.0046	57
30	55993.5407	0.0012	−0.0106	42
31	55993.6059	0.0023	−0.0101	57
61	55995.5631	0.0005	0.0064	54
62	55995.6264	0.0009	0.0049	58
77	55996.5919	0.0011	0.0000	58

*BJD−2400000.
†Against max $= 2455991.6105 + 0.064694E$.
‡Number of points used to determine the maximum.

3.28. V2051 Ophiuchi

Only one superhump was recorded during the 2012 February superoutburst: BJD 2455985.3378(2) ($N = 157$).

3.29. V1159 Orionis

V1159 Ori is one of the member of the ER UMa stars (Robertson et al. 1995; Nogami et al. 1995; Patterson et al. 1995). Although the object generally follows the ER UMa-type pattern with a short supercycle (Kato, Kunjaya 1995), the object is known to show variations of supercycles with a range of 44.6–53.3 d (Kato 2001). Since it has been demonstrated that the prototype ER UMa has recently been in a state of "negative superhumps" (Ohshima et al. 2012), it would be worth examining the current state of superhumps in V1159 Ori.

The observations were taken during its 2012 March superoutburst (the data were mainly from the AAVSO). The times of superhump maxima are listed in table 36. There was a ∼0.5 phase shift between $E = 31$ and $E = 77$, as seen in ER UMa in its "positive superhump" state (Kato et al. 2003a). A period analysis for $E \geq 61$ yielded a period of 0.06430(5) d, indicating that the period after the phase shift was that of positive superhumps, and not that of negative superhumps. The behavior well reproduced ER UMa in its "positive superhump" state (in the 1990s). V1159 Ori is currently the best target to investigate the ER UMa-type phenomena in "positive superhump" state and further detailed observations are required.

3.30. AR Pictoris

We observed the 2011 superoutburst of this object (=CTCV J0549−4921, Imada et al. 2008a). Kato et al. (2009) identified this object with a large negative $P_{\rm dot}$. The times of superhump maxima are listed in table 37. We only observed the terminal portion of the superoutburst, and the mean superhump period [0.08315(15) d] was much shorter than the value obtained during the 2006 superoutburst (Kato et al. 2009). During the post-superoutburst phase, we could detect a superhump period of 0.08225(9) d (PDM method). A lasso analysis yielded a combination of the superhump period and a period of 0.0801(1) d, which is potentially the orbital period. If this is indeed $P_{\rm orb}$, ϵ for the 2006 and 2011 superoutburst were 5.4% (average) and 3.7%, respectively. A comparison of $O-C$ diagrams (figure 27) indicates that the $O-C$ diagram in 2011 is in smooth extension of the 2006 one, which was obtained only during the early stage.

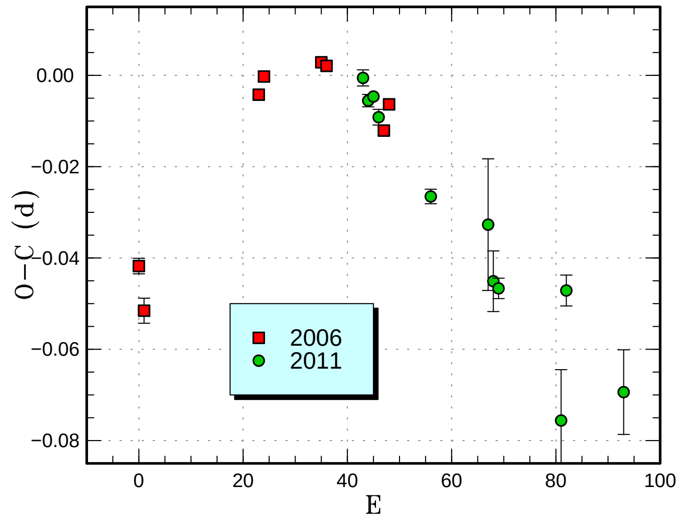

Fig. 27. Comparison of $O-C$ diagrams of AR Pic between different superoutbursts. A period of 0.08458 d was used to draw this figure. Approximate cycle counts (E) after the start of the superoutburst were used.

Table 37. Superhump maxima of AR Pic (2011).

E	max*	error	$O-C$†	N‡
0	55910.5774	0.0018	0.0038	20
1	55910.6570	0.0014	0.0002	25
2	55910.7425	0.0011	0.0026	29
3	55910.8225	0.0017	−0.0005	29
13	55911.6510	0.0016	−0.0036	25
24	55912.5752	0.0144	0.0059	19
25	55912.6474	0.0066	−0.0051	17
26	55912.7304	0.0022	−0.0052	23
38	55913.7164	0.0111	−0.0171	27
39	55913.8294	0.0034	0.0128	29
50	55914.7376	0.0093	0.0063	28

*BJD−2400000.
†Against max $= 2455910.5736 + 0.083154E$.
‡Number of points used to determine the maximum.

3.31. GV Piscium

The 2011 superoutburst of this object was detected by CRTS on October 17. Subsequent observations confirmed the presence of superhumps (vsnet-alert 13768). The times of superhump maxima are listed in table 38. There was little hint of period variation, and the mean period was close to that obtained during the 2008 superoutburst (Kato et al. 2009). Since the object faded relatively soon after the outburst detection, it looks likely that we also observed only stage C superhumps as in 2008.

Table 38. Superhump maxima of GV Psc (2011).

E	max*	error	$O-C$†	N‡
0	55852.3350	0.0003	−0.0003	95
1	55852.4291	0.0003	−0.0005	86
4	55852.7127	0.0003	0.0001	94
5	55852.8055	0.0003	−0.0014	87
11	55853.3728	0.0003	−0.0000	90
12	55853.4688	0.0005	0.0016	99
25	55854.6952	0.0003	0.0020	99
26	55854.7867	0.0004	−0.0008	90
61	55858.0892	0.0008	0.0007	62
62	55858.1814	0.0007	−0.0014	61

*BJD−2400000.
†Against max $= 2455852.3354 + 0.094313E$.
‡Number of points used to determine the maximum.

3.32. BW Sculptoris

This object (=HE 2350−3908, RX J2353.0−3852) was initially discovered in the Hamburg/ESO quasar survey (Augusteijn, Wisotzki 1997) and was also selected as a ROSAT CV (Abbott et al. 1997). Its remarkable similarity with WZ Sge was already noted at its very early history (Augusteijn, Wisotzki 1997). Despite monitoring, there had been no outbursts until 2011. Uthas et al. (2012) reported the ZZ Cet-type pulsation of the white dwarf and the presence of quiescent superhumps 11% longer than $P_{\rm orb}$.

The 2011 outburst was detected by M. Linnolt on October 21 at a visual magnitude of 9.6 (posting to AAVSO discussion), and subsequent observation soon confirmed early superhumps (vsnet-alert 13786; figure 28). The last observation before this outburst was on October 15 (by J. Hambsch; see also Hambsch 2012) when the object was still in quiescence. On October 31, ordinary superhumps developed (vsnet-alert 13815, 13819; figure 29). The object entered the rapid fading stage on November 12 (vsnet-alert 13847, 13850). The times of maxima of ordinary superhumps are listed in table 39. Following a period of stage A ($E \le 25$), there was stage B with $P_{\rm dot} = +4.3(0.3) \times 10^{-5}$. Although there was a suggestion of sudden shortening of the superhump period after $E = 210$, as seen in other WZ Sge-type dwarf novae [e.g. GW Lib and V455 And (Kato et al. 2009); OT J012059.6+325545 and SDSS J080434.20+510349.2 = EZ Lyn, (Kato et al. 2012a)], a discontinuity in the observation made the identification of hump phasing uncertain. We list times of hump maxima after this rapid fading in table 40, which were measured after subtracting the mean orbital variation (figure 30). The overall behavior of the outburst and $O-C$ diagram were very similar to those of GW Lib and V455 And. The period of early superhumps was 0.054308(2) d, 0.03% shorter than $P_{\rm orb}$. The ϵ for stage B superhumps was 1.3%.

A full analysis will be presented by Ohshima et al., in preparation.

Table 39. Superhump maxima of BW Scl (2011).

E	max*	error	$O-C$†	N‡
0	55865.5288	0.0016	−0.0209	89
1	55865.5827	0.0022	−0.0221	61
2	55865.6444	0.0031	−0.0155	89
3	55865.6992	0.0044	−0.0157	89
8	55865.9875	0.0003	−0.0026	426
9	55866.0407	0.0004	−0.0044	187
10	55866.0966	0.0006	−0.0035	154
17	55866.4844	0.0030	−0.0010	50
18	55866.5415	0.0005	0.0011	89
19	55866.6000	0.0004	0.0045	88
20	55866.6558	0.0004	0.0053	89
21	55866.7103	0.0008	0.0048	89
25	55866.9339	0.0003	0.0082	279
26	55866.9873	0.0002	0.0065	305
27	55867.0432	0.0003	0.0074	274
28	55867.0976	0.0004	0.0068	223
31	55867.2628	0.0001	0.0069	238
32	55867.3191	0.0001	0.0081	238
33	55867.3729	0.0001	0.0069	236
34	55867.4282	0.0003	0.0071	125
35	55867.4830	0.0001	0.0069	281
36	55867.5371	0.0001	0.0060	302
37	55867.5926	0.0002	0.0065	75
38	55867.6471	0.0002	0.0059	89
39	55867.7022	0.0002	0.0060	89
46	55868.0864	0.0002	0.0049	89
47	55868.1424	0.0002	0.0058	68
54	55868.5261	0.0004	0.0044	89
55	55868.5816	0.0003	0.0048	88
56	55868.6357	0.0003	0.0039	89
57	55868.6911	0.0003	0.0042	88
58	55868.7479	0.0005	0.0059	55
63	55869.0200	0.0002	0.0029	144
64	55869.0756	0.0003	0.0035	182
65	55869.1295	0.0003	0.0023	102
72	55869.5126	0.0006	0.0001	91
73	55869.5701	0.0012	0.0026	65
74	55869.6238	0.0004	0.0013	89
75	55869.6781	0.0005	0.0005	89
76	55869.7328	0.0005	0.0002	84
80	55869.9520	0.0005	−0.0008	141
81	55870.0068	0.0004	−0.0010	165
82	55870.0626	0.0004	−0.0003	237
83	55870.1169	0.0002	−0.0010	93
84	55870.1713	0.0003	−0.0017	84
90	55870.5005	0.0004	−0.0026	33
91	55870.5567	0.0004	−0.0015	37
92	55870.6106	0.0003	−0.0027	44
93	55870.6659	0.0003	−0.0024	43
94	55870.7217	0.0003	−0.0016	44
104	55871.2706	0.0001	−0.0030	238
105	55871.3265	0.0002	−0.0022	237
106	55871.3808	0.0003	−0.0029	197
108	55871.4894	0.0006	−0.0045	24
109	55871.5484	0.0006	−0.0004	33
110	55871.5994	0.0003	−0.0045	40

*BJD−2400000.
†Against max $= 2455865.5497 + 0.055038E$.
‡Number of points used to determine the maximum.

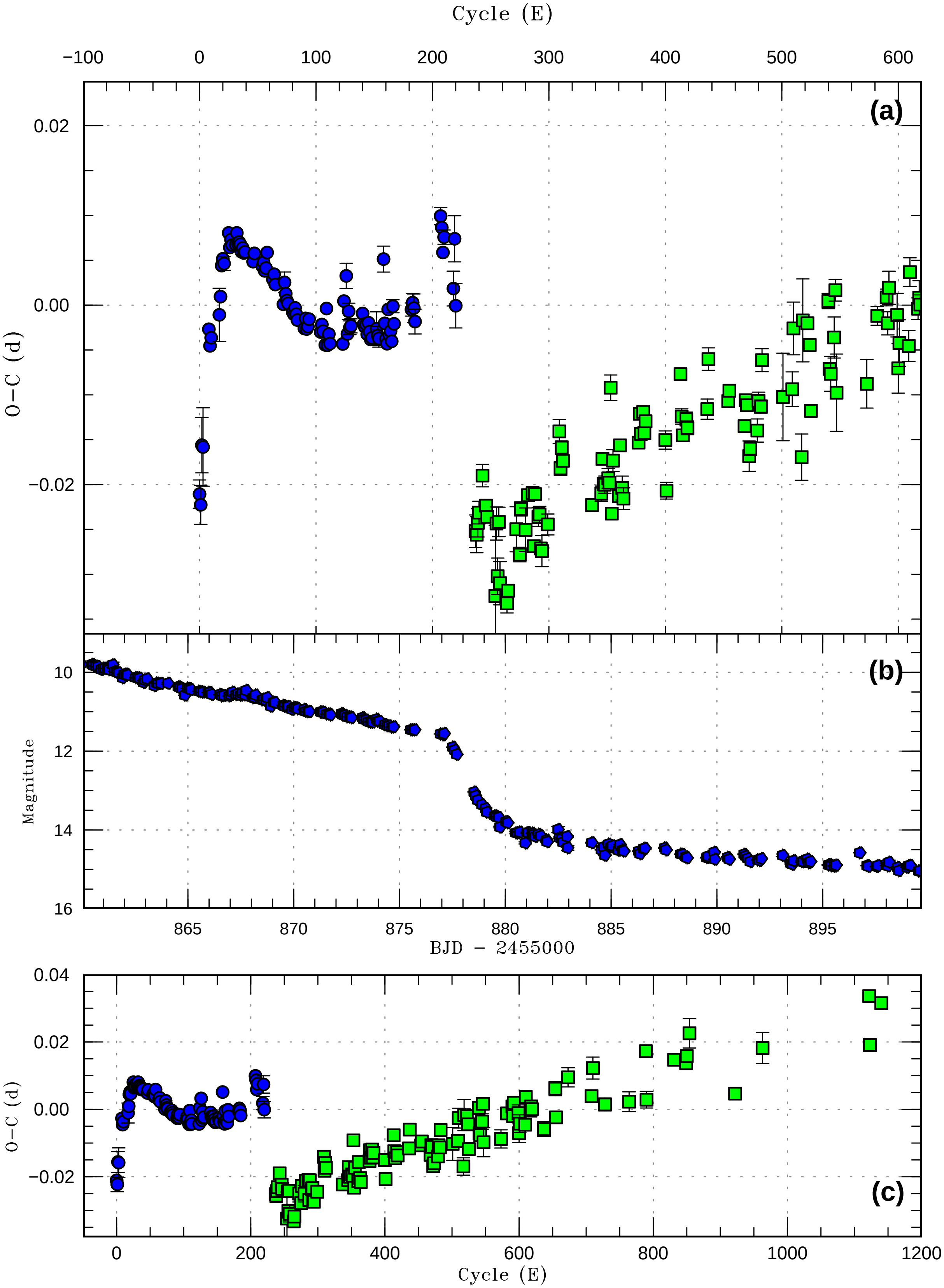

Fig. 31. $O-C$ diagram of superhumps in BW Scl (2011). (a) $O-C$. Filled circles and filled squares represent ordinary superhumps and late-stage superhumps after the rapid fading. We used a period of 0.055036 d for calculating the $O-C$ residuals. (b) Light curve. (c) $O-C$ diagram of the entire observation. The global evolution of the $O-C$ diagram is remarkably similar to those of GW Lib and V455 And (Kato et al. 2009).

Table 39. Superhump maxima of BW Scl (2011). (continued)

E	max*	error	$O-C$†	N‡
111	55871.6557	0.0004	−0.0033	40
112	55871.7096	0.0006	−0.0043	40
123	55872.3150	0.0003	−0.0044	219
124	55872.3748	0.0004	0.0004	237
126	55872.4877	0.0014	0.0032	222
127	55872.5363	0.0005	−0.0033	152
128	55872.5938	0.0009	−0.0007	40
129	55872.6470	0.0008	−0.0026	40
130	55872.7023	0.0008	−0.0024	41
140	55873.2540	0.0005	−0.0010	155
141	55873.3079	0.0002	−0.0022	238
142	55873.3626	0.0002	−0.0025	235
143	55873.4179	0.0002	−0.0022	240
144	55873.4718	0.0004	−0.0033	161
145	55873.5282	0.0006	−0.0021	32
146	55873.5822	0.0003	−0.0031	40
147	55873.6364	0.0004	−0.0039	41
148	55873.6916	0.0004	−0.0037	40
152	55873.9127	0.0019	−0.0027	76
153	55873.9670	0.0010	−0.0035	115
154	55874.0217	0.0010	−0.0038	114
158	55874.2507	0.0014	0.0050	133
159	55874.2986	0.0002	−0.0021	238
160	55874.3519	0.0004	−0.0039	235
161	55874.4064	0.0003	−0.0044	237
162	55874.4653	0.0004	−0.0006	237
163	55874.5174	0.0004	−0.0035	232
164	55874.5729	0.0004	−0.0030	40
165	55874.6268	0.0007	−0.0042	40
166	55874.6858	0.0007	−0.0003	40
167	55874.7388	0.0005	−0.0022	32
182	55875.5660	0.0007	−0.0006	40
183	55875.6218	0.0010	0.0001	40
184	55875.6762	0.0016	−0.0005	40
185	55875.7297	0.0014	−0.0020	40
207	55876.9523	0.0010	0.0097	60
208	55877.0060	0.0005	0.0084	50
209	55877.0583	0.0005	0.0057	100
210	55877.1150	0.0008	0.0074	58
218	55877.5496	0.0019	0.0016	24
219	55877.6102	0.0026	0.0072	25
220	55877.6578	0.0025	−0.0003	25

*BJD−2400000.
†Against max $= 2455865.5497 + 0.055038E$.
‡Number of points used to determine the maximum.

Table 40. Late-stage superhumps in BW Scl (2011).

E	max*	error	$O-C$†	N‡
0	55878.5682	0.0018	0.0005	25
1	55878.6229	0.0020	0.0000	25
2	55878.6792	0.0016	0.0013	25
3	55878.7354	0.0013	0.0024	22
6	55878.9046	0.0013	0.0063	106
9	55879.0664	0.0003	0.0028	83
10	55879.1202	0.0006	0.0014	84
17	55879.4966	0.0079	−0.0078	12
18	55879.5597	0.0019	0.0002	19
19	55879.6089	0.0020	−0.0058	20
20	55879.6700	0.0016	0.0002	19
21	55879.7182	0.0024	−0.0067	19
27	55880.0462	0.0011	−0.0093	110
28	55880.1026	0.0007	−0.0079	86
35	55880.4947	0.0025	−0.0015	10
38	55880.6570	0.0008	−0.0045	19
39	55880.7171	0.0008	0.0005	16
43	55880.9349	0.0024	−0.0021	61
45	55881.0489	0.0004	0.0016	97
49	55881.2693	0.0001	0.0016	390
50	55881.3184	0.0002	−0.0044	476
51	55881.3792	0.0002	0.0014	474
54	55881.5417	0.0010	−0.0014	18
55	55881.5971	0.0009	−0.0011	19
56	55881.6483	0.0005	−0.0050	20
57	55881.7031	0.0017	−0.0054	19
62	55881.9812	0.0012	−0.0027	76
72	55882.5419	0.0013	0.0070	20
73	55882.5929	0.0008	0.0028	20
74	55882.6502	0.0007	0.0051	20
75	55882.7038	0.0004	0.0035	19
100	55884.0747	0.0005	−0.0030	55
108	55884.5163	0.0008	−0.0022	57
109	55884.5752	0.0006	0.0016	59
110	55884.6275	0.0005	−0.0013	58
111	55884.6824	0.0010	−0.0014	58
114	55884.8482	0.0011	−0.0009	41
115	55884.9028	0.0005	−0.0014	38
116	55884.9684	0.0014	0.0091	31
117	55885.0094	0.0007	−0.0050	59
118	55885.0703	0.0012	0.0008	37
123	55885.3416	0.0004	−0.0034	127
124	55885.4023	0.0006	0.0021	99
126	55885.5076	0.0013	−0.0027	51
127	55885.5614	0.0012	−0.0040	59
140	55886.2831	0.0004	0.0014	110
141	55886.3414	0.0004	0.0046	127
142	55886.3942	0.0007	0.0023	39
144	55886.5067	0.0004	0.0046	48
145	55886.5594	0.0007	0.0022	59
146	55886.6157	0.0006	0.0034	44
163	55887.5493	0.0010	0.0003	59
164	55887.5986	0.0009	−0.0055	59
176	55888.2721	0.0003	0.0068	94
177	55888.3224	0.0009	0.0020	127

*BJD−2400000.
†Against max $= 2455878.5677 + 0.055100E$.
‡Number of points used to determine the maximum.

Table 40. Late-stage superhumps in BW Scl (2011). (continued)

E	max*	error	$O-C$†	N‡
178	55888.3753	0.0004	−0.0002	108
181	55888.5423	0.0008	0.0015	59
182	55888.5963	0.0008	0.0004	59
199	55889.5340	0.0011	0.0014	58
200	55889.5946	0.0013	0.0069	59
217	55890.5255	0.0005	0.0012	58
218	55890.5817	0.0006	0.0023	59
231	55891.2933	0.0005	−0.0025	127
232	55891.3512	0.0004	0.0003	127
233	55891.4057	0.0004	−0.0003	127
235	55891.5101	0.0017	−0.0061	56
236	55891.5659	0.0008	−0.0054	59
242	55891.8982	0.0013	−0.0037	55
243	55891.9565	0.0010	−0.0005	68
245	55892.0659	0.0007	−0.0012	22
246	55892.1261	0.0013	0.0039	19
264	55893.1127	0.0049	−0.0014	29
272	55893.5538	0.0019	−0.0010	31
273	55893.6157	0.0029	0.0057	24
280	55893.9866	0.0026	−0.0091	27
281	55894.0568	0.0046	0.0061	19
285	55894.2767	0.0004	0.0055	104
287	55894.3843	0.0004	0.0030	126
288	55894.4320	0.0004	−0.0044	127
303	55895.2698	0.0009	0.0068	90
304	55895.3173	0.0005	−0.0008	127
305	55895.3718	0.0019	−0.0014	127
308	55895.5409	0.0023	0.0025	30
309	55895.6012	0.0012	0.0077	30
310	55895.6448	0.0043	−0.0038	30
336	55897.0768	0.0027	−0.0045	31
345	55897.5796	0.0010	0.0025	30
353	55898.0220	0.0009	0.0041	22
354	55898.0742	0.0013	0.0011	30
355	55898.1331	0.0018	0.0050	20
362	55898.5154	0.0024	0.0015	26
363	55898.5645	0.0028	−0.0045	30
364	55898.6223	0.0026	−0.0017	17
372	55899.0623	0.0017	−0.0026	29
373	55899.1255	0.0016	0.0056	28
380	55899.5067	0.0012	0.0011	22
381	55899.5630	0.0019	0.0022	30
382	55899.6172	0.0011	0.0014	19
400	55900.6020	0.0022	−0.0057	15
417	55901.5496	0.0021	0.0053	20
418	55901.5961	0.0017	−0.0033	16
436	55902.5986	0.0028	0.0074	18
471	55904.5193	0.0017	−0.0004	30
473	55904.6377	0.0032	0.0078	19
491	55905.6176	0.0019	−0.0041	15
527	55907.5997	0.0029	−0.0056	16
552	55908.9906	0.0015	0.0078	30
553	55909.0312	0.0025	−0.0067	30
594	55911.2995	0.0009	0.0025	126
612	55912.2892	0.0012	0.0004	102

*BJD−2400000.
†Against max $= 2455878.5677 + 0.055100E$.
‡Number of points used to determine the maximum.

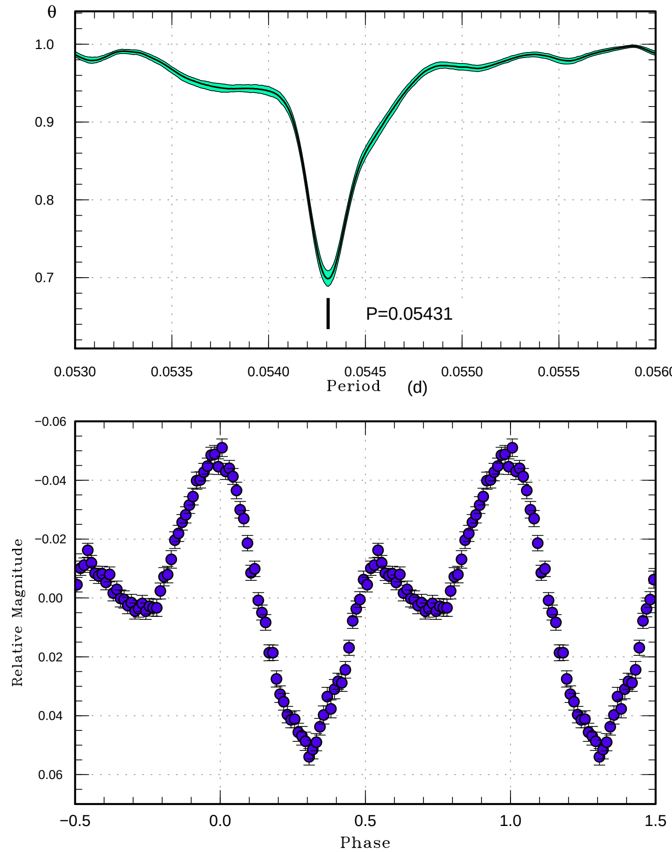

Fig. 28. Early superhumps in BW Scl (2011). (Upper): PDM analysis. (Lower): Phase-averaged profile.

Table 40. Late-stage superhumps in BW Scl (2011). (continued)

E	max*	error	$O-C$†	N‡
613	55912.3463	0.0008	0.0024	126
617	55912.5732	0.0044	0.0090	12
685	55916.2978	0.0005	−0.0133	116
726	55918.5678	0.0046	−0.0024	14
885	55927.3339	0.0011	0.0029	126
886	55927.3744	0.0019	−0.0117	105
903	55928.3225	0.0003	−0.0003	85

*BJD−2400000.
†Against max $= 2455878.5677 + 0.055100E$.
‡Number of points used to determine the maximum.

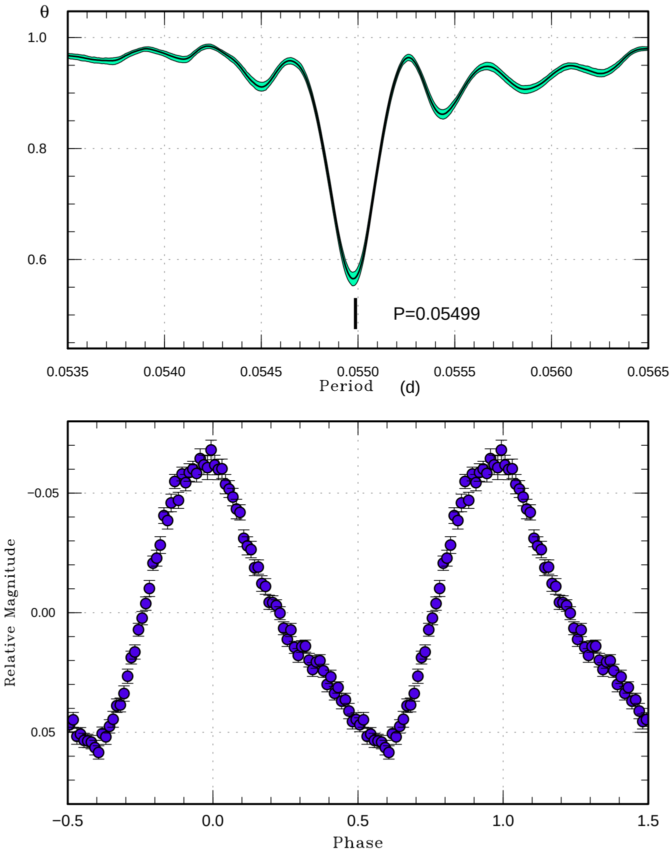

Fig. 29. Ordinary superhumps in BW Scl (2011). (Upper): PDM analysis. (Lower): Phase-averaged profile.

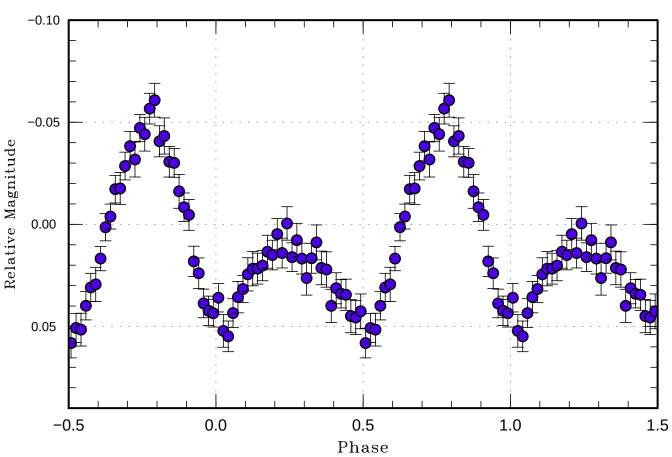

Fig. 30. Averaged orbital profile of BW Scl (2011) after the rapid decline.

3.33. CC Sculptoris

CC Scl was discovered as a ROSAT-selected CV (Schwope et al. 2000). During its 2000 October outburst (the second known), Ishioka et al. (2001a) detected likely superhumps with a period of 0.078 d and amplitudes of ∼0.3 mag. However, Augusteijn et al. (2000, vsnet-campaign 544) reported the detection of a photometric period of 0.058 d, which was considered as being the orbital period. Based on the discrepancy between the apparent period of superhumps and the orbital period, Ishioka et al. (2001a) suggested that the object may be an intermediate polar. The unusual short duration of the superoutburst was also noted. The 0.058 d period was later confirmed to be the orbital period (Chen et al. 2001; Tappert et al. 2004). Although there have been several outbursts since then, no confirmatory observations of superhumps have been reported.

The 2011 superoutburst was detected by CRTS Siding Spring Survey (SSS) and subsequent observations indicated the presence of low-amplitude (up to 0.1 mag) variations similar to superhumps with a period of 0.0603 d (vsnet-alert 13832). Although the observed variations had a definite underlying periodicity (vsnet-alert 13841, 13846), individual waveforms were rather irregular (vsnet-alert 13840; see also actual observations in figure 34) unlike most of SU UMa-type dwarf novae. Even after the object faded, the superhump signal persisted for at least eight days.

A PDM analysis yielded the stronger superhump signal and weaker orbital signal (figure 32 upper). A lasso analysis, which is less affected by aliasing, also indicated the presence of both signals (figure 32 lower). We adopted a refined orbital period of 0.0585845(10) d. We decomposed the observations into these two periodicities (figure 33), and tried to reproduce the observed light curve by combining these waves (figure 34). Although the result was not as remarkable as in OT J173516.9+154708, as we will see later (subsection 3.78), a part of the complex structure in the light curve appears to be understood as an effect of the orbital signal. We therefore subtracted the orbital variation and determined the time of superhump maxima (table 41). The relatively large scatter in the $O-C$ residuals suggests the presence of irregularities not attributable to the orbital variation. Despite these irregularities, the $O-C$ residuals itself did not show a strong trend of variation. Considering that the initial part of the outburst was likely missed, we probably observed only the stage C superhumps. We listed the value in table 2 based on this interpretation.

The unusualbehavior of superhumps in this system, as well as the strong presence of the orbital signal, might have led to a detection of a different period in (Ishioka et al. 2001a). Such unusual behavior may be related to a likely high orbital inclination (Tappert et al. 2004). The ϵ, however, was 2.4%, a normal value for this $P_{\rm orb}$. Future dense monitoring to detect the early stage of a superoutburst is desired.

Woudt et al. (2012) recently established that this object

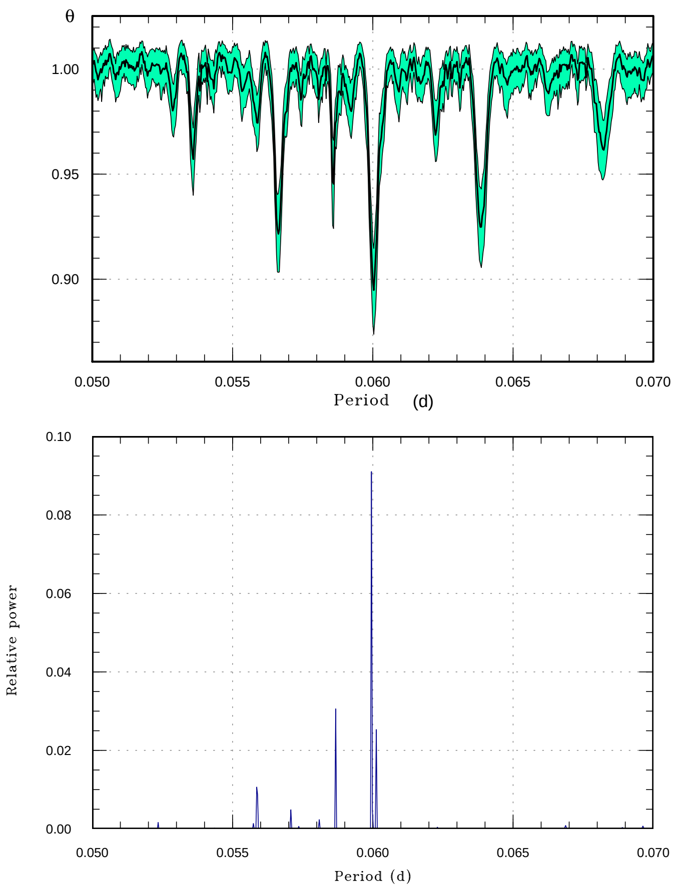

Fig. 32. Period analysis in CC Scl (2011). (Upper): PDM analysis. (Lower): lasso analysis ($\log \lambda = -5.05$).

is an intermediate polar similar to HT Cam. CC Scl is an intriguing case since HT Cam has not yet shown superoutbursts (Ishioka et al. 2002). The unusual behavior of the superhumps in CC Scl may be related to the magnetism of the white dwarf.

3.34. V1208 Tauri

We observed the 2011 December superoutburst of this object. The initial part of the outburst was likely missed. The times of superhump maxima are listed in table 42. The $O-C$ values were close to zero, which strengthens the identification of these superhump to be stage C superhumps. It is likely both 2000 and 2002 observations (Kato et al. 2009) also recorded stage C superhumps, which was not labelled as such in table 2 of Kato et al. (2009).

3.35. V1212 Tauri

Although the object underwent a superoutburst in 2011 January–February, it again underwent another superoutburst in September–October. The times of superhump maxima are listed in table 43. The period given in table 2 was determined with the PDM method. The value of the period suggests that we observed either the very start of stage B or stage C. The supercycle length of this object is about 240 d.

Table 41. Superhump maxima of CC Scl (2011).

E	max*	error	$O-C$†	N‡
0	55870.5914	0.0009	−0.0043	47
1	55870.6551	0.0040	−0.0006	48
2	55870.7078	0.0017	−0.0079	48
15	55871.5040	0.0011	0.0082	38
16	55871.5482	0.0011	−0.0077	37
17	55871.6251	0.0014	0.0092	44
18	55871.6732	0.0023	−0.0027	44
32	55872.5019	0.0011	−0.0142	36
33	55872.5826	0.0019	0.0065	45
51	55873.6608	0.0014	0.0045	44
52	55873.7157	0.0031	−0.0006	44
66	55874.5598	0.0009	0.0033	41
67	55874.6204	0.0020	0.0039	44
69	55874.7376	0.0014	0.0011	35
82	55875.5213	0.0034	0.0046	22
83	55875.5765	0.0014	−0.0002	43
84	55875.6400	0.0014	0.0033	43
85	55875.7007	0.0037	0.0040	43
99	55876.5243	0.0047	−0.0126	24
100	55876.5904	0.0086	−0.0065	27
117	55877.6246	0.0030	0.0076	28
118	55877.6874	0.0060	0.0103	26
119	55877.7551	0.0023	0.0181	14
133	55878.5726	0.0013	−0.0046	27
134	55878.6307	0.0027	−0.0065	27
149	55879.5368	0.0016	−0.0006	20
150	55879.5937	0.0048	−0.0037	21
151	55879.6535	0.0029	−0.0040	21
152	55879.7095	0.0011	−0.0080	20

*BJD−2400000.
†Against max $= 2455870.5957 + 0.060012E$.
‡Number of points used to determine the maximum.

Table 42. Superhump maxima of V1208 Tau (2011).

E	max*	error	$O-C$†	N‡
0	55919.4074	0.0007	0.0021	75
1	55919.4775	0.0008	0.0016	54
9	55920.0347	0.0008	−0.0050	75
10	55920.1086	0.0006	−0.0015	58
34	55921.8064	0.0009	0.0047	73
35	55921.8728	0.0007	0.0006	73
48	55922.7901	0.0007	0.0017	73
49	55922.8548	0.0012	−0.0041	73

*BJD−2400000.
†Against max $= 2455919.4054 + 0.070481E$.
‡Number of points used to determine the maximum.

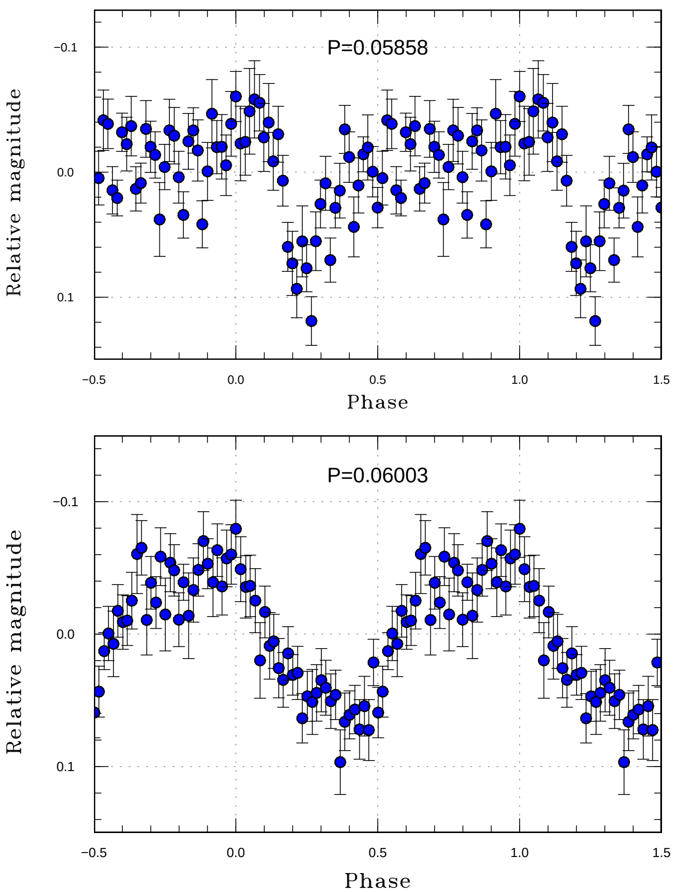

Fig. 33. Profiles of two periodicities in CC Scl (2011). (Upper) orbital variation. (Lower) superhump.

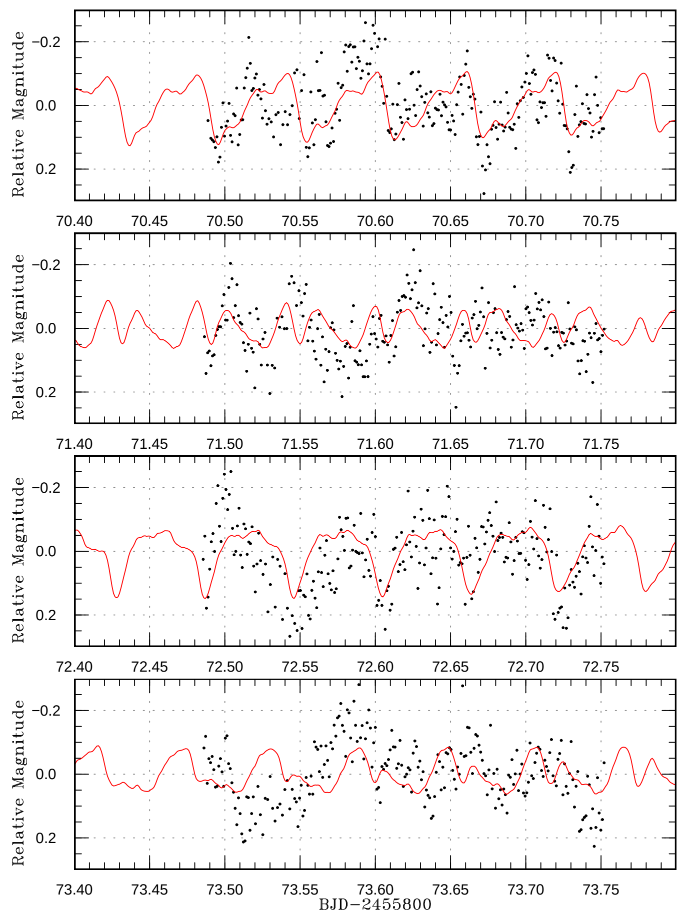

Fig. 34. Synthesized light curve of CC Scl (2011). The points represent observations. The curves represent the expected light curve by adding two waves in figure 33.

Table 43. Superhump maxima of V1212 Tau (2011b).

E	max*	error	$O-C$†	N‡
0	55834.4345	0.0034	−0.0001	21
1	55834.5065	0.0016	0.0021	63
2	55834.5735	0.0008	−0.0005	107
3	55834.6423	0.0010	−0.0016	90
15	55835.4805	0.0017	−0.0001	29
16	55835.5497	0.0019	−0.0006	66
17	55835.6201	0.0010	0.0000	35
18	55835.6906	0.0019	0.0008	19

*BJD−2400000.
†Against max $= 2455834.4346 + 0.069731E$.
‡Number of points used to determine the maximum.

3.36. *DI Ursae Majoris*

Since online data for Rutkowski et al. (2009) are available, we extracted times of superhump maxima for two superoutbursts in 2007 using our method (tables 44 and 45). The resultant values of P_{dot} were not very different from the analysis by Rutkowski et al. (2009). Although we listed times of maxima before the superoutburst ($E \leq 2$) and after the superoutburst ($E \geq 216$) for the first superoutburst, these maxima may not be equivalent to stage A and C superhumps in other SU UMa-type dwarf novae. Although there may be either a discontinuous period change or a phase shift between $E = 182$ and $E = 216$, we could not make a distinction from the available data. The second superoutburst was less observed and the resultant P_{dot} was less reliable. We have also analyzed the entire 2007 light curve to determine the orbital period. We detected a strong signal with a period of 0.0545665(8) d. This period is closer to the spectroscopic period of 0.054564(2) d obtained by Thorstensen et al. (2002b) than the one obtained by Rutkowski et al. (2009) and it likely represents the correct orbital period. The ϵ for the better determined first superoutburst was 1.4%,

Table 44. Superhump maxima of DI UMa (2007).

E	max*	error	$O-C$†	N‡
0	54204.3594	0.0028	−0.0185	20
1	54204.4108	0.0015	−0.0224	24
2	54204.4641	0.0011	−0.0244	44
18	54205.3793	0.0007	0.0070	20
19	54205.4336	0.0005	0.0061	25
20	54205.4894	0.0009	0.0066	35
35	54206.3165	0.0003	0.0050	39
36	54206.3715	0.0002	0.0048	37
37	54206.4246	0.0003	0.0027	39
53	54207.3080	0.0006	0.0022	79
54	54207.3630	0.0003	0.0020	102
55	54207.4200	0.0003	0.0037	69
56	54207.4745	0.0003	0.0030	67
57	54207.5293	0.0003	0.0025	66
71	54208.3073	0.0005	0.0072	40
72	54208.3535	0.0014	−0.0020	32
91	54209.4102	0.0013	0.0051	20
127	54211.4019	0.0010	0.0081	28
128	54211.4583	0.0016	0.0093	16
143	54212.2886	0.0020	0.0110	18
144	54212.3452	0.0008	0.0123	28
182	54214.4491	0.0010	0.0170	31
216	54216.3046	0.0006	−0.0058	39
217	54216.3615	0.0005	−0.0042	46
218	54216.4143	0.0009	−0.0065	28
219	54216.4696	0.0005	−0.0065	24
235	54217.3548	0.0018	−0.0052	11
236	54217.3952	0.0035	−0.0200	11

*BJD−2400000.
†Against max = 2454204.3779 + 0.055243E.
‡Number of points used to determine the maximum.

and there was no need to modify the ϵ by Rutkowski et al. (2009). This ϵ is fairly common for such short-$P_{\rm orb}$ objects and we cannot discriminate DI UMa from other SU UMa-type dwarf novae by ϵ only.

3.37. IY Ursae Majoris

We observed a superoutburst in 2011 June. Only two superhump maxima were recorded: BJD 2455717.0312(4) ($N = 60$) and BJD 2455718.0930(17) ($N = 68$).

3.38. KS Ursae Majoris

We observed a superoutburst in 2012 May. Only two superhump maxima were recorded: BJD 2456052.0468(13) ($N = 52$) and BJD 2456052.1159(18) ($N = 50$).

3.39. MR Ursae Majoris

The times of superhump maxima during the 2012 superoutburst are listed in table 46. Only the late stage of the outburst was observed and we recorded typical stage C superhumps. A comparison of $O-C$ diagrams between different superoutbursts is shown in figure 35.

Table 45. Superhump maxima of DI UMa (2007b).

E	max*	error	$O-C$†	N‡
0	54237.4668	0.0002	0.0044	29
16	54238.3514	0.0005	0.0035	36
17	54238.4042	0.0003	0.0009	39
18	54238.4571	0.0006	−0.0015	41
34	54239.3435	0.0003	−0.0005	33
35	54239.3951	0.0005	−0.0043	33
36	54239.4538	0.0004	−0.0009	30
71	54241.3914	0.0008	−0.0002	22
89	54242.3861	0.0008	−0.0016	29
90	54242.4357	0.0016	−0.0074	28
107	54243.3918	0.0007	0.0079	19
108	54243.4289	0.0018	−0.0103	26
126	54244.4451	0.0016	0.0098	27

*BJD−2400000.
†Against max = 2454237.4624 + 0.055340E.
‡Number of points used to determine the maximum.

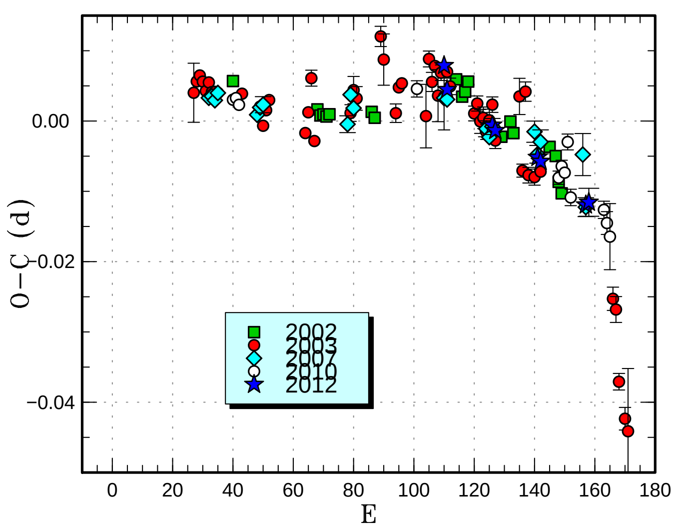

Fig. 35. Comparison of $O-C$ diagrams of MR UMa between different superoutbursts. A period of 0.06512 d was used to draw this figure. Approximate cycle counts (E) after the start of the 2007 superoutburst were used. Since the starts of the other superoutbursts were not well constrained, we shifted the $O-C$ diagrams to best fit the 2007 one.

Table 46. Superhump maxima of MR UMa (2012).

E	max*	error	$O-C$†	N‡
0	56094.3735	0.0005	0.0019	129
1	56094.4353	0.0006	−0.0011	135
16	56095.4070	0.0008	−0.0006	124
17	56095.4713	0.0010	−0.0010	131
31	56096.3792	0.0009	0.0004	133
32	56096.4438	0.0010	0.0003	134
47	56097.4144	0.0012	−0.0003	133
48	56097.4799	0.0020	0.0004	104

*BJD−2400000.
†Against max $= 2456094.3716 + 0.064746E$.
‡Number of points used to determine the maximum.

3.40. PU Ursae Majoris

PU UMa (=SDSS J090103.93+480911.1) is a deeply eclipsing CV below the period gap (Dillon et al. 2008), which was originally discovered by Szkody et al. (2003). Three past outbursts had been recorded before 2012: 2007 October (likely normal outburst), 2009 May (superoutburst; although superhumps were detected, the duration of the observation was insufficient to determine the period) and 2009 December (likely normal outburst).

The 2012 outburst was detected by J. Shears (BAAVSS alert 2830). Subsequent observations detected developing superhumps and eclipses (vsnet-alert 14201, 14214, 14215). The times of recorded eclipses were determined with the Kwee and van Woerden (KW) method (Kwee, van Woerden 1956; modified by the author, see appendix 1), after removing linearly approximated trends around eclipses in order to minimize the effect of superhumps, and are summarized in table 47. We obtained an updated ephemeris of

$$\mathrm{Min(BJD)} = 2453773.4875(3) + 0.07788054(1)E. \quad (2)$$

The times of superhump maxima outside the eclipses are listed in table 48. Except $E = 0$ (stage A), there is a hint of a stage B–C transition around $E = 48$. The overall pattern is similar to relatively long $P_{\rm orb}$-systems such as EG Aqr (Imada et al. 2008b) and NSV 4838 (Imada et al. 2009).

The ϵ for stage B and C superhumps were 4.1% and 3.7%, respectively, and is slightly larger than typical values of SU UMa-type dwarf novae with these $P_{\rm orb}$. A mean profile of stage B superhumps is shown in figure 36. Shears et al. (2012a) also reported observations of the same superoutburst, although they did not distinguish stage B and C superhumps.

3.41. SS Ursae Minoris

Olech et al. (2006) reported observations of the 2004 superoutburst and obtained a mean period of 0.070149(16) d with a negative (global) $P_{\rm dot}$. We observed the late stage of a superoutburst in 2012 March. As in Olech et al. (2006), the the main peak of the superhump was already diminishing and the secondary maximum was developing.

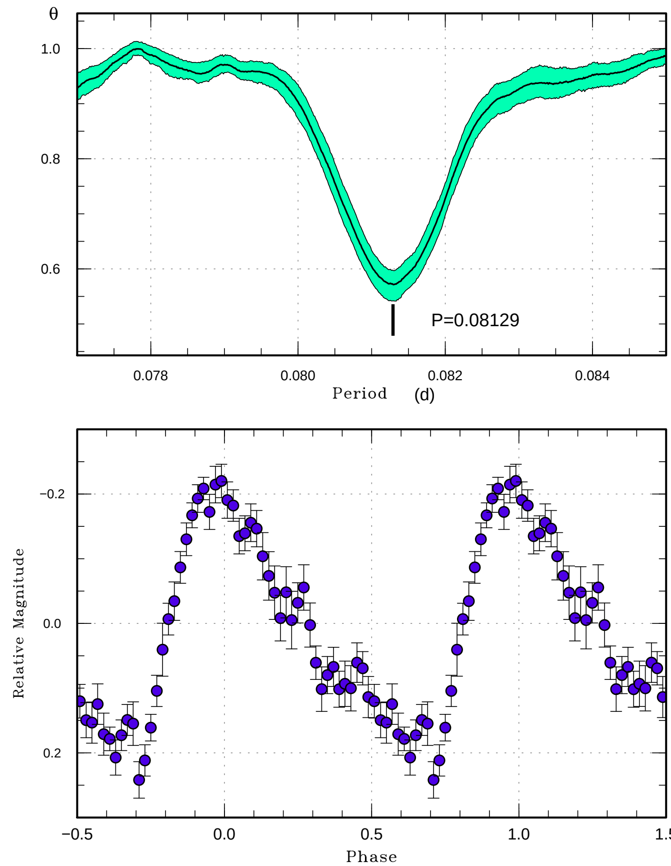

Fig. 36. Stage B superhumps in PU UMa (2012). (Upper): PDM analysis. (Lower): Phase-averaged profile.

Table 47. Eclipse minima of PU UMa (2012).

E	Minimum*	error	$O-C$†
28068	55959.43896	0.00006	0.00019
28069	55959.51692	0.00003	0.00027
28080	55960.37350	0.00005	0.00017
28081	55960.45131	0.00006	0.00010
28092	55961.30786	0.00002	-0.00004
28093	55961.38604	0.00004	0.00026
28110	55962.70976	0.00004	0.00001
28111	55962.78746	0.00004	-0.00017
28112	55962.86561	0.00003	0.00009
28118	55963.33222	0.00004	-0.00058
28119	55963.41032	0.00005	-0.00036
28173	55967.61633	0.00003	0.00010

*BJD−2400000.
†Against equation 2.

Table 48. Superhump maxima of PU UMa (2012).

E	max*	error	$O-C$†	phase‡	N§
0	55959.4659	0.0007	−0.0331	0.13	183
11	55960.3880	0.0009	−0.0029	0.16	123
12	55960.4712	0.0008	−0.0007	0.18	101
22	55961.2845	0.0012	0.0019	0.54	63
23	55961.3685	0.0006	0.0049	0.17	239
24	55961.4507	0.0015	0.0060	0.30	77
35	55962.3444	0.0011	0.0079	0.46	34
36	55962.4242	0.0011	0.0067	0.55	35
40	55962.7460	0.0005	0.0042	0.18	132
41	55962.8265	0.0008	0.0036	0.30	115
47	55963.3178	0.0014	0.0085	0.41	67
48	55963.3998	0.0011	0.0094	0.30	69
83	55966.2293	0.0045	0.0015	0.41	28
84	55966.3101	0.0015	0.0013	0.33	40
100	55967.5984	0.0006	−0.0076	0.19	96
121	55969.2966	0.0039	−0.0118	0.68	132

*BJD−2400000.
†Against max $= 2455959.4991 + 0.081068E$.
‡Orbital phase.
§Number of points used to determine the maximum.

Table 49. Superhump maxima of SS UMi (2012).

E	max*	error	$O-C$†	N‡
0	56009.5129	0.0007	0.0029	53
1	56009.5786	0.0009	−0.0017	53
2	56009.6468	0.0014	−0.0039	50
5	56009.8662	0.0043	0.0044	80
6	56009.9295	0.0014	−0.0026	80
7	56010.0062	0.0020	0.0037	54
15	56010.5616	0.0015	−0.0038	52
33	56011.8328	0.0053	0.0010	80

*BJD−2400000.
†Against max $= 2456009.5100 + 0.070358E$.
‡Number of points used to determine the maximum.

We list times of maxima of these humps in table 49. At this and following stages, the secondary humps were the dominant signal, which are listed in table 50. These secondary humps persisted during the quiescent state following the superoutburst, and the behavior is similar to the late stage of VW Hyi (subsection 3.22) and V344 Lyr (Kato et al. 2012a; Wood et al. 2011). Since SS UMi is considered to have a high mass-transfer rate comparable to ER UMa stars (Kato et al. 2000a; Olech et al. 2006), these secondary humps are possibly "traditional" late superhumps arising from the stream impact point. The signal became less convincing after the next normal outburst. A period analysis of the entire observation (BJD 2456007–2456038) yielded a photometric orbital period of 0.067855(7) d, which is slightly longer than the spectroscopic period of 0.06778(4) d in Thorstensen et al. (1996).

Table 50. Superhump maxima of SS UMi (2012) (secondary humps).

E	max*	error	$O-C$†	N‡
0	56009.5410	0.0012	−0.0003	52
1	56009.6083	0.0007	−0.0029	52
4	56009.8206	0.0009	−0.0004	80
5	56009.8899	0.0010	−0.0010	79
6	56009.9611	0.0006	0.0002	80
14	56010.5134	0.0007	−0.0070	53
15	56010.5876	0.0009	−0.0028	52
16	56010.6528	0.0010	−0.0075	50
18	56010.7969	0.0006	−0.0033	71
19	56010.8669	0.0006	−0.0032	79
20	56010.9348	0.0009	−0.0053	79
28	56011.4990	0.0009	−0.0006	52
29	56011.5696	0.0016	0.0000	86
30	56011.6398	0.0005	0.0003	74
33	56011.8523	0.0006	0.0030	79
34	56011.9197	0.0008	0.0004	79
35	56011.9931	0.0006	0.0039	69
42	56012.4833	0.0011	0.0044	52
43	56012.5527	0.0009	0.0039	64
44	56012.6247	0.0004	0.0059	104
45	56012.6965	0.0045	0.0078	48
56	56013.4677	0.0006	0.0097	53
57	56013.5267	0.0027	−0.0013	27
58	56013.6075	0.0015	0.0096	53
59	56013.6717	0.0011	0.0038	36
71	56014.5123	0.0012	0.0051	21
72	56014.5843	0.0008	0.0071	27
73	56014.6504	0.0011	0.0033	34
78	56014.9951	0.0015	−0.0017	46
85	56015.4873	0.0017	0.0009	27
86	56015.5525	0.0007	−0.0038	53
87	56015.6182	0.0014	−0.0081	53
88	56015.6914	0.0027	−0.0048	18
92	56015.9750	0.0008	−0.0010	52
100	56016.5337	0.0012	−0.0019	20
101	56016.5996	0.0009	−0.0059	28
102	56016.6762	0.0012	0.0008	27
106	56016.9480	0.0006	−0.0072	55

*BJD−2400000.
†Against max $= 2456009.5412 + 0.069943E$.
‡Number of points used to determine the maximum.

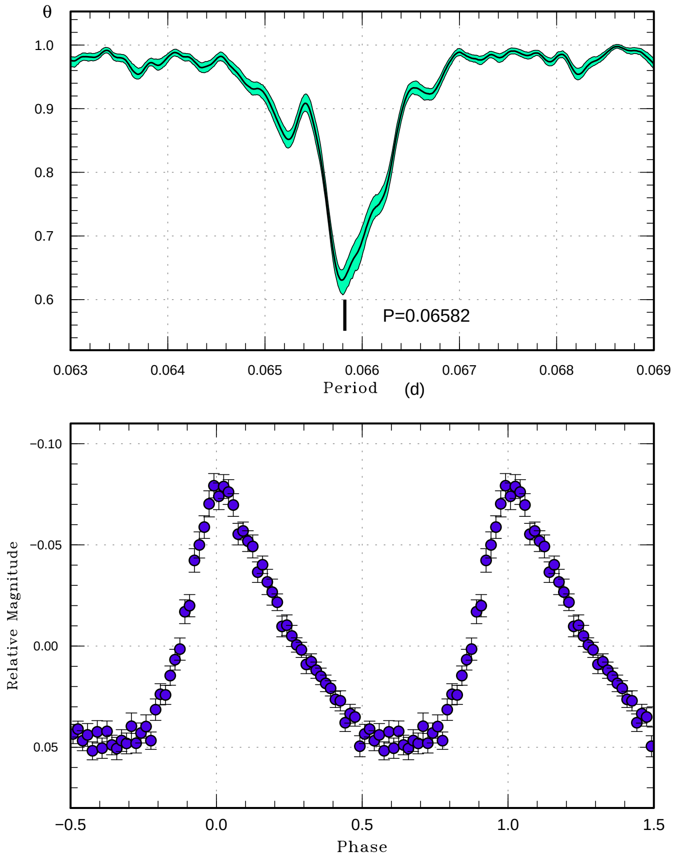

Fig. 37. Superhumps in 1RXS J231935 (2011). (Upper): PDM analysis. (Lower): Phase-averaged profile.

3.42. *1RXS J231935.0+364705*

This object (hereafter 1RXS J231935) was selected as a variable star, likely a dwarf nova, during the course of identification of the ROSAT sources (Denisenko, Sokolovsky 2011). The two previously known outbursts occurred in 2009 November and 2010 December, and both appear to be normal outbursts (H. Maehara detected no superhumps during the 2009 outburst). The 2011 September outburst was detected by E. Muyllaert (BAAVSS alert 2710). Subsequent observations confirmed the presence of superhumps (vsnet-alert 13711, 13712, 13719; figure 37). The times of superhump maxima are listed in table 51. The $O-C$ diagram clearly shows the familiar pattern of stages B and C. The $P_{\rm dot}$ for stage B superhumps was large [$+11.6(1.7) \times 10^{-5}$], typical for an object with this $P_{\rm SH}$.

3.43. *ASAS J224349+0809.5*

The 2011 June outburst of this object (hereafter ASAS J224349) was detected by Y. Maeda at a visual magnitude of 13.2 (vsnet-alert 13458). Due to the unfavorable seasonal condition, we obtained only two superhump maxima: BJD 2455740.6014(5) (N=40) and 2455741.5730(5) (N=49).

Table 51. Superhump maxima of 1RXS J231935.

E	max*	error	$O-C$†	N‡
0	55835.4280	0.0003	−0.0040	65
1	55835.4930	0.0003	−0.0048	68
2	55835.5596	0.0002	−0.0039	102
3	55835.6240	0.0002	−0.0052	203
4	55835.6920	0.0004	−0.0030	84
14	55836.3491	0.0004	−0.0035	49
15	55836.4142	0.0003	−0.0042	213
16	55836.4793	0.0002	−0.0049	362
17	55836.5457	0.0002	−0.0043	389
18	55836.6113	0.0002	−0.0044	217
19	55836.6764	0.0003	−0.0051	132
29	55837.3357	0.0003	−0.0035	157
30	55837.4024	0.0002	−0.0025	169
31	55837.4658	0.0002	−0.0049	250
32	55837.5312	0.0003	−0.0052	267
33	55837.5978	0.0002	−0.0044	267
34	55837.6649	0.0005	−0.0031	93
44	55838.3270	0.0007	0.0014	86
45	55838.3920	0.0006	0.0006	126
46	55838.4587	0.0006	0.0015	125
47	55838.5220	0.0038	−0.0009	41
56	55839.1186	0.0011	0.0038	94
57	55839.1859	0.0006	0.0054	123
59	55839.3162	0.0006	0.0041	98
60	55839.3808	0.0007	0.0030	116
61	55839.4481	0.0006	0.0045	121
62	55839.5133	0.0006	0.0039	85
63	55839.5871	0.0025	0.0120	77
64	55839.6491	0.0015	0.0082	41
75	55840.3753	0.0005	0.0110	51
76	55840.4449	0.0014	0.0149	50
77	55840.5081	0.0007	0.0123	57
78	55840.5728	0.0006	0.0112	57
79	55840.6379	0.0006	0.0106	44
102	55842.1444	0.0006	0.0045	112
103	55842.2125	0.0005	0.0068	119
104	55842.2761	0.0008	0.0047	66
118	55843.1927	0.0005	0.0005	95
140	55844.6357	0.0010	−0.0033	31
141	55844.7006	0.0011	−0.0041	31
142	55844.7650	0.0008	−0.0054	36
143	55844.8324	0.0009	−0.0038	33
144	55844.8970	0.0009	−0.0050	35
153	55845.4853	0.0036	−0.0086	54
154	55845.5512	0.0010	−0.0084	59
155	55845.6205	0.0010	−0.0049	83
157	55845.7555	0.0039	−0.0014	34
159	55845.8803	0.0010	−0.0081	28

*BJD−2400000.

†Against max $= 2455835.4320 + 0.065764E$.

‡Number of points used to determine the maximum.

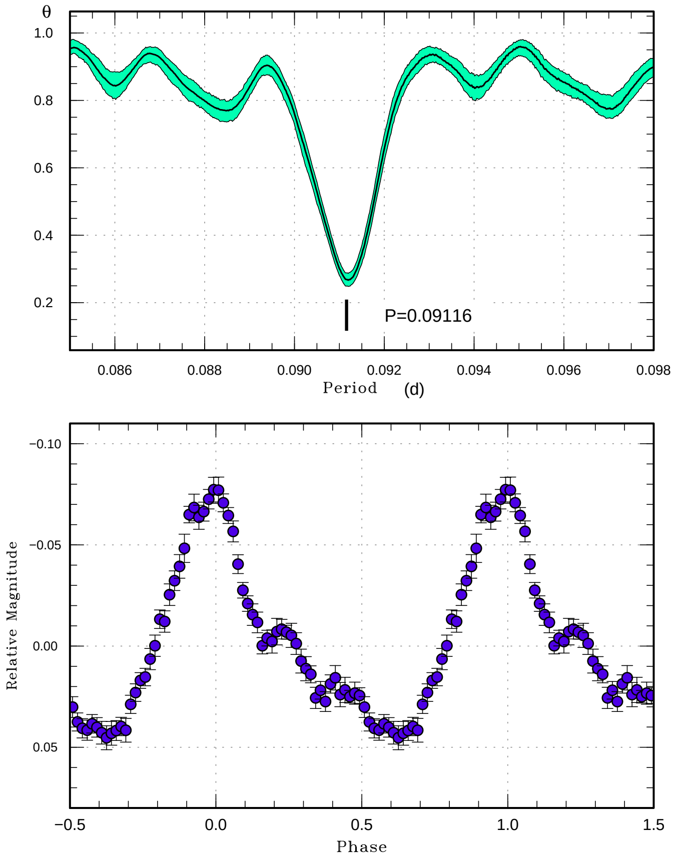

Fig. 38. Superhumps in DDE 19 (2011). (Upper): PDM analysis. (Lower): Phase-averaged profile.

3.44. DDE 19

DDE 19 is a CV discovered by D. Denisenko.[5] The object is located at $00^{\mathrm{h}}38^{\mathrm{m}}37\overset{\mathrm{s}}{.}40$, $+79^{\circ}21'37\overset{''}{.}5$ (J2000.0). During its outburst in 2011 November, superhumps were detected (vsnet-alert 13886, 13890; figure 38). The times of superhump maxima are listed in table 52. The object faded quickly after these observations, and we only observed the late stage of this superoutburst. We attributed the superhumps to stage C superhumps in table 2.

3.45. MASTER OT J072948.66+593824.4

This object (hereafter MASTER J072948) is a transient detected at an unfiltered CCD magnitude of 13.3 on 2012 February 17 (Balanutsa et al. 2012c; see also vsnet-alert 14249). Although subsequent observations detected superhump-like modulations (vsnet-alert 14252), their waveform was rather irregular and the variation did not appear to be expressed by a single period (vsnet-alert 14253, 14258, 14263). The observed maxima could not be expressed by any single period, and there was likely a superposition of two close periods (vsnet-alert 14265).

PDM and lasso analysis (see subsection 3.78 for the application of lasso and separation of two signals) is shown in figure 39. The lasso analysis favored the co-existence of two periods 0.06416(4) d and 0.06625(4) d. A period of 0.06208(3) d, a one-day alias of the 0.06625-d period, cannot be excluded instead of the 0.06625-d period. The mean profiles of these signals are shown in figure 40. While the 0.06416-d signal resembles a profile of superhumps (faster rise, sharper maximum), the other signal has a sharper minimum. A combination of these signals partly reproduced the actual light curve during the plateau phase (figure 41). Based on the profile, we may identify the 0.06416-d signal as superhumps. We might then interpret that the 0.06625-d period is the orbital period, and the 0.06416-d signal is 3.2% shorter than P_{orb}. Although negative superhumps are unexpected in ordinary SU UMa-type dwarf novae, this interpretation might explain why the profile of superhumps was so unstable (as in ER UMa, cf. Ohshima et al. 2012), and why the orbital signal is so strongly visible in a non-eclipsing system. Since the object started rapidly fading only three days after the start of our observation, the baseline for period analysis was insufficient to distinguish other possible periods or interpretations. Future observations in quiescence and in superoutbursts are absolutely needed.

[5] <http://hea.iki.rssi.ru/~denis/VarDDE.html>

Table 52. Superhump maxima of DDE 19 (2011).

E	max*	error	$O-C$†	N‡
0	55888.6444	0.0004	0.0018	97
2	55888.8256	0.0004	0.0006	96
11	55889.6458	0.0009	−0.0001	87
12	55889.7356	0.0008	−0.0014	96
13	55889.8258	0.0006	−0.0025	96
33	55891.6541	0.0007	0.0017	96
34	55891.7445	0.0013	0.0008	96
35	55891.8339	0.0010	−0.0010	96

*BJD−2400000.
†Against max $= 2455888.6425 + 0.091210E$.
‡Number of points used to determine the maximum.

3.46. MASTER OT J174305.70+231107.8

This object (hereafter MASTER J174305) is a transient detected at an unfiltered CCD magnitude of 15.6 on 2012 April 5 (Balanutsa et al. 2012a). Subsequent observations detected superhumps (vsnet-alert 14428; figure 42). Two superhump maxima were recorded: BJD 2456027.8604(12) ($N = 79$) and BJD 2456027.9281(9) ($N = 82$). The superhump period by the PDM method was 0.0670(5) d.

3.47. MASTER OT J182201.93+324906.7

This object (hereafter MASTER J182201) is a transient detected at an unfiltered CCD magnitude of 15.4 on 2012 April 29 (Balanutsa et al. 2012b). Subsequent observations detected superhumps (vsnet-alert 14529; figure 43). Two superhump maxima were recorded: BJD 2456050.4464(6) ($N = 33$) and 2456050.5081(4) ($N = 33$). The superhump period by the PDM method was 0.0618(2) d (figure 43).

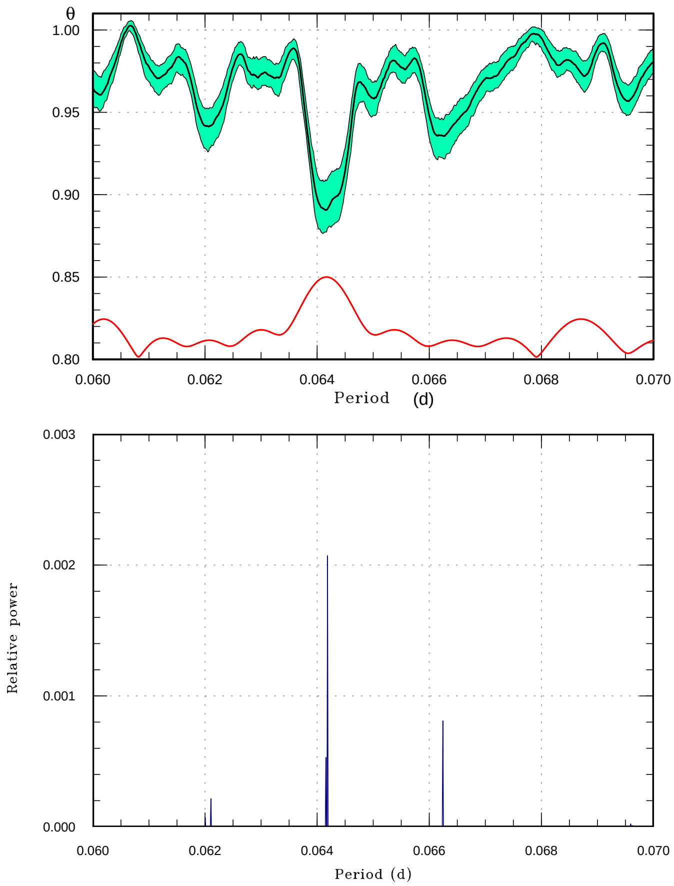

Fig. 39. Period analysis in MASTER J072948 (2012). (Upper): PDM analysis. The lower curve at the bottom indicates the window function. (Lower): lasso analysis ($\log\lambda = -4.34$).

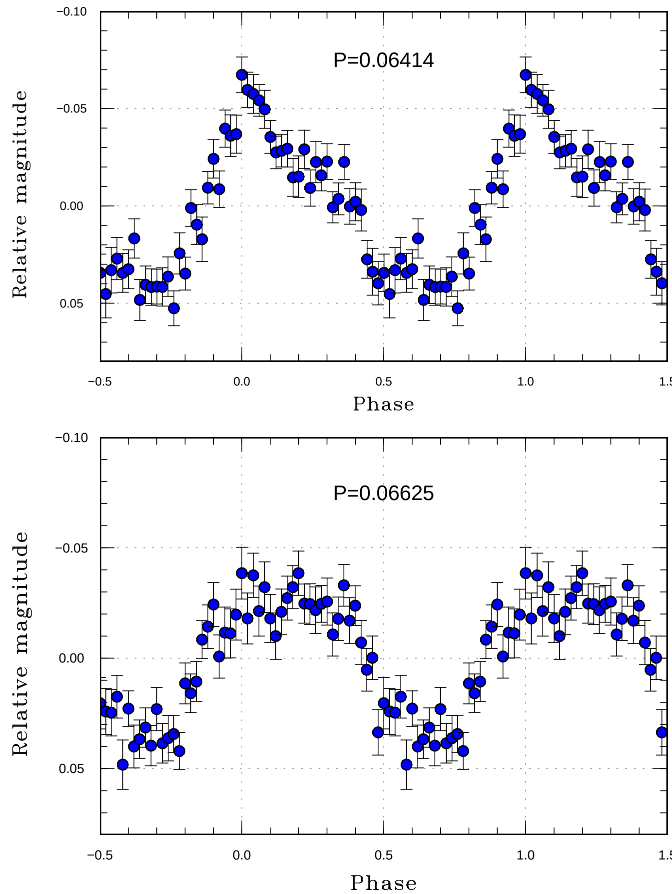

Fig. 40. Profiles of two periodicities in MASTER J072948 (2012).

3.48. MisV 1446

MisV 1446 was detected as a transient by the MISAO project, and it could be probably identified with the X-ray source 1RXS J074112.2−094529 (vsnet-alert 14080). The coordinates of the object are $07^{\mathrm{h}}41^{\mathrm{m}}12\overset{\mathrm{s}}{.}70$, $-09^{\circ}45'55\overset{''}{.}9$. Multicolor photometry by H. Sato was consistent with that of a color of a dwarf nova in outburst (vsnet-alert 14085). Subsequent observations recorded superhumps (vsnet-alert 14096, 14102, 14104; figure 44). The times of superhump maxima are listed in table 53. It appears that the observations recorded the late stage of a superoutburst, and that late part of stage B and stage C were recorded. It was impossible to measure P_{dot} for stage B.

3.49. SBS 1108+574

This object (hereafter SBS 1108) was originally selected as an ultraviolet-excess object during the course of the Second Byurakan Survey (SBS, Markarian, Stepanian 1983). An outburst of this object was detected by CRTS on 2012 April 22 (=CSS120422:111127+571239). The very blue color ($u-g=-0.3$) in quiescence was very notable (vsnet-alert 14475, 14483). Subsequent observations clarified that this object is an ultra-short period SU UMa-type dwarf nova showing superhumps (vsnet-alert 14480, 14484, 14493; figure 45). Although it was not initially clear whether this object belongs to AM CVn-type objects or hydrogen-rich objects, spectroscopic observation (Garnavich et al. 2012) confirmed that the object is hydrogen-rich.

The times of superhump maxima are listed in table 54. Although the epoch of the start of the outburst is unknown, the $O-C$ variation was very similar to that of ordinary short-P_{orb} SU UMa-type dwarf novae: consisting of stage B with a longer P_{SH} and a positive P_{dot} and stage C with a shorter P_{SH} with a relatively constant period (figure 46). The amplitudes of superhumps became smaller near the end of stage B as in ordinary short-P_{orb} SU UMa-type dwarf novae (Kato et al. 2012a) and became larger at the start of stage C (figure 47). The object also slightly brightened after the stage B–C transition (figure 46). This feature is commonly seen in objects with distinct stage B–C transitions (cf. Kato et al. 2003b; Kato et al. 2012a). The transition from stage B to C was abrupt, as in ordinary short-P_{orb} SU UMa-type dwarf novae. The stage C superhumps persisted after the rapid decline without a phase shift.

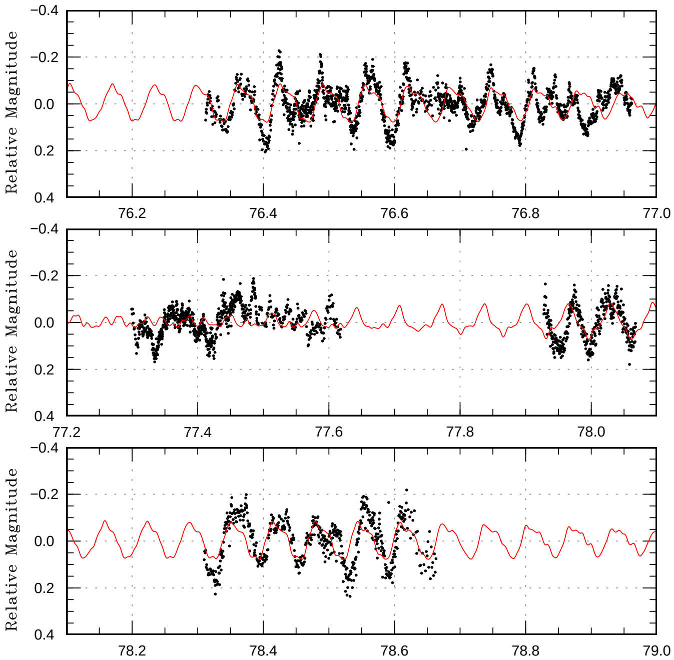

Fig. 41. Synthesized light curve of MASTER J072948 (2011). The points represent observations. The curves represent the expected light curve by adding two waves in figure 40

.

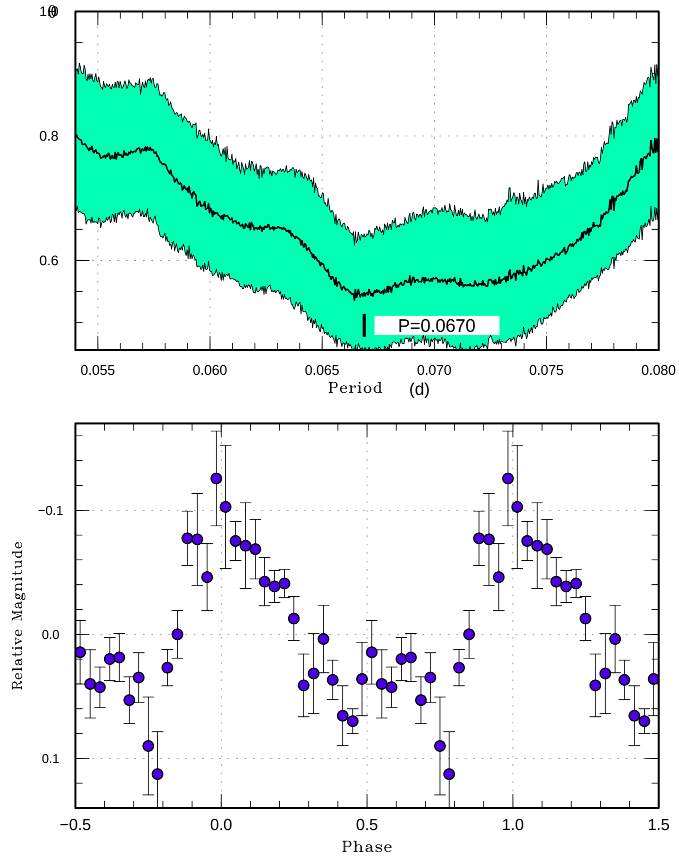

Fig. 42. Superhumps in MASTER J174305 (2012). (Upper): PDM analysis. (Lower): Phase-averaged profile.

In addition to superhumps, we detected a stable period of 0.038449(6) d, which we identified to be the orbital period (figure 48). The ϵ for stage B and C superhumps were 1.74(2)% and 1.11(2)%, respectively. By applying the ϵ–q relation in Kato et al. (2009) to the ϵ of stage C superhumps, we obtained $q = 0.06$. The ϵ or q is larger than those of many extreme WZ Sge-type dwarf novae, and this implies that the secondary is denser, or more massive, than in ordinary dwarf novae. The estimated volume radii of the Roche lobe of the secondary is located below the theoretical radius of a brown dwarf when we assume a typical mass (0.7 $M_{\odot}$) for a white dwarf in a dwarf nova (figure 49). Only with a massive ($\geq$1.0 $M_{\odot}$) white dwarf, the secondary can be a normal lower main-sequence star. Since sustained nuclear burning is not expected for a brown dwarf, this finding suggests that this secondary is a somewhat evolved star whose hydrogen envelope was mostly stripped during the mass-exchange. The spectrum taken in quiescence (Pavlenko et al. in preparation) showing the enhanced abundance of helium is consistent with this interpretation. The object may be analogous to OT J112253.3−111037 (= CSS100603:112253−111037) (Kato et al. 2010; Breedt et al. 2012; note also the unusual $u-g$ color mentioned in Kato et al. 2012b). Further detailed radial-velocity study would enable to clarify the nature of this binary.

3.50. SDSS J073208.11+413008.7

We observed the 2012 superoutburst of this object (hereafter SDSS J073208; the object was selected by Wils et al. 2010, see a comment in Kato et al. 2010). The times of superhump maxima are listed in table 55. The period listed in table 2 was determined by the PDM method. This period appears to be a global average of stage B and C superhumps.

3.51. SDSS J080303.90+251627.0

This object (hereafter SDSS J080303) was discovered as a CV during the course of the SDSS (Szkody et al. 2005). Szkody et al. (2005) identified a spectroscopic period of 0.071 d. The object showed multiple outbursts in the CRTS data. The 2011 outburst was detected by J. Shears (BAAVSS alert 2806). The detection was sufficiently early to observe the early evolution of superhumps (vsnet-alert 14006, 14015, 14033). The object showed large variation of the superhump period (vsnet-alert 14063). The mean superhump profile is shown in figure 50.

The times of superhump maxima are listed in table 56. The initial stage A with growing superhumps is immediately recognizable. We considered E =27–31 to be stage B–C transition and listed the period according to these identifications in table 2.

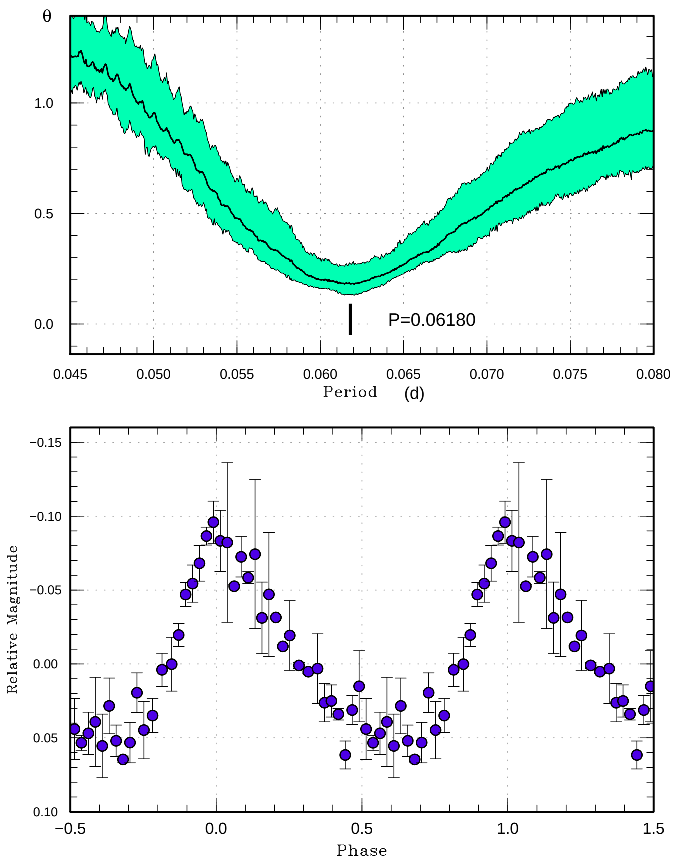

Fig. 43. Superhumps in MASTER J182201 (2012). (Upper): PDM analysis. (Lower): Phase-averaged profile.

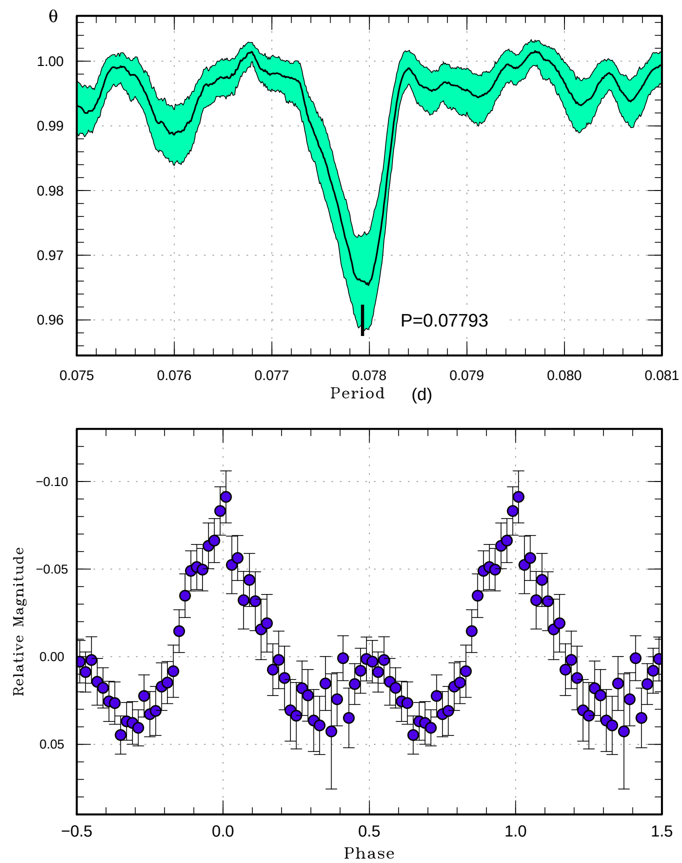

Fig. 44. Superhumps in MisV 1446 (2012). (Upper): PDM analysis. (Lower): Phase-averaged profile.

The large negative $P_{\rm dot}$ [global value of $-79(8)\times10^{-5}$] and the long $P_{\rm SH}$ resemble those of MN Dra (Pavlenko et al. 2010b).

3.52. SDSS J165359.06+201010.4

We observed a superoutburst in 2012 May of this SU UMa-type dwarf nova (hereafter SDSS J165359). The times of superhumps are listed in table 57. Since the object faded rapidly after our final observation, the superhumps recorded on the last three nights were most likely stage C superhumps. Although the identification of the stage of earlier observations was unclear due to the long gap in the observation, a comparison of the $O-C$ diagram with the 2010 superoutburst suggests that we observed the earlier stage of stage B (figure 51).

3.53. SDSS J170213.26+322954.1

This object (hereafter SDSS J170213) is an eclipsing SU UMa-type dwarf nova in the period gap (Boyd et al. 2006; Littlefair et al. 2006). Boyd et al. (2006) reported an analysis of the 2005 superoutburst. Kato et al. (2009) analyzed their data and concluded that this object showed increase in the $P_{\rm SH}$ during the middle-to-late stage of a superoutburst, contrary to most SU UMa-type dwarf novae with similar $P_{\rm SH}$.

The 2011 superoutburst by detected by G. Poyner with an unfiltered CCD magnitude of 13.93 (vsnet-outburst 13058). Subsequent observations confirmed the presence of superhumps and eclipses (vsnet-alert 13524, 13526, 13528, 13532). The times of recorded eclipses, determined with the KW method, after removing linearly approximated trends around eclipses in order to minimize the effect of superhumps, are summarized in table 58. We obtained an updated ephemeris of

$$\mathrm{Min(BJD)} = 2453648.23651(31) + 0.100082207(15)E. \quad (3)$$

The times of superhump maxima determined outside the eclipses are listed in table 59. There were clear stage A ($E \le 32$) and stage B with a positive $P_{\rm dot}$. There was no indication of a transition to stage C despite that the observation covered the early stage of the rapid decline. The large positive $P_{\rm dot}$ confirmed the 2005 results, and as suggested in Kato et al. (2009), this object mimics a short-$P_{\rm orb}$ system both in $O-C$ variation and stage transitions. The $\epsilon = 6.0\%$ is, however, much larger than those in systems with short-$P_{\rm orb}$. This object appears to have relatively infrequent outbursts [the only known outbursts have been in 2005 September–October (superoutburst), 2006 July (normal outburst), 2007 September (superoutburst), 2009 February (normal outburst), 2009 October (super-

Table 53. Superhump maxima of MisV 1446 (2012).

E	max*	error	$O-C$†	N‡
0	55938.0155	0.0031	−0.0006	134
1	55938.0949	0.0006	0.0010	207
2	55938.1682	0.0005	−0.0034	312
3	55938.2450	0.0006	−0.0044	281
4	55938.3233	0.0006	−0.0040	279
5	55938.4019	0.0015	−0.0031	113
13	55939.0278	0.0012	0.0003	178
14	55939.1040	0.0007	−0.0013	287
15	55939.1822	0.0007	−0.0009	158
16	55939.2639	0.0012	0.0030	155
17	55939.3371	0.0008	−0.0016	124
26	55940.0351	0.0031	−0.0038	138
27	55940.1209	0.0010	0.0042	108
35	55940.7515	0.0016	0.0123	81
36	55940.8206	0.0008	0.0035	67
37	55940.9001	0.0009	0.0053	82
40	55941.1329	0.0011	0.0046	225
41	55941.2098	0.0012	0.0038	157
42	55941.2873	0.0010	0.0034	155
44	55941.4427	0.0006	0.0032	301
45	55941.5184	0.0007	0.0011	407
48	55941.7484	0.0104	−0.0023	18
49	55941.8340	0.0123	0.0055	10
56	55942.3688	0.0037	−0.0043	191
57	55942.4462	0.0025	−0.0047	408
58	55942.5173	0.0010	−0.0114	336
69	55943.3793	0.0014	−0.0053	31

*BJD−2400000.
†Against max $= 2455938.0160 + 0.077806E$.
‡Number of points used to determine the maximum.

outburst), and 2011 July (superoutburst)] and probably indeed resembles EF Peg (cf. Howell et al. 1993; Kato 2002b) as proposed in Kato et al. (2009), rather than an unusual system with a large $P_{\rm dot}$, GX Cas (Kato et al. 2012a). The behavior of $O-C$ variation was similar between 2005 and 2011 outbursts (figure 52). It is noteworthy that stage A lasted much longer than in other systems.

3.54. SDSS J172102.48+273301.2

This object (hereafter SDSS J172102) was originally selected as a helium CV using the SDSS colors and confirmed by spectroscopy (Rau et al. 2010). Although there had been no record of outbursts, CRTS detected this object in outburst on 2012 June 8 at an unfiltered CCD magnitude of 16.4 (CSS120608:172102+273301). A quick follow-up observation confirmed the presence of superhumps on June 9 (vsnet-alert 14653). A retrospective study indicated that the object was recorded at unfiltered CCD magnitudes of 16.0–16.2 on June 5 at MASTER-Kislovodsk (vsnet-alert 14657). The object rapidly faded to 18.9 on June 11 (Goff) and 19.1 on June 15 (CRTS). The object was thus likely a superoutburst of an AM CVn-type object detected during its final stage. The object un-

Table 54. Superhump maxima of SBS 1108 (2012).

E	max*	error	$O-C$†	N‡
0	56040.6654	0.0007	−0.0064	67
1	56040.7056	0.0007	−0.0053	56
3	56040.7820	0.0006	−0.0070	63
11	56041.0923	0.0021	−0.0090	59
12	56041.1304	0.0010	−0.0099	80
13	56041.1755	0.0042	−0.0039	80
14	56041.2158	0.0045	−0.0027	53
18	56041.3662	0.0007	−0.0085	32
19	56041.4061	0.0005	−0.0076	40
20	56041.4448	0.0004	−0.0079	43
21	56041.4834	0.0005	−0.0084	42
22	56041.5227	0.0004	−0.0082	43
23	56041.5617	0.0005	−0.0082	42
24	56041.6002	0.0004	−0.0087	108
25	56041.6390	0.0005	−0.0090	71
26	56041.6778	0.0004	−0.0093	69
27	56041.7171	0.0006	−0.0089	69
33	56041.9475	0.0022	−0.0128	62
34	56041.9887	0.0012	−0.0107	121
35	56042.0287	0.0010	−0.0097	122
36	56042.0697	0.0042	−0.0078	35
44	56042.3807	0.0006	−0.0091	42
45	56042.4206	0.0005	−0.0083	42
46	56042.4600	0.0005	−0.0079	42
47	56042.4995	0.0005	−0.0075	43
48	56042.5390	0.0004	−0.0070	43
49	56042.5768	0.0005	−0.0083	42
50	56042.6166	0.0007	−0.0075	37
51	56042.6560	0.0007	−0.0072	67
52	56042.6963	0.0005	−0.0059	69
53	56042.7332	0.0005	−0.0081	61
54	56042.7724	0.0004	−0.0079	14
55	56042.8130	0.0011	−0.0064	10
56	56042.8522	0.0011	−0.0062	14
57	56042.8875	0.0019	−0.0099	14
68	56043.3183	0.0006	−0.0087	26
69	56043.3565	0.0005	−0.0095	26
70	56043.3964	0.0007	−0.0086	24
71	56043.4355	0.0008	−0.0086	26
72	56043.4770	0.0014	−0.0061	26
73	56043.5145	0.0009	−0.0077	26
94	56044.3342	0.0007	−0.0080	75
95	56044.3729	0.0006	−0.0083	98
96	56044.4121	0.0008	−0.0081	96
97	56044.4503	0.0024	−0.0089	21
98	56044.4894	0.0009	−0.0089	12
99	56044.5289	0.0012	−0.0085	12
100	56044.5709	0.0016	−0.0055	8
101	56044.6077	0.0009	−0.0077	38
102	56044.6465	0.0008	−0.0080	53
103	56044.6850	0.0010	−0.0085	50
104	56044.7266	0.0009	−0.0060	53

*BJD−2400000.
†Against max $= 2456040.6718 + 0.039046E$.
‡Number of points used to determine the maximum.

Table 54. Superhump maxima of SBS 1108 (2012) (continued).

E	max*	error	$O-C$†	N‡
105	56044.7671	0.0014	−0.0045	36
106	56044.8053	0.0014	−0.0054	14
107	56044.8460	0.0025	−0.0038	14
108	56044.8851	0.0014	−0.0037	14
109	56044.9287	0.0031	0.0009	10
118	56045.2718	0.0008	−0.0074	20
119	56045.3110	0.0009	−0.0073	21
120	56045.3523	0.0007	−0.0051	19
121	56045.3914	0.0012	−0.0050	19
122	56045.4288	0.0004	−0.0066	20
123	56045.4678	0.0007	−0.0067	22
124	56045.5092	0.0016	−0.0043	38
125	56045.5457	0.0009	−0.0068	35
128	56045.6634	0.0020	−0.0063	27
129	56045.7028	0.0009	−0.0060	31
130	56045.7438	0.0011	−0.0040	35
131	56045.7821	0.0015	−0.0048	36
132	56045.8224	0.0008	−0.0035	35
134	56045.8998	0.0013	−0.0042	12
136	56045.9809	0.0017	−0.0012	72
137	56046.0187	0.0012	−0.0024	81
144	56046.2898	0.0011	−0.0046	14
145	56046.3279	0.0007	−0.0056	20
146	56046.3673	0.0010	−0.0053	20
152	56046.6089	0.0022	0.0021	12
153	56046.6420	0.0008	−0.0039	13
154	56046.6783	0.0019	−0.0066	14
155	56046.7206	0.0017	−0.0033	13
156	56046.7576	0.0010	−0.0054	13
157	56046.7970	0.0008	−0.0050	14
158	56046.8373	0.0016	−0.0038	14
159	56046.8747	0.0019	−0.0055	14
160	56046.9123	0.0024	−0.0068	14
170	56047.3054	0.0016	−0.0042	20
171	56047.3472	0.0025	−0.0015	20
172	56047.3861	0.0013	−0.0017	35
173	56047.4238	0.0015	−0.0029	30
174	56047.4636	0.0008	−0.0022	13
175	56047.4987	0.0007	−0.0062	13
176	56047.5407	0.0007	−0.0032	9
178	56047.6210	0.0016	−0.0010	12
179	56047.6593	0.0017	−0.0017	14
180	56047.6971	0.0020	−0.0030	14
181	56047.7396	0.0029	0.0005	9
182	56047.7811	0.0043	0.0029	13
183	56047.8170	0.0036	−0.0002	14
184	56047.8543	0.0029	−0.0020	14
185	56047.8944	0.0018	−0.0009	14
195	56048.2844	0.0011	−0.0014	20
196	56048.3227	0.0010	−0.0021	20
197	56048.3627	0.0010	−0.0012	20

*BJD−2400000.
†Against max $= 2456040.6718 + 0.039046E$.
‡Number of points used to determine the maximum.

Table 54. Superhump maxima of SBS 1108 (2012) (continued).

E	max*	error	$O-C$†	N‡
198	56048.3996	0.0013	−0.0034	15
199	56048.4412	0.0012	−0.0007	19
200	56048.4785	0.0022	−0.0025	18
201	56048.5203	0.0010	0.0003	20
204	56048.6349	0.0018	−0.0023	14
205	56048.6749	0.0025	−0.0014	14
206	56048.7141	0.0025	−0.0012	14
207	56048.7513	0.0019	−0.0031	14
208	56048.7908	0.0014	−0.0026	13
209	56048.8291	0.0033	−0.0033	14
220	56049.2630	0.0047	0.0010	14
221	56049.2994	0.0049	−0.0016	17
222	56049.3368	0.0014	−0.0033	20
223	56049.3781	0.0048	−0.0010	20
224	56049.4163	0.0021	−0.0018	20
230	56049.6538	0.0026	0.0014	14
232	56049.7313	0.0024	0.0008	11
234	56049.8109	0.0040	0.0023	14
236	56049.8953	0.0031	0.0086	14
237	56049.9301	0.0010	0.0044	7
248	56050.3554	0.0020	0.0001	82
249	56050.4003	0.0022	0.0060	85
252	56050.5193	0.0017	0.0079	14
253	56050.5521	0.0010	0.0016	14
255	56050.6310	0.0033	0.0024	13
256	56050.6719	0.0013	0.0043	13
274	56051.3804	0.0024	0.0100	44
276	56051.4498	0.0025	0.0013	33
281	56051.6506	0.0042	0.0069	9
282	56051.7007	0.0029	0.0179	14
283	56051.7320	0.0035	0.0101	13
284	56051.7690	0.0024	0.0081	13
285	56051.8086	0.0020	0.0087	13
287	56051.8760	0.0019	−0.0020	12
306	56052.6258	0.0054	0.0059	13
307	56052.6741	0.0038	0.0151	14
308	56052.7138	0.0063	0.0158	32
309	56052.7508	0.0057	0.0137	35
310	56052.7808	0.0034	0.0047	31
311	56052.8246	0.0017	0.0094	34
312	56052.8690	0.0038	0.0148	29
313	56052.9066	0.0045	0.0134	25
323	56053.2924	0.0029	0.0088	16
324	56053.3230	0.0036	0.0002	16
332	56053.6286	0.0019	−0.0065	9
333	56053.6690	0.0019	−0.0052	14
334	56053.7237	0.0024	0.0105	13
335	56053.7632	0.0029	0.0110	10
338	56053.8731	0.0108	0.0038	11
352	56054.4292	0.0043	0.0132	46
354	56054.5078	0.0035	0.0137	29

*BJD−2400000.
†Against max $= 2456040.6718 + 0.039046E$.
‡Number of points used to determine the maximum.

Table 54. Superhump maxima of SBS 1108 (2012) (continued).

E	max*	error	$O-C$†	N‡
357	56054.6351	0.0027	0.0239	10
359	56054.7126	0.0010	0.0233	30
360	56054.7527	0.0020	0.0243	28
361	56054.7857	0.0062	0.0182	30
362	56054.8322	0.0016	0.0257	27
363	56054.8668	0.0067	0.0213	21
364	56054.9069	0.0038	0.0223	17
399	56056.2788	0.0015	0.0277	12
402	56056.3998	0.0016	0.0315	24
403	56056.4295	0.0015	0.0222	33
405	56056.5165	0.0028	0.0311	23
406	56056.5499	0.0038	0.0254	26
410	56056.7049	0.0009	0.0242	20
411	56056.7437	0.0026	0.0240	18
412	56056.7791	0.0024	0.0204	20
413	56056.8207	0.0013	0.0229	20
414	56056.8615	0.0018	0.0247	20
415	56056.9012	0.0017	0.0253	21
425	56057.2882	0.0014	0.0218	16
426	56057.3266	0.0025	0.0212	31
427	56057.3600	0.0033	0.0155	80
428	56057.4052	0.0009	0.0216	104
429	56057.4426	0.0015	0.0201	88
430	56057.4837	0.0013	0.0221	61
431	56057.5178	0.0014	0.0171	60
450	56058.2623	0.0018	0.0198	10
451	56058.3031	0.0021	0.0216	16
476	56059.2684	0.0080	0.0106	14
477	56059.3158	0.0012	0.0190	17
478	56059.3567	0.0007	0.0209	31
479	56059.3930	0.0016	0.0182	58
480	56059.4306	0.0010	0.0167	61
481	56059.4684	0.0009	0.0154	41
482	56059.5069	0.0012	0.0149	15
487	56059.7054	0.0014	0.0182	20
488	56059.7442	0.0009	0.0179	18
489	56059.7845	0.0013	0.0191	20
490	56059.8094	0.0012	0.0050	20
492	56059.9002	0.0022	0.0178	20
512	56060.6731	0.0020	0.0098	8
513	56060.7125	0.0012	0.0100	20
514	56060.7444	0.0013	0.0029	18
515	56060.7918	0.0017	0.0113	19
516	56060.8281	0.0018	0.0085	18
517	56060.8687	0.0029	0.0101	20
518	56060.9091	0.0038	0.0114	14
528	56061.3000	0.0034	0.0118	12
531	56061.4138	0.0019	0.0086	43
533	56061.4901	0.0028	0.0068	32
540	56061.7538	0.0013	−0.0028	20
541	56061.7907	0.0050	−0.0050	18

*BJD−2400000.
†Against max $= 2456040.6718 + 0.039046E$.
‡Number of points used to determine the maximum.

Table 54. Superhump maxima of SBS 1108 (2012) (continued).

E	max*	error	$O-C$†	N‡
542	56061.8396	0.0068	0.0048	19
543	56061.8850	0.0033	0.0112	17
556	56062.3817	0.0056	0.0003	72
558	56062.4634	0.0020	0.0039	72
559	56062.5072	0.0013	0.0087	29
564	56062.7000	0.0036	0.0062	20
565	56062.7351	0.0019	0.0023	19
566	56062.7764	0.0023	0.0046	20
582	56063.3952	0.0038	−0.0014	29
583	56063.4310	0.0020	−0.0046	28
584	56063.4683	0.0036	−0.0064	26
607	56064.3700	0.0033	−0.0028	42
608	56064.4070	0.0042	−0.0048	43
609	56064.4419	0.0022	−0.0090	42
634	56065.4115	0.0021	−0.0155	25
635	56065.4566	0.0023	−0.0094	26
657	56066.3051	0.0023	−0.0199	17
658	56066.3447	0.0008	−0.0194	29
659	56066.3833	0.0011	−0.0198	39
660	56066.4265	0.0034	−0.0157	38
662	56066.4951	0.0035	−0.0252	12
736	56069.3768	0.0026	−0.0329	9
738	56069.4499	0.0015	−0.0379	6
763	56070.4258	0.0012	−0.0382	11
770	56070.6959	0.0017	−0.0413	9
773	56070.8146	0.0013	−0.0398	8
872	56074.6617	0.0049	−0.0583	7
873	56074.7169	0.0034	−0.0421	7
875	56074.7828	0.0042	−0.0542	9
876	56074.8171	0.0018	−0.0591	9

*BJD−2400000.
†Against max $= 2456040.6718 + 0.039046E$.
‡Number of points used to determine the maximum.

Table 55. Superhump maxima of SDSS J073208 (2012).

E	max*	error	$O-C$†	N‡
0	55977.6385	0.0015	−0.0009	41
1	55977.7190	0.0008	0.0000	51
2	55977.7994	0.0012	0.0009	53
72	55983.3671	0.0025	−0.0000	43

*BJD−2400000.
†Against max $= 2455977.6394 + 0.079552E$.
‡Number of points used to determine the maximum.

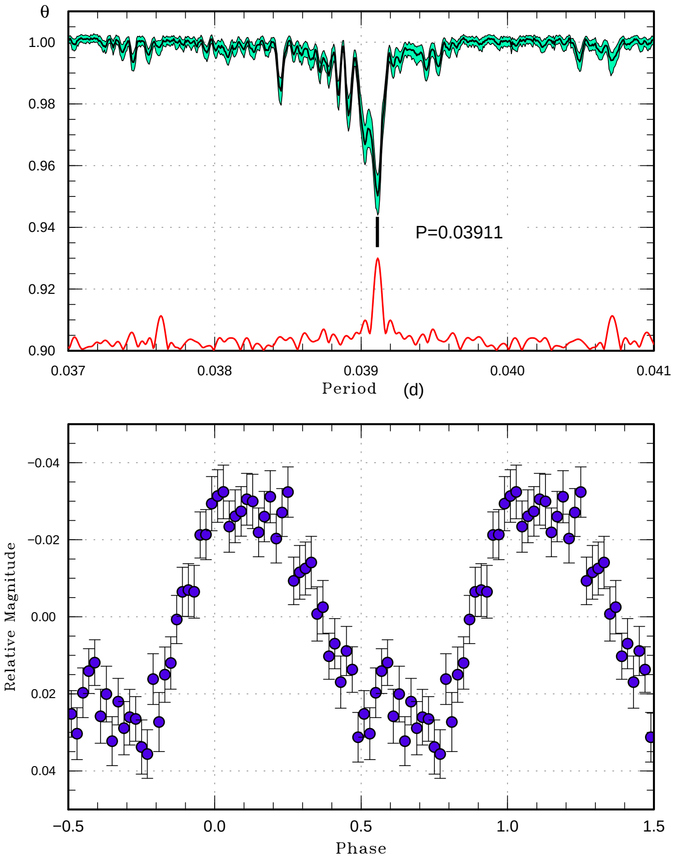

Fig. 45. Superhumps in SBS 1108 (2012). (Upper): PDM analysis. The curve at the bottom of the figure represents the window function. The signal at $P = 0.038449$ d is the candidate orbital period. (Lower): Phase-averaged profile.

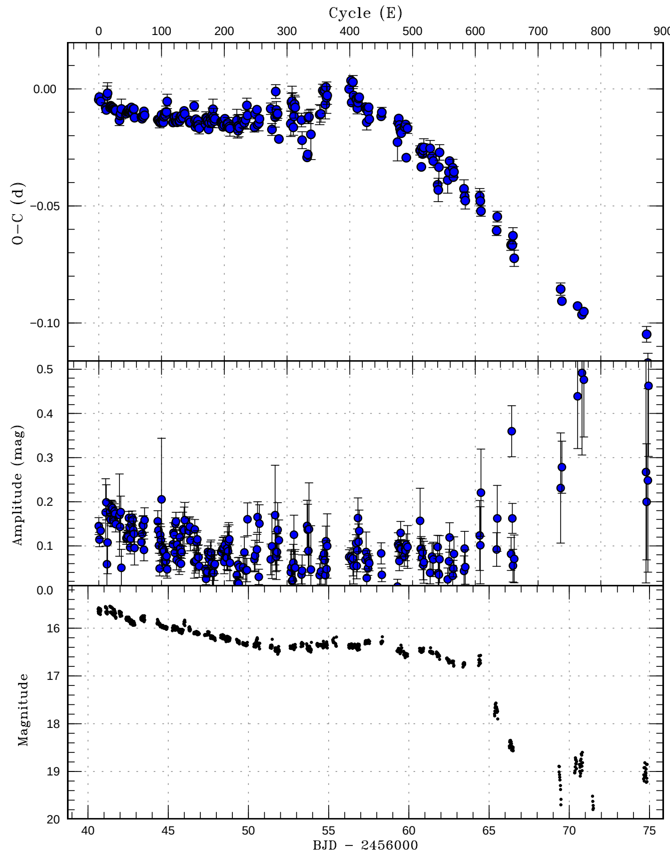

Fig. 46. $O-C$ diagram of superhumps in SBS 1108. (Upper:) $O-C$ diagram. We used a period of 0.03912 d for calculating the $O-C$ residuals. (Middle:) Amplitudes of superhumps. There was a slight tendency of regrowth of superhumps around the stage B–C transition. (Lower:) Light curve. The object slightly brightened after the stage B–C transition.

Table 56. Superhump maxima of SDSS J080303 (2011).

E	max*	error	$O-C$†	N‡
0	55921.6801	0.0015	−0.0524	96
1	55921.7738	0.0026	−0.0499	56
10	55922.6375	0.0004	−0.0071	187
11	55922.7343	0.0005	−0.0016	137
17	55923.2981	0.0008	0.0150	104
21	55923.6649	0.0003	0.0169	99
22	55923.7573	0.0005	0.0181	75
27	55924.2195	0.0005	0.0243	101
28	55924.3112	0.0009	0.0247	100
30	55924.4919	0.0006	0.0230	59
31	55924.5842	0.0006	0.0240	59
43	55925.6680	0.0006	0.0133	99
87	55929.6462	0.0020	−0.0220	97
88	55929.7332	0.0022	−0.0262	98

*BJD−2400000.
†Against max $= 2455921.7325 + 0.091215E$.
‡Number of points used to determine the maximum.

Table 57. Superhump maxima of SDSS J165359 (2012).

E	max*	error	$O-C$†	N‡
0	56062.5903	0.0004	0.0011	67
1	56062.6574	0.0004	0.0031	52
13	56063.4328	0.0004	−0.0025	105
14	56063.4999	0.0004	−0.0005	116
23	56064.0889	0.0009	0.0027	70
24	56064.1505	0.0011	−0.0008	52
28	56064.4077	0.0008	−0.0040	47
91	56068.5137	0.0007	0.0015	64
106	56069.4898	0.0009	0.0013	57
107	56069.5505	0.0007	−0.0032	55
115	56070.0719	0.0022	−0.0025	132
121	56070.4688	0.0013	0.0039	48

*BJD−2400000.
†Against max $= 2456062.5892 + 0.065089E$.
‡Number of points used to determine the maximum.

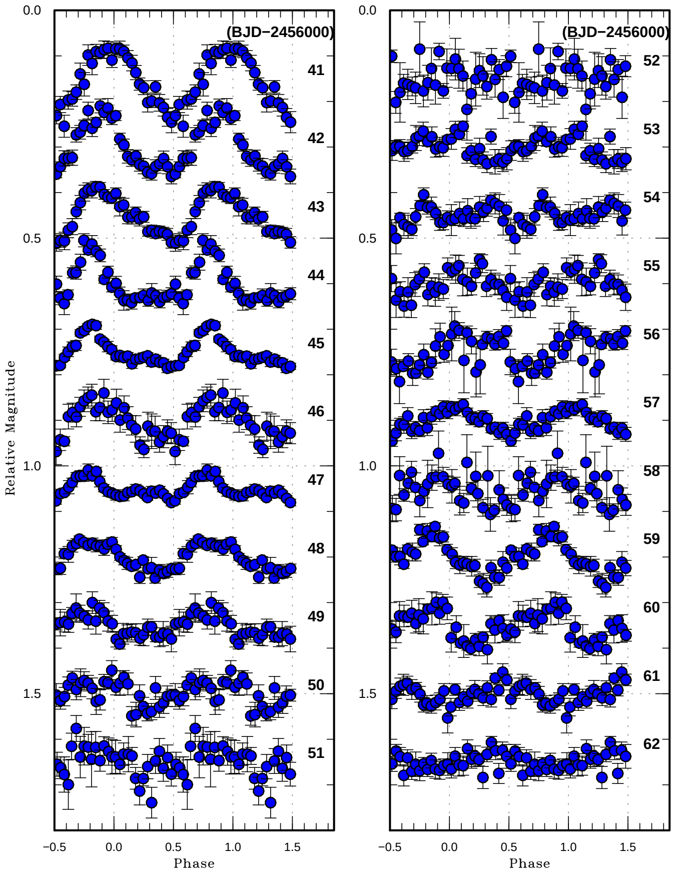

Fig. 47. Variation of superhump prfiles in SBS 1108 (2012). A period of 0.039111 d was assumed in phase-averaging. Although the amplitude of superhumps decreased for a time (BJD 2456050–2456056), it increased again (BJD 2456057–2456060).

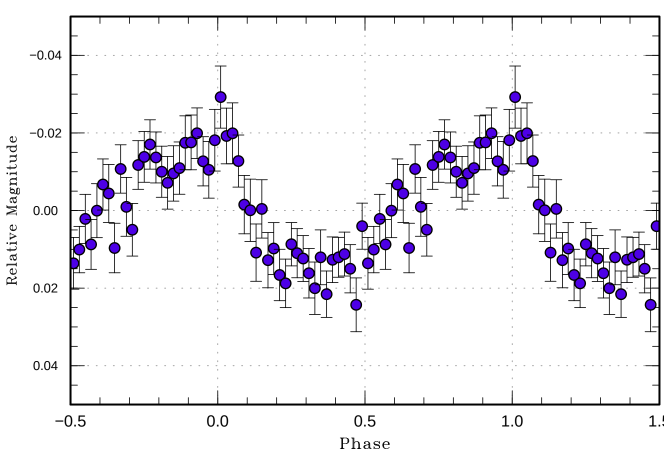

Fig. 48. Waveform of the candidate orbital period (0.038449 d) of SBS 1108.

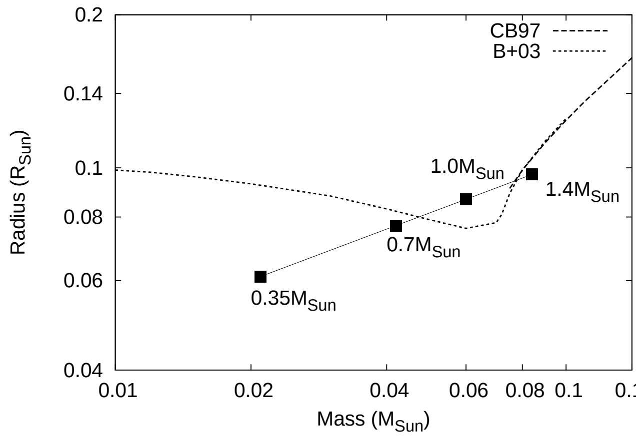

Fig. 49. Mass-radius relation of the secondary of SBS 1108. The volume radii of the Roche lobe of the secondary for various masses of the primary are plotted against the mass-radius relationship of 10 Gyr brown dwarfs and low-mass main-sequence stars by Baraffe et al. (2003) (B03) and Chabrier, Baraffe (1997) (CB97).

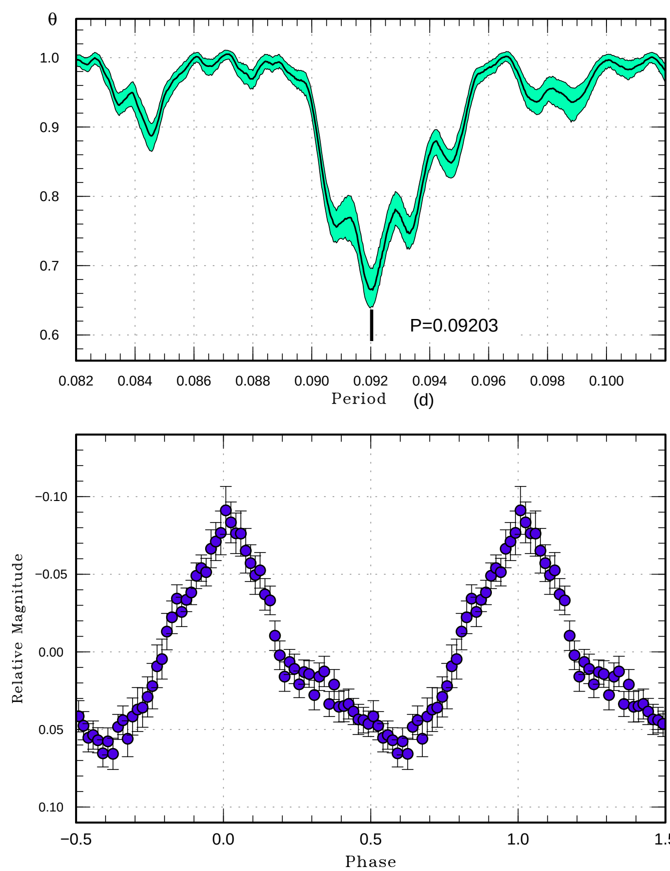

Fig. 50. Superhumps in SDSS J080303 (2011). (Upper): PDM analysis. (Lower): Phase-averaged profile.

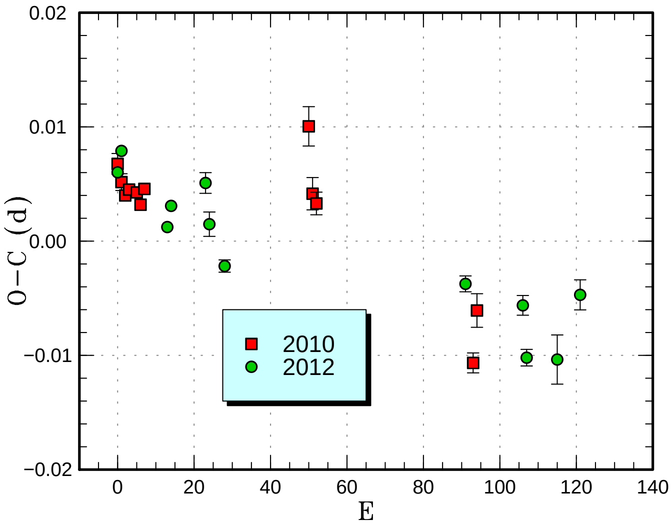

Fig. 51. Comparison of $O-C$ diagrams of SDSS J165359 between different superoutbursts. A period of 0.06520 d was used to draw this figure. Approximate cycle counts (E) after the start of the observation were used. We could not obtain a better match if we shifted the cycle number between these superoutbursts.

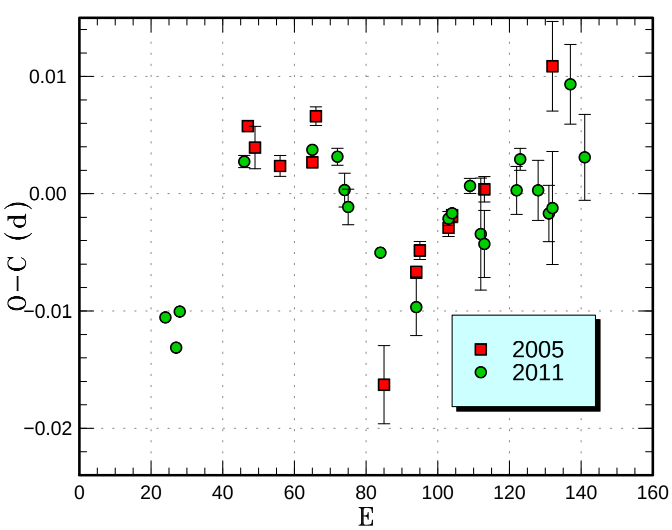

Fig. 52. Comparison of $O-C$ diagrams of SDSS J170213 between different superoutbursts. A period of 0.10510 d was used to draw this figure. Approximate cycle counts (E) after the start of the superoutburst were used.

Table 58. Eclipse minima of SDSS J170213 (2011).

E	Minimum*	error	$O-C$†
21165	55766.47660	0.00003	0.00018
21195	55769.47798	0.00004	-0.00091
21196	55769.57867	0.00004	-0.00029
21205	55770.48023	0.00004	0.00052
21214	55771.38036	0.00012	-0.00009
21215	55771.48107	0.00009	0.00054
21224	55772.38128	0.00003	0.00001
21225	55772.48149	0.00005	0.00013
21234	55773.38194	0.00003	-0.00015
21235	55773.48223	0.00003	0.00005
21245	55774.48296	0.00004	-0.00004
21248	55774.78356	0.00013	0.00032
21254	55775.38378	0.00003	0.00004
21255	55775.48378	0.00003	-0.00004
21264	55776.38464	0.00003	0.00008
21265	55776.48473	0.00005	0.00009
21270	55776.98509	0.00005	0.00004
21271	55777.08517	0.00006	0.00003
21274	55777.38503	0.00003	-0.00035
21280	55777.98583	0.00011	-0.00005
21281	55778.08560	0.00005	-0.00036
21284	55778.38640	0.00014	0.00020

*BJD−2400000.

†Against equation 3.

derwent a short post-superoutburst rebrightening on June 20 whose peak brightness must have been brighter than 17.5 (Goff). The times of superhump maxima are listed in table 60. Note that these observations were mostly made during the final stage of the superoutburst and subsequent post-superoutburst phase, and the maxima were rather difficult to identify due to the faintness. Our best estimate of the superhump period is 0.026673(8) d (figure 53). It is remarkable that both spectra in Rau et al. (2010) and the SDSS public archive were continuum-dominated (vsnet-alert 14650) in contrast to the quiescent state of many AM CVn-type objects showing dwarf-nova type outbursts.

3.55. SDSS J210449.94+010545.8

This object (hereafter SDSS J210449) was discovered as a CV during the course of the SDSS (Szkody et al. 2006). Szkody et al. (2006) recorded high and low states ranging 17.1–20.6 mag. Southworth et al. (2007) detected a photometric period of 0.07196(8) d. CRTS recorded multiple outbursts, and at least one of them (2006 November) lasted more than 18 d and was likely a superoutburst. During the superoutburst in 2011 September, I. Miller detected superhumps (vsnet-alert 13704). A PDM analysis yielded two equally acceptable one-day aliases (figure 54).

The times of superhump maxima are listed in table 61 The timing analysis prefers an alias of 0.0753 d, and we obtained a period of 0.07531(4) d with the PDM method,

Table 59. Superhump maxima of SDSS J170213 (2011).

E	max*	error	$O-C$†	phase‡	N§
0	55766.1025	0.0004	−0.0084	0.27	125
3	55766.4152	0.0003	−0.0111	0.39	187
4	55766.5234	0.0004	−0.0081	0.47	190
22	55768.4280	0.0005	0.0041	0.50	89
32	55769.4973	0.0010	0.0221	0.19	181
33	55769.5977	0.0011	0.0174	0.19	122
41	55770.4259	0.0004	0.0045	0.46	82
48	55771.1610	0.0007	0.0037	0.81	141
50	55771.3684	0.0014	0.0008	0.88	35
51	55771.4720	0.0015	−0.0007	0.92	77
60	55772.4140	0.0005	−0.0048	0.33	87
70	55773.4604	0.0024	−0.0098	0.78	96
79	55774.4138	0.0006	−0.0025	0.31	120
80	55774.5194	0.0005	−0.0021	0.37	110
85	55775.0472	0.0006	0.0001	0.64	169
88	55775.3584	0.0048	−0.0041	0.75	53
89	55775.4627	0.0029	−0.0050	0.79	100
98	55776.4132	0.0020	−0.0007	0.29	157
99	55776.5209	0.0009	0.0019	0.36	106
104	55777.0438	0.0026	−0.0009	0.59	231
107	55777.3571	0.0024	−0.0030	0.72	82
108	55777.4626	0.0048	−0.0026	0.77	79
113	55777.9987	0.0034	0.0078	0.13	148
117	55778.4129	0.0037	0.0015	0.27	138

*BJD−2400000.
†Against max $= 2455766.1110 + 0.105132E$.
‡Orbital phase.
§Number of points used to determine the maximum.

which is used in table 2. The ϵ of 4.7% inferred from this period is likely to be too large for this $P_{\rm orb}$, and there may have been negative superhumps at the time of observations by Southworth et al. (2007). The exact orbital period needs to be determined by radial-velocity studies.

3.56. SDSS J220553.98+115553.7

This object (hereafter SDSS J220553) was detected as a CV during the course of SDSS (Szkody et al. 2003). Szkody et al. (2003) showed the presence of the underlying white dwarf in the spectrum, suggesting the low mass-transfer rate. Warner, Woudt (2004) indicated that this system contains a ZZ Cet-type pulsating white dwarf (see also Szkody et al. 2007), also suggesting the low surface-temperature of the white dwarf (consistent with the low mass-transfer rate). Southworth et al. (2008) obtained the spectroscopic orbital period of 0.0575175(62) d, and they found that the pulsation of white dwarf ceased in 2007. Although the spectrum and the orbital period suggested an SU UMa-type or an even WZ Sge-type dwarf nova, no outburst had been recorded until 2011.

CRTS detected an outburst on 2011 May 20 (cf. vsnet-alert 13325) and the announcement of this detection was immediately followed by observations. Fully grown superhumps were soon detected (vsnet-alert 13329, figure 55),

Table 60. Superhump maxima of SDSS J172102 (2012).

E	max*	error	$O-C$†	N‡
0	56087.5334	0.0007	0.0035	18
1	56087.5601	0.0008	0.0036	19
82	56089.7123	0.0007	−0.0043	13
83	56089.7401	0.0007	−0.0032	14
84	56089.7687	0.0010	−0.0013	12
85	56089.7919	0.0017	−0.0047	14
86	56089.8217	0.0014	−0.0016	12
87	56089.8449	0.0008	−0.0050	10
88	56089.8753	0.0011	−0.0013	14
89	56089.9039	0.0016	0.0006	13
90	56089.9306	0.0015	0.0007	9
120	56090.7290	0.0011	−0.0010	13
122	56090.7869	0.0019	0.0036	14
123	56090.8112	0.0032	0.0012	14
124	56090.8354	0.0056	−0.0013	13
127	56090.9128	0.0041	−0.0039	13
233	56093.7449	0.0021	0.0015	13
234	56093.7751	0.0037	0.0050	14
236	56093.8200	0.0012	−0.0034	13
237	56093.8512	0.0013	0.0011	8
238	56093.8733	0.0019	−0.0035	14
239	56093.9027	0.0032	−0.0007	13
271	56094.7616	0.0007	0.0048	11
272	56094.7900	0.0030	0.0065	14
273	56094.8203	0.0050	0.0101	14
274	56094.8427	0.0012	0.0059	8
275	56094.8690	0.0033	0.0055	13
345	56096.7276	0.0019	−0.0026	11
346	56096.7560	0.0020	−0.0009	10
347	56096.7784	0.0019	−0.0051	14
350	56096.8612	0.0021	−0.0023	13
384	56097.7699	0.0025	−0.0004	11
387	56097.8535	0.0022	0.0033	11
388	56097.8736	0.0057	−0.0033	13
389	56097.9032	0.0033	−0.0004	14
390	56097.9289	0.0016	−0.0013	12
457	56099.7196	0.0050	0.0026	13
460	56099.8005	0.0044	0.0035	13
461	56099.8212	0.0034	−0.0025	9
462	56099.8486	0.0024	−0.0017	12
463	56099.8699	0.0050	−0.0071	14

*BJD−2400000.
†Against max $= 2456087.5299 + 0.026668E$.
‡Number of points used to determine the maximum.

Table 61. Superhump maxima of SDSS J210449 (2011).

E	max*	error	$O-C$†	N‡
0	55834.4629	0.0008	−0.0000	79
26	55836.4217	0.0015	0.0000	69
27	55836.4970	0.0011	−0.0000	55

*BJD−2400000.
†Against max $= 2455834.4629 + 0.075338E$.
‡Number of points used to determine the maximum.

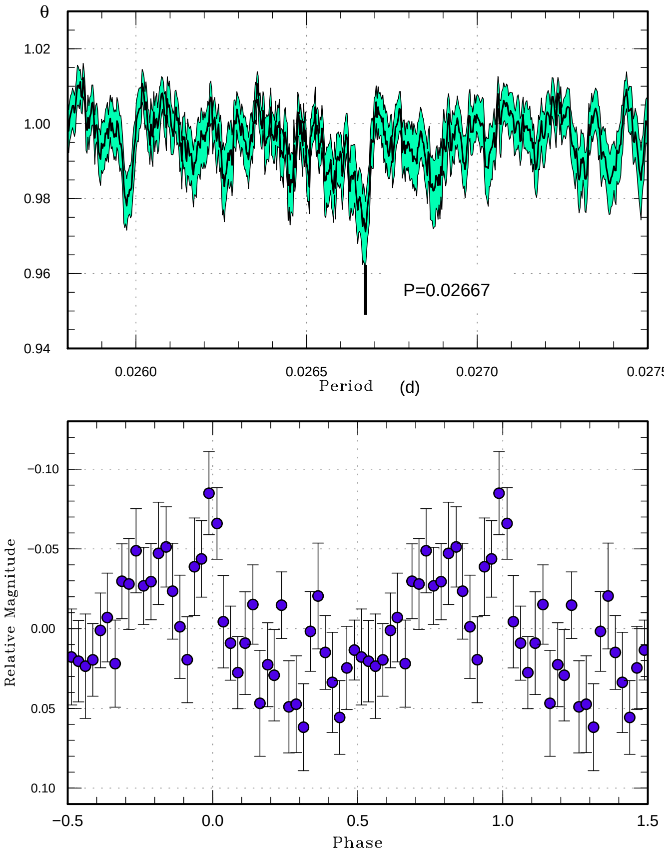

Fig. 53. Superhumps in SDSS J172102 (2012). (Upper): PDM analysis. The rejection rate for bootstrapping was reduced to 0.2 for better visualization. (Lower): Phase-averaged profile.

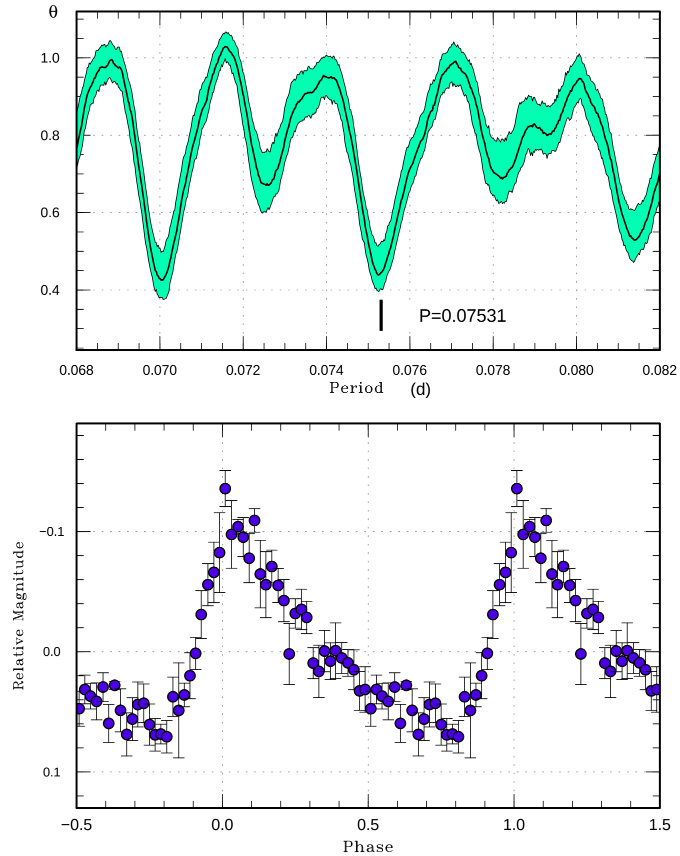

Fig. 54. Superhumps in SDSS J210449 (2011). (Upper): PDM analysis. The alias selection was based on superhump timing analysis. (Lower): Phase-averaged profile.

and the later development suggested a low ϵ, characteristic to a WZ Sge-type dwarf nova (vsnet-alert 13332, 13336). The $P_{\rm dot}$ was, however, unexpectedly large (vsnet-alert 13348).

The times of superhump maxima are listed in table 62. The resultant $P_{\rm dot}$ was $+7.7(0.9) \times 10^{-5}$. The ϵ for the mean period of stage B superhumps was 1.1%, which is much smaller than what would be expected for this large $P_{\rm dot}$.

According to the CRTS data, the object brighter than in usual quiescence four months after the outburst. This, combined with the low ϵ and the lack of previous outbursts in the CRTS data, suggest that the object is a WZ Sge-type dwarf nova. It may have been that the period of early superhumps was missed, and that the true maximum was much brighter.

3.57. OT J001952.2+433901

This transient (=CSS120131:001952+433901; hereafter OT J001952) was detected by CRTS on 2012 January 31. The large outburst amplitude ($\sim$ 6.5 mag) and the lack of previous outbursts attracted observers' attention (vsnet-alert 14182). Subsequent observations detected short-period superhumps (vsnet-alert 14189, 14202; figure 56).

Table 62. Superhump maxima of SDSS J220553 (2011).

E	max*	error	$O-C$†	N‡
0	55702.2039	0.0015	0.0042	109
1	55702.2618	0.0008	0.0039	119
12	55702.8979	0.0004	0.0003	60
13	55702.9551	0.0004	−0.0006	53
29	55703.8834	0.0004	−0.0028	87
30	55703.9436	0.0003	−0.0007	86
40	55704.5235	0.0010	−0.0024	31
46	55704.8715	0.0009	−0.0032	87
47	55704.9297	0.0005	−0.0032	86
63	55705.8626	0.0008	−0.0007	60
64	55705.9204	0.0005	−0.0010	61
97	55707.8427	0.0028	0.0023	36
98	55707.9006	0.0007	0.0021	60
99	55707.9586	0.0007	0.0018	43

*BJD−2400000.
†Against max $= 2455702.1998 + 0.058151E$.
‡Number of points used to determine the maximum.

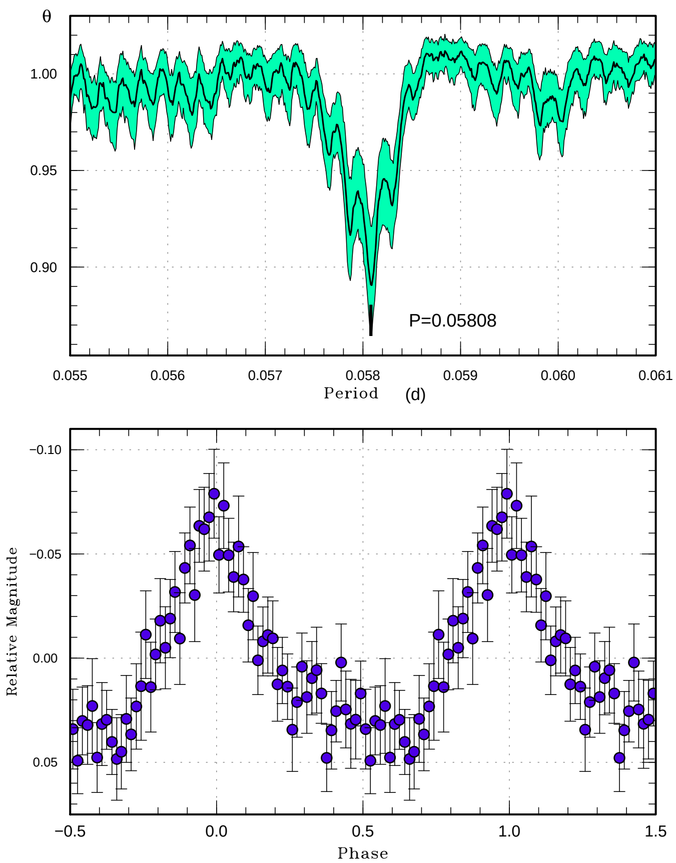

Fig. 55. Superhumps in SDSS J220553 (2011). (Upper): PDM analysis. (Lower): Phase-averaged profile.

Table 63. Superhump maxima of OT J001952.

E	max*	error	$O-C$†	N‡
0	55958.3297	0.0005	0.0005	61
1	55958.3856	0.0007	−0.0005	42
17	55959.2959	0.0006	0.0005	50
18	55959.3517	0.0008	−0.0005	60

*BJD−2400000.
†Against max $= 2455958.3292 + 0.056827E$.
‡Number of points used to determine the maximum.

The times of superhump maxima are listed in table 63. The large outburst amplitude and short superhump period suggest a possibility of a WZ Sge-type dwarf nova.

3.58. OT J011516.5+245530

This transient (=CSS101008:011517+245530; hereafter OT J011516) was detected by CRTS on 2010 October 8. Although several outbursts were known, the 2012 outburst was the brightest one (vsnet-alert 14142). Subsequent observations recorded superhumps (vsnet-alert 14147, 14149). Only single-night observation was available with superhump maxima of BJD 2455952.2518(7) (N=51) and 2455952.3253(10) (N=44). The best superhump period by the PDM was 0.0731(6) d (figure 57).

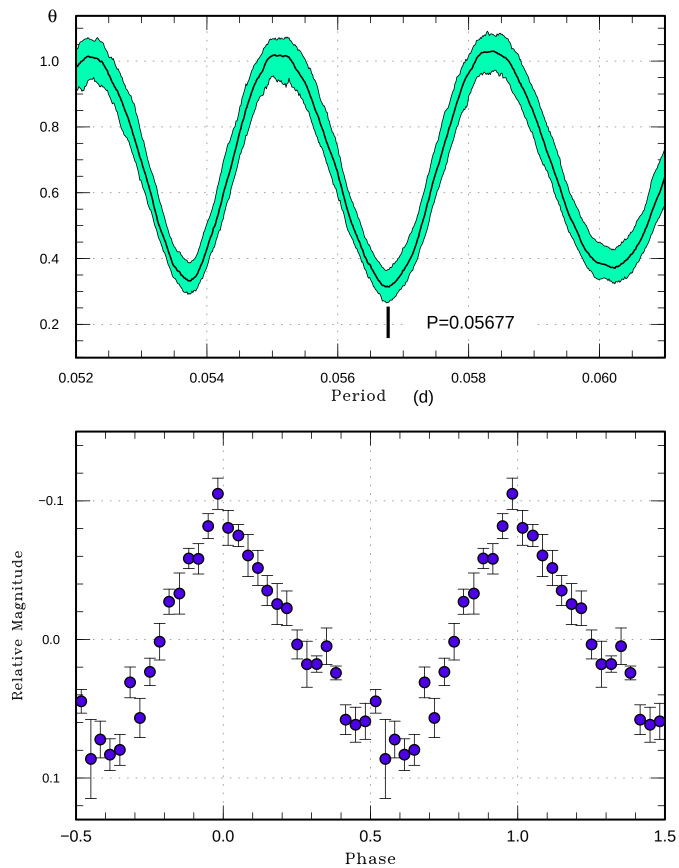

Fig. 56. Superhumps in OT J001952 (2011). (Upper): PDM analysis. The alias selection was based on continuous single-night observation. (Lower): Phase-averaged profile.

Table 64. Superhump maxima of OT J050716.

E	max*	error	$O-C$†	N‡
0	55952.4395	0.0009	−0.0012	31
1	55952.5075	0.0024	0.0015	19
14	55953.3518	0.0055	−0.0033	28
15	55953.4234	0.0018	0.0030	36

*BJD−2400000.
†Against max $= 2455952.4407 + 0.065317E$.
‡Number of points used to determine the maximum.

3.59. OT J050716.2+125314

This transient (=CSS081221:050716+125314; hereafter OT J050716) was detected by CRTS on 2008 December 21. The 2012 January outburst led to the detection of superhumps (vsnet-alert 14150, 14151). The times of superhump maxima are listed in table 64. Although the $O-C$ analysis favored an alias of 0.06592(8) d (adopted in table 2), the alias of 0.07055(9) d is not excluded (figure 58).

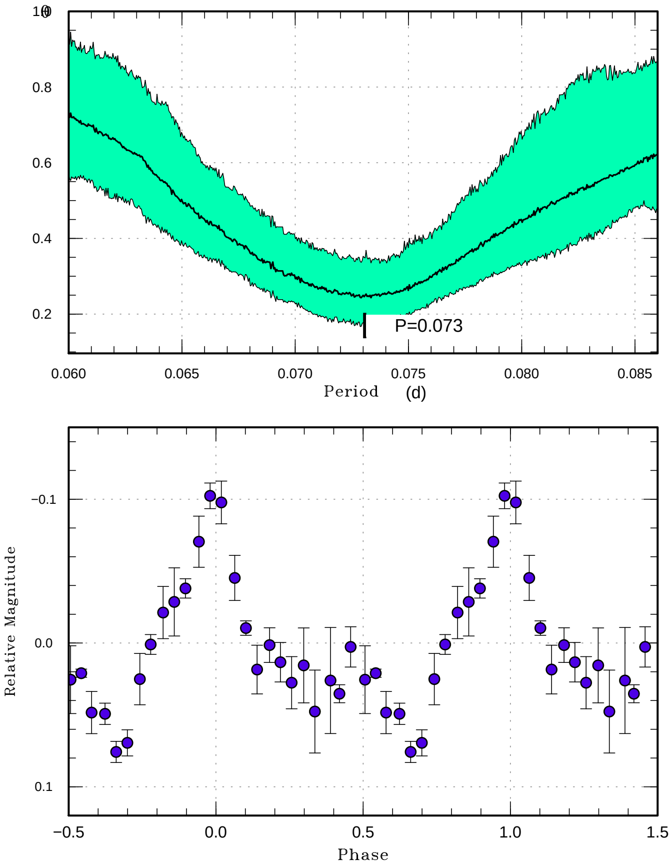

Fig. 57. Superhumps in OT J011516 (2012). (Upper): PDM analysis. (Lower): Phase-averaged profile.

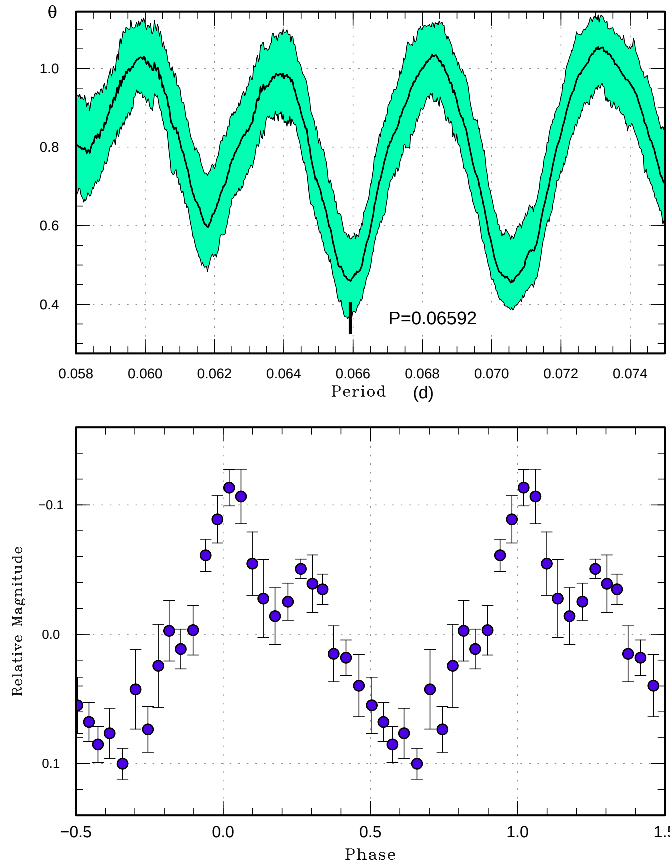

Fig. 58. Superhumps in OT OT J050716 (2012). (Upper): PDM analysis. (Lower): Phase-averaged profile.

3.60. OT J055721.8−363055

This transient (=SSS111229:055722−363055; hereafter OT J055721) was detected by CRTS SSS on 2011 December 29. The large outburst amplitude suggested an SU UMa-type, or even a WZ Sge-type object (vsnet-alert 14041). Subsequent observations detected superhumps (vsnet-alert 14052). The times of superhump maxima are listed in table 65. Although the observations in the middle of the outburst were rather sparse, we likely observed stage B superhumps with a positive $P_{\rm dot}$. The amplitude of superhumps (cf. figure 59) resembles those of ordinary SU UMa-type dwarf novae rather than those of extreme WZ Sge-type dwarf novae. The object, however, underwent a post-outburst rebrightening similar to those of WZ Sge-type dwarf novae (rebrightening followed by a short "dip"; vsnet-alert 14097).

3.61. OT J064608.2+403305

This transient (=CSS 080512:064608+403305; hereafter OT J064608) was detected by CRTS on 2008 May 12. A bright outburst in 2011 December was detected by E. Muyllaert (BAAVSS alert 2808). Subsequent observations confirmed the presence of superhumps (vsnet-alert 14023, 14036, 14039; figure 60). The time of superhump maxima are listed in table 66. The $P_{\rm dot}$ was $+11.1(2.6) \times 10^{-5}$, a typical value for stage B superhumps with this $P_{\rm SH}$.

3.62. OT J081117.1+152003

This transient (=CSS111030:081117+152003; hereafter OT J081117) was detected by CRTS on 2011 October 30. The object had a large ($\sim$ 6 mag) outburst amplitude and was considered as a good candidate for an SU UMa-type dwarf nova. As expected, short-period superhumps were detected (vsnet-alert 13816; figure 61). Due to the insufficient observation, we could not measure $P_{\rm SH}$ precisely. The times of superhump maxima are listed in table 67. We listed the most likely alias determined with the PDM method in table 2.

3.63. OT J084127.4+210053

This transient (=CSS090525:084127+210054; hereafter OT J084127) was detected by CRTS on 2009 May 25. There were other known outbursts (CRTS detections) in 2007 September, 2010 January and 2010 May. Kato et al. (2012b) suggested $P_{\rm orb}$=0.10 d from the SDSS colors. The 2012 March outburst was observed and superhumps were immediately detected (vsnet-alert 14391, 14392, 14396; figure 62). The times of superhump maxima are listed in table 68.

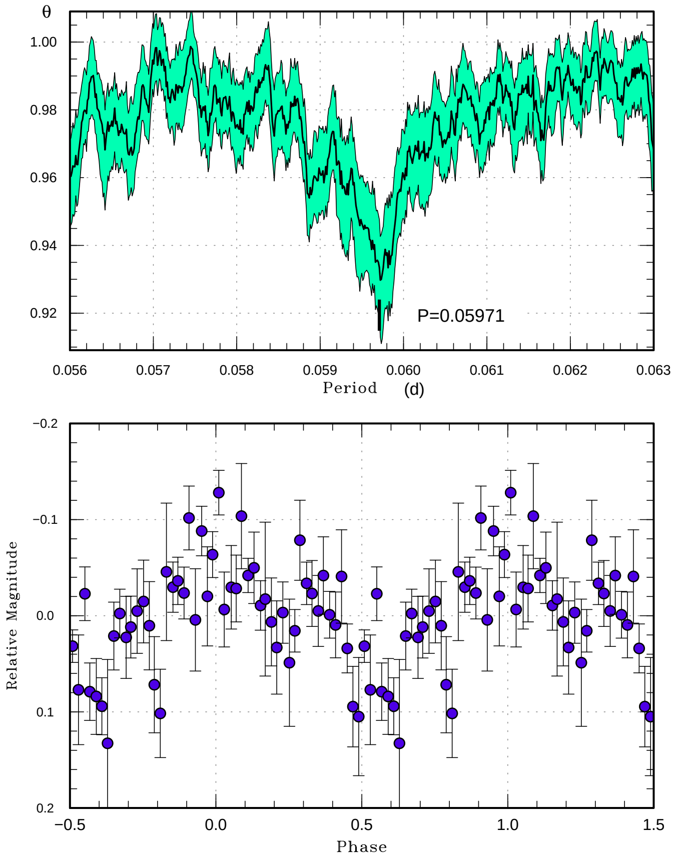

Fig. 59. Superhumps in OT J055721 (2011). (Upper): PDM analysis. The rejection rate for bootstrapping was reduced to 0.2 for better visualization. (Lower): Phase-averaged profile.

3.64. OT J094854.0+014911

This transient (=CSS120315:094854+014911; hereafter OT J094854) was detected by CRTS on 2012 March 15. There was no previous outbursts detected by CRTS. Immediately following this discovery superhumps were detected (vsnet-alert 14326, 14327; figure 63). The SDSS color of the quiescent counterpart resembles those of ordinary SU UMa-type dwarf novae rather than those of extreme WZ Sge-type dwarf novae (vsnet-alert 14328; see also Kato et al. 2012b). S. Yoshida pointed out that the object was already in outburst on March 11 (vsnet-alert 14330). The times of superhump maxima are listed in table 69. There was likely a stage B–C transition around $E = 77$. The early part of stage B was missed and the observations were not sufficient to determine the period of stage C superhumps.

3.65. OT J102842.9−081927

This object (=CSS090331:102843−081927, hereafter OT J102842) was originally discovered by CRTS. Kato et al. (2009) indicated that this object has a very short [0.038147(14) d] superhump period, suggesting an unusual evolutionary status similar to EI Psc (Thorstensen et al. 2002a; Uemura et al. 2002) or V485 Cen (Augusteijn

Table 65. Superhump maxima of OT J055721 (2011).

E	max*	error	$O-C$†	N‡
0	55926.5487	0.0010	0.0008	22
1	55926.6101	0.0006	0.0024	14
2	55926.6685	0.0005	0.0010	10
3	55926.7283	0.0015	0.0010	15
4	55926.7898	0.0011	0.0028	20
17	55927.5657	0.0006	0.0019	17
18	55927.6250	0.0012	0.0014	14
19	55927.6836	0.0006	0.0002	13
20	55927.7438	0.0005	0.0008	17
21	55927.8028	0.0007	0.0000	20
33	55928.5184	0.0024	−0.0015	17
34	55928.5806	0.0010	0.0010	15
35	55928.6376	0.0009	−0.0018	14
36	55928.6967	0.0008	−0.0024	16
37	55928.7549	0.0005	−0.0040	17
38	55928.8170	0.0006	−0.0016	19
94	55932.1550	0.0068	−0.0100	100
152	55935.6360	0.0036	0.0051	14
153	55935.6934	0.0029	0.0029	17

*BJD−2400000.
†Against max $= 2455926.5480 + 0.059756E$.
‡Number of points used to determine the maximum.

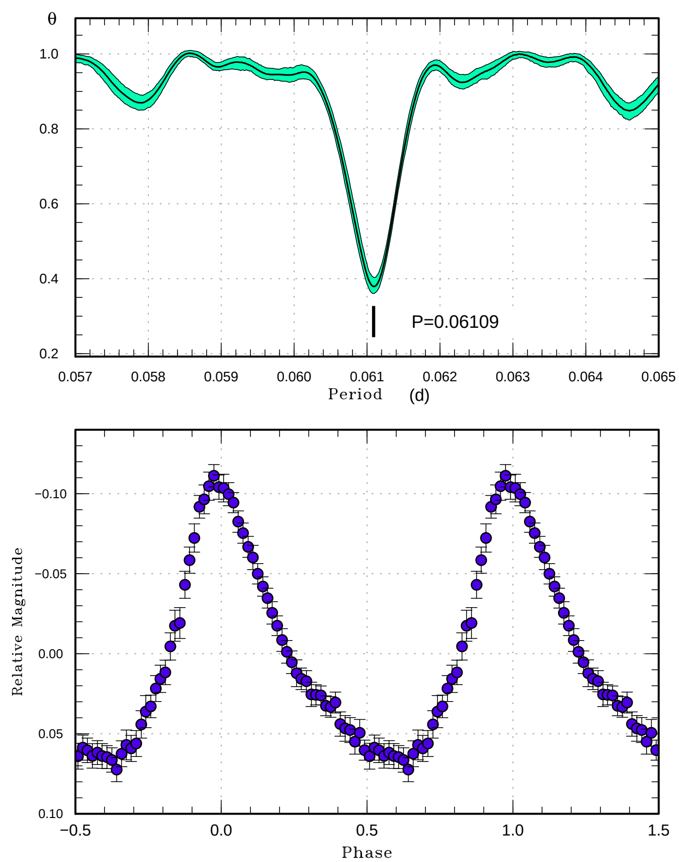

Fig. 60. Superhumps in OT J064608 (2011). (Upper): PDM analysis. (Lower): Phase-averaged profile.

Table 66. Superhump maxima of OT J064608 (2011).

E	max*	error	$O-C^{\dagger}$	$N^{\ddagger}$
0	55923.3629	0.0006	−0.0018	36
1	55923.4269	0.0002	0.0010	64
2	55923.4884	0.0002	0.0014	79
3	55923.5492	0.0002	0.0011	54
4	55923.6111	0.0002	0.0019	54
7	55923.7948	0.0002	0.0023	63
8	55923.8553	0.0002	0.0017	63
9	55923.9152	0.0006	0.0005	63
10	55923.9751	0.0003	−0.0007	64
17	55924.4049	0.0003	0.0013	64
18	55924.4661	0.0003	0.0015	64
23	55924.7705	0.0002	0.0004	64
24	55924.8319	0.0003	0.0006	64
25	55924.8923	0.0002	−0.0001	65
26	55924.9527	0.0003	−0.0007	64
27	55925.0124	0.0005	−0.0022	55
39	55925.7448	0.0008	−0.0031	36
40	55925.8078	0.0003	−0.0012	64
41	55925.8668	0.0003	−0.0032	64
42	55925.9280	0.0004	−0.0031	64
43	55925.9880	0.0005	−0.0043	63
56	55926.7855	0.0004	−0.0011	64
57	55926.8473	0.0003	−0.0004	64
58	55926.9074	0.0003	−0.0014	64
59	55926.9667	0.0008	−0.0032	63
60	55927.0366	0.0016	0.0055	34
82	55928.3828	0.0008	0.0075	65

*BJD−2400000.
†Against max $= 2455923.3648 + 0.061105E$.
‡Number of points used to determine the maximum.

Table 67. Superhump maxima of OT J081117 (2011).

E	max*	error	$O-C^{\dagger}$	$N^{\ddagger}$
0	55865.6525	0.0003	−0.0003	55
1	55865.7111	0.0004	0.0003	36
63	55869.3040	0.0031	−0.0000	20

*BJD−2400000.
†Against max $= 2455865.6529 + 0.057955E$.
‡Number of points used to determine the maximum.

Table 68. Superhump maxima of OT J084127 (2012).

E	max*	error	$O-C^{\dagger}$	$N^{\ddagger}$
0	56014.1263	0.0005	−0.0004	131
2	56014.3029	0.0004	0.0007	84
3	56014.3901	0.0004	0.0003	177
4	56014.4769	0.0007	−0.0006	91

*BJD−2400000.
†Against max $= 2456014.1268 + 0.087686E$.
‡Number of points used to determine the maximum.

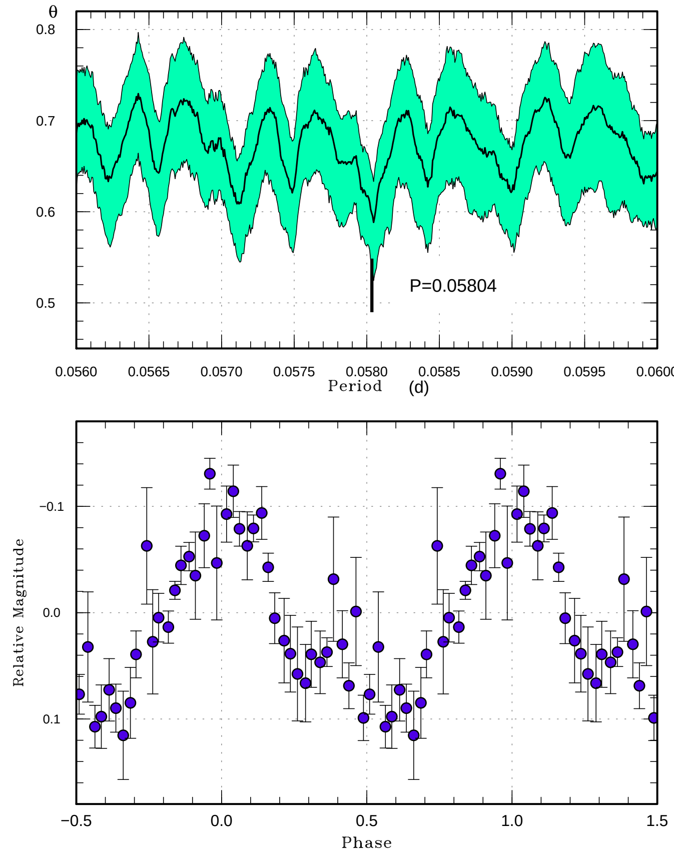

Fig. 61. Superhumps in OT J081117 (2011). (Upper): PDM analysis. The rejection rate for bootstrapping was reduced to 0.2 for better visualization. (Lower): Phase-averaged profile.

et al. 1993; Augusteijn et al. 1996; Olech 1997). The 2012 superoutburst, detected by CRTS, was also observed. The times of superhump maxima are listed in table 70. Contrary to Kato et al. (2009), the present observation gave a longer superhump period, particularly during the first half of the observation. It is difficult to reconcile with this disagreement of the periods unless we assume that the first half of the 2012 observation recorded stage A superhumps (sinec CRTS observations were typically made with 10-d intervals, it is difficult to determine the starting dates of outbursts). In table 2 and figure 64 we gave values and a comparison of $O-C$ diagrams based on this identification. This interpretation, however, has a problem in that it cannot explain the large amplitudes of superhumps at the initial stage of the 2012 observation. It may be either that the evolution of superhumps in this system is unusual, or that the period of superhumps greatly vary between superoutbursts. Further observations, particularly regular monitoring to record the epoch of the start of the outbursts, and to record superhumps during the full course of the outbursts.

3.66. OT J105122.8+672528

This transient (=CSS120101:105123+672528; hereafter OT J105122) was detected by CRTS on 2012 January 1.

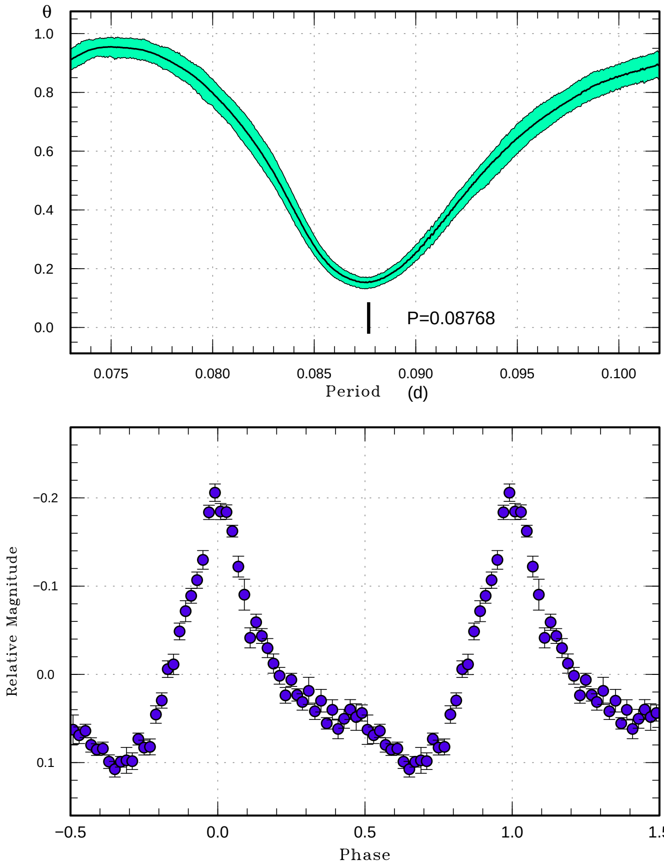

Fig. 62. Superhumps in OT J084127 (2012). (Upper): PDM analysis. (Lower): Phase-averaged profile.

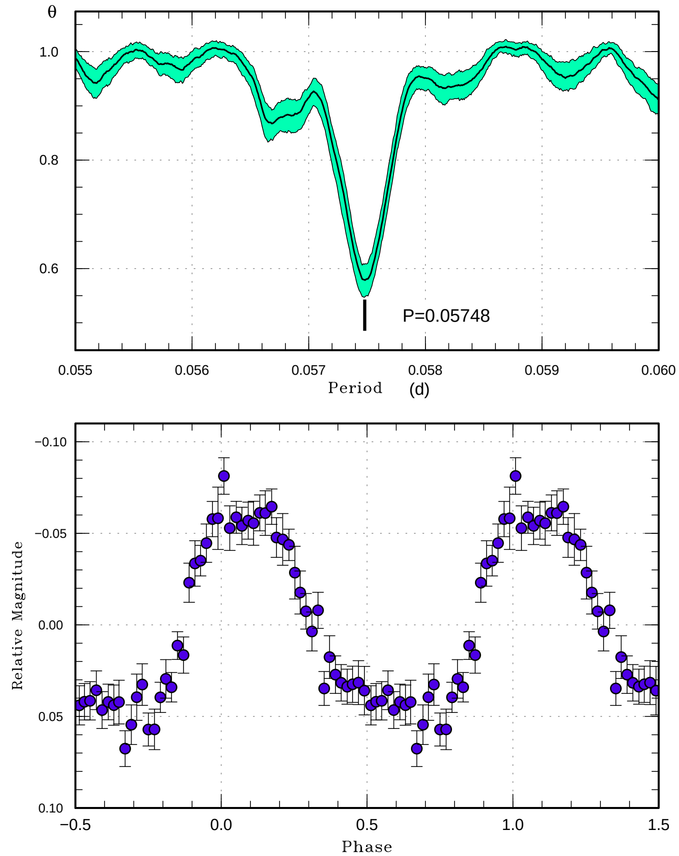

Fig. 63. Superhumps in OT J094854 (2012). (Upper): PDM analysis. (Lower): Phase-averaged profile.

There is an X-ray counterpart 1RXS J105120.5+672550. D. Denisenko reported that this object was recorded bright on a Palomer Sky Survey infrared plate taken on 1999 December 12 (vsnet-alert 14060). Subsequent observations detected superhumps (vsnet-alert 14067, 14072). MASTER team also independently detected this transient (Tiurina et al. 2012). Although it was classified as a CV (Sokolovsky et al. 2012), they couldn't detect variability. Pavlenko et al. (2012a) further observed this object in quiescence and recorded high-amplitude variations with a period of 0.0596(9) d, which was considered to be the orbital period.

The times of superhump maxima are listed in table 71. During these observations, the amplitudes of superhumps were small (figure 65), and not triangular as typically seen in early stage superhumps. Although these superhumps were likely recorded when the amplitudes get smaller (particularly before the stage B–C transition, cf. subsection 4.7 of Kato et al. 2012a), it was impossible to identify the stage in which they were observed.

3.67. OT J125905.8+242634

This transient (=CSS120424:125906+242634; hereafter OT J125905) was detected by CRTS on 2012 April 24. There was a previous outburst in 2009 February.

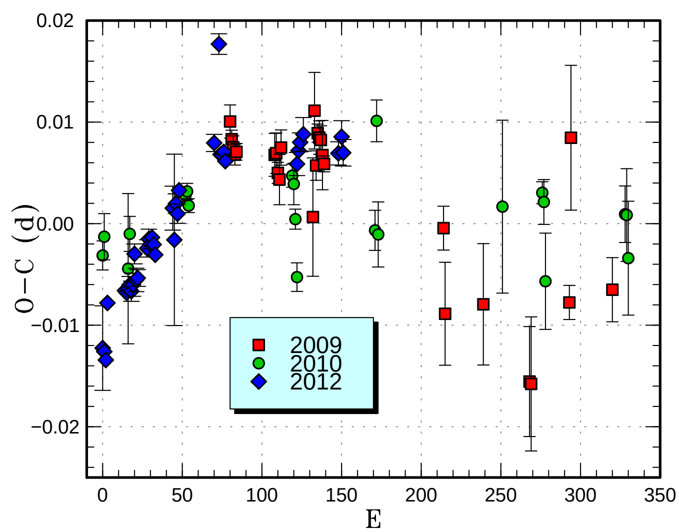

Fig. 64. Comparison of $O-C$ diagrams of J102842 between different superoutbursts. A period of 0.03816 d was used to draw this figure. Approximate cycle counts (E) after the start of the observations were used for 2009 and 2012, assuming that the observations started at the initial stage of the outbursts. The $O-C$ diagram for 2010 was shifted by 80 cycles.

Table 69. Superhump maxima of OT J094854 (2012).

E	max*	error	$O-C$†	N‡
0	56002.2812	0.0013	0.0024	24
1	56002.3383	0.0005	0.0019	40
2	56002.3946	0.0005	0.0007	31
18	56003.3141	0.0010	0.0002	40
19	56003.3720	0.0008	0.0007	40
22	56003.5445	0.0013	0.0006	20
23	56003.6031	0.0015	0.0018	16
24	56003.6583	0.0012	−0.0005	13
25	56003.7166	0.0005	0.0003	74
26	56003.7748	0.0016	0.0010	21
28	56003.8899	0.0009	0.0011	30
35	56004.2905	0.0007	−0.0008	31
36	56004.3477	0.0007	−0.0011	31
39	56004.5197	0.0008	−0.0017	26
40	56004.5798	0.0010	0.0010	19
41	56004.6341	0.0018	−0.0022	14
42	56004.6889	0.0010	−0.0049	13
43	56004.7467	0.0018	−0.0046	15
57	56005.5512	0.0016	−0.0051	14
58	56005.6125	0.0018	−0.0013	10
59	56005.6712	0.0009	−0.0001	9
60	56005.7287	0.0033	−0.0001	9
74	56006.5347	0.0040	0.0009	14
75	56006.5936	0.0016	0.0023	13
76	56006.6552	0.0017	0.0064	9
77	56006.7073	0.0025	0.0010	9
78	56006.7620	0.0016	−0.0017	9
91	56007.5118	0.0024	0.0006	17
92	56007.5717	0.0026	0.0030	14
93	56007.6220	0.0022	−0.0042	9
94	56007.6851	0.0027	0.0014	58
95	56007.7428	0.0013	0.0016	70
96	56007.7971	0.0013	−0.0016	60
97	56007.8572	0.0019	0.0010	60

*BJD−2400000.
†Against max $= 2456002.2789 + 0.057498E$.
‡Number of points used to determine the maximum.

Table 70. Superhump maxima of OT J102842 (2012).

E	max*	error	$O-C$†	N‡
0	55958.0498	0.0042	−0.0053	41
1	55958.0876	0.0007	−0.0058	64
2	55958.1250	0.0005	−0.0068	65
3	55958.1687	0.0007	−0.0013	60
14	55958.5897	0.0004	−0.0015	37
15	55958.6277	0.0004	−0.0018	36
16	55958.6663	0.0004	−0.0015	37
17	55958.7048	0.0008	−0.0013	31
18	55958.7423	0.0010	−0.0021	19
19	55958.7811	0.0011	−0.0016	20
20	55958.8223	0.0010	0.0013	12
21	55958.8579	0.0012	−0.0014	20
22	55958.8962	0.0008	−0.0013	11
28	55959.1281	0.0008	0.0008	68
29	55959.1672	0.0010	0.0016	68
30	55959.2048	0.0004	0.0010	123
31	55959.2437	0.0004	0.0015	113
32	55959.2811	0.0003	0.0007	113
33	55959.3183	0.0005	−0.0004	78
44	55959.7426	0.0022	0.0027	8
45	55959.7777	0.0084	−0.0005	5
46	55959.8194	0.0010	0.0029	7
47	55959.8566	0.0009	0.0018	11
48	55959.8970	0.0007	0.0040	5
70	55960.7412	0.0008	0.0058	9
73	55960.8654	0.0010	0.0151	24
74	55960.8927	0.0003	0.0041	44
75	55960.9308	0.0004	0.0039	39
76	55960.9693	0.0004	0.0041	39
77	55961.0065	0.0004	0.0031	40
122	55962.7235	0.0011	−0.0031	18
123	55962.7629	0.0008	−0.0019	15
124	55962.8019	0.0009	−0.0012	20
126	55962.8790	0.0017	−0.0007	20
148	55963.7167	0.0011	−0.0054	16
150	55963.7946	0.0016	−0.0040	20
151	55963.8312	0.0013	−0.0057	15

*BJD−2400000.
†Against max $= 2455958.0552 + 0.038290E$.
‡Number of points used to determine the maximum.

Subsequent observations detected superhumps (vsnet-alert 14500, 14501). The two superhumps maxima were BJD 2456045.3135(17) ($N = 28$) and 2456045.3795(14) ($N = 35$). We adopted a period of 0.0660(2) d from this timing analysis. The profile of the superhumps is shown in figure 66.

3.68. OT J131625.7−151313

This transient (=CSS080427:131626−151313; hereafter OT J131625) was detected by CRTS on 2008 April 27. Two further outbursts were detected by CRTS in 2010 February and 2011 April. The 2012 March outburst was also detected by CRTS. Subsequent observation clarified the presence of superhumps (vsnet-alert 14376, 14377). Since the observation was done only on one night, we obtained a single superhump maximum of BJD

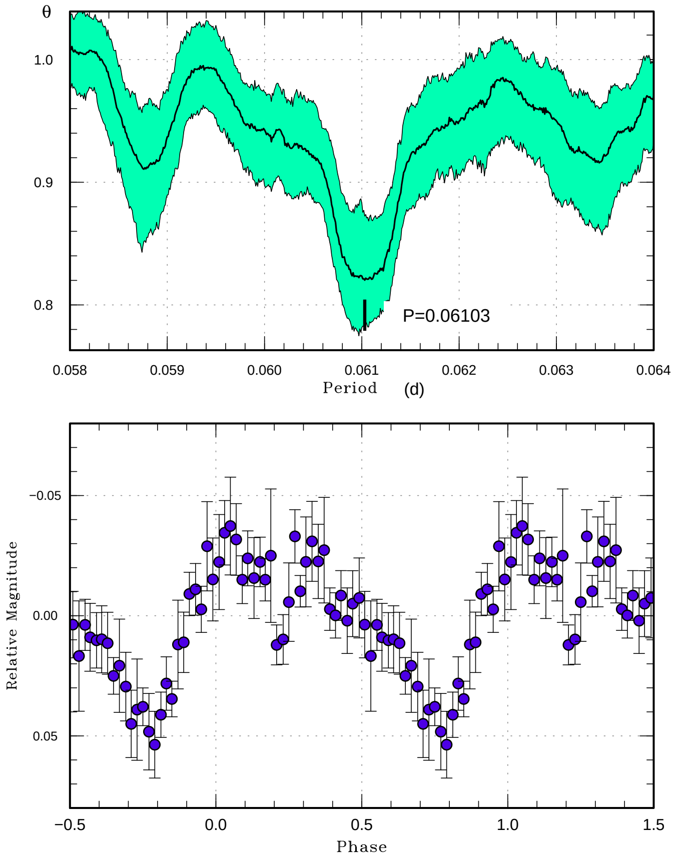

Fig. 65. Superhumps in OT J105122 (2012). (Upper): PDM analysis. (Lower): Phase-averaged profile.

Table 71. Superhump maxima of OT J105122 (2012).

E	max*	error	$O-C$†	N‡
0	55929.7466	0.0019	0.0007	64
1	55929.8069	0.0015	−0.0001	63
2	55929.8626	0.0009	−0.0055	63
3	55929.9291	0.0014	−0.0001	63
4	55929.9894	0.0009	−0.0008	57
12	55930.4884	0.0023	0.0098	16
26	55931.3292	0.0033	−0.0041	16
27	55931.3949	0.0024	0.0005	20
29	55931.5163	0.0072	−0.0003	23
30	55931.5776	0.0038	−0.0000	23

*BJD−2400000.
†Against max $= 2455929.7460 + 0.061054E$.
‡Number of points used to determine the maximum.

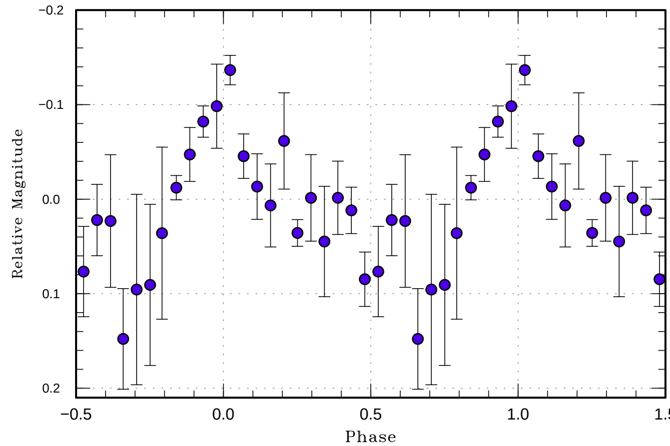

Fig. 66. Superhumps in OT J125905 (2012). A period of 0.0660 d was assumed in phase-averaging.

2456012.5086(9) ($N = 71$). The best superhump period is 0.0955(8) d (PDM method).

3.69. OT J142548.1+151502

This transient (=CSS110628:142548+151502; hereafter OT J142548) was detected by CRTS on 2011 June 28. Only single-night observation was available, which clearly showed superhumps (vsnet-alert 13474). The best superhump period (PDM method) was 0.0984(10) d and we obtained only two superhump maxima: BJD 2455742.3565(9) (N=34) and 2455742.4548(14) (N=27).

3.70. OT J144252.0−225040

This transient (=CSS120417:144252−225040; hereafter OT J144252) was detected by CRTS on 2012 April 17. The large outburst amplitude received attention (vsnet-alert 14448). Subsequent observations detected superhumps (vsnet-alert 14455, 14457; figure 67). The times of superhump maxima are listed in table 72. A clear pattern of stages B and C can be recognized. Despite the large outburst amplitude and the lack of past outbursts in the CRTS data, the $O-C$ diagram resembles those of ordinary SU UMa-type dwarf novae rather than those of extreme WZ Sge-type dwarf novae.

3.71. OT J144453.1−131118

This transient (=CSS120424:144453−131118; hereafter OT J144453) was detected by CRTS on 2012 April 24. There was a past outburst in 2005 December. Although there was a hint of superhumps in the first observation (vsnet-alert 14491), confirmatory observations became available after 4 d (vsnet-alert 14507). Later observations well characterized superhumps (vsnet-alert 14516, 14522, 14530; figure 68). The times of superhump maxima are listed in table 73. There was no hint of period variation. By taking the long initial gap of observation into account, we likely observed stage C superhumps. It is not, however, excluded that this object has a virtually zero $P_{\rm dot}$ as in some long-$P_{\rm orb}$ systems.

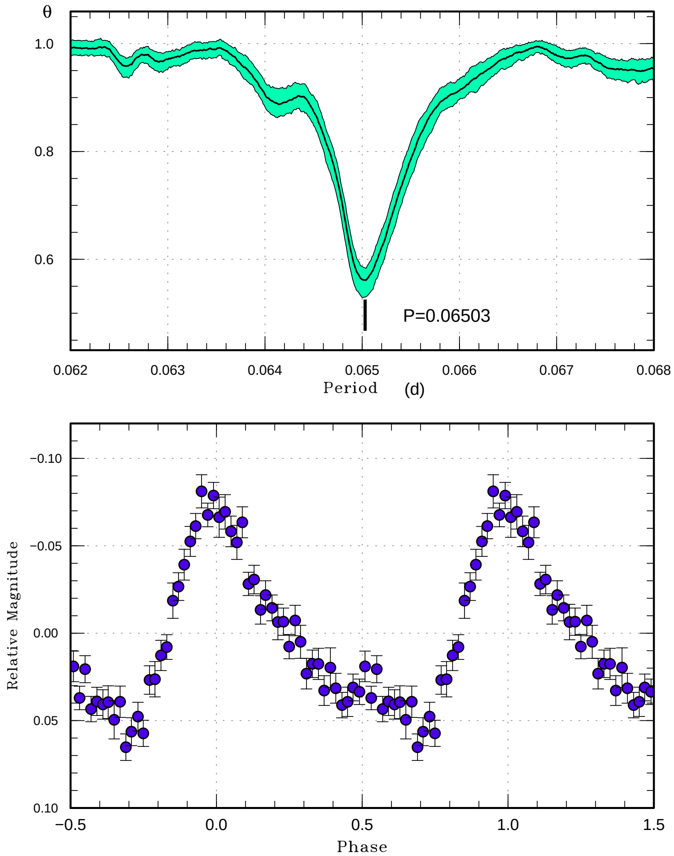

Fig. 67. Superhumps in OT J144252 (2012). (Upper): PDM analysis. (Lower): Phase-averaged profile.

Table 72. Superhump maxima of OT J144252 (2012).

E	max*	error	$O-C$†	N‡
0	56035.6984	0.0015	−0.0041	78
1	56035.7648	0.0010	−0.0027	89
2	56035.8322	0.0007	−0.0003	14
3	56035.8949	0.0006	−0.0025	18
12	56036.4809	0.0004	−0.0013	140
13	56036.5455	0.0006	−0.0017	152
14	56036.6126	0.0010	0.0004	75
15	56036.6742	0.0011	−0.0030	12
18	56036.8697	0.0009	−0.0024	18
27	56037.4552	0.0007	−0.0017	150
28	56037.5212	0.0008	−0.0006	133
29	56037.5855	0.0011	−0.0014	13
30	56037.6543	0.0016	0.0024	14
33	56037.8448	0.0014	−0.0020	17
34	56037.9103	0.0021	−0.0014	13
44	56038.5666	0.0031	0.0051	13
45	56038.6260	0.0017	−0.0004	13
48	56038.8248	0.0013	0.0034	14
49	56038.8921	0.0032	0.0057	18
59	56039.5453	0.0018	0.0092	12
60	56039.6056	0.0015	0.0045	13
61	56039.6725	0.0012	0.0064	11
64	56039.8669	0.0013	0.0059	19
75	56040.5781	0.0013	0.0023	13
76	56040.6422	0.0017	0.0014	13
79	56040.8370	0.0012	0.0013	18
80	56040.9001	0.0021	−0.0006	17
90	56041.5552	0.0069	0.0048	9
91	56041.6086	0.0013	−0.0068	13
106	56042.5791	0.0034	−0.0109	13
107	56042.6463	0.0026	−0.0087	13

*BJD−2400000.
†Against max $= 2456035.7025 + 0.064977E$.
‡Number of points used to determine the maximum.

3.72. OT J145921.8+354806

This transient (=CSS110613:145922+354806; hereafter OT J145921) was detected by CRTS on 2011 June 13. There was an earlier outburst in 2008 April. Subsequent observations detected superhumps (vsnet-alert 13427; figure 69). The times of superhump maxima are listed in table 74. The large amplitudes of the superhumps suggest that the outburst was detected in a relatively early stage. The resultant $P_{\rm dot}$ was less likely negative, as expected for an object with this $P_{\rm SH}$, and may be even positive. The object may be analogous to GX Cas (cf. Kato et al. 2012a) which showed a large positive $P_{\rm dot}$ despite its long $P_{\rm SH}$.

3.73. OT J155631.0−080440

The object was detected as a transient (=CSS090321:155631−080440; hereafter OT J155631) by CRTS on 2009 March 21. Although several outbursts were recorded since then, the 2012 March outburst was the brightest (15.3 mag) in its history. Superhumps were soon detected (vsnet-alert 14406, 14416; figure 70). The times of superhump maxima are listed in table 75.

3.74. OT J160410.6+145618

The object was detected as a transient (=CSS120326:160411+145618; hereafter OT J160410) by CRTS on 2012 March 26. There was another outburst in 2010 July (CRTS data). The large (>5 mag) outburst amplitude was noted (vsnet-alert 14384). Although there was only a single-night observation, two superhump maxima were recorded: BJD 2456014.5194(8) ($N = 35$) and BJD 2456014.5841(11) ($N = 34$). The superhump period by the PDM method is 0.0656(5) d.

3.75. OT J162806.2+065316

The object was detected as a transient (=CSS110611:162806+065316; hereafter OT J162806) by CRTS on 2011 June 11. The object had been selected as a candidate for QSO based on SDSS colors (Richards et al. 2009). The existence of two previous outbursts in the CRTS data confirmed the DN-type nature (vsnet-alert 13413). The object was soon confirmed to show

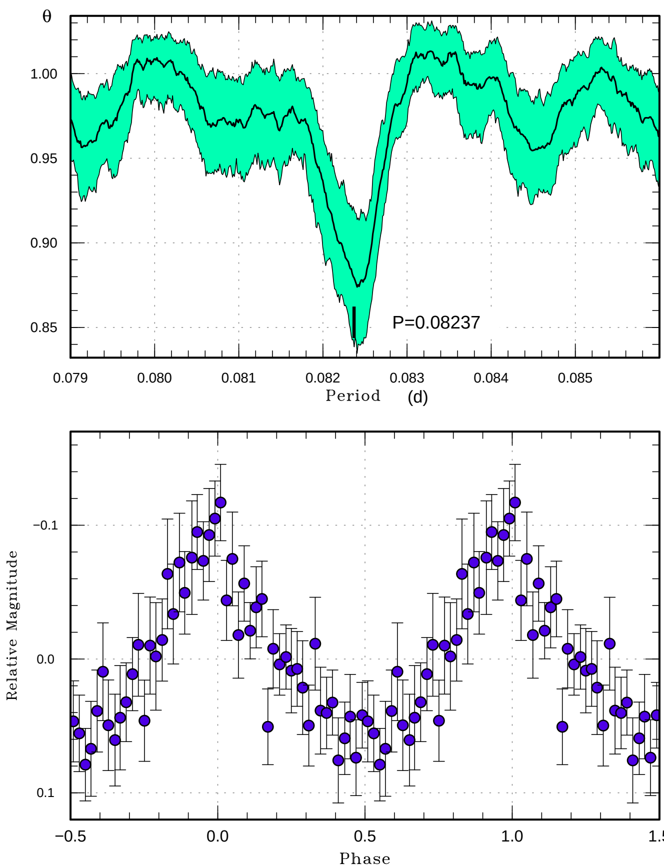

Fig. 68. Superhumps in OT J144453 (2011). (Upper): PDM analysis. (Lower): Phase-averaged profile.

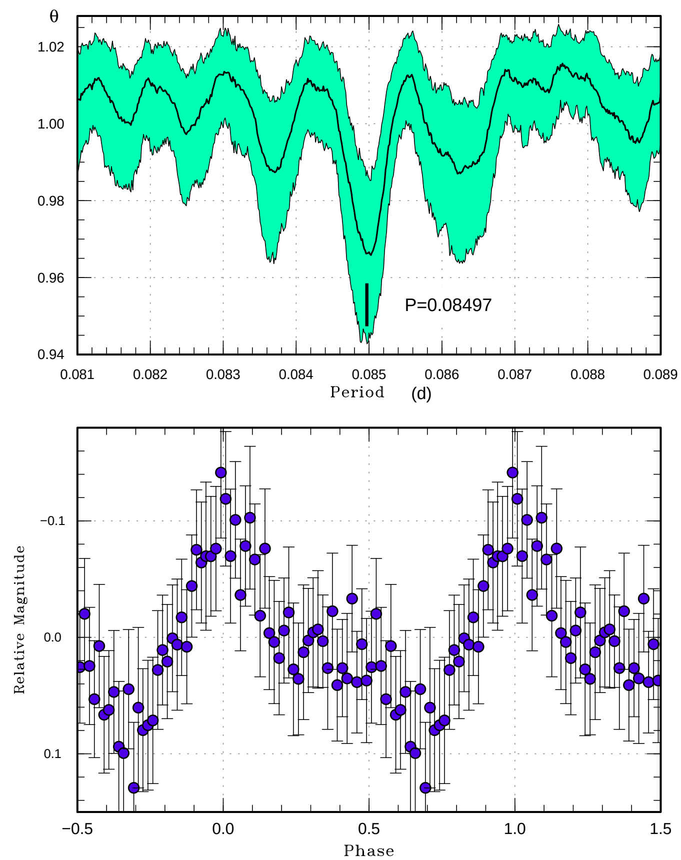

Fig. 69. Superhumps in OT J145921 (2011). (Upper): PDM analysis. (Lower): Phase-averaged profile.

Table 73. Superhump maxima of OT J144453 (2012).

E	max*	error	$O-C$†	N‡
0	56046.1078	0.0009	0.0001	170
17	56047.5119	0.0020	0.0053	13
18	56047.5888	0.0015	−0.0001	14
20	56047.7561	0.0009	0.0026	10
21	56047.8346	0.0010	−0.0011	25
32	56048.7402	0.0010	−0.0007	12
33	56048.8242	0.0012	0.0010	24
34	56048.9017	0.0016	−0.0039	19
42	56049.5541	0.0030	−0.0098	15
43	56049.6493	0.0045	0.0031	15
44	56049.7259	0.0205	−0.0025	12
45	56049.8057	0.0010	−0.0050	21
46	56049.8926	0.0020	−0.0004	22
55	56050.6386	0.0041	0.0050	14
56	56050.7191	0.0029	0.0032	12
57	56050.7967	0.0050	−0.0015	18
58	56050.8849	0.0028	0.0044	26

*BJD−2400000.
†Against max $= 2456046.1077 + 0.082289E$.
‡Number of points used to determine the maximum.

Table 74. Superhump maxima of OT J145921 (2011).

E	max*	error	$O-C$†	N‡
0	55728.4160	0.0011	0.0033	69
11	55729.3516	0.0003	0.0027	50
12	55729.4362	0.0005	0.0022	59
24	55730.4490	0.0023	−0.0064	30
25	55730.5413	0.0015	0.0008	33
35	55731.3891	0.0006	−0.0026	43
36	55731.4725	0.0007	−0.0043	36
58	55733.3492	0.0016	−0.0001	36
59	55733.4357	0.0011	0.0013	46
62	55733.6885	0.0018	−0.0013	125
63	55733.7754	0.0016	0.0005	126
71	55734.4462	0.0018	−0.0096	37
73	55734.6391	0.0082	0.0131	78
74	55734.7113	0.0032	0.0002	128

*BJD−2400000.
†Against max $= 2455728.4126 + 0.085114E$.
‡Number of points used to determine the maximum.

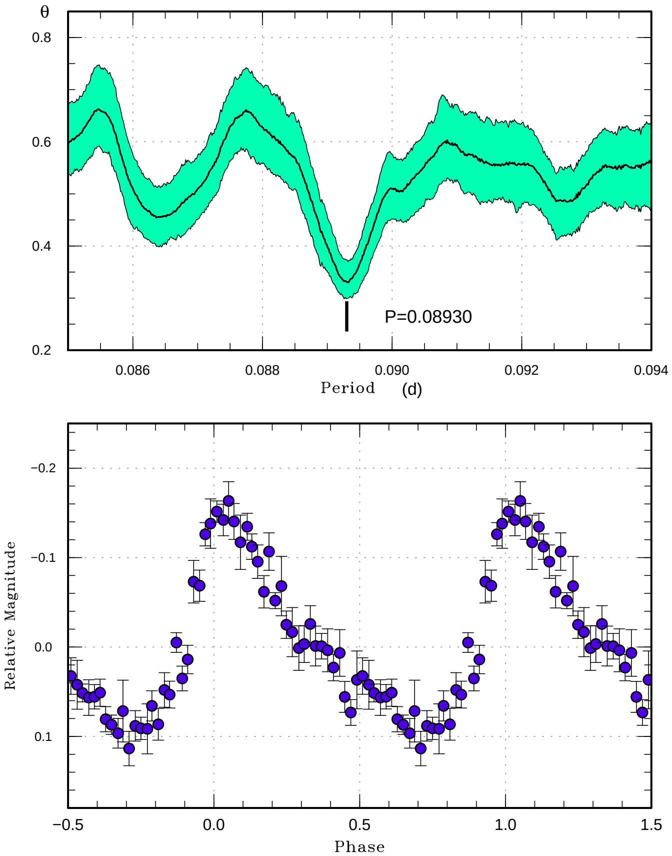

Fig. 70. Superhumps in OT J155631 (2012). (Upper): PDM analysis. (Lower): Phase-averaged profile.

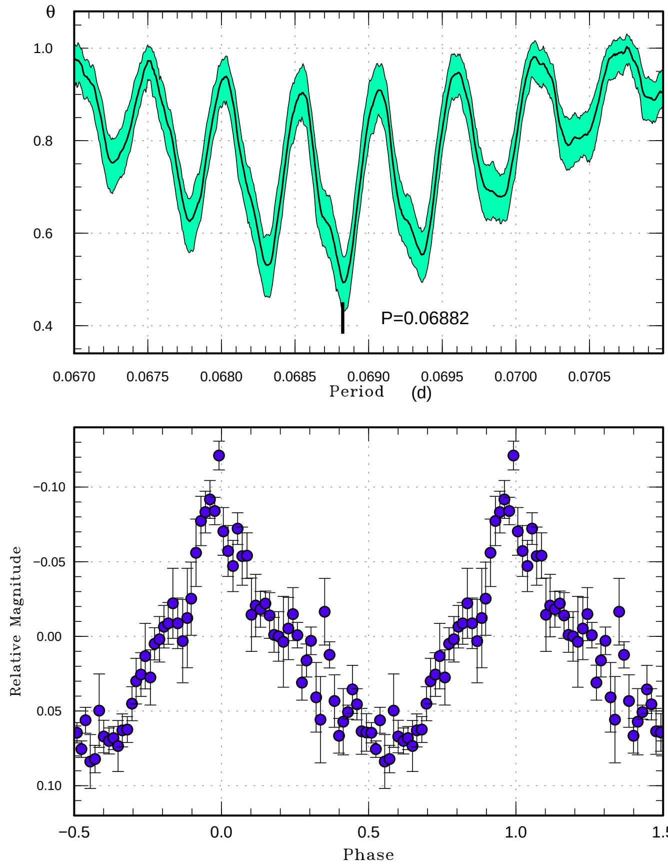

Fig. 71. Superhumps in OT J162806 (2011). (Upper): PDM analysis. (Lower): Phase-averaged profile.

Table 75. Superhump maxima of OT J155631 (2012).

E	max*	error	$O-C$†	N‡
0	56017.2322	0.0007	−0.0021	92
1	56017.3236	0.0005	−0.0000	95
18	56018.8443	0.0013	0.0024	13
29	56019.8257	0.0020	0.0015	10
30	56019.9149	0.0019	0.0013	14
40	56020.8067	0.0025	0.0001	9
41	56020.8928	0.0029	−0.0032	21

*BJD−2400000.
†Against max $= 2456017.2343 + 0.089309E$.
‡Number of points used to determine the maximum.

Table 76. Superhump maxima of OT J162806 (2011).

E	max*	error	$O-C$†	N‡
0	55724.4545	0.0003	0.0009	67
13	55725.3473	0.0005	−0.0013	38
14	55725.4175	0.0003	0.0000	64
15	55725.4866	0.0003	0.0003	55
139	55734.0220	0.0012	−0.0013	105
140	55734.0935	0.0022	0.0014	99

*BJD−2400000.
†Against max $= 2455724.4536 + 0.068847E$.
‡Number of points used to determine the maximum.

superhumps (vsnet-alert 13416; figure 71). The times of superhump maxima are listed in table 76.

3.76. OT J163942.7+122414

The object was originally detected as a transient (=CSS080131:163943+122414; hereafter OT J163942) by CRTS on 2008 January 31. We observed the 2012 April outburst detected by the CRTS. The observations confirmed the presence of superhumps (vsnet-alert 14474; figure 72). The times of superhump maxima are listed in table 77. The period in table 2 refers to the result of the

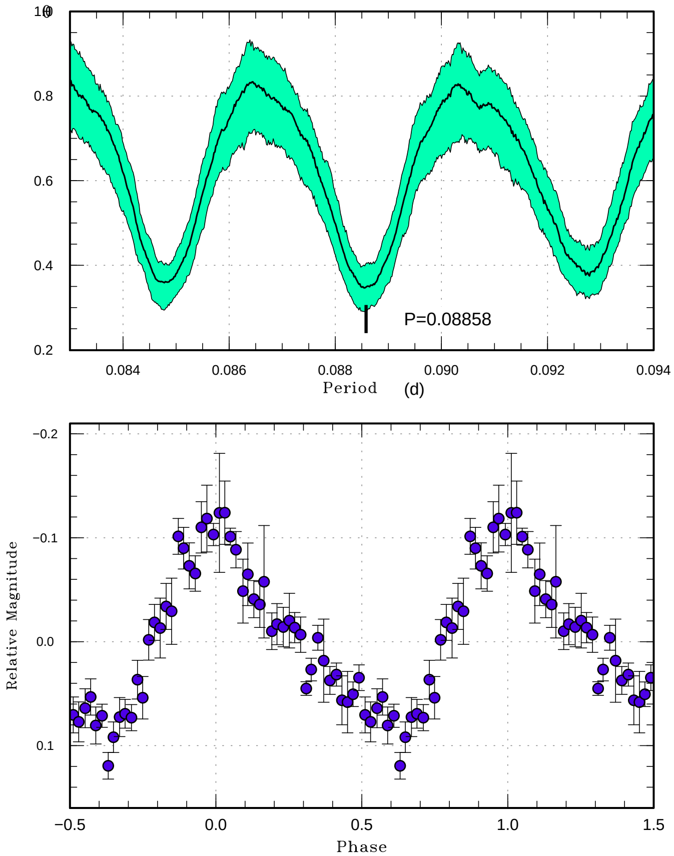

Fig. 72. Superhumps in OT J163942 (2012). (Upper): PDM analysis. The alias was selected by $O-C$ analysis of a continuous run on a single night. (Lower): Phase-averaged profile.

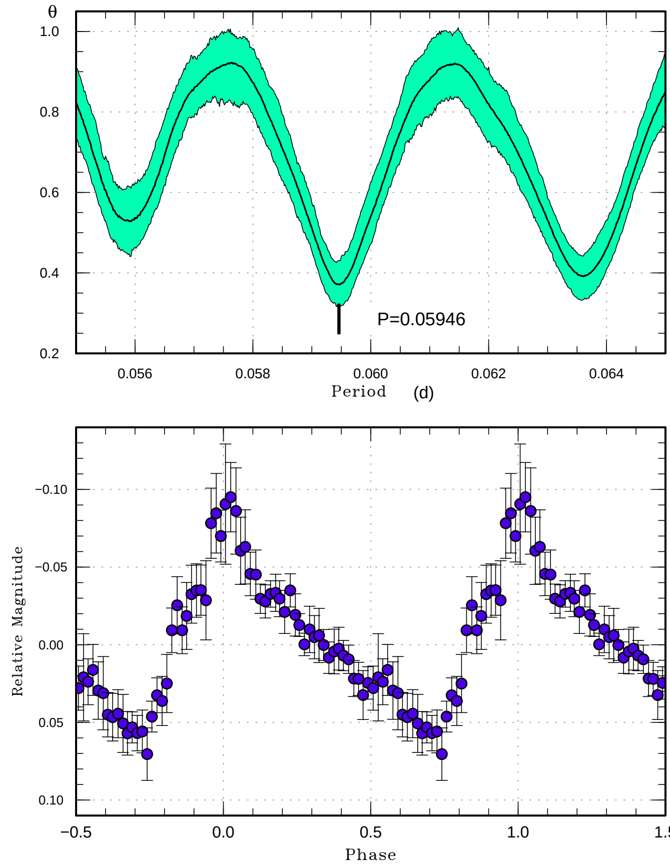

Fig. 73. Superhumps in OT J170609 (2011). (Upper): PDM analysis. (Lower): Phase-averaged profile.

Table 77. Superhump maxima of OT J163942 (2012).

E	max*	error	$O-C$†	N‡
0	56039.5603	0.0007	−0.0000	88
22	56041.5094	0.0024	0.0009	33
23	56041.5962	0.0011	−0.0008	39

*BJD−2400000.
†Against max $= 2456039.5603 + 0.088554E$.
‡Number of points used to determine the maximum.

Table 78. Superhump maxima of OT J170609 (2011).

E	max*	error	$O-C$†	N‡
0	55745.5333	0.0006	−0.0017	59
1	55745.5963	0.0015	0.0018	31
15	55746.4283	0.0004	−0.0003	57
16	55746.4884	0.0004	0.0002	60

*BJD−2400000.
†Against max $= 2455745.5350 + 0.059578E$.
‡Number of points used to determine the maximum.

PDM analysis. The object appears to be a long-$P_{\rm orb}$ system with frequent outbursts based on numerous outburst detections by the CRTS.

3.77. OT J170609.7+143452

The object was originally detected as a transient (=CSS090205:170610+143452; hereafter OT J170609) by CRTS on 2009 February 5. Although superhumps were detected during the 2009 outburst (vsnet-alert 11061), the period was not well determined because the object faded quickly after this observation.

The object underwent another outburst in 2011 June (CRTS detection, see also vsnet-alert 13456). Although the object once faded (vsnet-alert 13464), it showed a rebrightening in July (vsnet-alert 13481). The outburst turned out to be a superoutburst preceded by a precursor. Observations on two nights yielded a likely superhump period of 0.05946(8) d (PDM analysis; figure 73), although one-day aliases cannot be perfectly excluded. The selection of the alias appears to be justified by independently determined spectroscopic period of 0.0582 d (Thorstensen, Skinner 2012), yielding an ϵ of 2.2%. The times of superhump maxima are listed in table 78.

3.78. OT J173516.9+154708

The object was detected as a transient (=CSS110623:173517+154708; hereafter OT J173516) by CRTS on 2011 June 23. The object was also in outburst in GSC 1.2. Although early observations already recorded superhump-like modulations (vsnet-alert 13465, 13468, 13470), the times of maxima could not be well expressed by any trial period (vsnet-alert 13473, 13482). Although the main power of periodicities was recorded in a range of 0.05–0.06 d, we could not sort out a single superhump period at the time of the observation. On July 9, the object entered a rapid decline phase.

Using the best part (June 26–29) of our observation before the rapid decline, there appeared to be two strong signals around 0.05436 d and 0.05827 d with the PDM analysis. The lasso analysis, which is less affected by the window function, yielded the same two signals (figure 74). By partially subtracting mean profiles from the observations folded by each period, we have been able to decompose the light curve into these periods (figure 75). A simple superposition of these two waves has been shown to express the observation fairly well (figure 76).

The exact identifications of these periodicities are yet unclear. It might be that the shorter period is $P_{\rm orb}$ and the longer period is $P_{\rm SH}$. In this case, however, the ϵ is 7.2%, extremely too large for this $P_{\rm orb}$, and none of non-eclipsing SU UMa-type dwarf novae have yet shown similar amplitudes of orbital humps and superhumps at the same time. We suggest an alternative interpretation that the longer period is $P_{\rm orb}$ and the shorter period represents negative superhumps. The small amplitude of superhumps, compared to that of orbital humps, may be reconciled if negative superhumps were indeed excited. The exact identification of the periods should await future observations.

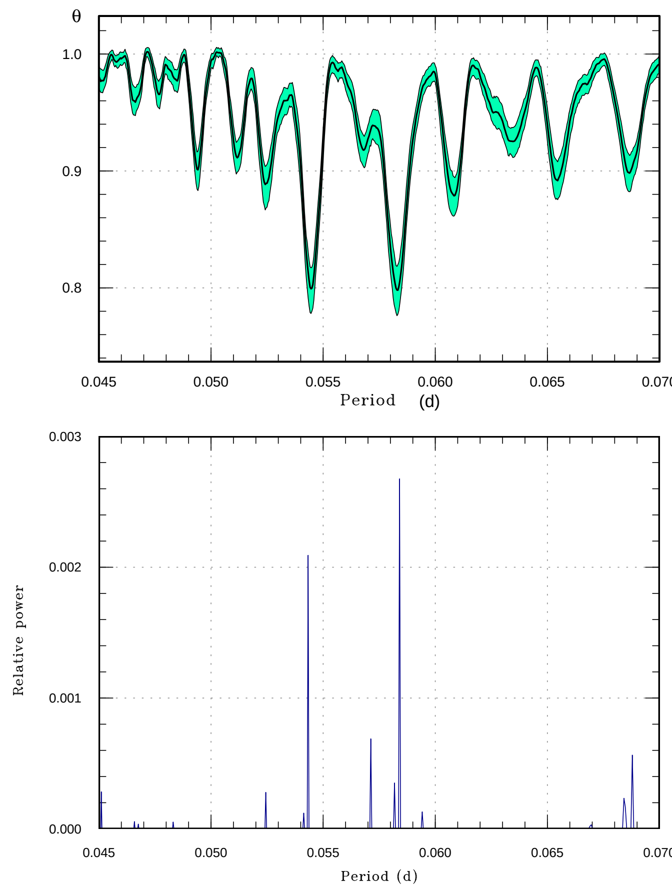

Fig. 74. Period analysis in OT J173516 (2011). (Upper): PDM analysis. (Lower): lasso analysis ($\log \lambda = -6.42$).

3.79. OT J184228.1+483742

This object (hereafter OT J184228) was discovered H. Nishimura on 2011 September 5.5293 UT at an unfiltered CCD magnitude of 11.8 (=PNV J18422792+4837425; Nakano et al. 2011). S. Kiyota's early multicolor photometry already suggested the dwarf nova-type nature (vsnet-alert 13645). M. Fujii, A. Ayani, C. Buil (vsnet-alert 13650, 13651, 13655) and A. Arai[6] reported spectra, all of which indicated Balmer lines in absorption with emission cores for Hα and Hβ, indicating that the object is indeed a dwarf nova in outburst. The relatively narrow absorption suggested a low-inclination of this object. U. Munari also reported a spectrum (Nakano et al. 2011). Although there were small-amplitude variations, the object started rapid fading on September 25 before the development of superhumps (we call this outburst "first plateau phase"; vsnet-alert 13703). The object brightened again on October 3 (vsnet-alert 13713) and object further brightened to the second plateau phase. During this plateau phase, ordinary superhumps finally developed (vsnet-alert 13726, 13728, 13729). Such development of the outburst was unprecedented in dwarf novae. On October 18, the object enter the rapid fading stage (vsnet-alert 13775). The object remained above quiescence even following the rapid decline, and there was another rebrightening following the second plateau phase (Katysheva et al. in preparation).

The times of superhump maxima during the second plateau phase and post-superoutburst stage are listed in table 79. The epochs $E=0,1$ were recorded during the rise to the second plateau phase. The times for $E>206$ were recorded during the post-superoutburst stage. Although the humps were clearly detected, the cycle counts for the latter maxima were slightly uncertain. As seen from $E=413$ and $E=428$, there appeared to have been double maxima during one superhump cycle. The short visibility in the evening during this stage hindered unambiguous identification of the nature of these maxima. We identified $E \le 64$ as the stage A superhumps because the superhumps evolved during this stage, and subsequent superhumps as stage B superhumps. These stages, however, may be inadequate considering the peculiar evolution of the entire outburst. In determining the period of stage A superhumps, we disregarded $E=0,1$. The period of stage B superhumps was very stable, and $P_{\rm dot}$ was almost zero.

[6] <http://www.cbat.eps.harvard.edu/unconf/followups/J18422792+4837425.html>.

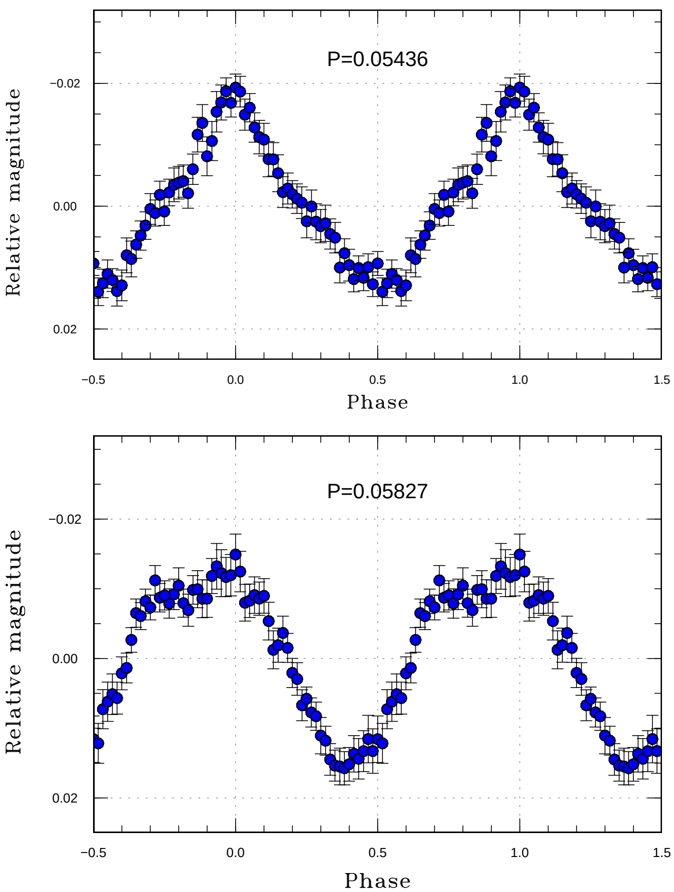

Fig. 75. Profiles of two periodicities in OT J173516 (2011).

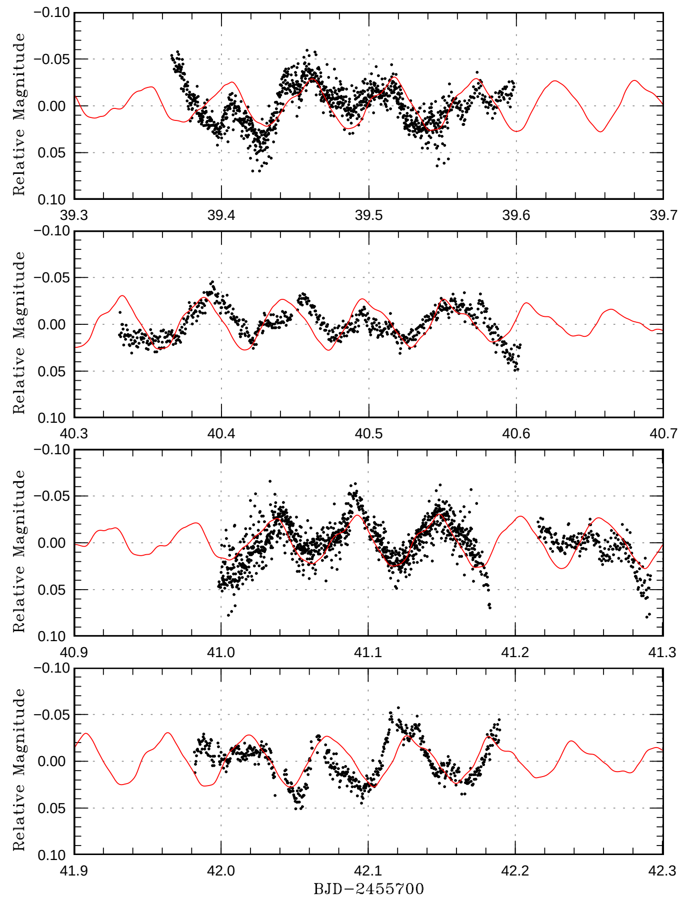

Fig. 76. Synthesized light curve of OT J173516 (2011). The points represent observations. The curves represent the expected light curve by adding two waves in figure 75.

Although these superhumps bore more characteristics of stage C superhumps in ordinary SU UMa-type dwarf novae, the identification of the nature should await future research. The amplitudes of superhumps were small (0.045 mag in full amplitude in average), suggesting a weak manifestation of the tidal instability.

During the first plateau phase, there was a possible signal of early superhumps with a period of 0.07168(1) d (figure 78). Since the signal had only a small amplitude, exact identification of the orbital period should await future observations. Assuming that this period is close to the orbital period, we obtained an ϵ of 0.9%, comparable to those of short-$P_{\rm orb}$ WZ Sge-type dwarf novae, but is unusually small for a $P_{\rm orb} = 0.07168$ d object. This might suggest the presence of an anomalously undermassive secondary and this object could be a good candidate for a period bouncer.

The unique feature of the outburst evolution might be also understood if the mass-ratio is anomalously low as explained in the following scenario. (1) The disk initially expanded enough to trigger the 2:1 resonance. (2) The disk started to cool down before the 3:1 resonance governs as in ordinary WZ Sge-type dwarf novae, and the object underwent a temporary excursion to a quiescent state, then (3) the 3:1 resonance started to grow slowly, and triggered a second thermal instability and entered the second plateau phase. The second plateau phase apparently started from an inside-out type outburst, as suggested by the slow rise. The small amplitude probably reflect the weak tidal torque resulting from a low mass-ratio.

The object resembles in its long $P_{\rm orb}$ and apparently in its low mass-ratio, suggesting a brown-dwarf secondary, the famous CV GD 552 (Hessman, Hopp 1990; Unda-Sanzana et al. 2008), which had never been observed to undergo an outburst (cf. Richter 1990). If GD 552 were to undergo an outburst, we might expect a phenomenon similar to OT J184228.

A more detailed analysis will be reported in Ohshima et al., in preparation.

3.80. OT J210950.5+134840

This object (hereafter OT J210950) was discovered as a possible nova (=PNV J21095047+1348396) by K. Itagaki as an 11.5 mag (unfiltered CCD magnitude) object (Yamaoka et al. 2011). Although the initial discovery announcement suggested the absence of the quiescent

Table 79. Superhump maxima of OT J184228 (2011).

E	max*	error	$O-C$†	N‡
0	55838.9637	0.0022	−0.0366	172
1	55839.0387	0.0005	−0.0341	83
17	55840.2225	0.0011	−0.0097	164
18	55840.2982	0.0009	−0.0065	322
19	55840.3668	0.0007	−0.0104	270
22	55840.5828	0.0017	−0.0117	51
31	55841.2434	0.0017	−0.0033	104
32	55841.3122	0.0009	−0.0070	76
33	55841.3884	0.0003	−0.0032	211
34	55841.4617	0.0008	−0.0024	134
35	55841.5395	0.0019	0.0029	91
36	55841.6068	0.0005	−0.0023	154
37	55841.6791	0.0008	−0.0024	113
41	55841.9707	0.0011	−0.0007	221
42	55842.0431	0.0015	−0.0007	355
43	55842.1302	0.0046	0.0139	36
45	55842.2669	0.0011	0.0057	76
46	55842.3374	0.0019	0.0037	76
49	55842.5624	0.0008	0.0113	118
50	55842.6314	0.0006	0.0079	131
56	55843.0700	0.0024	0.0117	87
58	55843.1943	0.0071	−0.0090	56
59	55843.2815	0.0018	0.0058	76
60	55843.3504	0.0022	0.0022	75
63	55843.5736	0.0010	0.0080	164
64	55843.6538	0.0017	0.0158	124
65	55843.7276	0.0020	0.0171	65
68	55843.9248	0.0013	−0.0030	172
69	55843.9854	0.0023	−0.0149	165
73	55844.3040	0.0008	0.0139	60
74	55844.3727	0.0011	0.0100	74
75	55844.4453	0.0010	0.0102	72
76	55844.5252	0.0010	0.0176	47
77	55844.5898	0.0011	0.0098	47
82	55844.9495	0.0010	0.0072	114
84	55845.0895	0.0020	0.0022	104
87	55845.3107	0.0012	0.0060	73
88	55845.3790	0.0015	0.0019	72
89	55845.4512	0.0022	0.0016	64
100	55846.2521	0.0009	0.0054	157
101	55846.3275	0.0005	0.0083	254
102	55846.4008	0.0008	0.0092	283
103	55846.4745	0.0024	0.0103	46
109	55846.9046	0.0013	0.0057	74
114	55847.2699	0.0015	0.0087	226
115	55847.3359	0.0017	0.0022	280
128	55848.2806	0.0014	0.0049	70
129	55848.3479	0.0012	−0.0002	144
130	55848.4222	0.0020	0.0015	145
141	55849.2102	0.0164	−0.0075	109
142	55849.2933	0.0024	0.0030	257

*BJD−2400000.

†Against max $= 2455839.0003 + 0.072464E$.

‡Number of points used to determine the maximum.

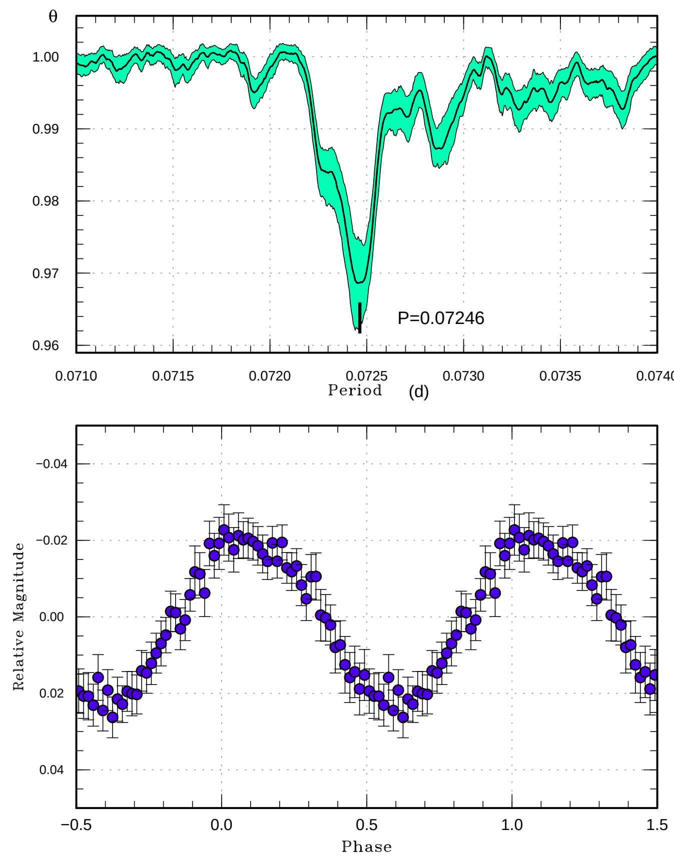

Fig. 77. Superhumps in OT J184228 (2011). (Upper): PDM analysis. (Lower): Phase-averaged profile.

counterpart, independent examinations of plate archives indicated the presence of an 18–19 mag counterpart (S. Korotkiy, vsnet-alert 13342; E. Guido and G. Sostero, Yamaoka et al. 2011, vsnet-alerr 13344). It was already suggested to be a WZ Sge-type dwarf nova with an amplitude exceeding 7 mag (vsnet-alert 13341). D. Denisenko also noted the presence of an M-dwarf having a common proper motion and the detection of this object in GALEX UV data (vsnet-alert 13343). Although only low-amplitude variations were detected soon after the discovery, superhumps appeared on May 30, 6 d after the discovery (vsnet-alert 13359). The obtained period was not suggestive of an extreme WZ Sge-type dwarf nova. There was a hint of evolving (double wave) superhumps on May 28 (vsnet-alert 13363). The object was spectroscopically confirmed to be a dwarf nova (Yamaoka et al. 2011).

The times of superhump maxima are listed in table 80. Distinct stages of A–C are present. Although the last two epochs were measured after the rapid fading, the times of maxima were well on the extension of the timings of stage C superhumps recorded before the rapid fading, and we consider them as persisting stage C superhumps as we already reported in earlier papers (Kato et al. 2009; Kato et al. 2010; Kato et al. 2012a). The resultant $P_{\rm dot}$ for the stage B was $+8.5(0.6) \times 10^{-5}$, whose large value is consistent with the idea that this object is not an extreme WZ

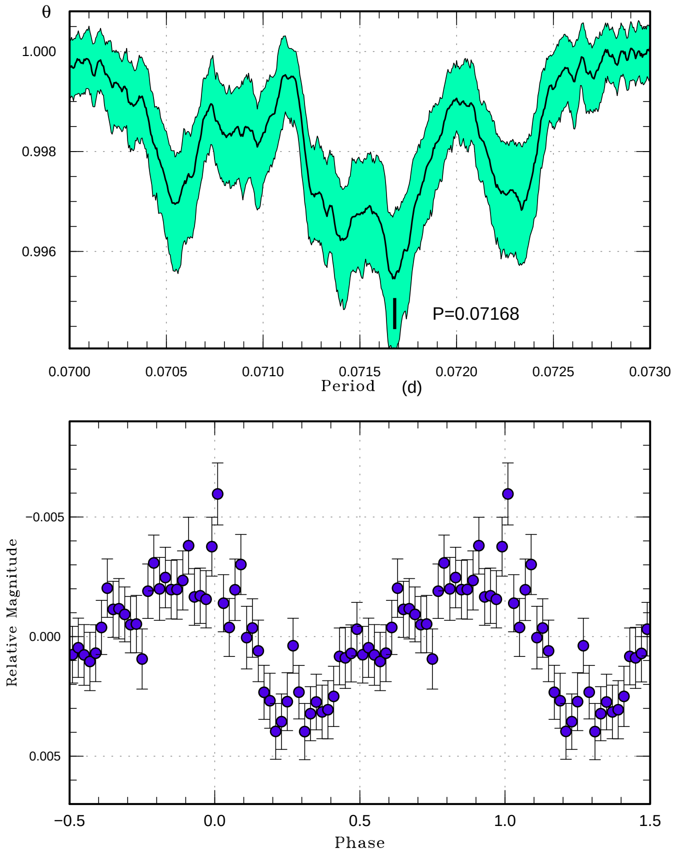

Fig. 78. Possible early superhumps in OT J184228 (2011). (Upper): PDM analysis. (Lower): Phase-averaged profile.

Table 79. Superhump maxima of OT J184228 (2011) (continued).

E	max*	error	$O-C$†	N‡
143	55849.3628	0.0013	0.0001	216
144	55849.4368	0.0021	0.0016	141
156	55850.3115	0.0015	0.0068	156
157	55850.3759	0.0013	−0.0013	138
158	55850.4445	0.0018	−0.0051	138
165	55850.9518	0.0014	−0.0051	150
170	55851.3083	0.0032	−0.0109	54
171	55851.3874	0.0041	−0.0043	71
183	55852.2622	0.0018	0.0009	187
184	55852.3280	0.0007	−0.0057	271
185	55852.4003	0.0010	−0.0059	272
186	55852.4717	0.0010	−0.0069	126
192	55852.9039	0.0011	−0.0095	167
193	55852.9774	0.0014	−0.0085	251
194	55853.0539	0.0018	−0.0044	150
198	55853.3424	0.0045	−0.0058	65
199	55853.4125	0.0026	−0.0082	55
198	55853.3424	0.0045	−0.0058	65
206	55853.9201	0.0018	−0.0078	110
226	55855.3771	0.0010	−0.0001	56
321	55862.2628	0.0015	0.0016	27
377	55866.3262	0.0018	0.0070	19
413	55868.9431	0.0010	0.0152	79
428	55869.9909	0.0009	−0.0241	91
472	55873.2097	0.0053	0.0064	9

*BJD−2400000.
†Against max $= 2455839.0003 + 0.072464E$.
‡Number of points used to determine the maximum.

Sge-type dwarf nova. No post-superoutburst rebrightening was recorded. CRTS data[7] did not record a prior outburst, and the data indicated that the object remained brighter than quiescence five months after the outburst. These features suggest that the outburst frequency is low, and the presence of a long-fading tail looks like those of WZ Sge-type dwarf novae (e.g. GW Lib, figure 33 in Kato et al. 2009). The object may be a WZ Sge-type dwarf nova with non-extreme properties, and showed a type-D superoutburst in terms of the lack of a post-superoutburst rebrightening. The $P_{\rm dot}$-ϵ relation (equation 6 in Kato et al. 2009) suggests ϵ of 2.6%.

In the PDM analysis (figure 79) there seems to be a slightly enhanced signal shorter than $P_{\rm SH}$, we employed lasso analysis to detect the possible $P_{\rm orb}$. The obtained candidate period was 0.05865(1) d, suggesting ϵ for stage B superhumps of 2.4%. Although this period is close to what was expected from the $P_{\rm dot}$-ϵ relation, it needs to be tested by future observations.

3.81. OT J214738.4+244553

The object was detected as a transient (=CSS111004:214738+244554; hereafter OT J214738) by CRTS on 2011 October 4. ASAS-3 (Pojmański 2002) recorded additional three outbursts. Subsequent observations recorded superhumps (vsnet-alert 13720, 13721; figure 80). The times of superhump maxima are listed in table 81. Although it is unclear whether we indeed observed the early stage of the outburst, the superhumps for $E \le 20$ appears to be stage A superhumps. There was no clear transition to stage C, and $P_{\rm dot}$ for $E \le 20$ was $+8.8(1.0) \times 10^{-5}$ anomalously high for a long-$P_{\rm SH}$ system. The behavior resembles those of SDSS J170213 (subsection 3.53) and GX Cas (Kato et al. 2012a). There is a strong signal at 0.09273(3) d (see figure 80), which we interpret as the orbital period. Assuming this period, the ϵ for the mean $P_{\rm SH}$ is 4.9%.

3.82. OT J215818.5+241925

This object (hereafter OT J215818) is an object reported by G. Sun and X. Gao to Central Bureau for Astronomical Telegrams (CBAT) Transient Objects Confirmation Page (TOCP) originally suspected to be a nova (=PNV J21581852+2419246). Soon after the discovery, R. Koff[8] detected modulations similar to superhumps. This finding was confirmed by subsequent obser-

[7] <http://nesssi.cacr.caltech.edu/catalina/20110606/1106061121124182967p.html>

[8] <http://www.cbat.eps.harvard.edu/unconf/followups/J21581852+2419246.html>.

Table 80. Superhump Maxima of OT J210950 (2011).

E	max*	error	$O-C$†	N‡
0	55710.5319	0.0009	−0.0188	168
1	55710.5897	0.0008	−0.0211	168
27	55712.1758	0.0006	0.0044	96
28	55712.2356	0.0003	0.0042	92
34	55712.5982	0.0002	0.0066	104
37	55712.7804	0.0003	0.0088	87
38	55712.8401	0.0002	0.0084	104
39	55712.9005	0.0002	0.0088	122
54	55713.7970	0.0002	0.0049	170
55	55713.8564	0.0003	0.0043	87
71	55714.8117	0.0004	−0.0008	86
72	55714.8706	0.0004	−0.0019	86
77	55715.1733	0.0008	0.0006	38
78	55715.2326	0.0004	−0.0001	48
84	55715.5900	0.0003	−0.0028	115
87	55715.7693	0.0004	−0.0036	61
88	55715.8315	0.0004	−0.0015	74
89	55715.8904	0.0004	−0.0026	75
104	55716.7890	0.0004	−0.0043	72
105	55716.8497	0.0002	−0.0036	146
106	55716.9099	0.0004	−0.0035	142
117	55717.5703	0.0003	−0.0033	168
117	55717.5703	0.0003	−0.0034	167
121	55717.8098	0.0006	−0.0040	106
122	55717.8708	0.0008	−0.0030	82
128	55718.2312	0.0005	−0.0027	101
148	55719.4352	0.0008	0.0008	120
165	55720.4667	0.0013	0.0119	122
166	55720.5259	0.0010	0.0110	133
187	55721.7886	0.0020	0.0132	68
188	55721.8463	0.0010	0.0109	69
220	55723.7585	0.0029	0.0023	35
221	55723.8227	0.0008	0.0064	48
222	55723.8818	0.0013	0.0055	49
288	55727.8236	0.0018	−0.0143	82
289	55727.8802	0.0019	−0.0178	93

*BJD−2400000.
†Against max $= 55710.5507 + 0.060025E$.
‡Number of points used to determine the maximum.

Table 81. Superhump maxima of OT J214738 (2011).

E	max*	error	$O-C$†	N‡
0	55839.3213	0.0002	−0.0289	244
1	55839.4206	0.0002	−0.0270	250
10	55840.3196	0.0002	−0.0038	253
11	55840.4178	0.0003	−0.0029	297
12	55840.5161	0.0003	−0.0019	252
13	55840.6173	0.0005	0.0020	260
14	55840.7175	0.0004	0.0049	140
21	55841.4019	0.0002	0.0081	408
22	55841.5001	0.0003	0.0090	237
24	55841.6948	0.0003	0.0090	175
25	55841.7914	0.0002	0.0083	186
27	55841.9864	0.0002	0.0087	160
28	55842.0864	0.0003	0.0114	88
31	55842.3748	0.0005	0.0078	152
32	55842.4717	0.0003	0.0074	327
33	55842.5686	0.0003	0.0070	135
34	55842.6645	0.0003	0.0056	237
35	55842.7619	0.0006	0.0057	64
44	55843.6347	0.0006	0.0027	60
45	55843.7323	0.0004	0.0030	69
51	55844.3131	0.0006	−0.0001	110
52	55844.4106	0.0007	0.0001	137
53	55844.5068	0.0008	−0.0011	96
55	55844.7015	0.0002	−0.0009	251
56	55844.7976	0.0002	−0.0022	212
65	55845.6732	0.0006	−0.0024	142
66	55845.7686	0.0003	−0.0043	186
71	55846.2559	0.0004	−0.0036	163
72	55846.3539	0.0003	−0.0029	381
73	55846.4503	0.0003	−0.0038	403
75	55846.6462	0.0051	−0.0026	94
76	55846.7457	0.0004	−0.0004	183
82	55847.3285	0.0003	−0.0015	180
86	55847.7168	0.0004	−0.0024	183
87	55847.8098	0.0007	−0.0067	166
96	55848.6900	0.0007	−0.0024	101
97	55848.7888	0.0007	−0.0009	102
107	55849.7643	0.0017	0.0015	24

*BJD−2400000.
†Against max $= 2455839.3502 + 0.097313E$.
‡Number of points used to determine the maximum.

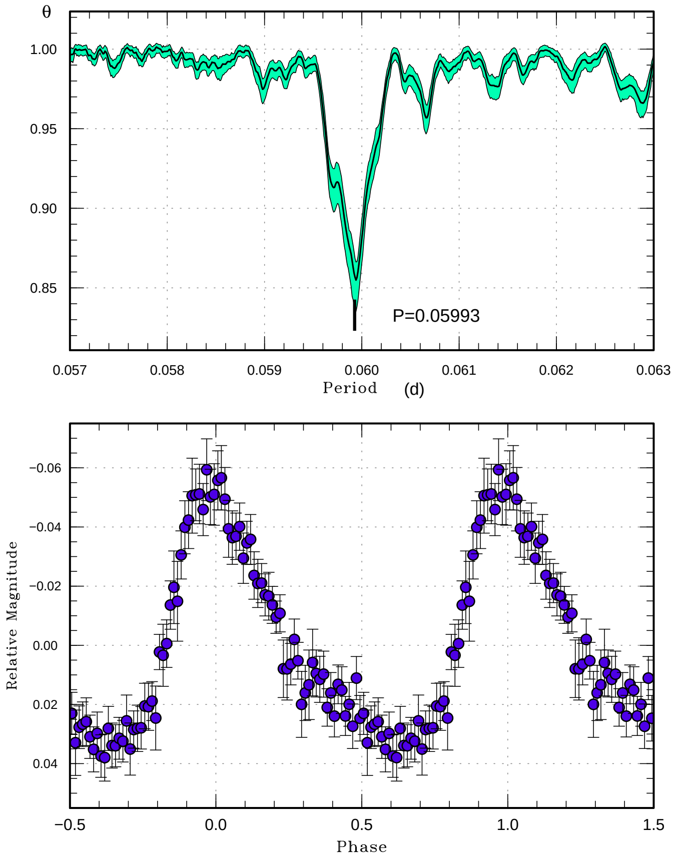

Fig. 79. Superhumps in OT J210950 (2011). (Upper): PDM analysis. (Lower): Phase-averaged profile.

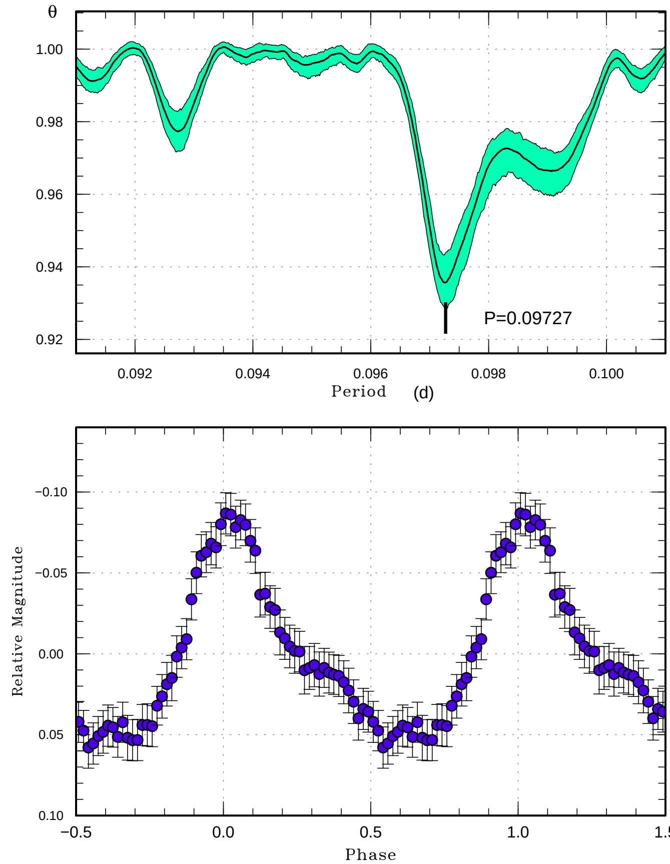

Fig. 80. Superhumps in OT J214738 (2011). (Upper): PDM analysis. (Lower): Phase-averaged profile.

vations (vsnet-alert 13803, 13805, 13807; figure 81), and the dwarf nova-type nature was confirmed. The times of superhump maxima are listed in table 82. The $O-C$ diagram shows typical stage B and C superhumps. The $P_{\rm dot}$ for stage B superhumps was not meaningfully determined because the outburst was apparently observed only during its late course. Shears et al. (2012b) reported a $P_{\rm dot}$ of 0.06728(21) d using a slightly different data set and obtained a similar pattern of $O-C$ variation with this analysis. Shears et al. (2012b) also reported the possible presence of an orbital signal at 0.06606(35) d. Our analysis yielded only a very weak signal (see figure 81), and it appears to be still inconclusive. Using lasso, we measured a period of 0.06607(5) d assuming that it is a real periodicity.

3.83. OT J221232.0+160140

The object was detected as a transient (=CSS 090911:221232+160140; hereafter OT J221232) by CRTS on 2009 September 11. A bright outburst was detected on 2011 December 23 by E. Muyllaert (BAAVSS alert 2804). Subsequent observations confirmed the presence of superhumps (vsnet-alert 14017, 14018, 14020; figure 82). The times of superhump maxima are listed in table 83. The early stage of the outburst was not observed. There was a likely stage B–C transition around $E = 29$.

3.84. OT J224736.4+250436

This object (=CSS120616:224736+250436, hereafter OT J224736) is a transient detected by CRTS on 2012 June 16. There was a previous outburst in 2006 November (CRTS data). An analysis of the SDSS color using the neural network (Kato et al. 2012b) suggested an object below the period gap (vsnet-alert 14682). Subsequent observation detected superhumps (vsnet-alert 14684; figure 83). The times of superhump maxima are listed in table 84. Due to the gap in observation, the other 2-d aliases are still viable. We used the period which gave the smallest residuals to superhump maxima on individual nights.

3.85. TCP J08461690+3115554

This object (hereafter TCP J084616) is a transient discovered by T. Kryachko et al. on 2012 March 19.[9] The object was soon recognized as a deeply eclipsing SU UMa-type dwarf nova (vsnet-alert 14347, 14348, 14351). The object has a $g = 21.8$ mag SDSS counterpart. Using the MCMC method (appendix 1), we obtained an eclipse ephemeris of

[9] <http://www.cbat.eps.harvard.edu/unconf/followups/J08461690+3115554.html>.

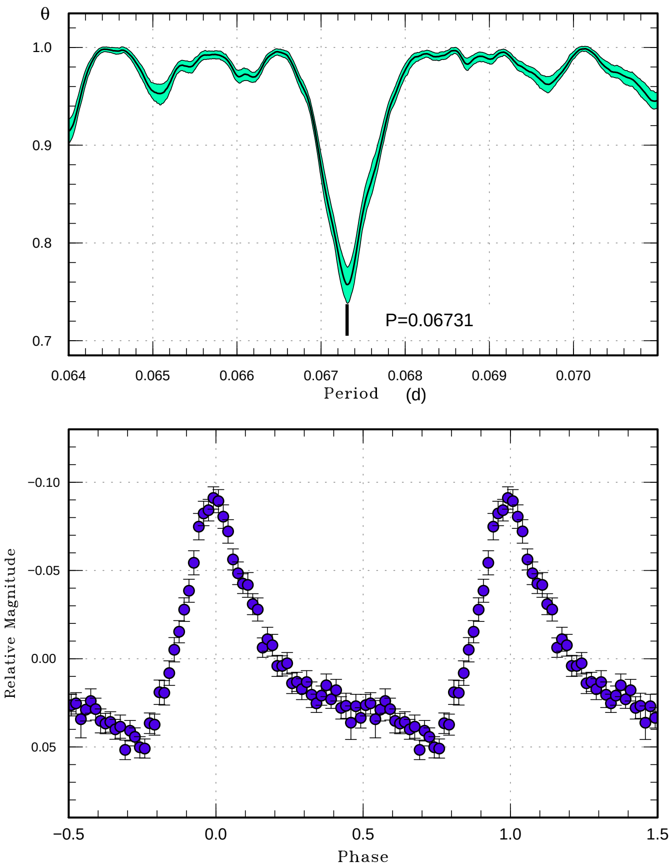

Fig. 81. Superhumps in OT J215818 (2011). (Upper): PDM analysis. (Lower): Phase-averaged profile.

$$\mathrm{Min(BJD)} = 2456007.33870(6) + 0.091383(6)E. \quad (4)$$

The times of superhumps maxima are listed in table 85. A PDM analysis (figure 84) yielded a period of 0.09633(11) d, giving $\epsilon = 5.4(1)\%$.

3.86. TCP J23130812+2337018

This object (hereafter TCP J231308) was discovered by Itagaki and Kaneda as a 14.3 mag (unfiltered CCD magnitude) object (TCP J23130812+2337018).[10] According to ASAS-3 data, the object underwent a brighter ($V = 13.4$) outburst in 2005 August. Subsequent observations confirmed the presence of superhumps (vsnet-alert 13438; figure 85). The times of superhump maxima are listed in table 86. The $O - C$ values clearly showed a stage B–C transition. The observation of stage B was not sufficiently long to determine $P_{\rm dot}$.

4. Discussion

4.1. Period Derivatives during Stage B

As in Kato et al. (2012a), we compared period derivatives during stage B (figure 86). The newly obtained $P_{\rm dot}$ for object for $P_{\rm orb} < 0.076$ d followed the trend obtained in the previous research. There were also two $P_{\rm dot} > 0$ systems (SDSS J170213 and OT J145921) for $P_{\rm orb} > 0.080$ d, as noted in Kato et al. (2012a). Among them, SDSS J170213 showed infrequent outbursts and indeed resembles EF Peg, the representative $P_{\rm dot} \sim 0$ object with a long $P_{\rm orb}$ (cf. Kato et al. 2009). The other object, OT J145921, showed more frequent outbursts and may resemble GX Cas, an unexpected object with $P_{\rm dot} > 0$ with typical SU UMa-type outburst behavior. There may be two classes of objects with $P_{\rm dot} > 0$ among SU UMa-type dwarf novae with long $P_{\rm orb}$.

4.2. Periods of Stage A Superhumps

Stage A superhumps recorded in the present study are listed in table 87. Although most of objects in this study

Table 82. Superhump maxima of OT J215818 (2011).

E	max*	error	$O-C$†	N‡
0	55863.2398	0.0003	−0.0043	134
1	55863.3048	0.0002	−0.0064	231
2	55863.3696	0.0004	−0.0088	277
3	55863.4404	0.0002	−0.0051	438
4	55863.5061	0.0003	−0.0065	185
17	55864.3810	0.0005	−0.0039	78
18	55864.4489	0.0002	−0.0031	209
19	55864.5162	0.0003	−0.0029	201
20	55864.5814	0.0006	−0.0048	204
21	55864.6512	0.0003	−0.0021	318
22	55864.7198	0.0004	−0.0006	259
23	55864.7865	0.0009	−0.0010	99
30	55865.2517	0.0023	−0.0056	31
31	55865.3245	0.0007	0.0002	112
32	55865.3927	0.0004	0.0012	193
33	55865.4587	0.0004	0.0002	195
34	55865.5280	0.0005	0.0023	155
36	55865.6653	0.0004	0.0054	175
37	55865.7313	0.0004	0.0044	175
40	55865.9351	0.0005	0.0068	119
41	55865.9970	0.0009	0.0016	114
50	55866.6093	0.0004	0.0100	179
51	55866.6757	0.0003	0.0093	226
52	55866.7436	0.0004	0.0101	176
55	55866.9400	0.0008	0.0052	116
56	55867.0100	0.0005	0.0081	74
61	55867.3408	0.0008	0.0034	147
62	55867.4088	0.0005	0.0042	193
63	55867.4778	0.0006	0.0061	143
80	55868.6185	0.0009	0.0061	91
81	55868.6812	0.0010	0.0017	93
125	55871.6216	0.0008	−0.0105	127
126	55871.6902	0.0008	−0.0090	176
127	55871.7544	0.0018	−0.0119	148

*BJD−2400000.
†Against max $= 2455863.2441 + 0.067104E$.
‡Number of points used to determine the maximum.

[10] <http://www.cbat.eps.harvard.edu/unconf/followups/J23130812+2337018.html>.

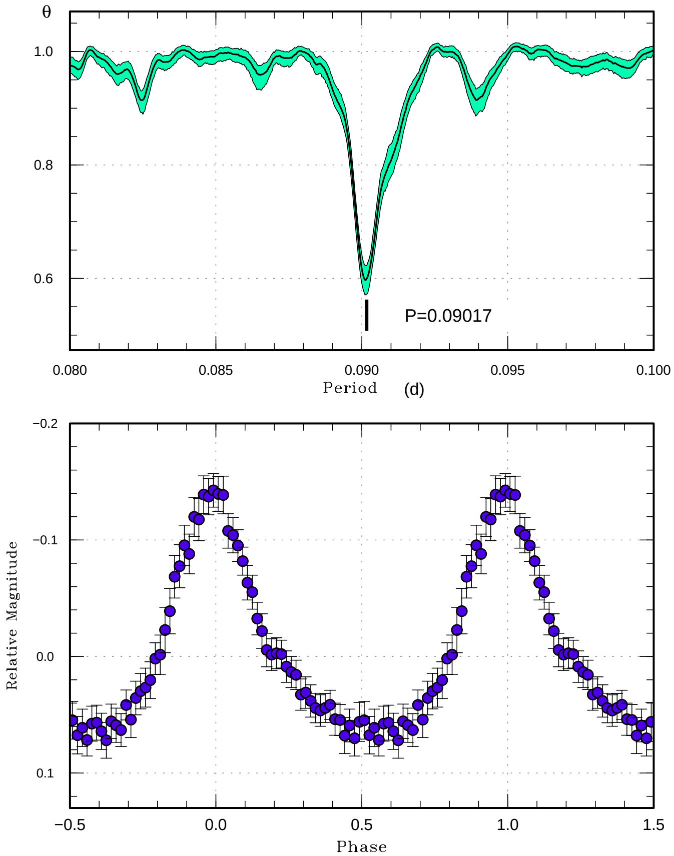

Fig. 82. Superhumps in OT J221232 (2011). (Upper): PDM analysis. (Lower): Phase-averaged profile.

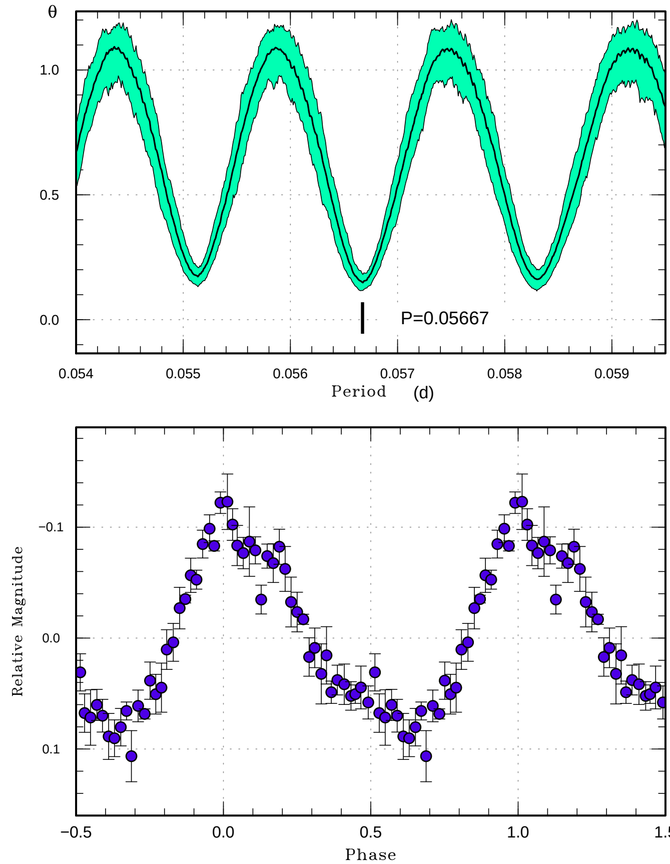

Fig. 83. Superhumps in OT J224736 (2012). (Upper): PDM analysis. (Lower): Phase-averaged profile.

Table 83. Superhump maxima of OT J221232 (2011).

E	max*	error	$O-C$†	N‡
0	55921.6566	0.0004	−0.0069	93
6	55922.2042	0.0003	−0.0000	116
7	55922.2925	0.0004	−0.0019	122
11	55922.6537	0.0005	−0.0012	91
14	55922.9302	0.0018	0.0050	45
17	55923.1942	0.0005	−0.0015	48
18	55923.2872	0.0005	0.0014	96
22	55923.6480	0.0005	0.0018	91
28	55924.1862	0.0023	−0.0008	84
29	55924.2797	0.0007	0.0026	221
33	55924.6417	0.0008	0.0040	90
55	55926.6221	0.0006	0.0017	82
73	55928.2400	0.0004	−0.0026	91
106	55931.2153	0.0024	−0.0016	30

*BJD−2400000.
†Against max $= 2455921.6635 + 0.090126E$.
‡Number of points used to determine the maximum.

Table 84. Superhump maxima of OT J224736 (2012).

E	max*	error	$O-C$†	N‡
0	56095.4674	0.0005	−0.0005	27
1	56095.5251	0.0004	0.0005	28
36	56097.5076	0.0007	−0.0006	30
37	56097.5653	0.0005	0.0005	29

*BJD−2400000.
†Against max $= 2456095.4679 + 0.056673E$.
‡Number of points used to determine the maximum.

Table 85. Superhump maxima of TCP J084616 (2012).

E	max*	error	$O-C$†	phase‡	N§
0	56007.2977	0.0006	−0.0009	0.35	32
1	56007.3955	0.0014	0.0006	0.33	27
11	56008.3626	0.0046	0.0046	0.62	35
12	56008.4500	0.0028	−0.0043	0.59	40

*BJD−2400000.
†Against max $= 2456007.2986 + 0.096303E$.
‡Orbital phase.
§Number of points used to determine the maximum.

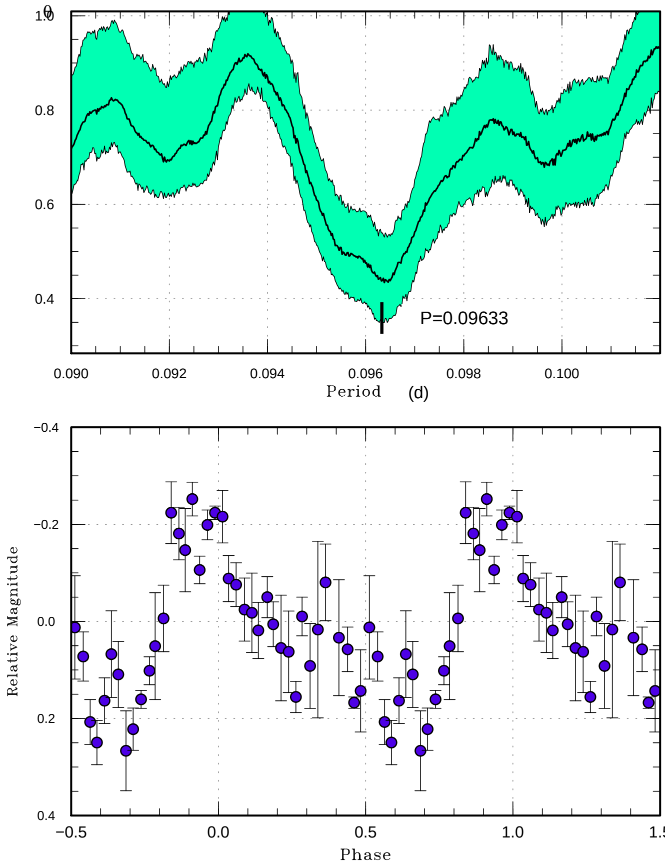

Fig. 84. Superhumps in TCP J084616 (2012). (Upper): PDM analysis. (Lower): Phase-averaged profile.

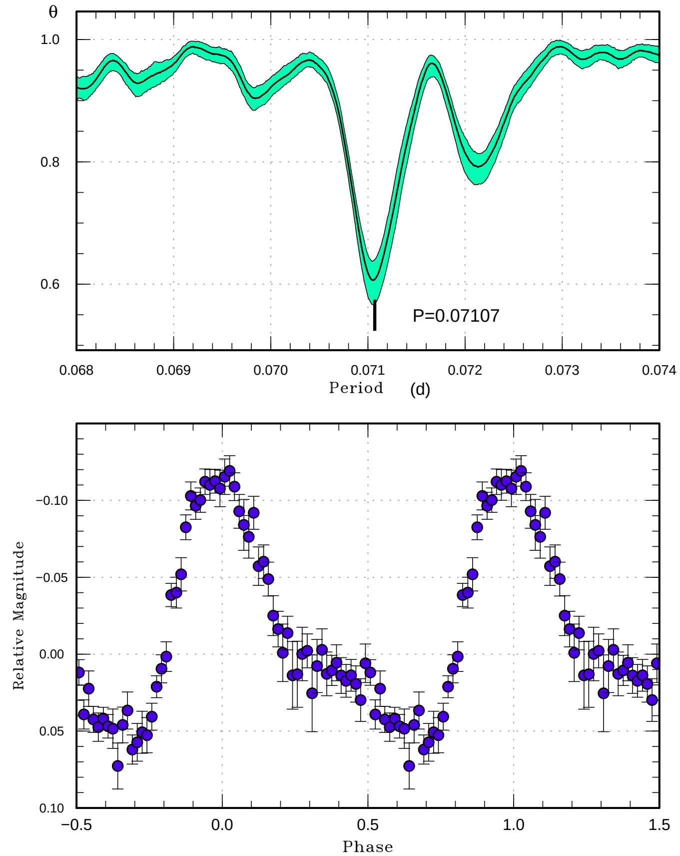

Fig. 85. Superhumps in TCP J231308 (2011). (Upper): PDM analysis. (Lower): Phase-averaged profile.

Table 86. Superhump maxima of TCP J231308 (2011).

E	max*	error	$O-C$†	N‡
0	55732.5371	0.0003	−0.0036	188
1	55732.6077	0.0002	−0.0041	212
14	55733.5369	0.0003	0.0015	91
15	55733.6066	0.0003	0.0001	59
19	55733.8916	0.0003	0.0009	94
23	55734.1796	0.0013	0.0047	176
24	55734.2488	0.0014	0.0029	118
28	55734.5318	0.0002	0.0017	78
29	55734.6024	0.0004	0.0013	50
51	55736.1610	0.0034	−0.0031	74
56	55736.5193	0.0003	−0.0001	45
57	55736.5888	0.0004	−0.0017	44
71	55737.5845	0.0003	−0.0006	176
85	55738.5799	0.0003	0.0001	199

*BJD−2400000.
†Against max $= 2455732.5407 + 0.071048E$.
‡Number of points used to determine the maximum.

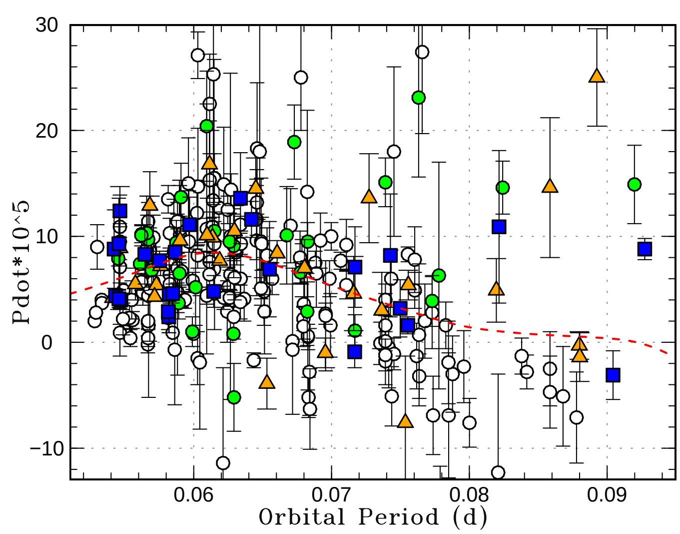

Fig. 86. $P_{\rm dot}$ for stage B versus $P_{\rm orb}$. Open circles, filled circles, filled triangles and filled squares represent samples in Kato et al. (2009), Kato et al. (2010), Kato et al. (2012a) and this paper, respectively. The curve represents the spline-smoothed global trend.

Table 87. Superhump Periods during Stage A

Object	Year	period (d)	err
SV Ari	2011	0.05575	0.00012
VW Hyi	2011	0.07770	0.00013
BW Scl	2011	0.05623	0.00012
PU UMa	2012	0.08382	–
SDSS J080303	2011	0.09540	0.00028
SDSS J170213	2011	0.10605	0.00011
OT J102842	2012	0.03844	0.00002
OT J184228	2011	0.07287	0.00008
OT J210950	2011	0.06087	0.00006
OT J214738	2011	0.09928	0.00022

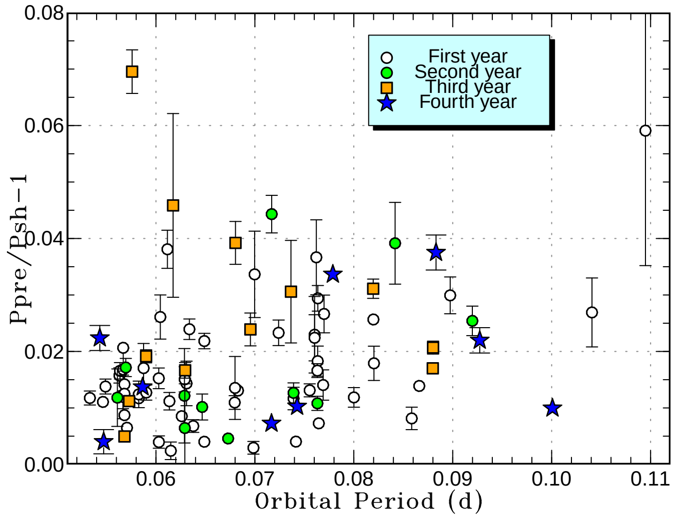

Fig. 87. Superhump periods during the stage A. Superhumps in this stage has a period typically 1.0–1.5% longer than the one during the stage B. There is a slight tendency of increasing fractional period excess for longer-$P_{\rm orb}$ systems. The symbols for first, second, third and fourth years represent data in Kato et al. (2009), Kato et al. (2010), Kato et al. (2012a) and this paper.

followed the trend obtained in the previous study, one object (SDSS J170213) has a substantially smaller fractional excess for stage A superhumps. This may have been either due to small number of observations (insufficient coverage for stage A), a systematic effect by overlapping eclipses, or the unusual period evolution of this object for this $P_{\rm orb}$ (cf. subsection 4.1). Although the object may also resemble short-$P_{\rm orb}$ objects in its small fractional excess for stage A superhumps, this needs to be confirmed by further observations.

4.3. WZ Sge-Type Stars

New WZ Sge-type dwarf novae and candidates are listed in table 88. Among them PR Her, BW Scl and OT J184228 were well characterized. SV Ari was observed only in the late stage of its superoutburst, and SDSS J220553 and OT J210950 were included in this table due to their resemblance to WZ Sge-type objects in the post-superoutburst behavior. For OT J001952 and OT J055721 we have only very limited information and these objects were included based on the large outburst amplitudes.

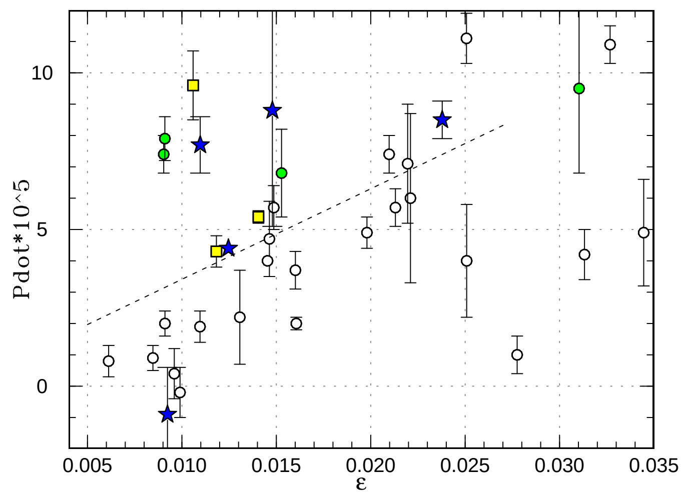

Fig. 88. $P_{\rm dot}$ versus ϵ for WZ Sge-type dwarf novae. Open circles, filled circles, filled squares and filled stars represent outbursts reported in Kato et al. (2009), Kato et al. (2010), Kato et al. (2012a) and this paper, respectively. The dashed line represents a linear regression for points with $\epsilon < 0.026$ as in Kato et al. (2009) figure 35.

The relation between $P_{\rm dot}$ versus ϵ for WZ Sge-type dwarf novae is shown in figure 88. Although there is a tendency of increasing $P_{\rm dot}$ for objects with larger ϵ as stated in Kato et al. (2009), several objects lie well above this relation, as discussed in Kato et al. (2012a). Although we may add two additional examples in the present study, these two objects, SDSS J220553 and PR Her, were not very well sampled and it is not certain whether these objects are outliers to this relation. The reverse case OT J184228 is remarkable in that it showed almost zero $P_{\rm dot}$. This object was indeed unusual in its "double plateau" superoutburst. The unusually small $P_{\rm dot}$ may be related to the unusual binary parameters (long $P_{\rm orb}$ and small expected q), and probably to its evolutionary stage as a candidate period bouncer.

Figure 89 indicates the updated relation between $P_{\rm dot}$ and $P_{\rm orb}$ and its relation to the type of post-superoutburst rebrightening phenomenon: type-A (long-lasting post-outburst rebrightening), type-B (multiple discrete rebrightenings), type-C (single rebrightening) and type-D (no rebrightening), cf. Kato et al. (2009). In the present study, type-C and type-D superoutbursts followed the same trend as in the past studies. There is noteworthy presence of a new type-B superoutburst (OT J184228) with an exceptionally long $P_{\rm orb}$ and small $P_{\rm dot}$. This presence seems to support the earlier suggestion (Kato et al. 2009; Kato et al. 2012a) that type-B superoutbursts are associated with low-q systems and they are likely period bouncers.

Table 88. Parameters of WZ Sge-type superoutbursts.

Object	Year	P_{SH}	P_{orb}	P_{dot}*	err*	ϵ	Type†	N_{reb}‡	delay§	Max	Min
SV Ari	2011	0.055524	–	4.0	0.2	–	D	0	–	]15.0‖	22.1
PR Her	2011	0.055022	0.05422	8.8	3.7	0.015	–	–	13	12.8	21.0
BW Scl	2011	0.055000	0.054323	4.4	0.3	0.012	D	0	10	9.0	16.4
SDSS J220553	2011	0.058151	0.05752	7.7	0.9	0.011	–	–	–	]14.4	20.1
OT J001952	2012	0.056770	–	–	–	–	–	–	–	]15.6	21.5:
OT J055721	2011	0.059756	–	4.6	0.9	–	C	1	–	]14.7	21.0:
OT J184228	2011	0.072342	0.07168	−0.9	1.5	0.009	B	]2	]29	]11.8	20.6
OT J210950	2011	0.060045	0.05865	8.5	0.6	0.024	D	0	]6	]11.5	18.7

*Unit 10^{-5}.
†A: long-lasting rebrightening; B: multiple rebegitehnings; C: single rebrightening; D: no rebrightening.
‡Number of rebrightenings.
§Days before ordinary superhumps appeared.
‖"]" represents the lower limit.

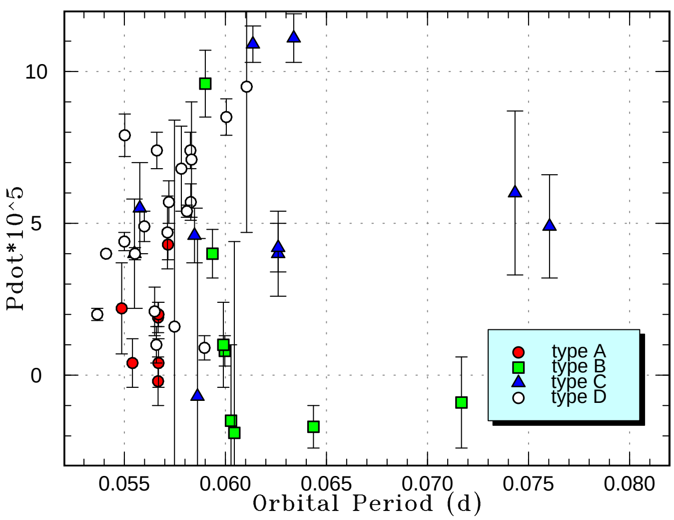

Fig. 89. P_{dot} versus P_{orb} for WZ Sge-type dwarf novae. Symbols represent the type (cf. Kato et al. 2009) of outburst: type-A (filled circles), type-B (filled squares), type-C (filled triangles), type-D (open circles).

4.4. VW Hydri – Revisiting the Prototype of SU UMa-Type Dwarf novae

In discussing superoutbursts and superhumps, we often refer to historical observations of bright southern SU UMa-type dwarf novae (VW Hyi, Z Cha and OY Car), from which our early knowledge of phenomenology of superhumps was established. These early findings were also summarized in textbooks such as Warner (1995). These early observations were, however, based on photoelectric photometry and only limited parts of the entire observations were published as figures, and these observations are not accessible in electronic form. This has been an obstacle in comparing the results of modern-day CCD observations with historical knowledge. Although Kepler observations of V344 Lyr and V1504 Cyg (Kato et al. 2012a; Wood et al. 2011) partly filled this gap, a direct comparison in the "prototype" object VW Hyi had been wanted. We have fortunately been able to obtain the entire course of the 2011 November–December superoutburst and two subsequent normal outbursts and the intervening quiescent period, although they were obtained only at a single observing location and suffered from unavoidable gaps in coverage. These data are available at the AAVSO database.

The results of these observations (subsection 3.22) can be summarized as follows:

1. The superoutburst started with a precursor outburst.
2. There was no hint of superhumps during the rising phase and the early phase of the precursor outburst.
3. During the later stage of the precursor outburst, superhumps started to grow and the object brightened.
4. The amplitudes of superhumps reached a maximum when the object reached the maximum brightness.
5. The amplitudes of superhumps decreased during the superoutburst plateau.
6. The global P_{dot} was negative.
7. Stage A was recognized during the evolving stage of superhumps.
8. There was likely stage B with an almost constant period, followed by likely stage C with a shorter period.
9. The transition to stage B to C was smoother than in short-P_{orb} systems. This feature is similar to the ones in Kepler data for V344 Lyr and V1504 Cyg.
10. Superhumps having phases ∼0.5 offset appeared during the late stage of the superoutburst. These superhumps indeed appear to be "traditional" late superhumps, rather than a simple extension of stage C superhumps as in short-P_{orb} systems.
11. The late superhumps persisted during the quiescent period before the next normal outburst and they were still detected even after this normal outburst. The signal became undetectable after the second normal outburst. The situation was very similar to the Kepler result for V344 Lyr.

12. In contrast to V344 Lyr, secondary maxima of superhumps were not prominent.

We thus confirmed most of the classical superhump phenomenology including the "traditional" late superhumps, whose presence has been questioned in most of recently observed objects (Kato et al. 2009; Kato et al. 2010; Kato et al. 2012a). Combined with the knowledge with V344 Lyr, the traditional descriptions of the development of superhumps and the appearance of late superhumps seem to be common among relatively long-$P_{\rm orb}$ and high mass-transfer systems, and VW Hyi can indeed be regarded as the prototype of these systems. Things, however, are somewhat different in shorter-$P_{\rm orb}$ and lower mass-transfer systems in the clear presence of stages B and C and no clear signature of "traditional" late superhumps. Although the systematics of superhumps in VW Hyi would be adequate for describing long-$P_{\rm orb}$ systems, we regard it dangerous to describe the phenomena seen in shorter-$P_{\rm orb}$ systems in the same manner. This will be particularly true for the term "late superhumps" which has been a major cause of confusion in describing the stage C superhumps. Although some authors refer superhumps seen in the late stages of superoutburst as late superhumps, this leads to a confusion since the original term "late superhumps" implies an $\sim$0.5 phase shift, while stage C superhumps don't show such a phase shift. This ambiguity in terminology could lead to a confusion in interpreting the mechanism [see e.g. Hessman et al. (1992), a work before the clarification between "traditional" superhumps and stage C superhumps, analyzed stage C superhumps with a term of "late superhumps" and an assumption of an $\sim$0.5 phase shift]. We propose that we should not use the term "late superhumps" unless there is a $\sim$0.5 phase shift.

Schreiber et al. (2004) recently compared the calculations of the pure thermal-tidal instability (TTI) model and the enhanced mass-transfer (EMT) model for VW Hyi. Although both models (TTI and EMT) well explain the many of observed characteristics, they claimed the advantage of the EMT model in that it can explain varieties in the observed light curve of single systems such as VW Hyi. Although we don't aim to validate or invalidate their claim here, we need to be specially careful in interpreting observations. They referred to varieties of light curves based on historical visual observations, and these observations may have not been very sensitive to subtle signatures of light curves. For example, while the present superoutburst showed a clear signature of a precursor, visual observations of the same superoutburst reported to the AAVSO did not recognize this feature. Considering that all six superoutbursts of V344 Lyr and all six superoutbursts of V1504 Cyg showed precursors in Kepler data (Cannizzo et al. 2012), and considering that these light curves are very similar to the present one of VW Hyi (figure 19, lower panel), we may postulate that precursors are more commonly present in superoutburst of these systems than assumed in Schreiber et al. (2004), and that variations within the single system is less pronounced. This stability of appearance of precursors might in turn favor the pure TTI model, and it needs to be examined further.

4.5. ER UMa Stars

Early years from the discovery of ER UMa-type stars (Kato, Kunjaya 1995; Robertson et al. 1995; Patterson et al. 1995), it was not feasible to fully analyze period variations and $O-C$ diagrams in these systems (Kato et al. 1996b; Kato et al. 2003a). Only recently superhumps in DI UMa (Rutkowski et al. 2009; subsection 3.36) and RZ LMi (Olech et al. 2008) were systematically studied. Although ER UMa showed positive superhumps at least until 2007 (our unpublished observations) and 2008 (AAVSO data),[11] the object now predominantly shows negative superhumps even during superoutbursts at least since 2011 (Ohshima et al. 2012) and in quiescence in 2008 (Kjurkchieva, Marchev 2010) [there was also a possible signature of negative superhumps in 1998 (Gao et al. 1999)], and it is now impossible to follow the evolution of positive superhumps during the entire course of a superoutburst of ER UMa as in the 1990s.

V1159 Ori, on the other hand, still shows positive superhumps (subsection 3.29), and it would be very desirable to study this object in detail. The recently recognized member of this family, BK Lyn, now shows almost the same behavior of ER UMa during its "negative superhump" (present) state.

We also studied RZ LMi and found some evidence of period variation (subsection 3.23). We also suggested a candidate orbital period from photometry, and this needs to be tested by further observations.

We list currently known ER UMa stars and their periods in table 89. The orbital periods were taken from Thorstensen et al. (1997) (ER UMa, V1159 Ori), Thorstensen et al. (2002b) (DI UMa), Ringwald et al. (1996) (BK Lyn). The superhump periods were from Kato, Kunjaya (1995) and Ohshima et al. (2012) (ER UMa), Rutkowski et al. (2009) (DI UMa), Olech et al. (2004) (IX Dra), and this work (V1159 Ori, RZ LMi, BK Lyn). Although Olech et al. (2004) suggested a possible orbital period, we did not include it because it is less likely to detect an orbital signal having a period close to the superhump period (as they claimed) from such a limited coverage. Since the behavior of IX Dra is very similar to that of ER UMa in the 1990s (Ishioka et al. 2001b), we would expect an ϵ similar to ER UMa. A search for the definite orbital period is still needed. It would be also interesting to see whether this object currently shows positive or negative superhumps.

4.6. Superoutbursts of AM CVn Stars

We analyzed the superhumps in a dwarf nova (CR Boo) belonging to AM CVn-type objects (subsection 3.5). CR Boo recently showed a regular pattern of superoutbursts similar to that of ER UMa (as noted in Kato et al. 2000b).

11 We don't completely rule out that negative superhumps may have appeared during the later course of superoutbursts in 2007 and 2008, since we don't have data during the late course of the superoutbursts.

Table 89. List of ER UMa-type stars

Object	P_{orb} (d)	P_{SH} (d)*	State†
ER UMa (1995–2008)	0.06366	0.0657	+
ER UMa (2011–)		0.06226	−
V1159 Ori	0.062178	0.0643	+
RZ LMi	(0.059053)	0.05944	+
DI UMa	0.054567	0.05531	+
IX Dra	–	0.06697	+
BK Lyn (2005–)	0.07498	0.07279	−

*The periods of dominant periodicities are given.
†positive (+) and negative (−) superhumps.

We recorded a stage B–C transition similar to hydrogen-rich SU UMa-type dwarf novae. This is the first indication that superhumps in helium dwarf novae evolve in a similar way to hydrogen-rich SU UMa-type dwarf novae. Since this pattern of stage B–C transition was also recorded in the black-hole X-ray transient KV UMa (Kato et al. 2009), the presence of stages B and C appear to be ubiquitous to all low-q systems. Theoretical studies for the origin of the superhump stages are required. Although the early stages of the superoutburst was not observed, SDSS J172102 underwent a superoutburst followed by a short post-superoutburst rebrightening resembling that of short-P_{orb} hydrogen-rich SU UMa-type dwarf novae. This also strengthens the similarity of phenomenology between helium-rich and hydrogen-rich SU UMa-type dwarf novae.

The peculiar object SBS 1108+574, a hydrogen-rich CV below the period minimum, also showed distinct stages B and C as in ordinary short-P_{orb} SU UMa-type dwarf novae (subsection 3.49). Although the system parameters of this object is similar to those of AM CVn-type stars, the superoutburst was much longer than those of AM CVn-type superoutbursts and there were no “dip”-like fadings during the superoutburst plateau (cf. Kotko et al. 2012). Such a difference in the behavior may be a result from the different properties of between pure-helium and hydrogen-rich accretion disks and warrants further study.

4.7. Double Periodic Superhumps?

In the present paper, we encountered three unusual objects (CC Scl, MASTER J072948, OT J173516) which showed superoutbursts similar to other SU UMa-type dwarf novae but with only low-amplitude and rather irregular superhumps. The light curves of these systems appear to be expressed by a combination of closely separated two periods. In CC Scl, these periods are almost certainly P_{orb} and positive superhumps, while the situation for MASTER J072948 and OT J173516 is unclear: either positive superhumps with an unusual ϵ or negative superhumps. Although these objects comprise only a minority of known SU UMa-type dwarf novae, there may have been “overlooked” systems since the amplitudes of variations are very small. We cannot explain the unusual behavior in these systems. If negative superhumps (or a tilted disk) were excited as in the present-day ER UMa, the coexistence of both signals of P_{orb} and negative superhumps and the rather irregular waveform may be easier to reconcile.

5. Summary

We studied the characteristics of superhumps for 86 SU UMa-type dwarf novae whose superoutbursts were mainly observed during the 2011–2012 season. Most of the new data for systems with short orbital periods basically confirmed the earlier findings.

Among WZ Sge-type dwarf novae, BW Scl showed an $O-C$ variation similar to other WZ Sge-type dwarf novae such as V455 And and GW Lib, and this pattern of period variation appears to be common among WZ Sge-type dwarf novae with shortest orbital periods. The WZ Sge-type object OT J184228.1+483742 showed an unusual pattern of double outbursts composed of an outburst with early superhumps and another with ordinary superhumps, separated by a temporary fading. We propose an interpretation that a very small growth rate of the 3:1 resonance due to an extremely low mass-ratio led to a quenching of the superoutburst before ordinary superhumps appeared. We suspect that this object is a good candidate for a period bouncer.

We studied VW Hyi during its superoutburst in 2011 November–December and subsequent two normal outbursts. We confirmed the presence of “traditional” late superhumps with a ∼0.5 phase shift. These late superhumps persisted until the second next normal outburst. The behavior was very similar to the results of Kepler observations of V344 Lyr and it is likely these late superhumps seem to be common among relatively long-P_{orb} and high mass-transfer systems.

We extended our research to the analysis of positive and negative superhumps in ER UMa-type dwarf novae, and found that the current V1159 Ori shows positive superhumps similar to ER UMa in the 1990s. In two extreme ER UMa stars (DI UMa and RZ LMi), there is an indication of positive period derivatives. We identified likely orbital periods for these objects, and both objects likely have small mass ratios. The recently identified ER UMa-type object BK Lyn has been in dwarf nova-type state at least since 2005, and its current variation is dominated by negative superhumps as in ER UMa at least since 2011.

We further examined superhumps in AM CVn-type objects, and for the first time established the pattern of period variations very similar to short-period hydrogen-rich SU UMa-type dwarf novae, and these objects are indeed a helium analogue of hydrogen-rich SU UMa-type dwarf novae.

We also studied a peculiar object SBS 1108+574, a hydrogen-rich dwarf nova below the period minimum, and showed a very similar pattern of period variations to those of short-period SU UMa-type dwarf novae. We detected a likely orbital period in this system and estimated the mass ratio to be $q=0.06$. This finding suggests that this secondary is a somewhat evolved star whose hydrogen envelope was mostly stripped during the mass-exchange.

We identified a new group of SU UMa-type dwarf novae (CC Scl, MASTER J072948 and OT J173516.9+154708) with low-amplitude superhumps with complex profiles. The complex profile in CC Scl is likely a result of combination of orbital humps and positive superhumps. The cases for MASTER J072948 and OT J173516.9+154708 are less clear and the second signal may be negative superhumps.

This work was supported by the Grant-in-Aid for the Global COE Program "The Next Generation of Physics, Spun from Universality and Emergence" from the Ministry of Education, Culture, Sports, Science and Technology (MEXT) of Japan. The authors are grateful to observers of VSNET Collaboration and VSOLJ observers who supplied vital data. We acknowledge with thanks the variable star observations from the AAVSO International Database contributed by observers worldwide and used in this research. This work is deeply indebted to outburst detections and announcement by a number of variable star observers worldwide, including participants of CVNET, BAA VSS alert and AVSON networks. We are grateful to the Catalina Real-time Transient Survey team for making their real-time detection of transient objects available to the public.

Appendix 1. MCMC Analysis of Eclipses

The KW method is widely used to determine the mid-eclipse times of eclipsing binaries. Although this method is useful for densely sampled light curves, it is difficult to determine the period of eclipsing binaries with sparse samples. This is particularly the case for TCP J084616 in which each eclipse was observed with low time-resolution and with large photometric errors due to the faintness of the object. In such cases, a usual approach to measure the mid-eclipse times by the KW method and then make a linear regression does not give a good result. We solved this problem by extending the application of the MCMC analysis introduced in Kato et al. (2010).

In this problem, $D = \{y_{\mathrm{obs}}(t_i)\}$ are the observed magnitudes (corrected for trends if necessary) for the epochs $\{t_i\}$, parameter space is $\theta = \{P, E_0, a, b, c\}$ defined by the model (y_{model}):

$$\begin{aligned} \phi_i =& 1/2 - |(t_i - E_0)/P \bmod 1 - 1/2| \\ y_{\mathrm{model}}(\phi_i) =& \quad b + c(a - \phi_i) \qquad (\phi_i < a) \\ y_{\mathrm{model}}(\phi_i) =& \quad b \qquad (\phi_i \geq a), \end{aligned} \tag{A1}$$

where P and E_0 are the period and epoch, respectively, and mod1 means the fractional part. and other parameters define the shape of the light curve. Assuming that $\epsilon_i = y_{\mathrm{obs}}(t_i) - y_{\mathrm{model}}(t_i)$ follows a normal distribution $N(0, \sigma_i^2)$, the likelihood function can be written as

$$\mathcal{L}(\theta) = \prod_i \frac{1}{\sqrt{2\pi\sigma_i^2}} \exp\left[-\frac{\{y_{\mathrm{obs}}(t_i) - y_{\mathrm{model}}(t_i)\}^2}{2\sigma_i^2}\right], \tag{A2}$$

and apply MCMC algorithm to this $\mathcal{L}(\theta)$. A sample of results is shown in figures 90, 91 and 92. We used the resultant P and E_0 in subsection 3.85. This method is also applicable to usual determination of minima of eclipsing binaries by appropriately defining the shape of the light curve. This method is advantageous to classical KW method in its plain formulation, robustness of the solution for noisy data, and easy incorporation of errors in individual measurements.

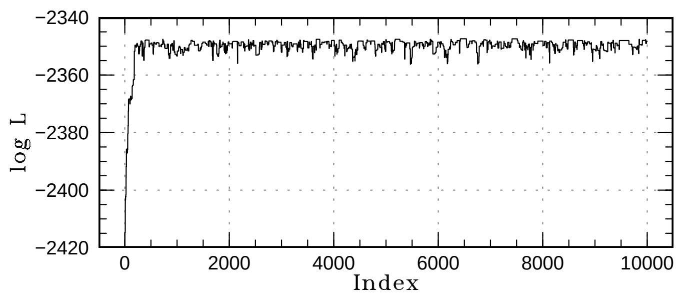

Fig. 90. MCMC analysis of TCP J084616: behavior of likelihood.

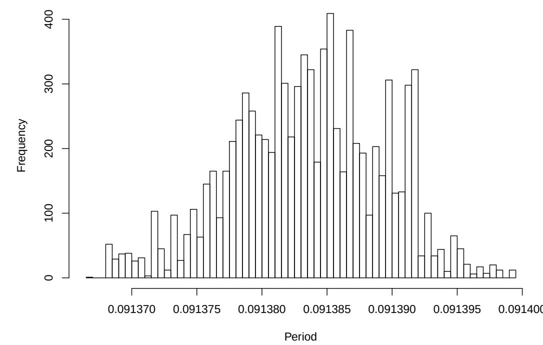

Fig. 91. Posterior probablistic function of P of TCP J084616.

References

Abbott, T. M. C., Fleming, T. A., & Pasquini, L. 1997, A&A, 318, 134

Augusteijn, T., van der Hooft, F., de Jong, J. A., & van Paradijs, J. 1996, A&A, 311, 889

Augusteijn, T., van Kerkwijk, M. H., & van Paradijs, J. 1993, A&A, 267, L55

Augusteijn, T., & Wisotzki, L. 1997, A&A, 324, L57

Balanutsa, P., et al. 2012a, Astron. Telegram, 4022

Balanutsa, P., et al. 2012b, Astron. Telegram, 4084

Balanutsa, P., et al. 2012c, Astron. Telegram, 3935

Baraffe, I., Chabrier, G., Barman, T. S., Allard, F., & Hauschildt, P. H. 2003, A&A, 402, 701

Boyd, D., Oksanen, A., & Henden, A. 2006, J. Br. Astron. Assoc., 116, 187

Breedt, E., Gänsicke, B. T., Marsh, T. R., Steeghs, D., Drake, A. J., & Copperwheat, C. M. 2012, MNRAS, 425, 2548

Cannizzo, J. K., Smale, A. P., Wood, M. A., Still, M. D., & Howell, S. B. 2012, ApJ, 747, 117

Cannizzo, J. K., Still, M. D., Howell, S. B., Wood, M. A., & Smale, A. P. 2010, ApJ, 725, 1393

Chabrier, G., & Baraffe, I. 1997, A&A, 327, 1039

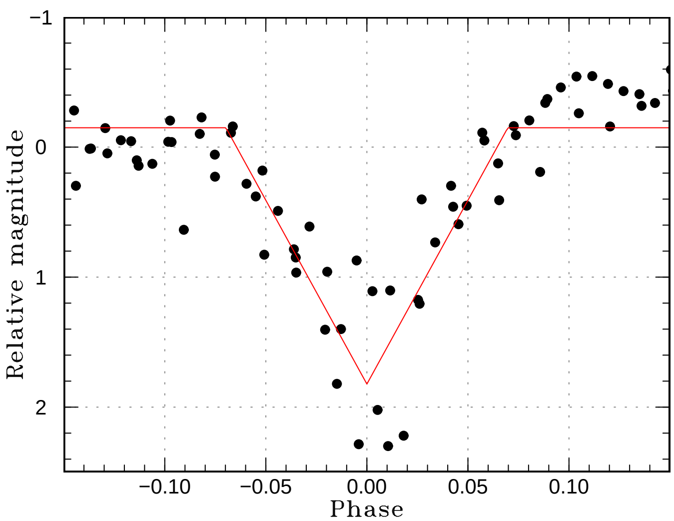

Fig. 92. Best-fit model for TCP J084616. Points are observations and line is the model.

Chen, A., O'Donoghue, D., Stobie, R. S., Kilkenny, D., & Warner, B. 2001, MNRAS, 325, 89

Denisenko, D. V., & Sokolovsky, K. V. 2011, Astron. Lett., 37, 91

Dillon, M., et al. 2008, MNRAS, 386, 1568

Duerbeck, H. W. 1987, Space Sci. Rev., 45, 1

Gao, W., Li, Z., Wu, X., Zhang, Z., & Li, Y. 1999, ApJL, 527, L55

Garnavich, P., Littlefield, C., Marion, G. H., Irwin, J., Kirshner, R. P., & Vinko, J. 2012, Astron. Telegram, 4112

Gessner, H. 1966, Veröff. Sternw. Sonneberg, 7, 61

Hambsch, F.-J. 2012, J. American Assoc. Variable Star Obs., 40, 1003

Harvey, D., Skillman, D. R., Patterson, J., & Ringwald, F. A. 1995, PASP, 107, 551

Hessman, F. V., & Hopp, U. 1990, A&A, 228, 387

Hessman, F. V., Mantel, K.-H., Barwig, H., & Schoembs, R. 1992, A&A, 263, 147

Hoffmeister, C. 1949, Erg. Astron. Nachr., 12, 12

Hoffmeister, C. 1951, Erg. Astron. Nachr., 12, 14

Hoffmeister, C. 1968, Astron. Nachr., 290, 277

Howell, S. B., Schmidt, R., DeYoung, J. A., Fried, R., Schmeer, P., & Gritz, L. 1993, PASP, 105, 579

Imada, A., et al. 2006, PASJ, 58, 143

Imada, A., Kato, T., Monard, L. A. G. B., Stubbings, R., Uemura, M., Ishioka, R., & Nogami, D. 2008a, PASJ, 60, 267

Imada, A., et al. 2008b, PASJ, 60, 1151

Imada, A., et al. 2009, PASJ, 61, 535

Ishioka, R., Kato, T., Matsumoto, K., Uemura, M., Iwamatsu, H., & Stubbings, R. 2001a, IBVS, 5023

Ishioka, R., et al. 2002, PASJ, 54, 581

Ishioka, R., Kato, T., Uemura, M., Iwamatsu, H., Matsumoto, K., Martin, B. E., Billings, G. W., & Novak, R. 2001b, PASJ, 53, L51

Ishioka, R., Sekiguchi, K., & Maehara, H. 2007, PASJ, 59, 929

Kato, T. 2001, PASJ, 53, L17

Kato, T. 2002a, PASJ, 54, L11

Kato, T. 2002b, PASJ, 54, 87

Kato, T., Hanson, G., Poyner, G., Muyllaert, E., Reszelski, M., & Dubovsky, P. A. 2000a, IBVS, 4932

Kato, T., et al. 2009, PASJ, 61, S395

Kato, T., Ishioka, R., & Uemura, M. 2002, PASJ, 54, 1029

Kato, T., & Kunjaya, C. 1995, PASJ, 47, 163

Kato, T., et al. 2012a, PASJ, 64, 21

Kato, T., Maehara, H., & Uemura, M. 2012b, PASJ, 64, 62

Kato, T., et al. 2010, PASJ, 62, 1525

Kato, T., Nogami, D., Baba, H., Hanson, G., & Poyner, G. 2000b, MNRAS, 315, 140

Kato, T., Nogami, D., Baba, H., Matsumoto, K., Arimoto, J., Tanabe, K., & Ishikawa, K. 1996a, PASJ, 48, L21

Kato, T., Nogami, D., & Masuda, S. 1996b, PASJ, 48, L5

Kato, T., Nogami, D., & Masuda, S. 2003a, PASJ, 55, L7

Kato, T., Nogami, D., Moilanen, M., & Yamaoka, H. 2003b, PASJ, 55, 989

Kato, T., Stubbings, R., Monard, B., Butterworth, N. D., Bolt, G., & Richards, T. 2004a, PASJ, 56, S89

Kato, T., & Uemura, M. 2012, PASJ, 64, 122

Kato, T., Uemura, M., Ishioka, R., Nogami, D., Kunjaya, C., Baba, H., & Yamaoka, H. 2004b, PASJ, 56, S1

Kemp, J., et al. 2012, Society for Astronom. Sciences Ann. Symp., 31, 7

Kjurkchieva, D., & Marchev, D. 2010, Publ. de l'Observatoire Astronomique de Beograd, 90, 147

Kotko, I., Lasota, J.-P., Dubus, G., & Hameury, J.-M. 2012, A&A, 544, A13

Kwee, K. K., & van Woerden, H. 1956, Bull. Astron. Inst. Netherlands, 12, 327

Levitan, D., et al. 2011, ApJ, 739, 68

Littlefair, S. P., Dhillon, V. S., Marsh, T. R., & Gänsicke, B. T. 2006, MNRAS, 371, 1435

Markarian, B. E., & Stepanian, D. A. 1983, Astrofizika, 19, 639

Mennickent, R. E., Patterson, J., O'Donoghue, D., Unda, E., Harvey, D., Vanmuster, T., & Bolt, G. 1999, Ap&SS, 262, 1

Nakano, S., Nishimura, H., Noguchi, T., & Munari, U. 2011, Cent. Bur. Electron. Telegrams, 2818, 1

Nogami, D., Kato, T., Masuda, S., & Hirata, R. 1995, IBVS, 4155

Nogami, D., Monard, B., Retter, A., Liu, A., Uemura, M., Ishioka, R., Imada, A., & Kato, T. 2004, PASJ, 56, L39

Ohshima, T., et al. 2012, PASJ, 64, L3

Ohshima, T., et al. 2011, PASJ, submitted

Olech, A. 1997, Acta Astron., 47, 281

Olech, A., Mularczyk, K., Kędzierski, P., Złoczewski, K., Wiśniewski, M., & Szaruga, K. 2006, A&A, 452, 933

Olech, A., Wisniewski, M., Zloczewski, K., Cook, L. M., Mularczyk, K., & Kedzierski, P. 2008, Acta Astron., 58, 131

Olech, A., Zloczewski, K., Mularczyk, K., Kedzierski, P., Wisniewski, M., & Stachowski, G. 2004, Acta Astron., 54, 57

Pastukhova, E. N. 1988, Astron. Tsirk., 1534, 17

Patterson, J., Jablonski, F., Koen, C., O'Donoghue, D., & Skillman, D. R. 1995, PASP, 107, 1183

Patterson, J., et al. 1997, PASP, 109, 1100

Pavlenko, E., et al. 2010a, in AIP Conference Proceedings, 17th European White Dwarf Workshop, ed. K. Werner & T. Rauch (Maryland: AIP), p. 320

Pavlenko, E., Kato, T., Pit, N., Baklanov, A., Antonyuk, K., & Stein, W. 2012a, Astron. Telegram, 3889, 1

Pavlenko, E. P., Samsonov, D. A., Antonyuk, O. I., Andreev, M. V., Baklanov, A. V., & Sosnovskij, A. A. 2012b, Astrophysics, 55, 494

Pavlenko, E. P., et al. 2010b, Astron. Rep., 54, 6

Pojmański, G. 2002, Acta Astron., 52, 397

Provencal, J. L., et al. 1997, ApJ, 480, 383

Ramsay, G., Barclay, T., Steeghs, D., Wheatley, P. J., Hakala, P., Kotko, I., & Rosen, S. 2011, MNRAS, 419, 2836

Ramsay, G., Barclay, T., Steeghs, D., Wheatley, P. J., Hakala, P., Kotko, I., & Rosen, S. 2012, MNRAS, 419, 2836

Rau, A., Roelofs, G. H. A., Groot, P. J., Marsh, T. R., Nelemans, G., Steeghs, D., Salvato, M., & Kasliwal, M. M. 2010, ApJ, 708, 456

Richards, G. T., et al. 2009, ApJS, 180, 67

Richter, G. A. 1990, Mitteil. Veränderl. Sterne, 12, 59

Ringwald, F. A., Thorstensen, J. R., Honeycutt, R. K., & Robertson, J. W. 1996, MNRAS, 278, 125

Robertson, J. W., Honeycutt, R. K., Hillwig, T., & Jurcevic, J. 1998, in ASP Conf. Ser. 137, Wild Stars in the Old West, ed. S. Howell, E. Kuulkers, & C. Woodward (San Francisco: ASP), p. 469

Robertson, J. W., Honeycutt, R. K., Hillwig, T., Jurcevic, J. S., & Henden, A. A. 2000, AJ, 119, 1365

Robertson, J. W., Honeycutt, R. K., & Turner, G. W. 1995, PASP, 107, 443

Rutkowski, A., Olech, A., Wiśniewski, M., Pietrukowicz, P., Pala, J., & Poleski, R. 2009, A&A, 497, 437

Schoembs, R., & Vogt, N. 1980, A&A, 91, 25

Schreiber, M. R., Hameury, J.-M., & Lasota, J.-P. 2004, A&A, 427, 621

Schwope, A., et al. 2000, Astron. Nachr., 321, 1

Shears, J., Hambsch, F.-J., Littlefield, C., Miller, I., Morelle, E., Pickard, R., Pietz, J., & Sabo, R. 2012a, J. Br. Astron. Assoc., in press (arXiv astro-ph/1209.4062)

Shears, J., et al. 2012b, J. Br. Astron. Assoc., in press (arXiv astro-ph/1205.0898)

Skillman, D. R., & Patterson, J. 1993, ApJ, 417, 298

Sokolovsky, K. V., Baryshev, K. O., & Korotkiy, S. A. 2012, Astron. Telegram, 3849

Solheim, J.-E. 2010, PASP, 122, 1133

Southworth, J., et al. 2008, MNRAS, 391, 591

Southworth, J., Marsh, T. R., Gänsicke, B. T., Aungwerojwit, A., Hakala, P., de Martino, D., & Lehto, H. 2007, MNRAS, 382, 1145

Stellingwerf, R. F. 1978, ApJ, 224, 953

Szkody, P., et al. 2003, AJ, 126, 1499

Szkody, P., et al. 2006, AJ, 131, 973

Szkody, P., et al. 2005, AJ, 129, 2386

Szkody, P., et al. 2007, ApJ, 658, 1188

Tappert, C., Augusteijn, T., & Maza, J. 2004, MNRAS, 354, 321

Thorstensen, J. R., Fenton, W. H., Patterson, J. O., Kemp, J., Krajci, T., & Baraffe, I. 2002a, ApJL, 567, L49

Thorstensen, J. R., Patterson, J. O., Kemp, J., & Vennes, S. 2002b, PASP, 114, 1108

Thorstensen, J. R., Patterson, J. O., Shambrook, A., & Thomas, G. 1996, PASP, 108, 73

Thorstensen, J. R., & Skinner, J. N. 2012, AJ, 144, 81

Thorstensen, J. R., Taylor, C. J., Becker, C. M., & Remillard, R. A. 1997, PASP, 109, 477

Tiurina, N., et al. 2012, Astron. Telegram, 3845

Tsugawa, M., & Osaki, Y. 1997, PASJ, 49, 75

Uemura, M., et al. 2002, PASJ, 54, L15

Uemura, M., Kato, T., Pavlenko, E., Baklanov, A., & Pietz, J. 2001, PASJ, 53, 539

Uemura, M., et al. 2005, A&A, 432, 261

Unda-Sanzana, E., et al. 2008, MNRAS, 388, 889

Uthas, H., et al. 2012, MNRAS, 420, 379

Vogt, N. 1983, A&A, 118, 95

Warner, B. 1995, Cataclysmic Variable Stars (Cambridge: Cambridge University Press)

Warner, B., & Woudt, P. A. 2004, in ASP Conf. Ser. 310, IAU Colloq. 193: Variable Stars in the Local Group, ed. D. W. Kurtz & K. R. Pollard (San Francisco: ASP), p. 382

Wils, P., Gänsicke, B. T., Drake, A. J., & Southworth, J. 2010, MNRAS, 402, 436

Wolf, M., & Wolf, G. 1905, Astron. Nachr., 169, 415

Wood, M. A., Still, M. D., Howell, S. B., Cannizzo, J. K., & Smale, A. P. 2011, ApJ, 741, 105

Woudt, P. A., et al. 2012, MNRAS, 427, 1004

Yamaoka, H., et al. 2011, Cent. Bur. Electron. Telegrams, 2731, 1